

**AN INVESTIGATION OF EFFECTIVENESS AND
DAMPING CAPABILITIES OF HYDRAULIC
SHOCK ABSORBERS**

THESIS

submitted in fulfillment of the requirement of the degree of

DOCTOR OF PHILOSOPHY

to

YMCA UNIVERSITY OF SCIENCE & TECHNOLOGY

by

DEV DUTT

Registration No.: YMCAUST/ Ph21/ 2010

Under the Supervision of

Dr. M. L. AGGARWAL

PROFESSOR



DEPARTMENT OF MECHANICAL ENGINEERING

Faculty of Engineering & Technology

YMCA University of Science & Technology

Sector-6, Mathura Road, Faridabad, Haryana, India

FEBRUARY, 2016

DECLARATION

I hereby declare that this thesis entitled **AN INVESTIGATION OF EFFECTIVENESS AND DAMPING CAPABILITIES OF HYDRAULIC SHOCK ABSORBERS** by **DEV DUTT**, being submitted in fulfillment of the requirements for the Degree of Doctor of Philosophy in **MECHANICAL ENGINEERING** under Faculty of Engineering & Technology of YMCA University of Science & Technology Faridabad, during the academic year 2016, is a bona fide record of my original work carried out under guidance and supervision of **Dr. M. L. AGGARWAL, PROFESSOR in MECHANICAL ENGINEERING DEPARTMENT, YMCAUST, FARIDABAD** and has not been presented elsewhere.

I further declare that the thesis does not contain any part of any work which has been submitted for the award of any degree either in this university or in any other university.



Devdutt

Registration No. YMCAUST/ Ph21/ 2010

CERTIFICATE

This is to certify that this Thesis entitled **AN INVESTIGATION OF EFFECTIVENESS AND DAMPING CAPABILITIES OF HYDRAULIC SHOCK ABSORBERS** by DEVDUTT, submitted in fulfillment of the requirement for the Degree of Doctor of Philosophy in **MECHANICAL ENGINEERING** under Faculty of Engineering & Technology of YMCA University of Science & Technology Faridabad, during the academic year 2016, is a bona fide record of work carried out under my guidance and supervision.

I further declare that to the best of my knowledge, the thesis does not contain any part of any work which has been submitted for the award of any degree either in this university or in any other university.



Dr. M. L. Aggarwal
PROFESSOR

Department of Mechanical Engineering
Faculty of Engineering & Technology

Dated: 8/2/2016

YMCA University of Science & Technology, Faridabad

ACKNOWLEDGEMENT

I would like to express my sincere gratitude to my Supervisor **Dr. M. L. Aggarwal** for giving me the opportunity to work in this area. It would never be possible for me to take this thesis to this level without his innovative ideas and his relentless support and encouragement.

I would also like to extend thanks to my family members for their patience and moral support throughout this thesis work. Finally, I wish to acknowledge my parents who taught me the value of education as well as for their blessings.



Devdutt

Registration No. YMCAUST/ Ph21/ 2010

ABSTRACT

This thesis presents the damping force generation ability of dual tube passive dampers with various piston and valve design parameters. The application of magnetorheological (MR) damper in semi-active suspension system for passenger ride comfort and safety is also studied, taking three-degree-of-freedom quarter car system. Various compression and rebound tests are performed on Measurement Testing Machine (MTS) machine to observe the influence of piston design parameters such as number of orifices, diameter of orifices, piston material, piston weight and thickness of piston as well as valve design parameters on the damping properties of dual tube passive hydraulic dampers.

The selected MR damper is tested on MTS machine under various experimental conditions in terms of current, amplitude, frequency values to generate various force-displacement and force-velocity curves. Polynomial model is selected for matching simulated curves with experimental results. Forward and Inverse controllers are designed for damping force generation through assembled MR damper. Forward control strategies include PID controller, Fuzzy Logic controller, Hybrid Fuzzy PID controller (HFPID) and Hybrid Fuzzy PID controller with Coupled Rules (HFPIDCR) respectively. Forward controllers are responsible for generation of desired damping force in suspension system. Inverse controller's designs are based on the concept of Fuzzy Logic. Inverse controllers are responsible for generation of current signals which is supplied to MR damper coils for generation of actual damping force.

The aim of the control system design and application in semi-active quarter car suspension system with MR damper is to achieve the improved performance in terms of passenger ride comfort and safety. For simulation work of quarter car suspension system, three different cases as primary suspension controlled, secondary suspension controlled and fully controlled suspension system are considered. In present case, four different types of road profiles such as pulse road profile, bump road profile, sinusoidal road profile and random road profiles are considered. The considered criterion is maximum and root mean square values of passenger seat acceleration and displacement response. The achieved performances through simulation work in these cases are compared between the passive or uncontrolled and controlled suspension system results in time domain. The simulation results showed the effectiveness of HFPIDCR controller in combination with MR damper for achieving best ride comfort

and safety of passengers compared to uncontrolled, PID controlled, Fuzzy controlled and HFPIID controlled suspension systems. The fully controlled semi-active quarter car system with HFPIIDCR controller in combination with MR damper provided best performance related to passenger ride comfort issues out of passive, primary suspension controlled and secondary suspension controlled quarter car systems for various passenger and sprung mass values.

TABLE OF CONTENTS

Candidate's Declaration	i
Certificate of the supervisor	ii
Acknowledgement	iii
Abstract	iv
Table of Contents	vi
List of Tables	xi
List of Figures	xvi
List of Symbols	xxi
List of Abbreviations	xxiii

1 INTRODUCTION

1.1 BACKGROUND.....	1
1.2 SUSPENSION SYSTEM.....	2
1.2.1 Primary Suspension System.....	3
1.2.2 Secondary Suspension System.....	3
1.3 CLASSIFICATION OF SUSPENSION SYSTEM.....	4
1.3.1 Passive Suspension System.....	4
1.3.2 Active Suspension System.....	5
1.3.3 Semi-active Suspension System.....	5
1.4 HYDRAULIC DAMPER.....	6
1.5 TYPES OF HYDRAULIC DAMPERS.....	7
1.5.1 Passive Hydraulic Dampers.....	7
1.5.1.1 Monotube Damper	8
1.5.1.2 Twin Tube Damper	9
1.5.2 Semi-Active Hydraulic Dampers.....	10
1.6 MAGNETORHEOLOGICAL FLUID TECHNOLOGY.....	11
1.7 RESEARCH OBJECTIVES.....	13
1.8 APPROACH.....	14
1.9 ORGANIZATION OF THE THESIS.....	16

2 LITERATURE REVIEW

2.1 OVERVIEW.....	19
-------------------	----

2.2 PASSIVE SHOCK ABSORBER.....	19
2.3 MAGNETORHEOLOGICAL DAMPER DESIGN.....	22
2.4 MR DAMPER MODELLING.....	23
2.4.1 Parametric Models.....	23
2.4.2 Non-parametric Models.....	25
2.5 CONTROL SYSTEM FOR SEMI-ACTIVE QUARTER CAR SYSTEMS.....	26
2.6 IDENTIFIED GAPS IN THE LITERATURE.....	31
2.7 SUMMARY.....	31
3 PASSIVE DAMPER TESTING	
3.1 INTRODUCTION.....	32
3.2 CONFIGURATION OF DUAL TUBE PASSIVE DAMPER.....	32
3.3 EXPERIMENTAL SET UP.....	33
3.3.1 Experimental Test Equipment.....	34
3.3.2 Experimentation.....	35
3.4 EXPERIMENTAL RESULTS.....	35
3.4.1 Variation in Number of Piston Orifice.....	36
3.4.2 Variation in Diameter of Piston Orifice	38
3.4.3 Variation in Valve Thickness.....	40
3.4.4 Variation in Cuts in Valve.....	42
3.4.5 Piston with Different Material.....	44
3.4.6 Piston with Different Thickness.....	44
3.4.7 Piston with Different Weight.....	45
3.4.8 Summary of the Parameter Design Results.....	45
3.5 THEORETICAL ESTIMATION OF DAMPING COEFFICIENT.....	46
3.6 OPTIMIZATION OF SELECTED PARAMETERS USING TAGUCHI METHOD.....	49
3.6.1 Geometrical optimization of passive damper using Taguchi method.....	50
3.6.2 Analysis of Signal – to - Noise (S/N) Ratio.....	51
3.6.3 Contribution of selected parameters on performance.....	53
3.6.4 Regression Analysis	53
3.6.5 Confirmation of Result.....	54

3.7 SUMMARY.....	54
4 MR DAMPER TESTING & MODELING	
4.1 OVERVIEW.....	55
4.2 MR DAMPER RD-1005-3 TESTING.....	55
4.2.1 Configuration of MR Damper.....	55
4.2.2 Experimental Set Up.....	56
4.2.3 Test Parameters & Results.....	57
4.3 MR DAMPER MODELING.....	58
4.4 SUMMARY.....	62
5 MATHEMATICAL MODELING OF QUARTER CAR SYSTEM	
5.1 INTRODUCTION.....	63
5.2 MODELLING ASSUMPTIONS.....	63
5.3 QUARTER CAR WITH PASSIVE AND SEMI-ACTIVE SUSPENSION SYSTEM.....	63
5.4 SUMMARY.....	67
6 CONTROLLERS DESIGN	
6.1 INTRODUCTION.....	68
6.2 FORWARD CONTROLLERS.....	68
6.2.1 PID Controller.....	68
6.2.2 Fuzzy Logic Controller.....	69
6.2.3 Hybrid Fuzzy PID Controller (HFPID).....	72
6.2.4 Hybrid Fuzzy PID Controller with Coupled Rules (HFPIDCR).....	73
6.3 INVERSE CONTROLLERS.....	74
6.4 SUMMARY.....	78
7 PERFORMANCE SPECIFICATIONS	
7.1 OVERVIEW.....	79
7.2 PERFORMANCE EVALUATION PARAMETERS.....	79
7.2.1 Peak Amplitude Criterion.....	79
7.2.2 RMS Criterion.....	80
7.3 SIMULATION PARAMETERS.....	80
7.3.1 Quarter Car Simulation Parameters.....	80

7.3.2 Controller Parameters.....	81
7.4 INPUT ROAD EXCITATIONS.....	82
7.4.1 Pulse Road Profile.....	82
7.4.2 Bump Road Profile.....	82
7.4.3 Sinusoidal Road Profile.....	83
7.4.4 Random Road Profile.....	83
7.5 ROBUSTNESS ANALYSIS.....	83
7.6 SUMMARY.....	84
8 PRIMARY SUSPENSION CONTROLLED SEMI-ACTIVE QUARTER CAR SYSTEM	
8.1 INTRODUCTION.....	85
8.2 PASSENGER SEAT SIMULATION RESULTS.....	85
8.2.1 Pulse Input Disturbance.....	85
8.2.2 Bump Input Disturbance.....	90
8.2.3 Sinusoidal Input Disturbance.....	95
8.2.4 Random Input Disturbance.....	100
8.3 SPRUNG MASS SIMULATION RESULTS.....	105
8.4 SUMMARY.....	110
9 SECONDARY SUSPENSION CONTROLLED SEMI-ACTIVE QUARTER CAR SYSTEM	
9.1 INTRODUCTION.....	111
9.2 PASSENGER SEAT SIMULATION RESULTS.....	111
9.2.1 Pulse Input Disturbance.....	111
9.2.2 Bump Input Disturbance.....	116
9.2.3 Sinusoidal Input Disturbance.....	121
9.2.4 Random Input Disturbance.....	126
9.3 SPRUNG MASS SIMULATION RESULTS.....	131
9.4 SUMMARY.....	136
10 FULLY CONTROLLED SEMI-ACTIVE QUARTER CAR SYSTEM	
10.1 INTRODUCTION.....	137
10.2 PASSENGER SEAT SIMULATION RESULTS.....	137

10.2.1 Pulse Input Disturbance.....	137
10.2.2 Bump Input Disturbance.....	144
10.2.3 Sinusoidal Input Disturbance.....	150
10.2.4 Random Input Disturbance.....	157
10.3 SPRUNG MASS SIMULATION RESULTS.....	163
10.4 SUMMARY.....	168
11 FREQUENCY RESPONSE ANALYSIS OF QUARTER CAR MODEL	
11.1 INTRODUCTION.....	169
11.2 NATURAL FREQUENCIES OF QUARTER CAR MODEL.....	170
11.3 ROAD PROFILE AND QUARTER CAR TRAVEL.....	170
11.4 SUMMARY.....	172
12 CONCLUSIONS AND SCOPE FOR FURTHER WORK	
12.1 CONCLUSIONS.....	173
12.1.1 SUMMARY.....	173
12.2 RESEARCH LIMITATIONS.....	183
12.3 SCOPE FOR FURTHER WORK.....	183
REFERENCES.....	185
APPENDIX A	197
BRIEF PROFILE OF THE RESEARCH SCHOLAR.....	202
LIST OF PUBLICATIONS OUT OF THESIS.....	203

LIST OF TABLES

Table 3.1 Parameters for experimental work.....	35
Table 3.2 Variation in number of orifice.....	36
Table 3.3 Peak Damping Force Values.....	37
Table 3.4 Variation in orifice diameter.....	38
Table 3.5 Peak Damping Force Values.....	40
Table 3.6 Variation in valve thickness.....	40
Table 3.7 Peak Damping Force Values.....	42
Table 3.8 Variation in cuts in valve.....	42
Table 3.9 Peak Damping Force Values.....	44
Table 3.10 Summary of Parameter Design Results at 0.3 m/s velocity.....	45
Table 3.11 Damping coefficient comparison.....	49
Table 3.12 Signal-to-Noise (S/N) ratio equations.....	50
Table 3.13 Selected parameters and levels for Taguchi method.....	50
Table 3.14 L9 Orthogonal Array.....	50
Table 3.15 Assigned Factors to L9 Orthogonal Array.....	51
Table 3.16 Damping Force and S/N Ratios for L9 Array.....	51
Table 3.17 S/N Ratios for each level of factors.....	52
Table 3.18 Specified optimum levels of S/N Ratios.....	52
Table 3.19 Optimum geometry.....	53
Table 3.20 Analysis of Variance.....	53
Table 3.21 Confirmation of result.....	54
Table 4.1 Technical details of MR shock absorber RD-1005-3.....	56
Table 4.2 Calculated coefficients b_i and c_i of fitted curve with values.....	60
Table 6.1 Fuzzy Rule Base for computing F_d	71
Table 6.2 Rule base description of Forward FLC.....	71
Table 6.3 Fuzzy Rule Base for computing I	76
Table 6.4 Rule base description of Inverse FLC.....	77
Table 7.1 Parameters of quarter car model for simulation.....	81
Table 7.2 Forward controller parameters for primary suspension system.....	81
Table 7.3 Forward controller parameters for secondary suspension system...	81

Table 8.1 Performance comparison of quarter car results under Pulse road profile ($M_p = 70$ kg).....	87
Table 8.2 Performance comparison of quarter car results under Pulse road profile ($M_s = 325$ kg).....	88
Table 8.3 Calculated Max. desired damping force using Forward controller 1 (N).....	89
Table 8.4 Calculated Max. input current using Inverse controller 1 (A).....	90
Table 8.5 Performance comparison of quarter car results under Bump road profile ($M_p = 70$ kg).....	92
Table 8.6 Performance comparison of quarter car results under Bump road profile ($M_s = 325$ kg).....	93
Table 8.7 Calculated Max. desired damping force using Forward controller 1 (N).....	94
Table 8.8 Calculated Max. input current using Inverse controller 1 (A).....	95
Table 8.9 Performance comparison of quarter car results under Sinusoidal road profile ($M_p = 70$ kg).....	97
Table 8.10 Performance comparison of quarter car results under Sinusoidal road profile ($M_s = 325$ kg).....	98
Table 8.11 Calculated Max. desired damping force using Forward controller 1 (N).....	99
Table 8.12 Calculated Max. input current using Inverse controller 1 (A).....	100
Table 8.13 Performance comparison of quarter car results under Random road profile ($M_p = 70$ kg).....	102
Table 8.14 Performance comparison of quarter car results under Random road profile ($M_s = 325$ kg).....	103
Table 8.15 Calculated Max. desired damping force using Forward controller 1 (N).....	104
Table 8.16 Calculated Max. input current using Inverse controller 1 (A).....	105
Table 8.17 Performance comparison of Sprung mass response.....	109
Table 9.1 Performance comparison of quarter car results under Pulse road profile ($M_p = 70$ kg).....	113
Table 9.2 Performance comparison of quarter car results under Pulse road profile ($M_s = 325$ kg).....	114

Table 9.3 Calculated Max. desired damping force using Forward controller 2 (N).....	115
Table 9.4 Calculated Max. input current using Inverse controller 2 (A).....	116
Table 9.5 Performance comparison of quarter car results under Bump road profile ($M_p = 70$ kg).....	118
Table 9.6 Performance comparison of quarter car results under Bump road profile ($M_s = 325$ kg).....	119
Table 9.7 Calculated Max. desired damping force using Forward controller 2 (N).....	120
Table 9.8 Calculated Max. input current using Inverse controller 2 (A)...	121
Table 9.9 Performance comparison of quarter car results under Sinusoidal road profile ($M_p = 70$ kg).....	123
Table 9.10 Performance comparison of quarter car results under Sinusoidal road profile ($M_s = 325$ kg).....	124
Table 9.11 Calculated Max. desired damping force using Forward controller 2 (N).....	126
Table 9.12 Calculated Max. input current using Inverse controller 2 (A).....	126
Table 9.13 Performance comparison of quarter car results under Random road profile ($M_p = 70$ kg).....	128
Table 9.14 Performance comparison of quarter car results under Random road profile ($M_s = 325$ kg).....	129
Table 9.15 Calculated Max. desired damping force using Forward controller 2 (N).....	130
Table 9.16 Calculated Max. input current using Inverse controller 2 (A).....	131
Table 9.17 Performance comparison of Sprung mass response.....	135
Table 10.1 Performance comparison of quarter car results under Pulse road profile ($M_p = 70$ kg).....	139
Table 10.2 Performance comparison of quarter car results under Pulse road profile ($M_s = 325$ kg).....	140
Table 10.3 Calculated Max. desired damping force using Forward controller 1 (N).....	141
Table 10.4 Calculated Max. input current using Inverse controller 1 (A).....	142
Table 10.5 Calculated Max. desired damping force using Forward controller 2 (N).....	143

Table 10.6 Calculated Max. input current using Inverse controller 2 (A).....	144
Table 10.7 Performance comparison of quarter car results under Bump road profile ($M_p = 70$ kg).....	146
Table 10.8 Performance comparison of quarter car results under Bump road profile ($M_s = 325$ kg).....	147
Table 10.9 Calculated Max. desired damping force using Forward controller 1 (N).....	148
Table 10.10 Calculated Max. input current using Inverse controller 1 (A)....	149
Table 10.11 Calculated Max. desired damping force using Forward controller 2 (N).....	149
Table 10.12 Calculated Max. input current using Inverse controller 2 (A)....	150
Table 10.13 Performance comparison of quarter car results under Sinusoidal road profile ($M_p = 70$ kg).....	152
Table 10.14 Performance comparison of quarter car results under Sinusoidal road profile ($M_s = 325$ kg).....	153
Table 10.15 Calculated Max. desired damping force using Forward controller 1 (N).....	154
Table 10.16 Calculated Max. input current using Inverse controller 1 (A)....	155
Table 10.17 Calculated Max. desired damping force using Forward controller 2 (N).....	156
Table 10.18 Calculated Max. input current using Inverse controller 2 (A)...	157
Table 10.19 Performance comparison of quarter car results under Random road profile ($M_p = 70$ kg).....	158
Table 10.20 Performance comparison of quarter car results under Random road profile ($M_s = 325$ kg).....	159
Table 10.21 Calculated Max. desired damping force using Forward controller 1 (N).....	161
Table 10.22 Calculated Max. input current using Inverse controller 1 (A)....	161
Table 10.23 Calculated Max. desired damping force using Forward controller 2 (N).....	163
Table 10.24 Calculated Max. input current using Inverse controller 2 (A).....	163
Table 10.25 Performance comparison of Sprung mass response.....	167
Table 11.1 Quarter car model natural frequencies.....	170
Table 11.2 Base excitation frequency at various quarter car velocities...	172

Table 12.1 Performance comparison of Passenger seat response under Pulse road profile.....	174
Table 12.2 Performance comparison of Passenger seat response under Bump road profile.....	175
Table 12.3 Performance comparison of Passenger seat response under Sinusoidal road profile.....	176
Table 12.4 Performance comparison of Passenger seat response under Random road profile.....	177
Table 12.5 Influence of various piston design parameters.....	178
Table 12.6 Influence of various valve design parameters.....	179
Table 12.7 Primary suspension system good desired damping force range....	182
Table 12.8 Secondary suspension system good desired damping force range	182
Table 12.9 Primary suspension system fair desired damping force range.....	182
Table 12.10 Secondary suspension system fair desired damping force range	182
LIST OF PUBLICATIONS OUT OF THESIS.....	203

LIST OF FIGURES

Figure 1.1 Primary suspension system.....	3
Figure 1.2 Secondary suspension system.....	3
Figure 1.3 Types of suspension systems.....	4
Figure 1.4 Quarter car model with a passive suspension.....	4
Figure 1.5 Quarter car model with an active suspension system.....	5
Figure 1.6 Quarter car model with a semi-active suspension system.....	6
Figure 1.7 Hydraulic damper in vehicle.....	7
Figure 1.8 Monotube passive damper.....	8
Figure 1.9 Twin-tube passive damper.....	9
Figure 1.10 Sectional view of magnetorheological damper.....	10
Figure 1.11 Magnetorheological damper.....	11
Figure 1.12 Illustration of MR fluid activation behaviour: (a) Without magnetic field (b) Initial stage during magnetic field application (c) Fully developed stage.....	12
Figure 1.13 Working modes of MR fluid.....	13
Figure 1.14 Research Methodology for Phase I.....	14
Figure 1.15 Research Methodology for Phase II.....	15
Figure 2.1 Classification of Literature Review.....	19
Figure 2.2 Bingham model.....	24
Figure 2.3 Bouc-Wen hysteretic model.....	24
Figure 2.4 Modified Bouc-Wen model.....	24
Figure 2.5 Hyperbolic tangent function based model.....	25
Figure 2.6 Modified Dahl model.....	25
Figure 3.1 Dual tube passive damper.....	33
Figure 3.2 Piston valve assembly.....	33
Figure 3.3 Schematic diagram of passive damper test set up.....	34
Figure 3.4 Passive damper testing.....	34
Figure 3.5 Test results for variation in number of piston orifice.....	37
Figure 3.6 Combined test results of variation in number of piston orifice.....	38

Figure 3.7 Test results for variation in diameter of piston orifice.....	39
Figure 3.8 Combined test results of variation in dia. of piston orifices.....	40
Figure 3.9 Test results for variation in valve thickness.....	41
Figure 3.10 Combined test results of variation in valve thickness.....	42
Figure 3.11 Test results for variation in cuts in valve.....	43
Figure 3.12 Combined test results of variation in cuts in valve.....	44
Figure 3.13 Viscosity-Temperature relationship.....	46
Figure 3.14 S/N Ratio plot for maximization of damping force.....	52
Figure 4.1 MR damper RD-1005-3.....	55
Figure 4.2 Schematic diagram of MR damper test set up on MTS.....	56
Figure 4.3 Experimental setup of MR damper with test machine.....	57
Figure 4.4 Experimental results (2.5 Hz, \pm 6.3 mm): force vs. displacement; (b) force vs. velocity.....	58
Figure 4.5 Polynomial model.....	59
Figure 4.6 The relationship between a_i and input current.....	60
Figure 4.7 Comparison of model fitted curves and experimental results (2.5 Hz, \pm 6.3 mm): (a) force vs displacement; (b) force vs velocity.....	61
Figure 5.1 (a) Passive quarter car model (b) Primary suspension controlled semi-active quarter car model (c) Secondary suspension controlled semi- active quarter car model (d) Fully controlled semi-active.....	64
Figure 6.1 Conventional PID controller applied in secondary suspension system.....	68
Figure 6.2 Forward FLC with plant or system.....	70
Figure 6.3 MFs for FLC (a) Input side, e and de (b) Output side, F_d	71
Figure 6.4 Forward FLC input / output surface.....	72
Figure 6.5 Structure of HFPID controller.....	73
Figure 6.6 Structure of HFPIDCR controller.....	74
Figure 6.7 Inverse controller design using Forward controller output.....	74
Figure 6.8 Inverse fuzzy logic controller with plant or system.....	75
Figure 6.9 MFs for FLC (a) Input side, F_d and de (b) Output side, I	76
Figure 6.10 Inverse Input / Output surface.....	77
Figure 7.1 Peak / Maximum amplitude.....	79

Figure 7.2 Pulse road profile.....	82
Figure 7.3 Bump road profile.....	83
Figure 7.4 Sinusoidal road profile.....	83
Figure 7.5 Random road profile.....	83
Figure 8.1 Block diagram of primary suspension controlled semi-active quarter car system.....	85
Figure 8.2 (a) Passenger seat acceleration (b) Passenger seat displacement...	86
Figure 8.3 Desired damping force signals supplied by different controllers...	89
Figure 8.4 Input current signal generated by different controllers.....	90
Figure 8.5 (a) Passenger seat acceleration (b) Passenger seat displacement...	91
Figure 8.6 Desired damping force signals supplied by different controllers...	94
Figure 8.7 Input current signal generated by different controllers.....	95
Figure 8.8 (a) Passenger seat acceleration (b) Passenger seat displacement...	96
Figure 8.9 Desired damping force signals supplied by different controllers...	99
Figure 8.10 Input current signal generated by different controllers.....	100
Figure 8.11 (a) Passenger seat acceleration (b) Passenger seat displacement	101
Figure 8.12 Desired damping force signals supplied by different controllers	104
Figure 8.13 Input current signal generated by different controllers.....	105
Figure 8.14 Sprung mass response under pulse road input (a) Acceleration (b) Displacement.....	106
Figure 8.15 Sprung mass response under bump road input (a) Acceleration (b) Displacement.....	107
Figure 8.16 Sprung mass response under sinusoidal road input (a) Acceleration (b) Displacement.....	107
Figure 8.17 Sprung mass response under random road input (a) Acceleration (b) Displacement.....	108
Figure 9.1 Block diagram of secondary suspension controlled semi-active quarter car system.....	111
Figure 9.2 (a) Passenger seat acceleration (b) Passenger seat displacement...	112
Figure 9.3 Desired damping force signals supplied by different controllers...	115
Figure 9.4 Input current signal generated by different controllers.....	116
Figure 9.5 (a) Passenger seat acceleration (b) Passenger seat displacement...	117
Figure 9.6 Desired damping force signals supplied by different controllers...	120
Figure 9.7 Input current signal generated by different controllers.....	121

Figure 9.8 (a) Passenger seat acceleration (b) Passenger seat displacement...	122
Figure 9.9 Desired damping force signals supplied by different controllers...	125
Figure 9.10 Input current signal generated by different controllers.....	126
Figure 9.11 (a) Passenger seat acceleration (b) Passenger seat displacement	127
Figure 9.12 Desired damping force signals supplied by different controllers	130
Figure 9.13 Input current signal generated by different controllers.....	131
Figure 9.14 Sprung mass response under pulse road input (a) Acceleration (b) Displacement.....	132
Figure 9.15 Sprung mass response under bump road input (a) Acceleration (b) Displacement.....	133
Figure 9.16 Sprung mass response under sinusoidal road input (a) Acceleration (b) Displacement.....	133
Figure 9.17 Sprung mass response under random road input (a) Acceleration (b) Displacement.....	134
Figure 10.1 Block diagram of fully suspension controlled semi-active quarter car system.....	137
Figure 10.2 (a) Passenger seat acceleration (b) Passenger seat displacement	138
Figure 10.3 Desired damping force signals supplied by different controllers	141
Figure 10.4 Input current signal generated by different controllers.....	142
Figure 10.5 Desired damping force signals supplied by different controllers	143
Figure 10.6 Input current signal generated by different controllers.....	144
Figure 10.7 (a) Passenger seat acceleration (b) Passenger seat displacement	145
Figure 10.8 Desired damping force signals supplied by different controllers	148
Figure 10.9 Input current signal generated by different controllers.....	148
Figure 10.10 Desired damping force signals supplied by different control.....	149
Figure 10.11 Input current signal generated by different controllers.....	150
Figure 10.12 (a) Passenger seat acceleration (b) Passenger seat displacement.....	151
Figure 10.13 Desired damping force signals supplied by different controllers.....	154
Figure 10.14 Input current signal generated by different controllers.....	155
Figure 10.15 Desired damping force signals supplied by different controllers.....	156
Figure 10.16 Input current signal generated by different controllers.....	156

Figure 10.17 (a) Passenger seat acceleration (b) Passenger seat displacement.....	157
Figure 10.18 Desired damping force signals supplied by different controllers.....	160
Figure 10.19 Input current signal supplied to MR shock absorber by different controllers.....	161
Figure 10.20 Desired damping force signals supplied by different controllers.....	162
Figure 10.21 Input current signal supplied to MR shock absorber by different controllers.....	162
Figure 10.22 Sprung mass response under pulse road input (a) Acceleration (b) Displacement.....	164
Figure 10.23 Sprung mass response under bump road input (a) Acceleration (b) Displacement.....	164
Figure 10.24 Sprung mass response under sinusoidal road input (a) Acceleration (b) Displacement.....	165
Figure 10.25 Sprung mass response under random road input (a) Acceleration (b) Displacement.....	166
Figure 11.1 Quarter car travel over sinusoidal road profile.....	171
Figure A.1 Uncontrolled and controlled quarter car simulink models.....	198
Figure A.2 Overview of quarter car model input-output signals.....	199
Figure A.3 Overview of Inverse Fuzzy Logic Controller in quarter car model.....	200

List of Symbols

a_{RMS}	RMS value of vertical acceleration
c_p	Primary suspension damping coefficient
c_s	Secondary suspension damping coefficient
d_{RMS}	RMS value of vertical displacement
$de(t)$	Change of error signal
$e(t)$	Error signal
F_d	Desired damping force signal
F_{d1}	Desired damping force signal generated by forward controller 1
F_{d2}	Desired damping force signal generated by forward controller 2
F_{a1}	Active damping force supplied by controller 1
F_{a2}	Active damping force supplied by controller 2
F_{MRp}	Damping force generated by primary suspension MR damper
F_{MRs}	Damping force generated by secondary suspension MR damper
h	Bump height
I	Supplied current to MR damper
I_1	Current signal generated by inverse controller 1
I_2	Current signal generated by inverse controller 2
K_P	Proportional gain
K_I	Integral gain
K_D	Derivative gain
K_{PI}	Proportional Integral gain
K_{PD}	Proportional Derivative gain
k_p	Primary suspension spring stiffness
k_s	Secondary suspension spring stiffness
m_1	Passenger seat mass
m_2	Sprung mass
m_3	Unsprung mass
n	Number of variables

v	Piston rod actual velocity
v_{ref}	Piston rod reference velocity
w	Threshold value
y	Current position of piston rod
y_{ref}	Reference position of piston rod
k_t	Tire stiffness
z_1	Passenger seat displacement
z_2	Sprung mass displacement
z_3	Unsprung mass displacement
z_r	Road input displacement
\dot{z}_1	Passenger seat velocity
\dot{z}_2	Sprung mass velocity
\dot{z}_3	Unsprung mass velocity
\ddot{z}_1	Passenger seat acceleration
\ddot{z}_2	Sprung mass acceleration
\ddot{z}_3	Unsprung mass acceleration
λ_{uss}	Calculated value with uncontrolled suspension system
λ_{css}	Calculated value with controlled suspension system

List of Abbreviations

ANFIS	Adaptive Neuro Fuzzy Inference System
ANOVA	Analysis of variance
ASD	Amplitude Selective Damping
BBM	Black Box Model
CFD	Computational Fluid Dynamics
CCFD	Coupled Computational Fluid Dynamics
DC	Direct Current
DSSA	Displacement Sensitive Shock Absorber
ER	Electro Rheological
FEA	Finite Element Analysis
FEMM	Finite Element Method Magnetics
FLSC	Fuzzy Lyapunov Skyhook Controller
FNNC	Fuzzy Neural Network Control
FSI	Fluid Structure Interaction
HFPID	Hybrid Fuzzy PID
HFPIDCR	Hybrid Fuzzy PID controller with Coupled Rules
HILS	Hardware In Loop Simulation
IFLC	Inverse Fuzzy Logic Controller
LQ	Linear Quadratic
LQG	Linear Quadratic Gaussian
LSM	Least Squares Method
MATLAB	MATRIX LABORATORY
MR	Magneto Rheological
MRF	Magneto Rheological Fluid
MTS	Measurement Testing System
NSGA	Non-dominated Sorting Genetic Algorithm
OEM	Original Equipment Manufacturer
PI	Proportional Integral

PID	Proportional Integral Derivative
PSO	Particle Swarm Optimization
RMS	Root Mean Square
SMC	Sliding Mode Control
SN	Signal to Noise

CHAPTER I

INTRODUCTION

1.1 BACKGROUND

The aim of vehicle suspension system is to provide support to the automotive body mass and to suppress/ eliminate the vibrations and disturbances generated by uneven road surfaces for safe, comfortable and pleasant ride. Thus, suspension system plays a crucial role in vehicle assembly by fulfilling multiple tasks and requirements related to vehicle stability, road holding ability, passenger's ride comfort and safety during changing road conditions, loading conditions and vehicle speed variations. The main concern in automotive suspension system design and development is to achieve the above said conflicting and challenging issues i.e. suspension should be soft enough to achieve a comfortable ride whereas stiff suspension system is needed for good road handling capability and vehicle stability [1].

Bad road conditions and harsh driving habits induce severe vibrations in the vehicle structure, causing discomfort to the passengers and sometimes even leading to the damage of the assembled parts. The protection of vehicle parts and its occupants as well as loaded objects under road induced vibrations can be achieved by application of various methods such as improving the structural design, rigidity of assembled parts, damping of vehicle structure etc. Comfort level for travelling passengers is affected by intensity and duration of vibrations transmitted to the vehicle system as well as to the sitting occupants. Acceleration transmitted to the vehicle body through road surface is finally experienced by the passengers as a disturbing external force which affects the ride comfort. High intensity of acceleration in combination with high level of passenger seat displacement and its long time duration can generate fatal results for human health and safety. Exposure to high level of vibrations for longer time is very uncomfortable to traveling passengers and may result in injury to human body. Human exposure to small level of vibrations is also harmful if its duration is long enough, making it a crucial factor for drivers driving the vehicles continuously for longer time on regular basis.

Automotive manufacturing industries are struggling hard to achieve these increasing customer demands by putting efforts, time and money in research and development activities. The new developments in the vibration control technology of vehicles and comfort needs for driver and occupants against road induced jerks and health hazards

motivated scientists and engineers to do research in the field of automotive control technology. Finally, long term efforts in the field of suspension system have opened the doors to controllable suspension system related technology. Automotive industries have started working towards the development of controllable and intelligent mechatronics based suspension system technology which includes active and semi-active ones. Such smart suspension systems working is based on the devices such as computers and controllable actuators [2- 4].

1.2 SUSPENSION SYSTEM

Every vehicle model has got its own designed and assembled suspension system, which is responsible for comfortable ride on different road conditions varying from smooth to rough. A vehicle suspension system structure consist the assembly of various parts such as dampers, springs, torsion bars and arms etc. The two main assembled parts in suspension system are spring and damper. Technically, during the vehicle vibration duration, the spring element stores the energy in potential form, which is instantaneously converted into kinetic energy of vehicle body and dissipated to the environment in the form of thermal energy through the outer walls of the damper [5]. The suspension system must be designed and developed in such a way so as to keep wheels in contact with road surface i.e. wheel lifting must be avoided during turning, braking and accelerating conditions.

During the changing load conditions on the vehicle i.e. during loaded and unloaded situations, the suspension system must support this weight with minimum disturbance to suspension components. A minimum movement and rapid settling time of primary as well as secondary suspension system components during harsh travelling conditions will provide a design choice for suspension working space setting within certain limits. It is helpful for passengers ride comfort and safety as well as longer life of assembled components.

A possible cause for the difference in behavior of the vehicle on a smooth road and on a rough road is the nonlinear behavior of the dampers of the vehicle. During driving, the roughness of the road will determine the level of vibrations present at the wheel. The generated damping characteristics need to be selected or tuned during the design phase to achieve the optimum compromise between ride comfort and vehicle handling performance for different types of road travelling conditions.

1.2.1 Primary Suspension System

The parts connecting the axle-wheel assembly of a vehicle to the frame of the vehicle is known as primary suspension as shown in Figure 1.1 [6]. The spring and damper assembly helps in controlling the road induced vibrations from transmitting to the passenger seat and occupants while these are connected between the sprung mass (vehicle body mass) and unsprung mass (tyre and wheel mass) in the suspension system.

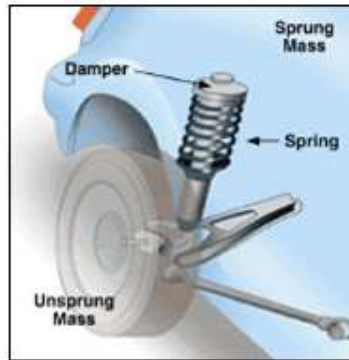


Figure 1.1 Primary suspension system

The damper performs the critical function of reducing and slowly eliminating the effects of undesirable road generated vibrations in the vehicle system during the travelling period. In the absence of suitable damper in vehicle suspension system, the desired characteristics related to the road holding i.e. adequate wheel-ground contact, steering and braking as well as passenger safety would reduce drastically.

1.2.2 Secondary Suspension System

Here, parts connecting the components to the body of a vehicle such as seat suspensions, engine mounts and cab mounts are known as secondary suspension. The secondary suspension system includes passenger seat mass, spring as well as damper as shown in Figure 1.2.

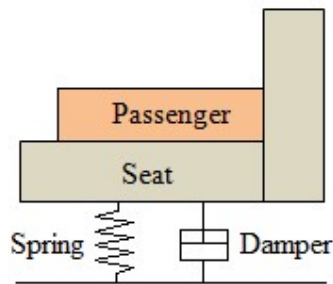


Figure 1.2 Secondary suspension system

1.3 CLASSIFICATION OF SUSPENSION SYSTEM

Vehicle overall performance related to suspension system action in terms of passengers ride comfort, vehicle structure safety and road holding ability depends mainly on three types of suspension systems, which can be categorized as: passive suspension system, active suspension system and semi-active suspension system as shown in Figure 1.3.

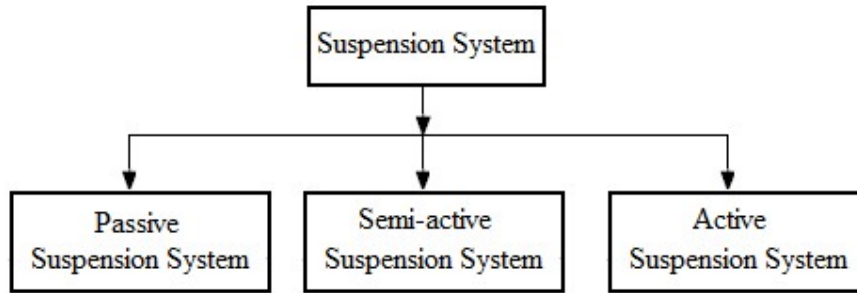


Figure 1.3 Types of suspension systems

1.3.1 Passive Suspension System

In passive suspension system, the characteristics of main vibration controlling components such as springs and dampers are fixed within certain limits by the designer as per the type and application of the vehicle as shown in Figure 1.4. These characteristics cannot be changed or varied or tuned externally as per the changing conditions such as road, load, comfort and vehicle handling requirements.

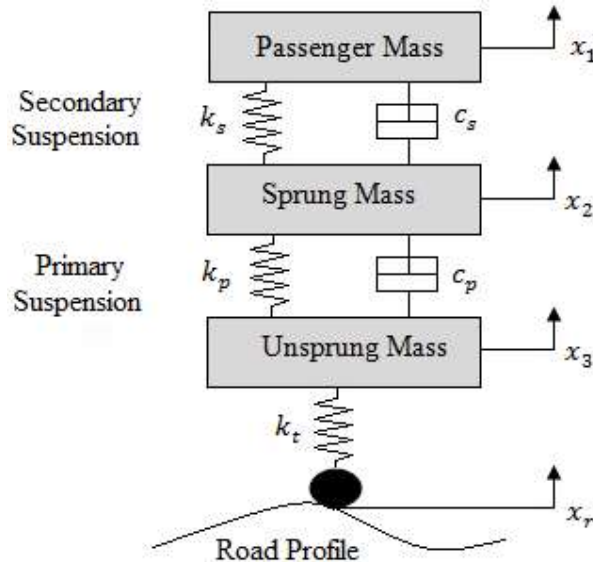


Figure 1.4 Quarter car model with a passive suspension system

Thus, during the changing road, load and braking conditions of vehicle, suspension system is totally dependent on passive parts, which cannot provide optimal

performance due to restricted or limited technology. In today's world, passive suspension system is mostly used in automotive sector, having an acceptable level between ride comfort and vehicle handling.

1.3.2 Active Suspension System

Active suspension system provides superior and improved ride comfort and handling characteristics in a wider frequency band due to application of independent force supplied by actuators and controllers. In case of active suspension, assembly of mechatronics based devices forms the integral part of suspension system and responsible for damping force generation and controlling instead of traditional passive components such as spring and damper. A quarter car model with active suspension system is shown in Figure 1.5.

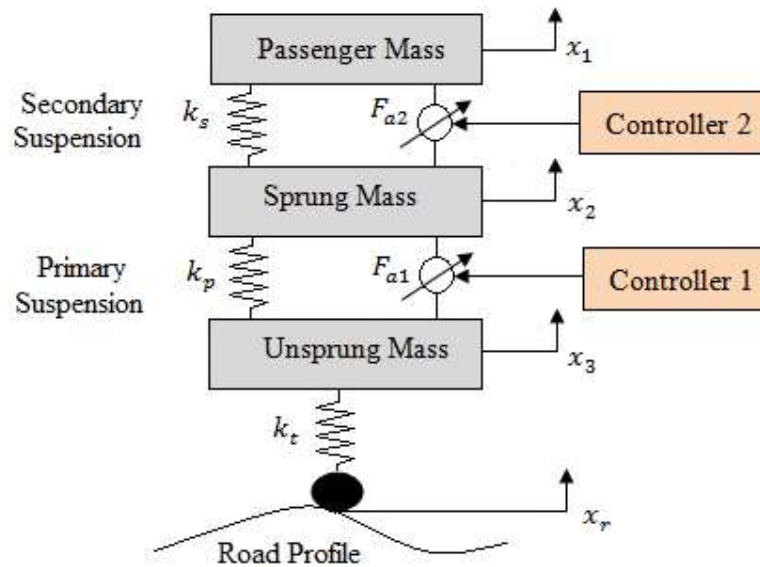


Figure 1.5 Quarter car model with an active suspension system

Here, F_{a1} and F_{a2} represents the active damping force supplied by controller 1 in primary suspension system and by controller 2 in the secondary suspension system respectively. This technology is very costly, requires high input power for system working, including other serious drawbacks such as size as well as weight of sensors and controllers. Thus, application and implementation of this technology is limited to some high end and costly vehicles.

1.3.3 Semi-active Suspension System

Semi-active suspension system technology came into existence in early 1970s by the efforts of Karnopp et al. while working with Lord Corporation and using the "skyhook" damping approach by the application of hydraulically adjustable damper

[7]. These suspension systems became an alternate choice in terms of desired performance with economical price, lower weight and compact size of controllable damper, simple assembly and much less power consumption as compared to active suspension system. It inherits the advantages of both passive as well as active suspension systems and provides the additional safety factor to the vehicle and passengers during the travelling duration. In case of the failure of control system, the assembled damper unit automatically shifts or switch over to passive mode, making the damping device still workable by working as passive suspension system.

Practically, a semi-active vehicle suspension system assembly consists of a helical spring and a MR or ER damper as main parts. An external controller is used to vary or control the damping force generated by MR or ER damper. The damping coefficient of such dampers can be externally controlled for effective suspension system behavior without adding external energy to suspension system [8-9]. A schematic of semi-active suspension system in combination with controllable dampers and controllers is depicted in Figure 1.6.

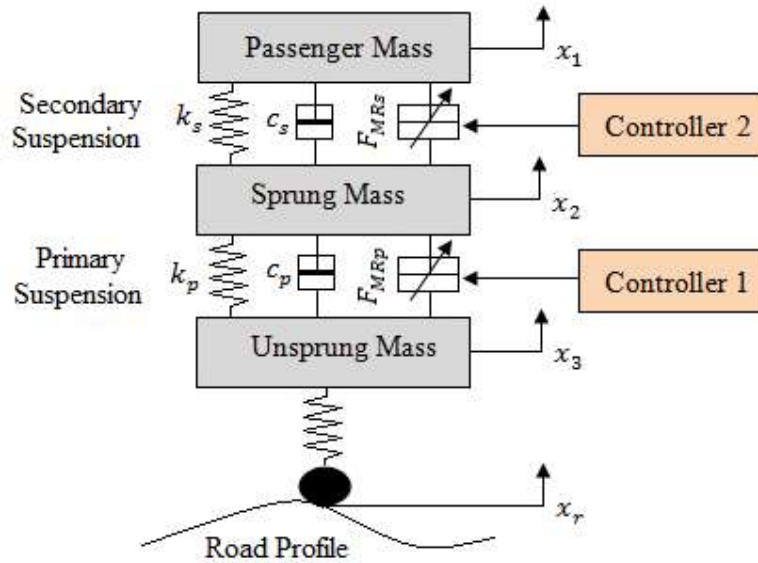


Figure 1.6 Quarter car model with a semi-active suspension system

Here, F_{MRp} and F_{MRS} represents damping force generated by MR damper in the primary and secondary suspension respectively.

1.4 HYDRAULIC DAMPER

A damper is an assembly of small components working on the concept of fluid flow. In damper, thermal energy is generated due to fast movement of hydraulic oil inside the tube, which is dissipated to external environment through the outer walls of the

damper. During each stroke of the piston rod in vertical direction, volume of the fluid displaced from high pressure side to the low pressure side is equivalent to the swept volume of the piston rod. A damper generates damping forces during the compression and rebound strokes as shown in Figure 1.7.

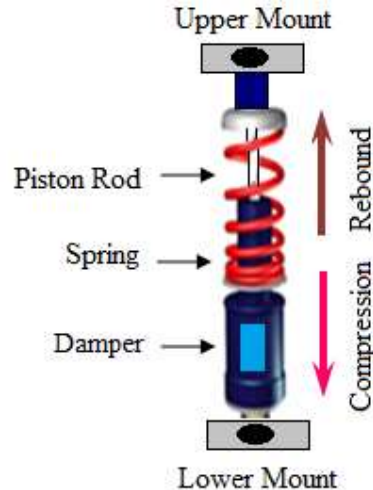


Figure 1.7 Hydraulic damper in vehicle

Compression damping involves the generation of damping force during the compression stage of the damper from its normal position. It results in to the decrease in the measured length of the damper from its normal length. Magnitude of the generated compression damping force decides the ride comfort and vehicle handling criterion. Too low compression damping results into loss of wheel contact with road surface leading to poor vehicle handling while in case of too high compression damping the road transmitted force is directly transferred to chassis and passenger seat of the vehicle leading to harsh ride experience.

Rebound damping is followed by compression damping of the damper. During this stage, the damper tries to attain its equilibrium position. A low rebound damping generates a very soft ride experience while a high rebound damping results into prevention of wheel to attain its equilibrium state leading to uncontrolled vehicle handling situation.

1.5 TYPES OF HYDRAULIC DAMPERS

1.5.1 Passive Hydraulic Dampers

A passive damper assembly mainly consists of a cylindrical tube filled with oil having particular characteristics in which piston assembly with rod is submerged. In such type of dampers, the damping behavior is controlled by the design and assembly of piston valves and washers. The accumulator side is generally filled with gas (air or

nitrogen) to provide cushioning effect in case of sudden jerk to piston rod. The pressure drop due to rapid oil flow through orifices is responsible for damping force generation. The fluid flow between the compression and extension chambers during the piston movement occurs through two paths:

- (i) through the orifices in the piston and
- (ii) between the piston outer wall and inner wall of the cylindrical tube.

This concept is applied in design and development work of monotube and twin tube dampers.

1.5.1.1 Monotube Damper

Monotube damper is having single cylinder, filled with fluid which is easier to manufacture, lighter in weight and contains a high pressurised gas filled in it. The filled gas provides cushioning or spring effect to the damping force generated by the damper, controlling the damper at its full extended position when there is no force applied [10]. A floating piston is assembled for separating the fluid and gas chambers. The gas chamber provides additional advantage by preventing the vacuum creation resulting into the absence of cavitation of the fluid during the piston extension stroke, which is necessary for effectiveness of damper in the smooth generation of damping force. The monotube damper with its main components such as housing, piston and piston rod assembly as well as accumulator is shown in Figure 1.8.

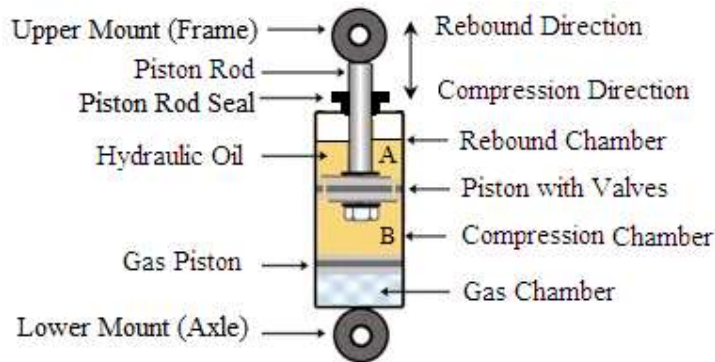


Figure 1.8 Monotube passive damper

During the compression stroke, the piston and rod moves in the downwards direction in the cylinder, which causes a small pressure drop in the chamber labeled A, above the piston. Now, the volume of the chamber labeled B, below the piston is reduced resulting into a high pressure fluid in the chamber labeled B. This causes the flow of fluid from chamber B to chamber A through the piston orifices by the deflection of piston valves.

The monotube damper can be mounted/ assembled in any orientation making it a versatile device for vibration control applications. In such type of dampers, dissipation of generated heat during working is fast and smooth which is prime requirement for sports vehicles having racing applications.

1.5.1.2 Twin Tube Damper

Twin-tube damper is having outer and inner tubes making two chambers filled with oil as shown in Figure 1.9. The piston movement occurs in the inner chamber while the outer chamber equalizes the change in oil volume. Twin-tube assembly contains two valves : a base valve and a piston valve. During the piston movement, the oil movement takes place from inner housing to outer housing and vice-versa through the base valve.

On bump, or compression, the piston and rod move downwards in the cylinder, resulting in a small pressure drop in the chamber labeled A, above the piston. At the same time, the volume of the chamber labeled B, below the piston, is reduced, causing a high fluid pressure. This unseats the piston valve, and fluid flows up through the outer passages in the piston, and into chamber A. But the piston rod is also now entering A, and displacing a quantity of fluid equal to its volume, so, all of the oil in B cannot flow into A, The displaced fluid is forced down through a base valve and out into the reservoir labeled C.

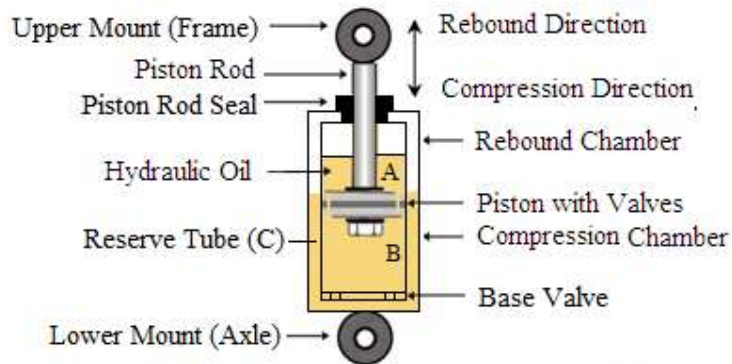


Figure 1.9 Twin-tube passive damper

In the rebound, or extension phase, the piston and rod move upwards and the volume of chamber A is reduced. Chamber A becomes a high-pressure area, and fluid flows through the extension valve in the piston, into chamber B. However the withdrawal of the piston from B greatly increases its volume, and fluid flow from A is insufficient to fill the space. Pressure in B falls below that of the reservoir, causing

the base intake valve to be unseated. Fluid flows from the reserve tube C into chamber B, keeping the inner tube full.

A twin tube damper has got certain advantages and disadvantages compared to mono tube damper. It can operate with longer stroke range and contains more oil volume in two tubes which provides a comfortable ride experience and proper vehicle handling and control. It can operate with lower gas pressure and more safe against damage from outer environment due to additional outer cylinder. But the heat dissipation to the outer environment is not rapid as well as the design and assembly procedure is complex compared to monotube damper.

1.5.2 Semi-Active Hydraulic Dampers

In past few decades, industrial attention is towards design and development of semi-active suspension system based technology providing reliable choice in terms of performance related to passenger ride comfort and vehicle handling due to controllable variable damping. Semi-active control technology integrates attractive features of both passive and active control systems. The advancement and research in the field of damper technology lead to the development of Electro-Rheological (ER) and Magneto-Rheological (MR) fluid dampers having great and promising potential compared to traditional passive dampers. Figure 1.10 shows the sectional view of MR damper while MR damper assembly consisting of a cylindrical tube, piston assembly having magnetic coil is shown in Figure 1.11.

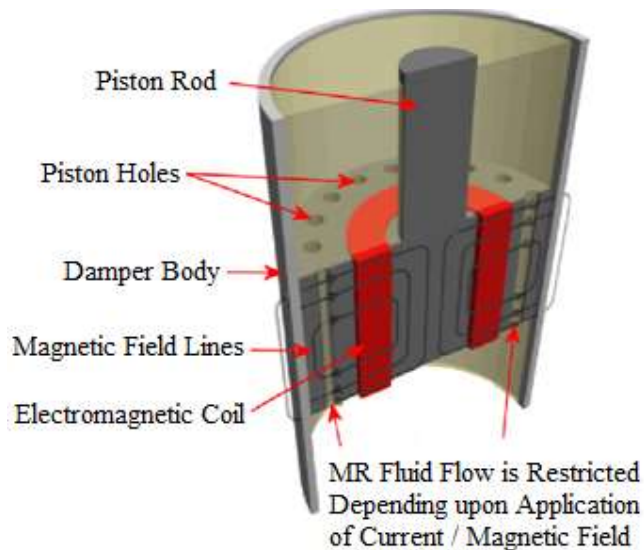


Figure 1.10 Sectional view of magnetorheological damper

It only requires changing the behavior of working fluid for controllable damping instead of mechanically disturbing the internal assembled components. It contains a

smart fluid which can be externally controlled and relaxed within few milliseconds i.e. damping force can be altered with the application of externally applied electric field. In such dampers, design criterion is such that, controllable damper force is directly related to the piston velocity inside the damper [11].

There is a flow of MR fluid from one reservoir to another, with the connection being through a small diameter passage. If the passage is subjected to a variable intensity of magnetic field, the amount of fluid that is able to flow will be altered due to the fluctuating strength of the bonds between the magnetized iron particles. The generation of high intensity of magnetic field causes the increase in the viscosity of the fluid and it becomes more resistant to the passage through the restrictions in damper. This approach is used in MR fluid damper design.

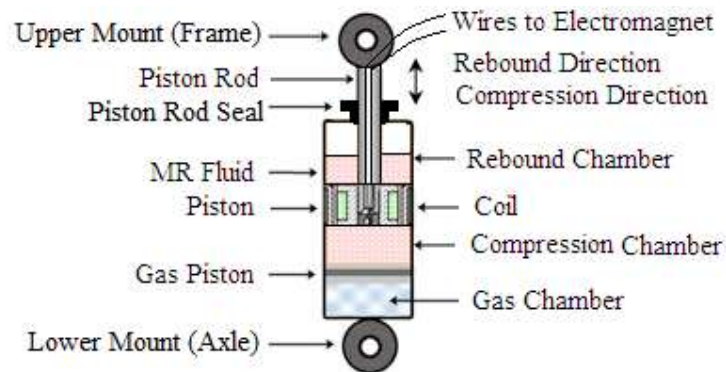


Figure 1.11 Magnetorheological damper

Research and development work by Lord Corporation in the field of MR damper technology has attracted many industries and researchers in recent years due to its applicability in semi-active controlled technology. Many automotive manufacturing industries including Ferrari, Honda and Cadillac have started the application of MR dampers in semi-active suspension system related technology for achieving enhanced performance in terms of ride comfort and vehicle handling. Recently, research and development related to working and controllable behaviour of MR dampers has resulted into its selection and application in various devices ranging from civil structures, seat suspensions, military weapons and vehicles [12-16].

1.6 MAGNETORHEOLOGICAL FLUID TECHNOLOGY

The research and development work by Jacob Rabinow in 1940s at the US National Bureau of Standards led to the discovery of MR fluids [17-18]. MR fluids are the mixture of normal fluid and micron-sized particles. When exposed to external electric or magnetic fields, these particles align themselves in a chain like structures resulting

into increase of fluid viscosity. The conversion from low viscous fluid to high viscous fluid takes place within certain milliseconds of time while the flowing ability or resistance to fluid flow also changes from free flowing to semi-solid state. Since the rheology of the fluid can be varied or manipulated with application of the externally applied field i.e. electric or magnetic, such fluids are also called “smart fluids” [19-20].

MR fluids are the mixture of small freely suspended micron-sized spherical or ellipsoidal magnetizable particles in a base or carrier fluid as main part i.e. mineral or silicone oil. Their behavior can be easily controlled and varied under the application of externally applied magnetic field as shown in Figure 1.12, making them a top choice for various practical applications related to semi-active control technology. In the presence of electric field or magnetic field, the particles attains alignment in particular direction by formation of chain-like structures [21]. In the absence of magnetic field, MR fluid behaves as a normal free-flowing as well as linear viscous liquid. The degree of chain formation is directly affected by the intensity of applied magnetic field strength.

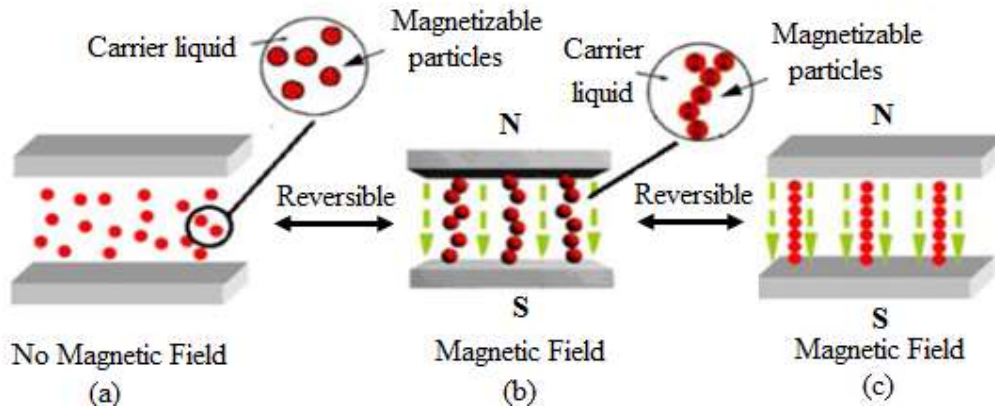


Figure 1.12 Illustration of MR fluid activation behaviour: (a) Without magnetic field
 (b) Initial stage during magnetic field application (c) Fully developed stage

The fluid behavior variation is reversible as well as controllable and very rapid; taking time of response less than a few milliseconds and requiring very small magnitude of electric power in terms of watts. Under the effect of a magnetic field, MR fluid also experiences certain other properties variation such as thermal, electrical as well as acoustic etc. Additionally, MR fluid related devices provide excellent reliability related to performance and unaffected by temperature variations or impurities mixed in the carrier fluid during working period. MR fluid works as a bridge between mechanical and electrical / electronic based systems for the development of vibration

control devices [22]. Figure 1.13 shows the working modes of magnetorheological fluid, classified into three categories as: (a) Flow mode (b) Shear mode, and (c) Squeeze mode respectively.

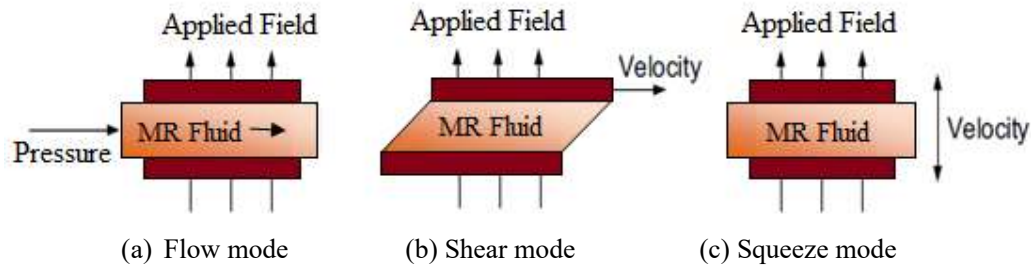


Figure 1.13 Working modes of MR fluid

1.7 RESEARCH OBJECTIVES

The main objectives of present research work are to study the effectiveness and damping capabilities of hydraulic dampers. Passive and magnetorheological dampers are used to achieve the desired objectives. Passive dampers are used in many automotive industries for assembly in suspension system whereas the development and application of magnetorheological dampers in automotive suspension system is the latest area of research. To achieve desired passenger ride comfort and vehicle handling issues, it is very essential to study the performance capabilities of hydraulic dampers related to effectiveness and damping force generation ability in vehicle suspension system.

The main objectives of the present research work are as follows:

1. To investigate different hydraulic shock absorbers employing various piston designs and discuss their influence on force-velocity and force-displacement curves i.e. on shock absorber performance.
2. Design of different pistons and analyze the effect of piston design parameters such as number of orifices, diameter of orifices, piston material, piston weight and thickness of piston on the damping properties of hydraulic shock absorbers by carrying out the compression and rebound tests on MTS machine.
3. Find ranges for which the operator can say the shock absorbers are good, fair and unacceptable for particular requirement.
4. To establish relationships between valve design parameters and shock absorber's performance.
5. To compare between force-velocity and force-displacement curves of different hydraulic shock absorbers with different piston designs.

1.8 APPROACH

The research methodology adopted in this Thesis is presented in stepwise sequence in Phase I as shown in Figure 1.14 and in Phase II as shown in Figure 1.15 and explained as follows:

Phase I

1. Development of dual tube passive dampers with various piston and valve design parameters.
2. Testing of developed passive dampers on MTS machine to get experimental data in terms of force-displacement and force-velocity curves.
3. Conclusions based on the experimental results.

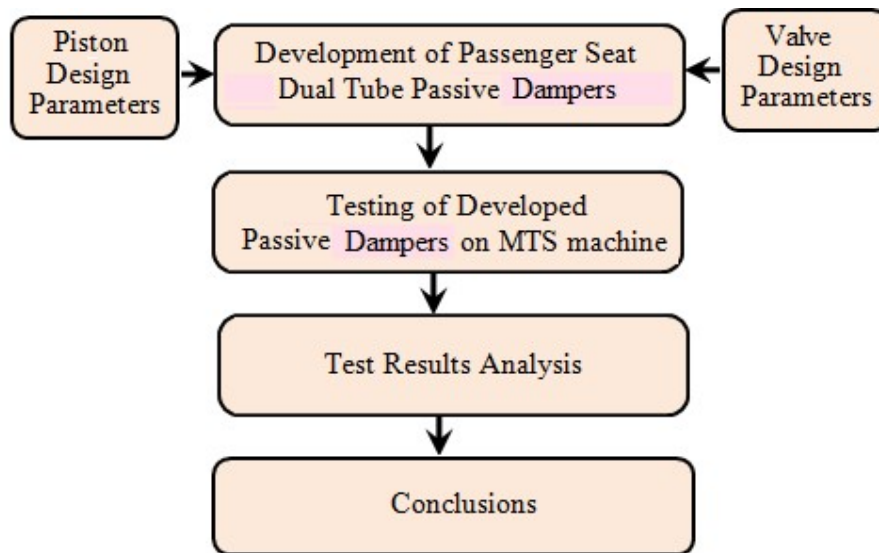


Figure 1.14 Research Methodology for Phase I

Phase II

In this phase, the procedure adopted is related to the MR damper RD-1005-3 experimental and simulation work as explained below:

1. Testing of magnetorheological damper RD-1005-3 on MTS machine to get experimental data in terms of force-velocity and force-displacement curves.
2. Mathematical modeling of experimental data using polynomial curve fitting method.
3. Mathematical modeling of passive and semi-active quarter car models with three degrees of freedom.
4. Development of forward and inverse controllers for application in semi-active quarter car system.

5. Simulation work is carried out in MALAB/Simulink environment using simulink models of passive and semi-active quarter car systems.
6. Simulation results are compared in terms of passenger seat acceleration and displacement responses for passive and various semi-active quarter car models with different control strategies.
7. Conclusion based on MR damper experimental and simulation results.

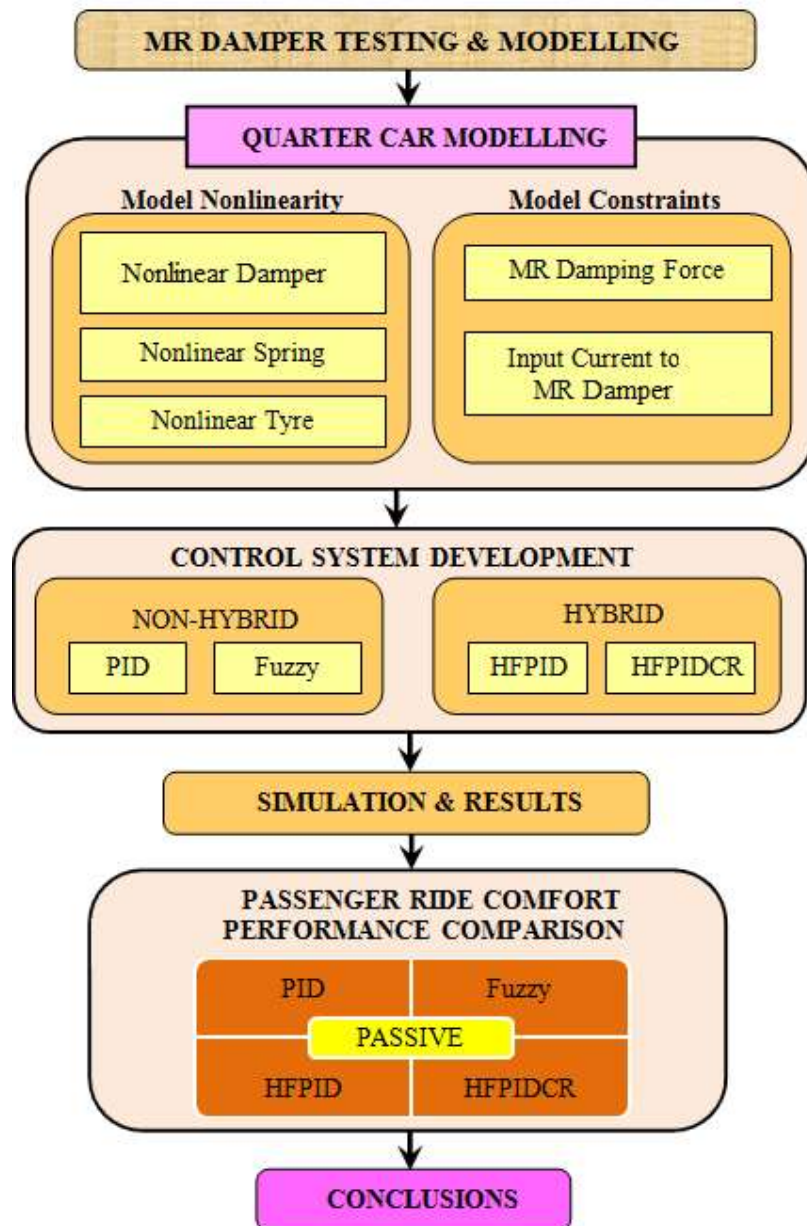


Figure 1.15 Research Methodology for Phase II

1.9 ORGANIZATION OF THE THESIS

This thesis work is divided into twelve chapters. Each chapter provides a platform for achieving the presented objectives as well as a proper direction for completion of research work. The organization of present Ph. D thesis work in various chapters is as follows:

CHAPTER 1: INTRODUCTION

In this chapter, introduction about hydraulic dampers and suspension systems is discussed. The research objectives and the adopted research methodology is also presented. A brief summary of the organization of the chapters in present thesis work is also discussed.

CHAPTER 2: LITERATURE REVIEW

This chapter presents the research work done in the field of design, development, testing, simulation and application of passive and magnetorheological dampers/ shock absorbers by various researchers. This chapter also presents the research publications related to vibration control of semi-active quarter vehicle system regarding ride comfort and vehicle handling issues. Based on the literature survey, research gaps were identified which provided the platform for this dissertation work in the field of hydraulic damper technology.

CHAPTER 3: PASSIVE DAMPER TESTING

In this chapter, developed dual tube passive dampers with various piston design and shim design parameters were tested on Measurement Testing System (MTS) machine under compression and rebound strokes. The selected piston design parameters were number of orifices, diameter of orifices, piston material, piston weight and thickness of piston whereas valve design parameters were thickness variation of valve and number of cuts in valve.

CHAPTER 4: MR DAMPER TESTING & MODELING

This chapter presents magnetorheological damper testing and modeling issues. A particular type of magnetorheological damper was selected for experimental work. Laboratory testing was performed on MTS machine under particular excitation condition and supplied current. Experimental results in terms of force-displacement and force-velocity curves were taken for modeling purpose. Polynomial model was selected to match the experimental results of tested MR damper.

CHAPTER 5: MATHEMATICAL MODELING OF QUARTER CAR SYSTEM

In present chapter, a quarter car model with three degrees of freedom consisting one fourth mass of the whole car body is considered. It is required for simulation work and comparative analysis of passive and semi-active suspension control strategies under various road inputs. Quarter car model takes into account the vertical dynamics of vehicle body accurately.

CHAPTER 6: CONTROLLERS DESIGN

In this chapter, designing of forward and inverse controllers is mentioned. The selected four different control strategies are: PID controller, Fuzzy Logic controller, Hybrid Fuzzy-PID controller (HFPID) and Hybrid Fuzzy controller with Coupled Rules (HFPIDCR). These control strategies are used for vibration suppression in semi-active quarter car suspension system.

CHAPTER 7: PERFORMANCE SPECIFICATIONS

In present chapter, peak and root mean square (RMS) values of passenger seat acceleration and displacement responses are the criteria selected for performance evaluation. The parameters selected for simulation purpose of quarter car model with three degrees of freedom as well as controller parameters are mentioned. The four types of selected road profiles such as pulse, bump, sinusoidal and random road excitations are also shown.

CHAPTER 8: PRIMARY SUSPENSION CONTROLLED SEMI-ACTIVE QUARTER CAR SYSTEM

In this chapter, simulation work is done using uncontrolled and primary suspension controlled semi-active quarter car system under selected road excitations for comparative analysis of passenger seat acceleration and displacement response.

CHAPTER 9: SECONDARY SUSPENSION CONTROLLED SEMI-ACTIVE QUARTER CAR SYSTEM

In this chapter, quarter car model is having MR shock absorber assembled between sprung mass and passenger seat. Simulation work is performed using uncontrolled and secondary suspension controlled semi-active quarter car system related to passenger ride comfort issues.

CHAPTER 10: FULLY SUSPENSION CONTROLLED SEMI-ACTIVE QUARTER CAR SYSTEM

In this chapter, semi-active quarter car model is assembled with MR shock absorbers in primary as well as secondary suspension systems. Simulation work is done using

uncontrolled and fully suspension controlled semi-active quarter car system for comparative analysis of passenger seat acceleration and displacement response.

CHAPTER 11: FREQUENCY RESPONSE ANALYSIS OF QUARTER CAR MODEL

In this chapter, three natural frequencies of quarter car model having three degrees of freedom are calculated. Finally, sinusoidal road profile is considered for travelling of quarter model and road excitation frequencies are calculated for the velocity ranging from 20 km/hr to 120 km/hr.

CHAPTER 12: CONCLUSIONS AND SCOPE FOR FURTHER WORK

In this chapter, contributions of the present research work are discussed. Based on the research work, conclusions, limitations, recommendations and future scope for further research work are also presented.

CHAPTER II

LITERATURE REVIEW

2.1 OVERVIEW

Research publications related to passive shock absorber as well as vibration control of vehicle suspension system taking semi-active quarter car model were studied regarding ride comfort and vehicle handling issues. Particular areas of interest for literature search were grouped into different categories related to the design, development, testing, simulation and application of passive shock absorbers as well as MR shock absorbers in semi-active suspension systems using available control algorithms as shown in Figure 2.1. Finally, gaps were identified based on the literature survey which provided the platform for this dissertation work in the field of passive and MR shock absorber technology.

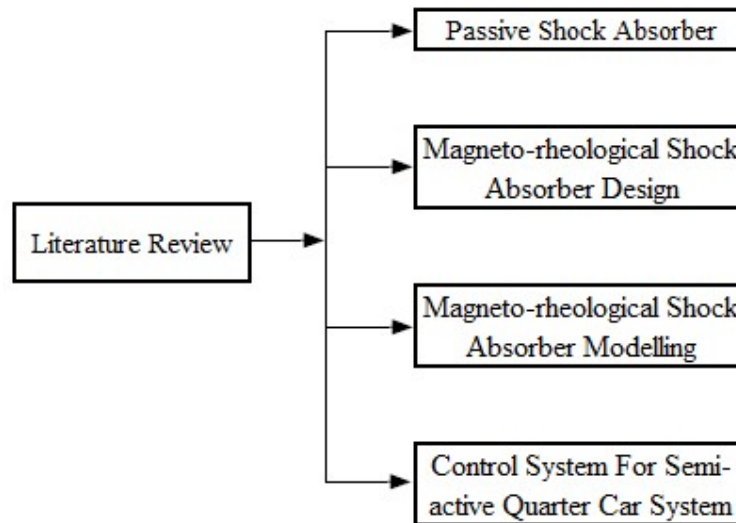


Figure 2.1 Classification of Literature Review

2.2 PASSIVE SHOCK ABSORBER

This section is based on the literature review in the field of passive shock absorbers. The main selected parameters were related to valve influence, shim stack influence, mathematical modelling, simulation work, computational fluid dynamics (CFD), Finite Element Analysis (FEA) as well as experimental work.

Lee (1997) [23] selected a monotube damper for computer modeling purpose. The model was designed using principles of mechanics and helpful in selection of damper valve and/or size to achieve target performance. Monotube damper model results as

well as test results were compared taking certain parameters such as stroke conditions, valve combinations and gas charge pressure and acceptable similarities were found.

Talbott and Starkey (2002) [24] presented a mathematical model of a racing damper. The selected damper was a gas charged mono-tube type. In this model, the selected parameters were bleed orifice flow, piston leakage flow, shim stack flow as well as floating piston and shim stack stiffness respectively. Experimental work was performed on Ohlins WCJ 22/6 damper to validate the developed model.

Akutain et al. (2006) [25] developed an explicit parametric model for mono tube damper and validated the designed model through experimental work. A dynamometer was used to validate the damper model. Further, testing work was developed to validate the desired results in an acceptable manner during driving conditions of a single seat sports car on a track.

Lee and Moon (2006) [26] studied the effectiveness of displacement-sensitive shock absorber (DSSA) in terms of damping behavior of vehicle related to the ride comfort issues. The generated two modes of damping force (i.e. soft and hard) of the DSSA were dependent on the piston position. The fluid flow characteristic in chamber and valve of DSSA was considered for mathematical modeling. A quarter car model was selected to analyze the vehicle dynamics behavior of the DSSA. The simulation results related to damping characteristics of the DSSA were compared with the experimental data. Based on the simulation results, it was concluded that the ride comfort and driving safety of the DSSA was dependent on the low and high amplitude road conditions respectively.

Guzzomi et al. (2007) [27] studied the valve performance of a Tenneco Automotive hydraulic damper. Tenneco damper valve assembly was composed of shims and a spring preloaded disc for controlling the fluid flow through the main flow orifices. Sequential geometry and simulation updating technique was used to investigate the pressure distribution acting on the valve assembly.

Shams et al. (2007) [28] applied Coupled Computational Fluid Dynamics (CCFD) analysis under various intake valve deflections and piston velocities to obtain the force acting on the valve under deflection stage. Finite Element Analysis (FEA) method was applied to establish valve deflection-force relationship. Numerical and test results showed good agreements with each other.

Farjoud and Ahmadian (2010) [29] provided a model of the shim stack assembly to properly predict the damping level for different designs of the shim stack. The

analysis was done on the deflection of shim stack and compared with the single disk approximation.

Zhou and Xu (2010) [30] established the formula for the deformation of single throttle slice for shock absorber using elastic mechanics. The analytic formula of equivalent thickness of multi-throttle slices was established using the deformation of multi-throttle-slices with the pressure on each slice.

Goldasz (2011) [31] applied amplitude-selective-damping (ASD) valving approach to improve the performance of a hydraulic shock absorber. A complete state space model taking geometric and performance factors of the ASD valve was derived and analyzed. The results of the selected twin-tube shock absorber were presented in the phase plane plots of force-displacement diagrams.

Czop et al. (2012) [32] considered the reduction of the aeration and cavitation effects to improve the shock absorber performance by optimization of the design of a disc spring valve system. To achieve this, the geometry of the valve interior was modified using fluid structure interaction (FSI) model as well as pressure distribution was analyzed along the flow paths inside the valve cavity. The criterion selected for valve improvement was related to reduction in the damping force level provided by shock absorber against the number of cycles performed during working period.

Farjoud et al. (2012) [33] studied the shim stack properties and their influence on the damper performance in a monotube hydraulic damper. Various parameters were considered to study their effect on the hysteresis region. The mathematical model was compared with experimental test results of OHLINS CCJ 23/8 monotube damper.

Liang et al. (2012) [34] considered the deflection of the shock absorber valve due to oil flow as well as the contact between the superposition valves. The valve deflection results between the FEM work and the calculated results using Mechanical Design Handbook were compared. The simulation results obtained generated by mathematical model showed good fit with the experimental data.

Satpute et al. (2013) [35] discussed the mathematical modeling of the damper having various shim controlled orifices. FEA work was performed to compute the stiffness of the selected shims while MATLAB programming was done to calculate the variation in pressure and damping force across the piston using continuity equation of fluid flow. Finally, displacement transmissibility was found using damper model in single degree of freedom model in MATLAB / Simulink software.

2.3 MAGNETORHEOLOGICAL DAMPER DESIGN

In past, numerous studies related to MR damper design and developments have been performed to enhance its effectiveness in vibration control of suspension system through damping force generation ability. Various analytical, experimental and simulation based work have been selected to improve the performance characteristics of MR damper.

Yang et al. (2002) [36] used an axisymmetric and a parallel-plate model for the force-velocity relationship of MR damper and model results were compared with the experimental data. Dynamic response time was also taken into consideration for evaluating the performance of MR damper.

Hong et al. (2005) [37] considered four non - dimensional design parameters for design of a magneto-rheological mixed mode damper. A single degree of freedom vibration model with a spring and MR damper was utilized for evaluating the effectiveness of the proposed MR damper design concept related to damping force behavior. Finally, experimental damping force characteristics of developed MR damper were compared with the predicted data.

Chooi et al. (2008) [38] derived the solutions and presented the methodology related to fluid flow with a yield stress through annuli. Computational fluid dynamics simulation work was used for validation of the presented mathematical expressions.

Nguyen et al. (2009) [39] designed an optimal MR damper using finite element analysis by considering force, dynamic range and inductive time constant. A semi-active quarter car suspension system was designed to evaluate the vibration control response of optimally designed MR damper while the vehicle travels over bump and sinusoidal road excitations.

Kciuk et al. (2011) [40] used finite element method for modeling the effect of magnetic field on the magnetorheological fluid. Experimental and simulation work was carried out for a semi-active suspension system taking prototype damper into account.

Parlak et al. (2012) [41] used finite element method (FEM), electromagnetic analysis of magnetic field and CFD analysis of magneto-rheological fluid flow to achieve two objectives i.e. target damping force and maximum magnetic flux density of MR damper. Two MR dampers with optimal design parameters were manufactured and the test results were compared with simulated data for validation purpose.

Prabakar et al. (2013) [42] considered the application of MR damper in a semi-active quarter car model under random road excitation. The characterization of MR damper hysteretic behavior was done using Bingham and modified Bouc-Wen models. The optimal parameters of MR damper were determined using Non-dominated Sorting Genetic Algorithm II (NSGA II).

Lee et al. (2013) [43] designed a rotary MR damper for unmanned vehicle suspension system. Finite element model was developed to study the roles of sealing location and cover case curvature on the performance of MR damper. The proposed MR damper calculated damping torque values were compared and validated with the experimental measurements.

Mangal et al. (2014) [44] developed an MR damper using finite element method (FEM) concept and tested it experimentally in the semi-active vibration control laboratory. Based on the obtained test results, it was concluded that the FEM based model was effective in portraying the damping test results of MR damper.

Yazid et al. (2014) [45] presented a combination of shear and squeeze working mode for the design of MR damper. Finite Element Method Magnetics (FEMM) was used to simulate the generated magnetic field through coils of MR damper. The simulation data was used to design and fabricate the MR damper whereas the experimental work was done under quasi-static loading in shear mode, squeeze mode and combination of both modes.

2.4 MR DAMPER MODELLING

Generally, two types of models exist to model the nonlinear dynamic nature of MR damper, known as parametric and non-parametric models.

2.4.1 Parametric Models

In parametric method, the damping force generated by MR damper is presented by a combination of linear and non-linear elements. Parametric models are composed of certain mechanical elements which include dashpot, spring and friction elements controlling the operation of MR damper [46]. Various available parametric models can be described as follows:

Stanway et al. (1987) [47] developed the first parametric model known as Bingham model to represent the nonlinear hysteretic behavior of an electrorheological (ER) shock absorber and later applied for MR shock absorbers. It consists a Coulomb frictional element in combination with a dash-pot as shown in Figure 2.2 [47].

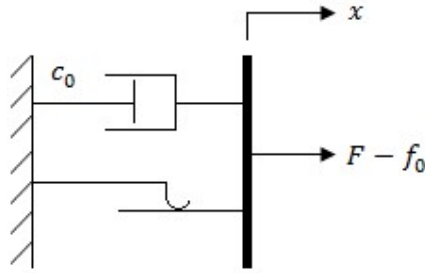


Figure 2.2 Bingham model

Wen (1976) [48] used the concept given by Bouc hysteretic model to develop the widely used model for showing the hysteretic behavior of the MR shock absorber. The model is the combination of a spring, a dash-pot and a Bouc-Wen hysteretic element attached in parallel as shown schematically in Figure 2.3 [48].

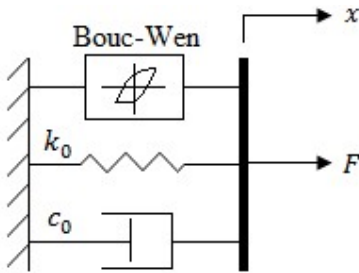


Figure 2.3 Bouc-Wen hysteretic model

Spencer et al. (1997) [49] proposed an upgraded model based on the modification of the Bouc-Wen model. To enhance and improve the performance of the MR shock absorber at small magnitude of velocities, damping and spring coefficients c_1 and k_1 were added in Bouc Wen model as shown in Figure 2.4 [49].

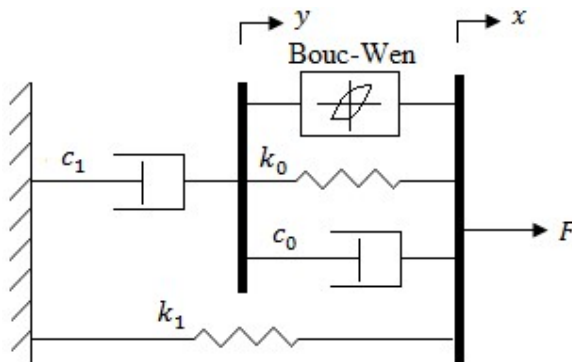


Figure 2.4 Modified Bouc-Wen model

Bass and Christenson (2007) [50] used a hyperbolic tangent function to develop a mathematical expression based model for MR shock absorbers known as hyperbolic tangent function model as shown in Figure 2.5 [50].

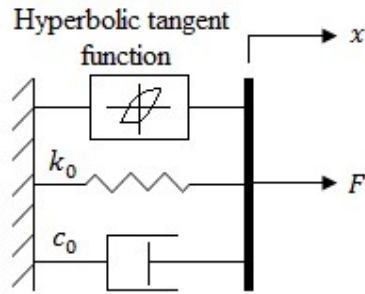


Figure 2.5 Hyperbolic tangent function based model

Dahl (1976) [51] proposed a model to simulate the control systems having friction in which differential equation was used to model the stress-strain curve.

Zhou and Qu (2002) [52] proposed an improved version of Dahl [51] model for MR dampers as shown in Figure 2.6 [52]. Here, Dahl hysteresis model was used to simulate Coulomb force. The modified Dahl model was successful in tracing the force-velocity relationship in the low velocity region.

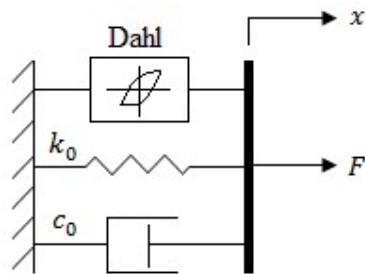


Figure 2.6 Modified Dahl model

2.4.2 Non-parametric Models

Non-parametric modeling is based on the mathematical functions such as polynomial, hyperbolic, tangent and delay etc.

Ehrgott and Masri (1992) [53] used Chebyshev polynomials to model the dynamic behaviour of electro-rheological shock absorbers. The MR shock absorber generated force was emulated using two approaches. First approach considered damping force dependency on the displacement and velocity while in second approach, the damping force was related to the velocity and acceleration. In both the cases, two-dimensional orthogonal Chebyshev polynomials were used to describe the damping force values.

Schurter and Roschke (2000) [54] proposed a neuro-fuzzy model to predict the hysteretic behaviour of a small-scale MR shock absorber. Neural network was selected to train the designed membership functions to simulate the relationship between inputs (damper displacement, velocity, voltage signal) and output (damper

force). The parameters for modeling the damper were determined using Adaptive Neuro-Fuzzy Inference System (ANFIS).

Choi et al. (2001) [55] developed the polynomial model to predict the forward dynamics of magneto-rheological (MR) damper. In present model, hysteresis curve of MR shock absorber is divided into two parts i.e. upper curve (negative acceleration) and lower curve (positive acceleration) respectively.

Wang and Liao (2004) [56] proposed a neural network based technique to identify the forward dynamics of MR shock absorbers. A recurrent neural-network structure was used having Levenberg-Marquardt algorithm as training method.

Du et al. (2006) [57] developed an approach to approximate the forward and inverse dynamic behaviors of a magneto-rheological (MR) damper using evolving radial basis function (RBF) networks.

Truong (2010) [58] presented a black-box model (BBM) for direct identification of forward dynamics of MR shock absorber. Fuzzy parameters were trained using the back propagation algorithm and gradient descent method to enhance the accuracy of the BBM.

Boada et al. (2011) [59] proposed a recursive lazy learning method based on neural networks to model the MR damper behavior.

2.5 CONTROL SYSTEM FOR SEMI-ACTIVE QUARTER CAR SYSTEMS

To achieve the desired ride comfort and vehicle handling issues, variety of control algorithms have been developed and tested in semi-active quarter car system in combination with MR shock absorber. This section is related to the review of various control algorithms used in semi-active quarter car system with MR damper/ shock absorber, for application in suspension system vibration control.

Kim and Jeon (1999) [60] designed an Magneto-Rheological (MR) damper for application in semi-active quarter car model. Experimental work was performed for comparative analysis of passive method, LQ control and frequency shaped LQ control. The proposed frequency shaped LQ control provided best results in the human sensitive frequency range of 4 Hz and 8 Hz as well as improved driving safety near the resonance frequency of unsprung mass i.e. 11 Hz.

Ahmadian et al. (2000) [61] studied experimentally the performance of skyhook, groundhook and hybrid control policies in quarter car rig. The sprung mass and unsprung mass transmissibility results showed the promising performance of hybrid

control policy in achieving better ride comfort and vehicle stability compared to other two considered policies.

Yao et al. (2002) [62] used sky-hook control strategy in a semi-active quarter car model with magnetorheological (MR) damper. Bouc-Wen model was selected to characterize the forward dynamics of MR damper. Simulation results demonstrated the effectiveness of semi-active control strategy in vibration control of suspension system.

Lam et al. (2003) [63] considered sliding mode controller and skyhook system in semi-active quarter car system with two degree of freedom. The transmissibility of MR suspension system was considered for the performance evaluation by simulation under bump and random road excitations.

Goncalves and Ahmadian (2003) [64] performed experimental work on a quarter car rig with a magneto-rheological damper to study the response of hybrid control policy. The test results of control policy in terms of peak-to-peak displacement and peak-to-peak acceleration of sprung and unsprung mass were obtained under steady state and step input road profiles. Experimental results showed the effectiveness of hybrid control policy in reducing the peak-to-peak displacement and acceleration of both masses.

Guo et al. (2004) [65] presented a neural network control in semi-active vehicle suspension assembled with magnetorheological damper. The simulation and experimental results for quarter car model showed the superior performance of semi-active suspension system compared to passive suspension in a low frequency range for ride comfort issues.

Hudha et al. (2005) [66] evaluated the performance of various semi-active control algorithms in quarter car model with a magneto-rheological damper. The selected control algorithms were modified skyhook, modified groundhook and modified hybrid skyhook-groundhook controllers. Simulation and experimental responses showed superior response provided by the modified hybrid skyhook-groundhook controller in vibration control of body acceleration, body displacement, suspension displacement as well as lower wheel acceleration.

Du et al. (2005) [67] studied H_∞ control of semi-active suspension system in combination with MR damper. A polynomial model was selected to characterize the experimental results of MR damper. A quarter-car model with two-degrees of freedom was used for analysis and simulation purpose under random road input.

Simulation results proved that the designed H_∞ controller can achieve good performance in semi-active suspension vibration control compared to passive one.

Miao et al. (2006) [68] proposed an adaptive fuzzy-neural network control (FNNC) scheme for the transient course for control of MR suspension. Comparison between passive and semi-active suspension system was done using numerical example and real road test taking quarter car model into consideration. The simulation and road test results showed the effectiveness of MR vehicle with FNNC strategy in controlling the vibrations in terms of peak acceleration and reduction of settling time compared to passive system.

Rashid et al. (2007) [69] selected Fuzzy controller for the development of a semi-active suspension system. The performance of semi-active quarter car model having two-degrees of freedom was compared using PID, Fuzzy and Hybrid-Fuzzy controllers against passive quarter car model. Simulation results provided the encouraging results for selection of semi-active suspension with Fuzzy-hybrid controller and MR damper for achieving good ride comfort and steering stability.

Batterbee et al. (2007) [70] performed experimental work to investigate the controller performance in semi-active suspension system with MR shock absorber using the hardware-in-the-loop-simulation (HILS) method. The experimental results were validated using simulation work on a two-degree-of-freedom quarter car model related to passenger ride comfort, road holding and suspension working space issues.

Rashid et al. (2008) [71] developed and implemented hybrid fuzzy logic based controller in semi-active suspension system of a quarter car model. PID, Fuzzy logic and Fuzzy Hybrid controllers were used to control the semi-active suspension system. Experimental results showed that Fuzzy-hybrid controller was most suitable to control vibrations in semi-active suspension system compared to Fuzzy and PID controlled suspension systems.

Turnip et al. (2008) [72] investigated the performance of sensitivity control in semi-active quarter car system with two degrees of freedom for ride quality and handling issues. Numerical simulation results demonstrated the improved performance delivered by proposed algorithm compared to passive suspension system to achieve the desired objectives.

Uradniecek and Musil (2008) [73] presented a study related to adaptive control of semi-active quarter car model in vibration isolation of suspension system. The simulation work was performed in time domain under sine sweep excitation.

Simulation results were used to demonstrate the effectiveness of proposed controller compared to skyhook controller and passive suspension system in vibration control.

Ubaidillah et al. (2009) [74] used multi-order PI control for semi-active MR damper suspension system with outer loop and inner loop controller. Simulation and experimental work on quarter car system showed the improved performance of semi-active suspension system compared to its counterparts.

Dong et al. (2010) [75] compared the performance of five control algorithms i.e. skyhook controller, the hybrid controller, the LQG controller, the sliding mode controller and the fuzzy logic controller in semi-active suspension system of quarter car model with two-degrees of freedom. Numerical simulation as well as road test was performed to observe the controller performance under various road inputs. The results showed that sliding mode controller was highly successful in vibration control of semi-active suspension system compared to passive and other control strategies.

Nguyen et al. (2010) [76] investigated a road-frequency adaptive control in semi-active suspension system to enhance the vehicle suspension effectiveness. The selected target was to achieve ride comfort and wheel handling issues in all frequency regions due to road induced disturbances. A displacement sensor was used to measure the data based on which a state estimator was designed using Kalman filter to know the desired state variables. Numerical simulation was performed to evaluate the efficiency of the proposed control algorithm.

Rashid et al. (2011) [77] selected PID, Fuzzy and Hybrid-Fuzzy controllers in semi-active quarter car model having two-degrees of freedom. Simulation results provided the encouraging results for selection of semi-active suspension with Fuzzy-hybrid controller and MR damper for achieving good ride comfort and steering stability.

Hudha, and Jamaluddin (2011) [78] used PI controller in a quarter car suspension system to track the force generated by magnetorheological fluid damper. Skyhook algorithm was used for the development of a fuzzy controller to improve the ride comfort. The performance delivered by skyhook algorithm based fuzzy logic was found better compared to on-off and fuzzy logic control algorithm in time domain.

Jiang et al. (2012) [79] used a full scale two degree of freedom quarter car system to study the vehicle suspension. On off skyhook controller and Fuzzy Lyapunov skyhook controller (FLSC) were employed to control the input current for MR damper so as to achieve the desired damping force. In comparison with OEM damper,

on off and FLSC controlled MR dampers reduced the acceleration of vehicle sprung mass by about 15% and 24%, respectively.

El-Kafafy et al. (2012) [80] investigated the effectiveness of sliding mode control (SMC) in semi-active quarter car model. Simulation work showed the effectiveness and improvement in results of proposed controller under a road hump and random road conditions for vehicle road holding ability.

Zong et al. (2012) [81] used a linear quadratic gauss (LQG) controller as the system controller and an adaptive neuro-fuzzy inference system (ANFIS) inverse model as the damper controller in semi-active quarter car system. Simulation results demonstrated the ability of LQG controller in vibration control of suspension system compared to passive suspension system.

Rahman et al. (2012) [82] studied the application of Proportional Integral Derivative and clipped-optimal controllers in semi-active quarter car suspension system having two degrees of freedom. Simulation work using quarter car model was performed under step input road profile to evaluate the performance of control algorithms.

Shojaei et al. (2013) [83] studied Fuzzy logic, skyhook and On-Off control techniques in semi-active quarter car vehicle suspension system through theoretical and experimental work. Simulation and experimental results of fuzzy logic controller were compared with other control strategies in time and frequency domain under bump and random road disturbances.

Yildiz et al. (2013) [84] designed a nonlinear observer to calculate the internal state values of the MR damper. A semi-active quarter car model with magnetorheological (MR) was selected for vibration control purposes.

Qazi et al. (2014) [85] used Fuzzy logic controller in semi-active quarter car model for vibration control purpose. Particle swarm optimization (PSO) was implemented to obtain the optimal gain parameters of Fuzzy logic controller. Simulation results of optimized fuzzy controller were compared with passive, fuzzy skyhook, fuzzy groundhook and fuzzy hybrid controllers. The results achieved by optimized fuzzy controller were best related to ride comfort and road holding compared to passive and other controlled cases.

Nugroho et al. (2014) [86] implemented adaptive neuro fuzzy inference system (ANFIS) technique in quarter vehicle suspension system to improve the passenger ride comfort and road holding ability. Numerical simulations using MATLAB/

Simulink showed the effectiveness of the ANFIS controller under step, sinusoidal and bump type road disturbances compared to passive and hybrid controller.

2.6 IDENTIFIED GAPS IN THE LITERATURE

After extensive study of available literature related to passive dampers/ shock absorbers and application of MR dampers/ shock absorbers in semi-active quarter car model with different controllers, a number of research gaps were identified.

- Literature related to testing of passenger seat damper taking piston design parameters and valve design parameters needs consideration.
- Many of the proposed control strategies and simulation work was based on the two-degrees-of-freedom of semi-active quarter vehicle system that utilized MR damper.
- Most of the research work was focussed on controlling the vibration of sprung mass as well as unsprung mass taking acceleration and displacement factors into account.
- There is little research work available for three-degrees-of-freedom of semi-active quarter vehicle system taking passenger seat into account for ride comfort and vibration control using MR damper.

2.7 SUMMARY

In this chapter, a critical literature review on passive dampers/ shock absorbers, MR dampers/ shock absorber design, modeling and application in quarter car suspension system is presented. It started with passive shock absorber design and modeling issues. Then a short description related to design of MR damper is given. This was followed by modeling of experimental results of MR damper using parametric and nonparametric modeling techniques. Research related to the application of MR damper/ shock absorbers in vibration control of semi-active quarter car system using various controllers was studied. Based on the literature review, research gaps were identified which is the basis for present research work.

CHAPTER III

PASSIVE DAMPER TESTING

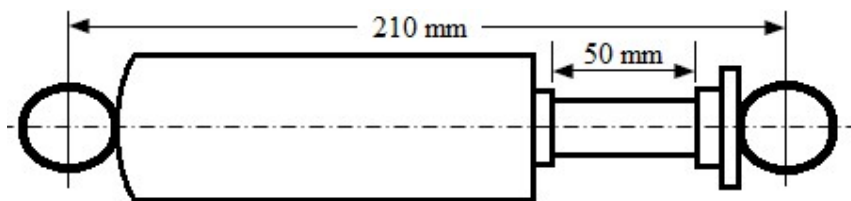
3.1 INTRODUCTION

A greater damping force attenuates vehicle suspension vibration faster. However, the damping force is always designed larger in the tension stage than in the compression stage. The purpose is to make damper improve the vehicle dynamic behavior. The damping force is produced on account of resistance developed by damper which depends on the speed of the suspension, the number and size of the holes of the piston etc. All modern dampers are velocity sensitive hydraulic damping devices. The selection of holes and controlled fluid flow within the damper determines the comfort feeling and handling of the vehicle.

This chapter presents experimental setup and testing of dual tube passive damper on MTS machine. Test results in terms of damping force vs. displacement and damping force vs. velocity provides data about damper performance. These test results are helpful in determining the performance of damper in vehicles during travelling period. Various compression and rebound tests were performed on MTS machine to observe the influence of various piston design parameters such as number of orifices, diameter of orifices, piston material, piston weight and thickness of piston as well as valve design parameters on the damping properties of dual tube passive damper.

3.2 CONFIGURATION OF DUAL TUBE PASSIVE DAMPER

The dual tube passive damper was used in this research work for experimental work. It was a small scale damper for assembly under the passenger seat to control the vibrations. Figure 3.1 shows the dimensional model as well as real picture of the used damper. Its total length during the full extension period was 210 mm while during the full compressed state it was 160 mm. The working stroke length of the damper was 50 mm. The diameter of piston rod was 11 mm. The outer diameter of inner and outer tube was 27.5 mm and 34 mm respectively with the wall thickness of 1 mm. The diameter of the piston was 25.4 mm while its thickness was 12.7 mm.



(a) Dimensional model



(b) Original damper

Figure 3.1 Dual tube passive damper

Figure 3.2 shows the various components used for the piston valve assembly [88]. It was assembled with the piston rod and responsible for controlling the damper generated damping force during the compression and rebound period respectively.

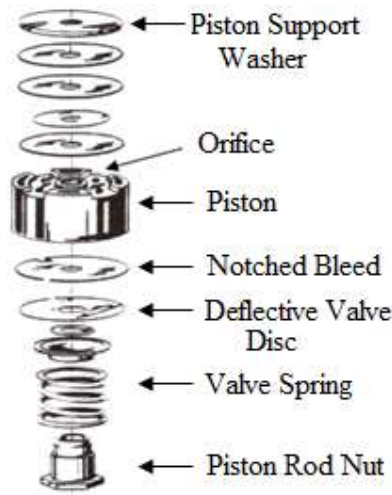


Figure 3.2 Piston valve assembly

3.3 EXPERIMENTAL SET UP

The schematic diagram of experimental set up is shown in Figure 3.3 while the real experimental work performed on MTS machine is shown in Figure 3.4. The used MTS machine was servo hydraulic in nature and controlled by computer generated commands. The MTS machine contains upper head as well as lower head with assembled grippers to hold the damper at the desired location. The lower head of MTS machine was having fixed base used to hold the lower head of passive damper. The upper head was movable in vertical up and down direction through hydraulic actuator and was attached with a load cell of 15 kN. The load cell measures the applied force acting on the passive damper. Passive damper was excited by the hydraulic actuator with a sinusoidal displacement at the room temperature of 25-33°C. In present case the amplitude of excitation was 25 mm with velocity of 0.05 m/s (frequency 0.636 Hz), 0.1 m/s (frequency 1.273 Hz) and 0.3 m/s (frequency 3.819 Hz) respectively.

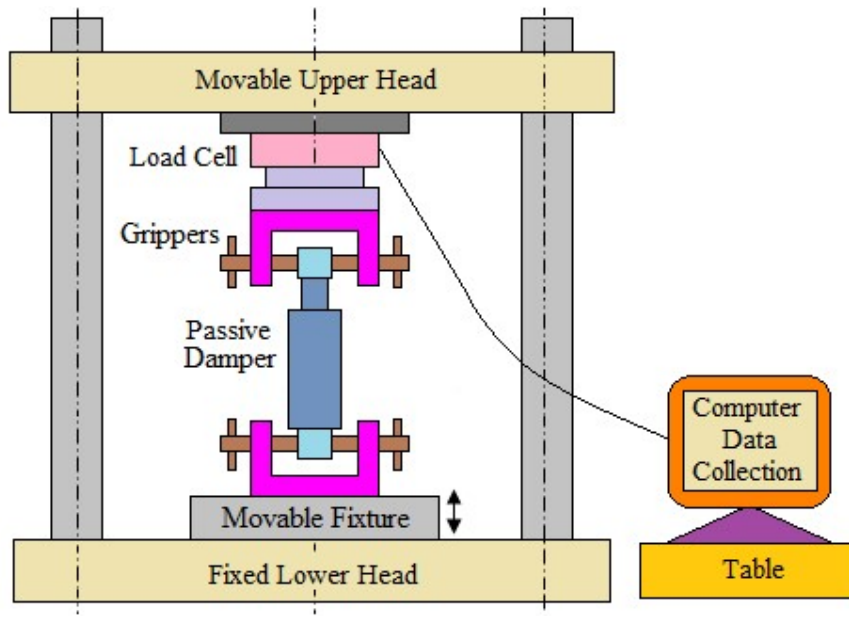


Figure 3.3 Schematic diagram of passive damper test set up

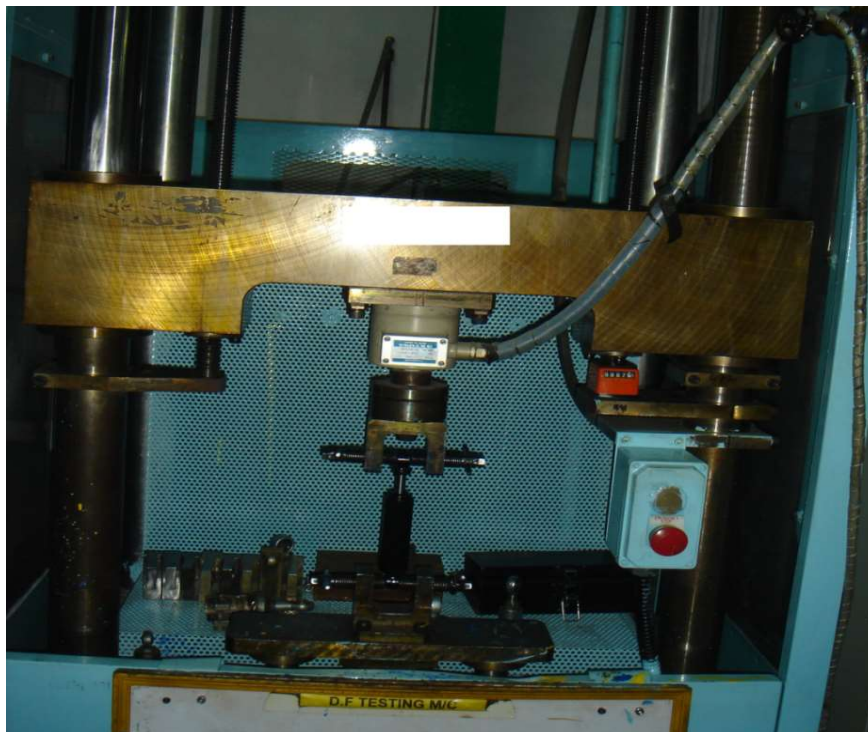


Figure 3.4 Passive damper testing

3.3.1 Experimental Test Equipment

Damper test was performed to get experimental results for force-displacement and peak force-velocity characteristics. The details of machine equipment are as follows:

1. Displacement and Velocity Transducer: The mathematical data for velocity and displacement in the dynamometer comes from the velocity and displacement

transducers. This measured data was stored on the computer and provides Force – Displacement and Force – Velocity plots.

2. Load Cell: The damping forces are sensed by the load cell mounted in the load path at the cylindrical end of the damper.
3. Mounting Clevises: There are two mounting clevises provided on the machine for gripping the upper and lower end of the damper during test work.
4. Computer Control: The test mechanism work on the commands provided by a computer. The transfer of data between the computer and the dynamometer is by a USB connection. The computer program allows the user to input the test data in terms of displacement and desired velocity.

3.3.2 Experimentation:

1. Damper Clamping: During the testing work, the lower end of the passive damper was gripped to the hydraulic servo-platform while the upper end was gripped to the rigid beam assembled with force sensor.
2. Test Parameters: The data for testing the damper was typed into the computer in terms of amplitude as well as the excitation velocity. Then the damper was given excitation in vertical direction through servo mechanism according to input test data to the damper.
3. Data Collection: After completion of the testing work on the damper, the test data was collected in terms of force-displacement and peak force-velocity curves from the computer system. Test data was stored into the Microsoft excel files.

3.4 EXPERIMENTAL RESULTS

In the present research work, total sixteen numbers of passive dampers with different piston and valve design parameters were developed as shown in Table 3.1. These pistons were used in the assembly of passive hydraulic dampers.

Table 3.1 Parameters for experimental work









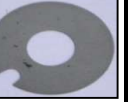
Sr. No.	Parameter	Qty.	Values
1	Different number of piston orifice	3	1, 2 and 3
2	Different diameter of piston orifice (mm)	3	0.8, 0.9, 1
3	Valve Thickness Variation (mm)	3	0.15, 0.30, 0.45
4	Cuts in Valve	3	1, 2 and 3
5	Piston with different material	2	-----
6	Piston with different thickness (mm)	2	11.7, 12.7
7	Piston with different weight	--	-----

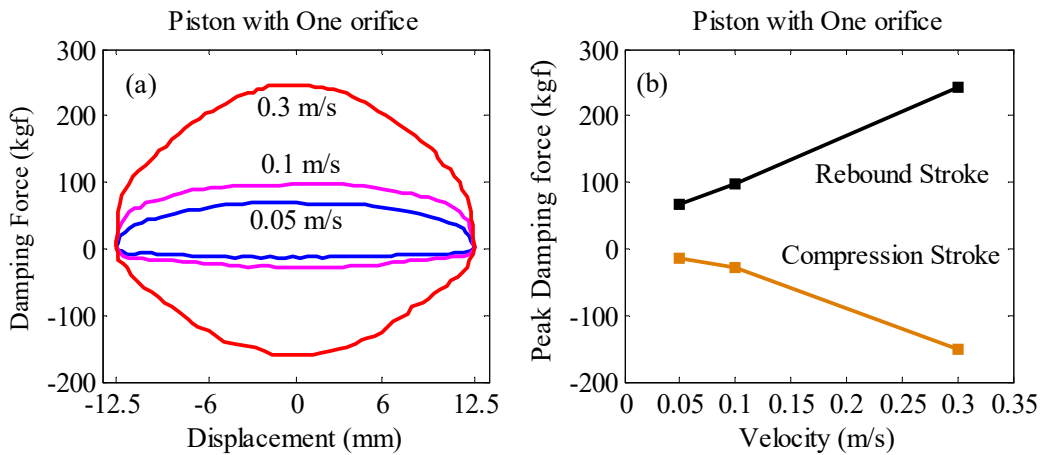
The assembled sixteen passive hydraulic dampers were tested on MTS machine under piston rod velocity of 0.05 m/s, 0.1 m/s and 0.3 m/s respectively. The test results were obtained in terms of force-displacement and peak force-velocity curves to observe the effect of selected design parameters on the damping properties of hydraulic dampers as discussed below:

3.4.1 Variation in Number of Piston Orifice

In present case, three pistons with different number of orifice having dia. 1.5 mm and with valve thickness 0.15 mm were tested on MTS machine. The variations in number of orifice in developed pistons are shown in Table 3.2 while measured test results are shown in Figure 3.5.

Table 3.2 Variation in number of orifice

Piston No.	1	2	3
No. of Orifice	1	2	3
Compression Side			
Rebound Side			
Valve			



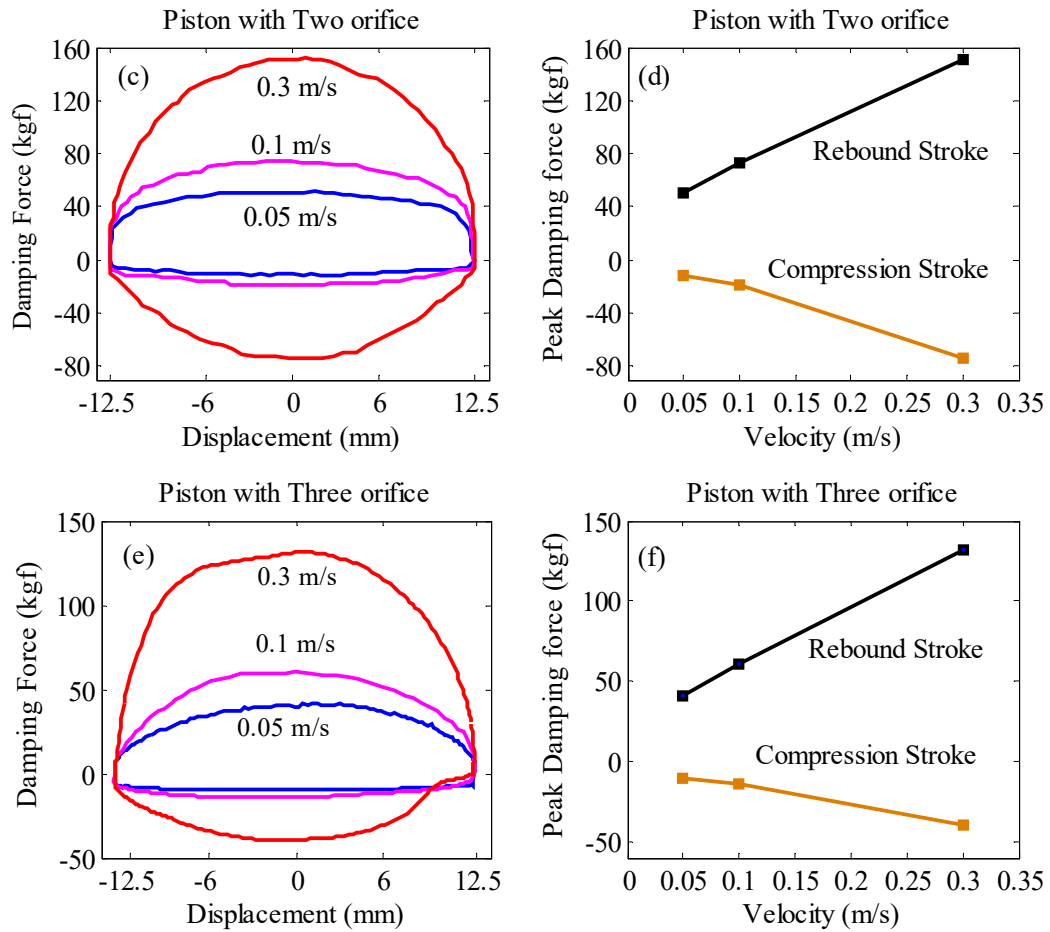


Figure 3.5 Test results for variation in number of piston orifice

Table 3.3 Peak Damping Force Values (kgf)

Sample No.	No. of Piston Orifice	Piston Rod Velocity (m/s)					
		0.05	0.1	0.3	0.05	0.1	0.3
		Peak Rebound Force (kgf)			Peak Compressive Force (kgf)		
1	1	69.9	98.3	246.0	-15.3	-29.5	-160.2
2	2	52.0	74.6	152.0	-12.0	-18.7	-73.3
3	3	41.4	60.3	131.6	-10.0	-14.4	-39.8

Table 3.3 shows the peak damping force values for compression and rebound stage while Figure 3.6 represents the combined test results for the developed dampers with 3 different pistons.

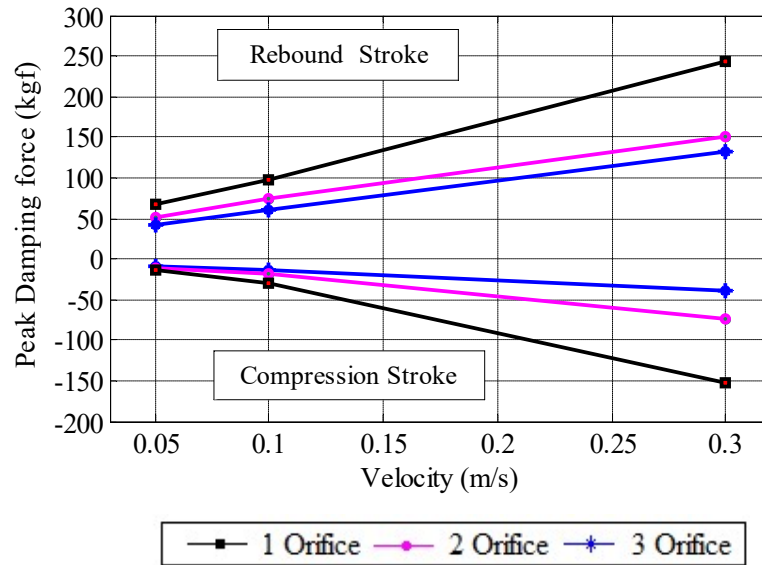











Figure 3.6 Combined test results of variation in number of piston orifice

3.4.2 Variation in Diameter of Piston Orifice

In present case, three pistons with different diameter of orifice as well as with 4 number of orifice and valve thickness as 0.15 mm were tested on MTS machine. The variations in diameter of orifice in developed pistons are shown in Table 3.4 while the measured test results are shown in Figure 3.7.

Table 3.4 Variation in orifice diameter

Piston No.	4	5	6
Dia. of Orifice	0.8 mm	0.9 mm	1 mm
Compression Side			
Rebound Side			
Valve			

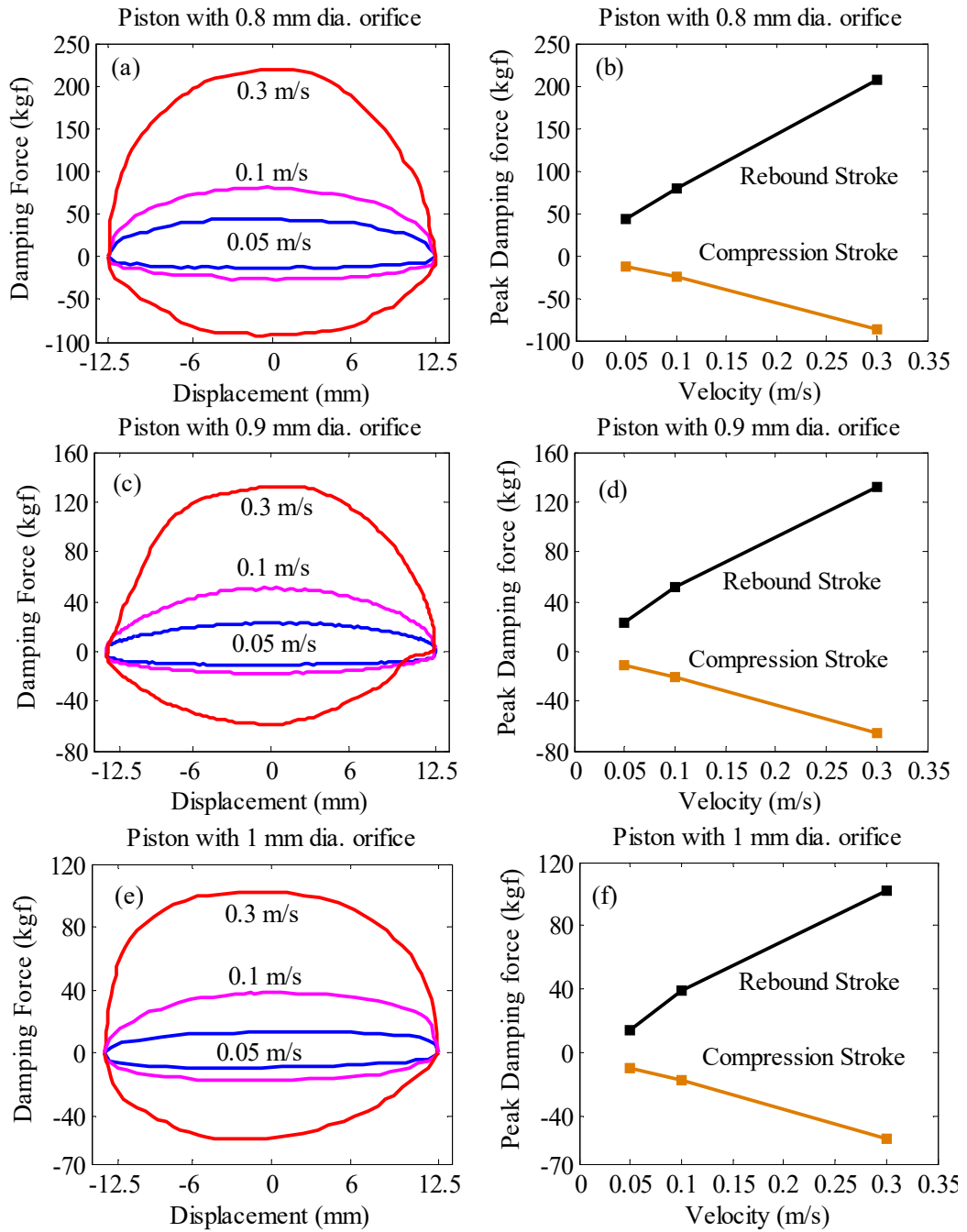


Figure 3.7 Test results for variation in diameter of piston orifice

Table 3.5 shows the peak damping force values for compression and rebound stage while Figure 3.8 represents the combined test results for the developed dampers with 3 different diameters of orifice.

Table 3.5 Peak Damping Force Values (kgf)

Sample No.	Dia. of Piston Orifice (mm)	Piston Rod Velocity (m/s)					
		0.05	0.1	0.3	0.05	0.1	0.3
		Peak Rebound Force (kgf)			Peak Compressive Force (kgf)		
1	0.8	43.8	82.8	206.5	-12.5	-28.0	-92.2
2	0.9	23.0	51.4	132.0	-11.2	-20.8	-65.6
3	1	13.7	38.7	102.5	-9.5	-17.5	-54.7

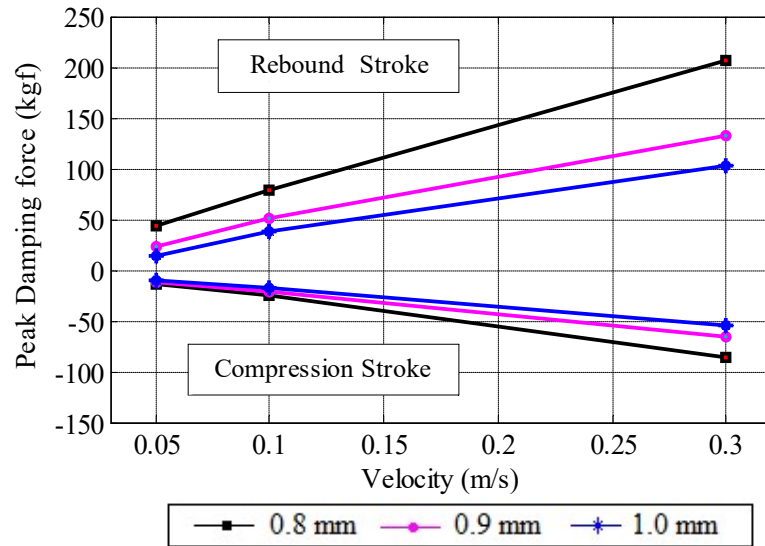











Figure 3.8 Combined test results of variation in dia. of piston orifices

3.4.3 Variation in Valve Thickness

In present case, three pistons with different valve thickness on rebound side as well as with 4 number of orifice having 1 mm diameter were tested on MTS machine. The variations in valve thickness on rebound side of pistons are shown in Table 3.6. The measured test results are shown in Figure 3.9.

Table 3.6 Variation in valve thickness

Piston No.	7	8	9
Valve Thickness	0.15 mm	0.30 mm	0.45 mm
Compression Side			
Rebound Side			
Valve			

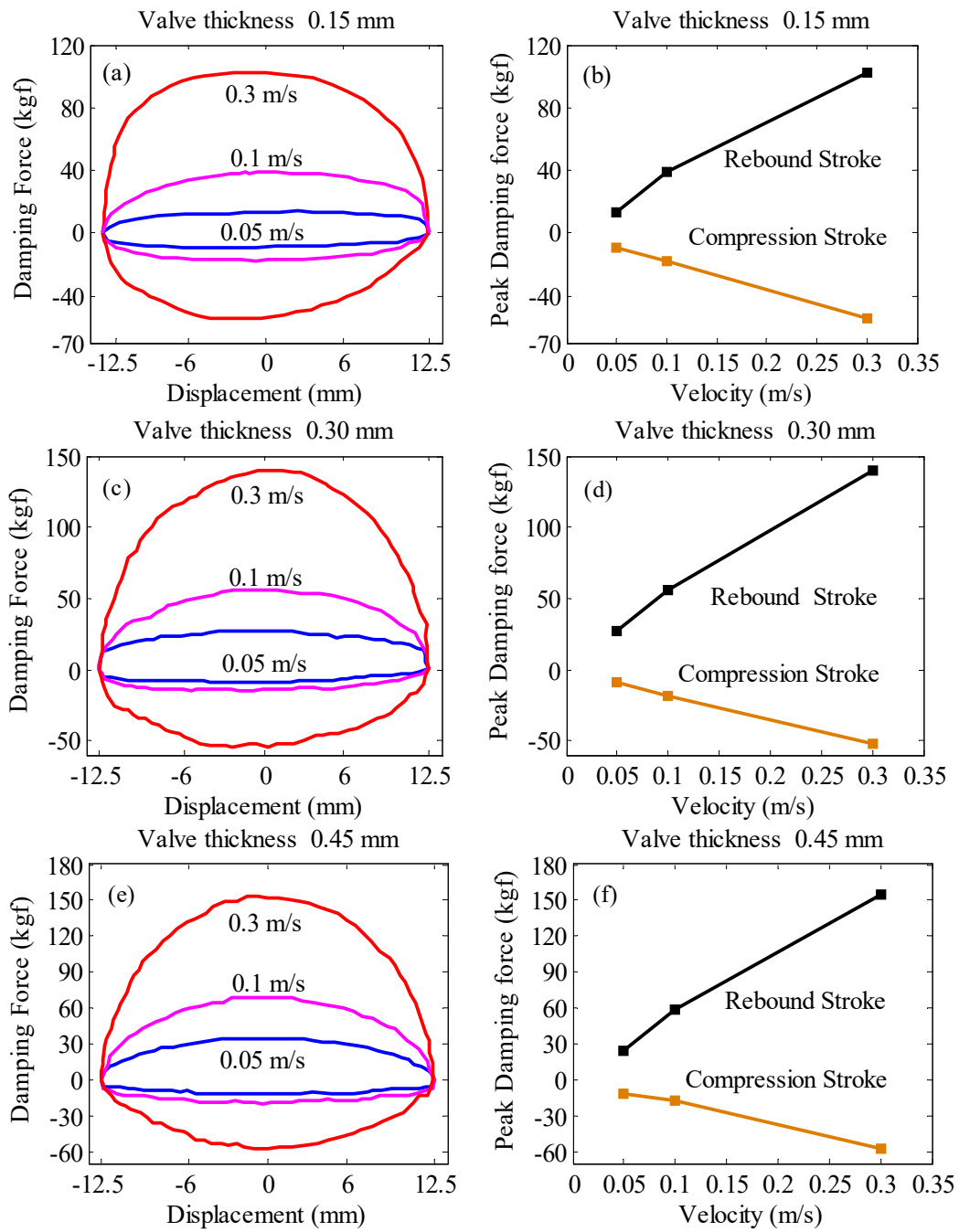


Figure 3.9 Test results for variation in valve thickness

Table 3.7 shows the peak damping force values for compression and rebound stage while Figure 3.10 represents the combined test results for the developed dampers with 3 different valve thicknesses on rebound side.

Table 3.7 Peak Damping Force Values (kgf)

Sample No.	Valve Thickness (mm)	Piston Rod Velocity (m/s)					
		0.05	0.1	0.3	0.05	0.1	0.3
		Peak Rebound Force (kgf)			Peak Compressive Force (kgf)		
1	0.15	13.7	38.7	102.5	-9.5	-17.5	-54.7
2	0.30	26.9	55.7	140.2	-9.2	-18.7	-52.6
3	0.45	34.5	68.0	153.5	-11.3	-20.9	-57.2

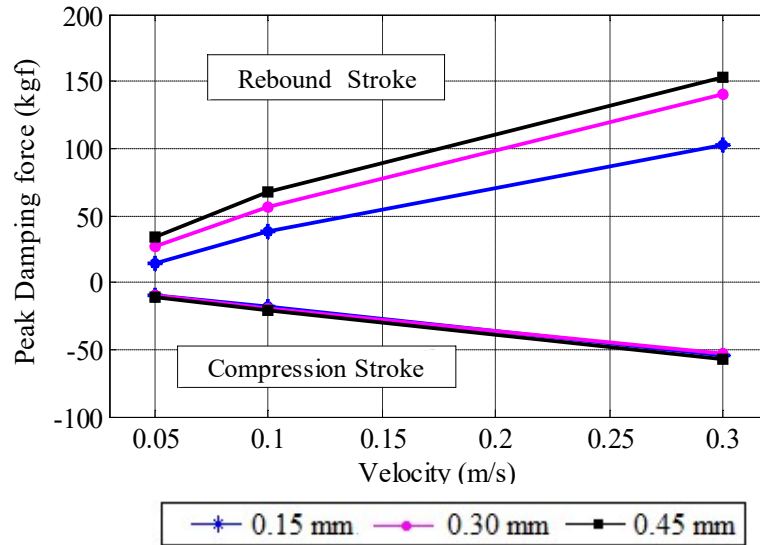











Figure 3.10 Combined test results of variation in valve thickness

3.4.4 Variation in Cuts in Valve

In present case, three pistons with different number of cuts in the valve on rebound side as well as with 4 number of orifice with dia. 1 mm and valve thickness 0.15 mm were tested on MTS machine. The variations in cuts in the valve on rebound side of pistons are shown in Table 3.8. The measured test results are shown in Figure 3.11.

Table 3.8 Variation in cuts in valve

Piston No.	10	11	12
Cuts in Valve	1	2	3
Compression Side			
Rebound Side			
Valve			

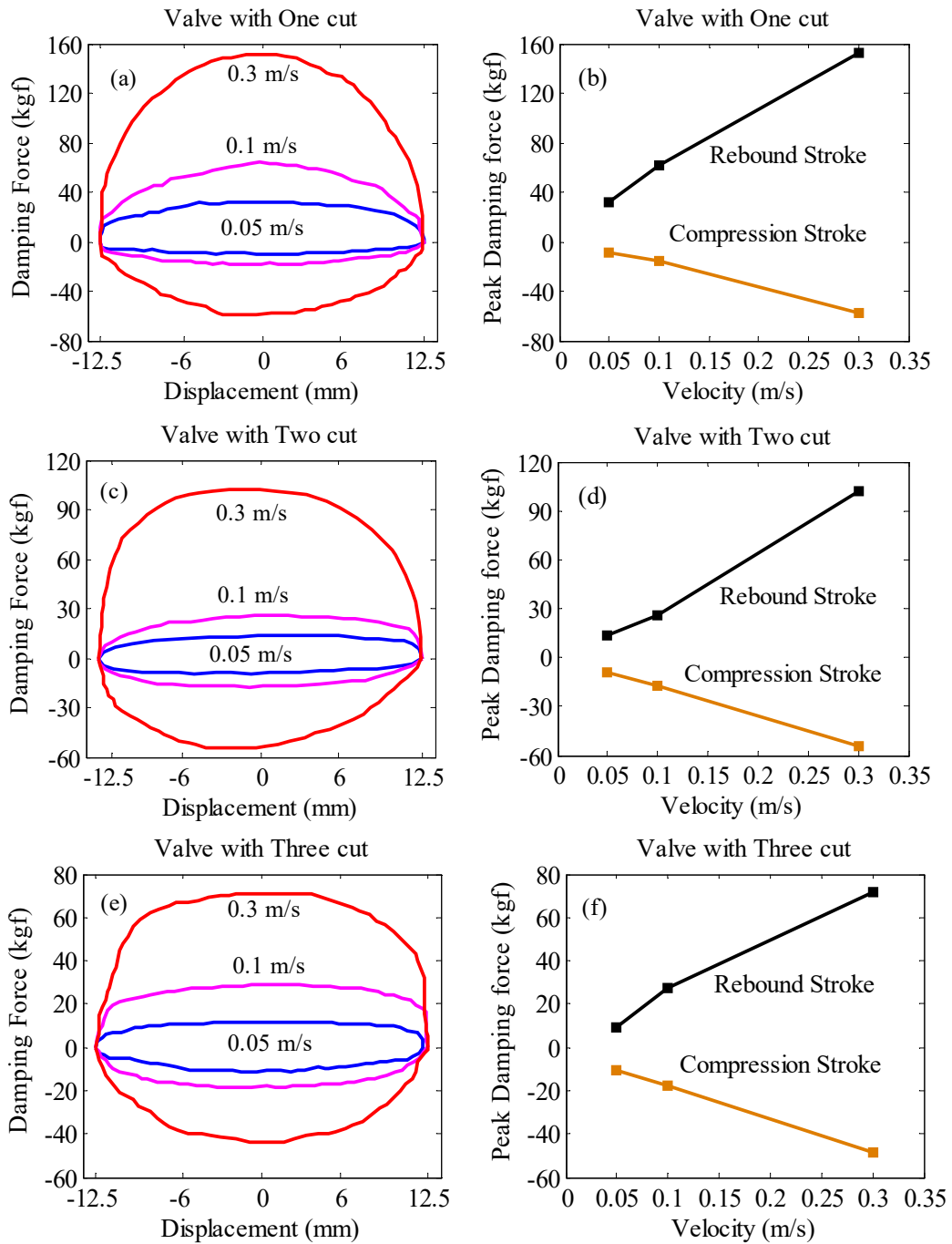


Figure 3.11 Test results for variation in cuts in valve

Table 3.9 shows the peak damping force values for compression and rebound stage while Figure 3.12 represents the combined test results for the developed dampers with 3 different cuts in valve on rebound side.

Table 3.9 Peak Damping Force Values (kgf)

Sample No.	No. of Cuts	Piston Rod Velocity (m/s)					
		0.05	0.1	0.3	0.05	0.1	0.3
		Peak Rebound Force (kgf)			Peak Compressive Force (kgf)		
1	1	32.0	64.2	150.5	-9.9	-17.9	-58.4
2	2	13.7	38.7	102.5	-9.5	-17.5	-54.7
3	3	11.6	29.2	71.2	-11.2	-18.5	-47.8

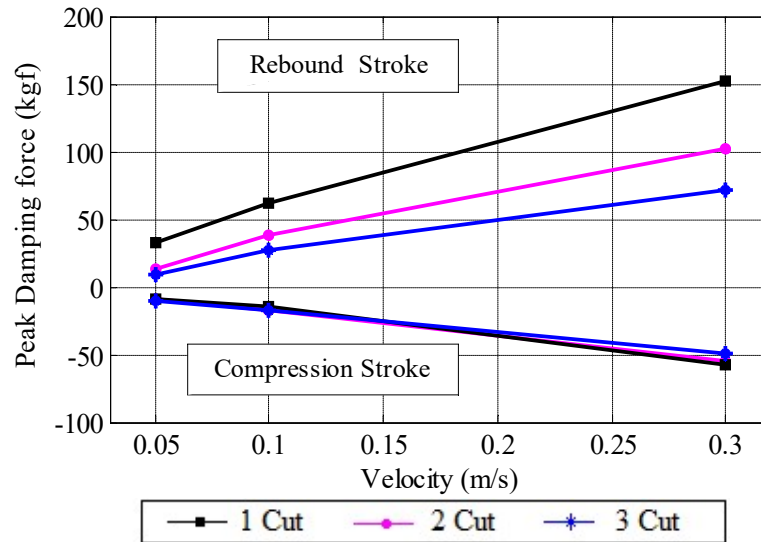


Figure 3.12 Combined test results of variation in cuts in valve

3.4.5 Piston with Different Material

In present case, two pistons with different materials and same dimensions were developed. The number and diameter of orifice were same in each case. The types of piston material used were as follows:

- (a) Ductile iron
- (b) 7075 aluminium alloy

The developed pistons were assembled in passive hydraulic dampers for compression and rebound tests using MTS machine to obtain test results. It was observed from test results that there was negligible effect on the force-displacement and peak force-velocity curves due to two pistons of different materials.

3.4.6 Piston with Different Thickness

In present case, two aluminium alloy pistons with different thickness of 11.7 mm and 12.7 mm were tested. The developed pistons with same number and orifice diameter were assembled in passive hydraulic dampers to perform compression and rebound tests using MTS machine. It was observed that there was negligible effect on the

force-displacement and peak force-velocity curves due to thickness variation of two pistons.

3.4.7 Piston with Different Weight

The weight of piston may be calculated as follows:

Weight of piston = Mass Density x (Total Volume of piston – Volume of the slots/holes in piston)

Piston material density = 6.7 g/cm³ for ductile iron and 2.8 g/cm³ for Al alloy.

Here, above test results in sections 3.4.1, 3.4.2, 3.4.5 and 3.4.6 of passive hydraulic dampers related to various piston weights are considered.

3.4.8 Summary of the Parameter Design Results

Table 3.10 shows the summary of the parameter design results at the piston rod velocity of 0.3 m/s.

Table 3.10 Summary of Parameter Design Results at 0.3 m/s velocity

Factor	Values	Peak Damping Force (kgf)		Compression to Rebound Force Ratio (r)	Variation in Range of 'r'
		Rebound Force	Compression Force		
No. of Orifice	1	246.0	160.2	0.65	0.30 to 0.65
	2	152.0	73.3	0.48	
	3	131.6	39.8	0.30	
Orifice Diameter (mm)	0.8	206.5	92.2	0.44	0.44 to 0.53
	0.9	132.0	65.6	0.49	
	1	102.5	54.7	0.53	
Valve Thickness (mm)	0.15	102.5	54.7	0.53	0.37 to 0.53
	0.3	140.2	52.6	0.38	
	0.45	153.5	57.2	0.37	
Cuts in Valve	1	150.5	58.4	0.39	0.39 to 0.67
	2	102.5	54.7	0.53	
	3	71.2	47.8	0.67	

The damping force is always designed larger in the tension stage than in the compression stage and this ratio may be taken as 0.4 to 0.5 in many cases to make damper for improving the vehicle dynamic behaviors [88]. It may also be seen that with orifice diameter varying from 0.8 mm to 1 mm and number of holes 4 at a testing velocity of 0.3 m/s, the variation range of peak compression force to peak rebound force i.e. 'r' is least and acceptable.

3.5 THEORETICAL ESTIMATION OF DAMPING COEFFICIENT

The following methods may be opted for theoretical calculation of damping coefficient:

1. Dampers produce force based on how fast you move them, or their velocity. Therefore, the amount of damping force (F) produced is proportional to velocity (v).

$$F = cv \quad (3.1)$$

where c is called viscous damping coefficient.

The viscosity-temperature curves for some lubricating oils are shown in Figure 3.13 [89].

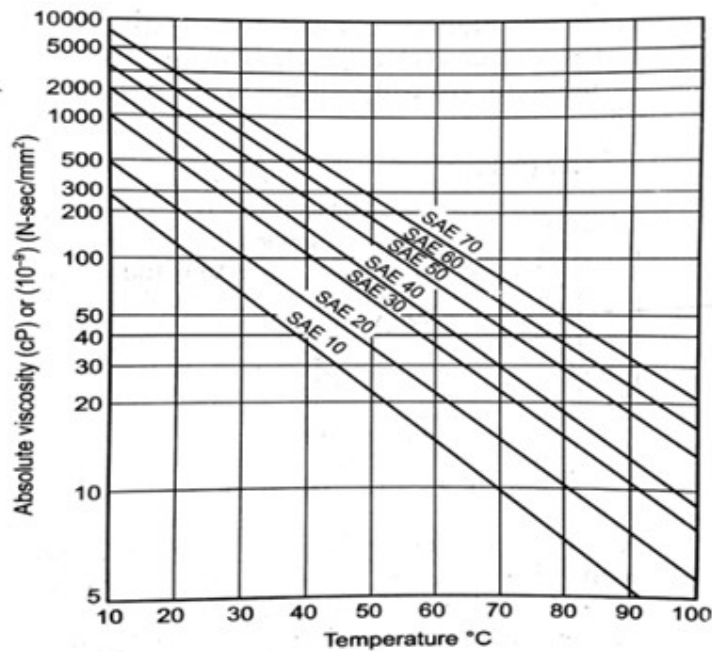


Figure 3.13 Viscosity-Temperature relationship

Approximate value of viscous damping coefficient for a piston and cylinder arrangement is given by [90]:

$$c = \frac{12\mu (A_p - A_r)L}{\pi D_m e^3} \quad (3.2)$$

where,

c : viscous damping coefficient,

μ : absolute viscosity of fluid,

$A_p - A_r$: difference in area of flat side of piston and piston rod diameter,

L : length of piston,

D_m : mean diameter of the cylinder and piston,

e : clearance between piston and the cylinder,

Taking appropriate values for piston cylinder arrangement as follows:

$$\mu = 0.017 \text{ N}\cdot\text{s}/\text{m}^2 \quad (\text{for SAE 10 oil at } 60^\circ\text{C})$$

$$D_m = 25.0 \text{ mm}, \quad \text{Piston rod diameter} = 11.0 \text{ mm}, \quad L = 12.7 \text{ mm}, \quad e = 1 \text{ mm}$$

Here, the calculated value of viscous damping coefficient (c) is 12.0 kN.s/m.

2. The ideal viscous damper is such one in which the damping force is proportional to the first power of velocity. The mean value of damping coefficient (μ) is determined from the required rate of amplitude of damping represented by the ratio of amplitudes (δ) of two successive cycles as follows [91]:

$$\mu = \frac{1.41 \ln \delta}{\sum_1^{kd} l_i^2} \sqrt{\frac{J_y \sum_1^k C_i l_i^2}{4\pi^2 + (\ln \delta)^2}} \quad (3.3)$$

where,

kd : number of dampers on one side of vehicle,

J_y : mass moment of inertia of vehicle about its lateral axis,

C_i : stiffness of suspension system at the i^{th} road wheel,

l_i : distance of the i^{th} road wheel from vehicle center of gravity.

In automobiles, the damping coefficient is smaller when the wheel moves downwards (damper compression) than when wheel moves upwards (damper rebound). The two coefficients ratio (r) has a range between 0.4 and 0.5 in most of cases and the following parameters were selected for shockers in automobiles [88]:

$$J_y = 24 \text{ kN}\cdot\text{m}\cdot\text{s}^2, \quad kd1 = 2, \quad kd2 = 1, \quad C_i = 127 \text{ kN}/\text{m}.$$

It was found that for an average value of $r = 0.5$, the damping coefficient in compression $\mu_1 = 11.5 \text{ kN}\cdot\text{s}/\text{m}$ and in rebound $\mu_2 = 23 \text{ kN}\cdot\text{s}/\text{m}$ and mean damping coefficient was $17.25 \text{ kN}\cdot\text{s}/\text{m}$.

3. Lu et al. [92] selected the Besinger model for identifying damping force. The LSM (Least Squares Method) method was utilized to identify the damper parameters based on experimental data. The model had three features: nonlinear relationship between the tension and compression stages, hysteresis loop and saturation in high-speed stage during the tension stage. In the Besinger model, the damping force F_v is defined as:

$$F_v = C(v)v \quad \text{for } v < v_{lim} \quad (3.4)$$

where,

$$C(v) = \frac{C_1(v - \alpha)}{\alpha \sqrt{1 + \left(\frac{v - \alpha}{\alpha}\right)^2}} + C_2$$

$C(v)$: A function of the piston velocity relative to cylinder tube,

C_c : The damping coefficient of damper in the compression stroke,

C_e : The damping coefficient of damper at the low-speed stage of the tension stroke,

v_{lim} : The speed at the turning speed between high speed and low speed during the tension stroke,

α : A transition parameter between compression and tension damping force and

$$C_1 = (C_e + C_c)/2 \text{ and } C_2 = (C_e - C_c)/2.$$

Based on the testing data with frequency 2 Hz and amplitude 10 mm, the LMS method was used to calculate the damping parameters of the selected shock absorber.

The specific damping coefficients were: $C_c = 14.4$ Ns/mm, $C_e = 15.6$ Ns/mm, $v_{lim} = 0.125$ m/s and $\alpha = 0.7$ m/s.

Damping coefficient is variable for various types of damper parameters. The damper is a typical nonlinear system and its damping force modeling has become a research highlight. The nonlinear modeling methods consist of parametric model and non-parametric model. Parametric model accounts for the damper's internal fluid flow and the real structure, while non-parametric model is mainly based on actual measurement ignoring its inner structure. It is difficult to work in terms of damping coefficient of a damper due to following reasons:

1. Size of piston and holes, number of holes, quantity and type of hydraulic oil, valve and shim is different for variety of dampers used in automotive vehicles.
2. Dampers provide a resistive force by passing oil through small passages. The energy associated with creating the resistive force is dissipated as heat, which raises the temperature of the oil in the damper. Oils are inherently temperature sensitive, their viscosity varies greatly between 0°C and 120°C. Figure 3.13 shows how viscosity varies over this temperature range for SAE grade 10 oil, commonly used in dampers,.
3. In case of MR dampers, viscosity of MR fluid varies due to application of varied current near the piston hence it is not practically possible to calculate viscosity.
4. Damping force is different in compression and rebound stroke at the same velocity.
5. Theoretically, damping coefficient is difficult to calculate for a damper and its results may have large variations because of number of variables. Research work

related to measurement of damping force in the literature is mostly based on experimentation.

Due these reasons mentioned above, it is not appropriate to work in terms of damping coefficient. Table 3.11 shows the calculated damping coefficient using theoretical and experimental results.

Table 3.11 Damping coefficient comparison

Parameters	Damping coefficient (kN.s/m)		
	Rebound	Compression	Average value
Ref. [87] : Piston cylinder arrangement, viscous damping coefficient (theoretical)	-	-	12.0
Ref. [88] : Passive damper (theoretical)	23.0	11.5	17.25
Ref. [90] : Passive damper (theoretical)	15.6	14.4	15.0
Piston rod velocity 0.3 m/s, 4 holes in piston, 0.8 mm diameter, passive damper (experimental)	6.75	2.85	4.80

3.6 OPTIMIZATION OF SELECTED PARAMETERS USING TAGUCHI METHOD

Taguchi developed the orthogonal array method to study the systems in a more convenient and rapid way, whose performance is affected by different factors when the system study become more complicated with the increase in the number of factors. This method can be used to select best results by optimization of parameters with a minimum number of test runs. Application of Taguchi method can support significantly to achieve the best results out of various tests by selection of optimum combination of different factors. Final product quality can be improved ranging from industrial products to service sector in terms of process optimization, product design and system analysis [93-96].

Experimental results are used to determine the corresponding values in terms of signal-to-noise (S/N) ratio for each run. It projects the performance of each test run depending on the obtained S/N ratio. Basically, three types of S/N ratios are used in Taguchi method such as: lower is better (LB), higher is better (HB) and nominal is best (NB) as shown in Table 3.12:

Table 3.12 Signal-to-Noise (S/N) ratio equations

<i>Quality characteristics</i>	<i>S/N ratio</i>
Lower is better	$-10\log\left(\frac{1}{n}\sum y_i^2\right)$
Nominal is best	$-10\log\left(\frac{1}{n}\sum(y_i - y_0)^2\right)$
Higher is better	$-10\log\left(\frac{1}{n}\sum\frac{1}{y_i^2}\right)$

where:

n = number of observations

y_i = the measured data.

3.6.1 Geometrical optimization of passive damper using Taguchi method

The objective of present study is to obtain optimum combination of three parameters (no. of holes, dia. of holes and shim thickness), to maximize the peak rebound damping force of the dual tube passive damper. In order to maximize the damping force value, higher is better S/N ratios are computed. Three different levels have been selected related to every parameter for damping force maximization (Table 3.13). In this case, Taguchi's L9 orthogonal array was selected, leading to nine experiments (Table 3.14).

Table 3.13 Selected parameters and levels for Taguchi method

Parameter	Level 1	Level 2	Level 3
No. of Holes	4	6	8
Dia of Holes	0.8	1.0	1.2
Shim Thickness	0.15	0.3	0.45

Table 3.14 L9 Orthogonal Array

Exp. No.	Factor 1	Factor 2	Factor 3
1	1	1	1
2	1	2	2
3	1	3	3
4	2	1	2
5	2	2	3
6	2	3	1
7	3	1	3
8	3	2	1
9	3	3	2

The corresponding factors were placed in Table 3.15. Total nine passive dampers were developed as per L9 orthogonal array and experimental results in terms of damping force values at 0.3 m/s and at the piston rod displacement of 25 mm were selected. The obtained damping force values at the piston velocity of 0.3 m/s were placed in Table 3.16.

Table 3.15 Assigned Factors to L9 Orthogonal Array

Exp. No.	No. of Holes	Dia. of Holes	Shim Thickness
1	4	0.8	0.15
2	4	1.0	0.30
3	4	1.2	0.45
4	6	0.8	0.30
5	6	1.0	0.45
6	6	1.2	0.15
7	8	0.8	0.45
8	8	1.0	0.15
9	8	1.2	0.30

3.6.2 Analysis of Signal – to - Noise (S/N) Ratio

In Taguchi method, S/N ratio considers both the mean and the variability during the optimization process. Here, the term ‘S’ i.e. signal represents the desired value (mean) related to output characteristics while the term ‘N’ i.e. noise (standard deviation) represents the undesirable value related to output characteristics. Thus, S/N ratio is helpful to measure the quality characteristics deviation from the desired value. The calculated S/N ratio using Minitab 17 as per “Higher is better” objective for maximization of peak rebound damping force values for dual tube passive damper is shown in Table 3.16.

Table 3.16 Damping Force and S/N Ratios for L9 Array

Exp. No.	No. of Holes	Dia. of Holes	Shim Thickness	Peak Rebound Damping Force	S/N Ratio
1	4	0.8	0.15	206.5	46.298
2	4	1.0	0.30	142.2	43.058
3	4	1.2	0.45	121.7	41.706
4	6	0.8	0.30	115.2	41.229
5	6	1.0	0.45	95.3	39.582
6	6	1.2	0.15	71.6	37.098
7	8	0.8	0.45	80.5	38.116
8	8	1.0	0.15	61.1	35.721
9	8	1.2	0.30	42.5	32.568

The calculated S/N ratios for selected piston and shim design parameters related to passive dampers for defined levels i.e. from Level 1 to Level 3 in terms of damping force values are written in Table 3.17.

Table 3.17 S/N Ratios for each level of factors

Level	No. of Holes	Dia. of Holes	Shim Thickness
1	43.69	41.88	39.71
2	39.30	39.45	38.95
3	35.47	37.12	39.80

S/N plots for damping force values are presented in Figure 3.14, helpful in selection of optimum combination of piston and shim design parameters as A1B1C3 having largest S/N ratios for individual piston and shim design parameters.

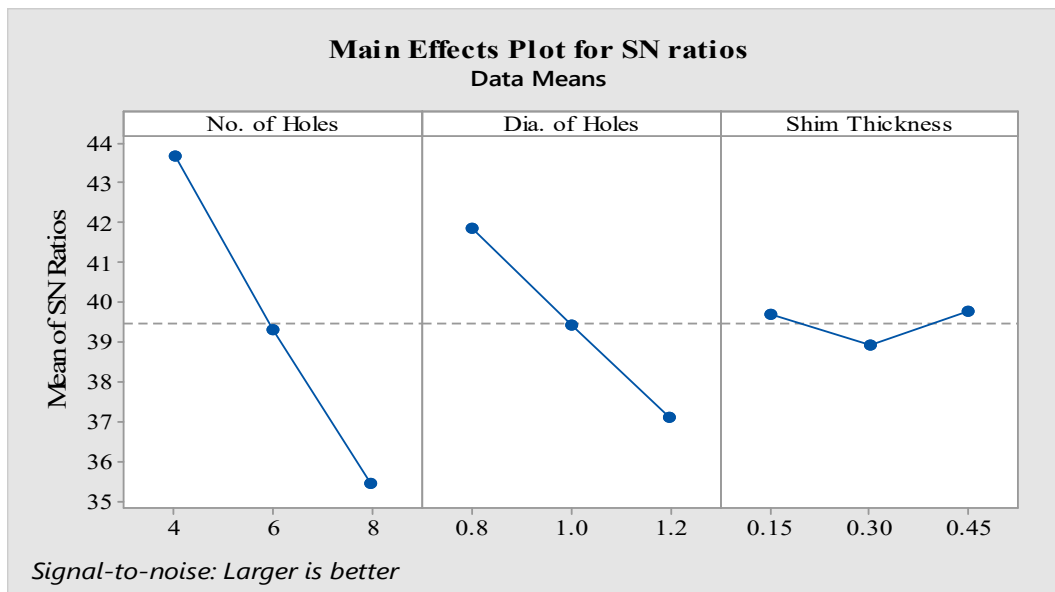


Figure 3.14 S/N Ratio plot for maximization of damping force

Table 3.18 shows the selected best levels for each factor using S/N ratio analysis.

Table 3.18 Specified optimum levels of S/N Ratios

Parameters	Delta	Rank	Value
No. of Holes	8.22	1	4
Dia. of Holes	4.76	2	0.8
Shim Thickness	0.85	3	0.45

The optimal selection with no. of holes, dia. of holes and shim thickness using Taguchi L9 experimental design method are summarized in Table 3.19.

Table 3.19 Optimum geometry

Parameters	Value
No. of Holes	4
Dia. of Holes	0.8 mm
Shim Thickness	0.45 mm

3.6.3 Contribution of selected parameters on performance

Analysis of Variance (ANOVA) is performed to investigate which design parameter contributes highly in the desired performance characteristics of maximum damping force value. ANOVA results are presented in Table 3.20. It can be seen from Table 3.20 that no. of holes affects the maximum damping force value with maximum percentage share of 74.20 % while parameter dia. of holes affects the maximum damping force value with percentage share of 24.82 %.

Table 3.20 Analysis of Variance

Source	DF	Adj SS	Adj MS	F-Value	P-Value	% Contribution
No. of Holes	2	101.485	50.742	4130.40	0.000	74.20
Dia of Holes	2	33.951	16.975	1381.79	0.001	24.82
Shim Thickness	2	1.300	0.649	52.90	0.019	0.95
Error	2	0.025	0.0123			0.01
Total	8	136.760				

DF : Degrees of Freedom; Adj SS : Adjusted sum of squares; Adj MS : Adjusted Mean Squares; P : Percentage.

Model Summary:

S = 0.11, R-sq = 99.98 %, R-sq (adj.) = 99.93 %, R-sq (pred.) = 99.64 %.

3.6.4 Regression Analysis:

Regression analysis was done for modeling the relationship between the output parameter or dependent variable i.e. damping force and input independent variables i.e. no. of holes, dia. of holes and shim thickness respectively using Minitab 17 statistical software.

The obtained regression equation is:

Optimum Damping Force

$$= 399.8 - 23.86 \times \text{No. of Holes} - 138.7 \times \text{Dia. of Holes} - 46.3 \times \text{Shim Thickness}$$

Now, the optimum parameters were placed in the above equation to get the optimum value of quality characteristic which in present case is maximum damping force value.

$$\begin{aligned} \text{Optimum Damping Force} &= 399.8 - 23.86 \times 4 - 138.7 \times 0.8 - 46.3 \times 0.45 \\ &= 172.56 \text{ kgf (Predicted by Regression Equation)} \end{aligned}$$

3.6.5 Confirmation of Result

One damper was developed using optimal parameters i.e. A1B1C3 and experimental work was performed on it by taking three trials. The predicted results in terms of peak rebound damping force obtained by regression equation and the average peak rebound damping force show the error of 1.76 % as seen in Table 3.21.

Table 3.21 Confirmation of result

Trial No.	1	2	3	Average		% Error
				Exp.	Pred.	
Damping Force (kgf)	175.1	178.2	173.6	175.6	172.5	1.76

3.7 SUMMARY

In this chapter, dual tube hydraulic passive dampers with various piston design and valve design parameters were tested on MTS machine under piston rod velocity of 0.05 m/s, 0.1 m/s and 0.3 m/s respectively. Test results in terms of damping force vs. displacement and peak damping force vs. velocity were presented in graphical and tabular form. Taguchi method was applied for geometrical optimization of three selected parameters (no. of holes, dia. of holes and shim thickness) i.e. selection of optimum combination of these parameters to maximize the peak rebound damping force generation ability of the dual tube passive damper using S/N ratio. ANOVA was performed to investigate the contribution of each design parameter on the maximum rebound damping force generation ability of the selected damper.

CHAPTER IV

MR DAMPER TESTING & MODELING

4.1 OVERVIEW

This chapter presents MR damper testing and modeling issues. The configuration of selected MR damper for experimental work is mentioned. Experimental setup with necessary machine and components is described. MR damper test results are presented under different input current values as well as with particular magnitude of amplitude and frequency. Finally, the applicability of selected polynomial model is discussed in reproducing the desired non-linear hysteresis behavior of MR damper.

4.2 MR DAMPER RD-1005-3 TESTING

4.2.1 Configuration of MR Damper

Magnetorheological damper selected for experimental work was RD-1005-3 while its schematic diagram is shown in Figure 4.1 [97]. Its technical details are given in Table 4.1. It can generate peak to peak damping force up to 2224 N at the excitation velocity of 51 mm/s and at a continuous current input of 1 A. The damper can work continuously at the supplied current of 1 A while the maximum current can reach up to 2 A for intermittent supply.

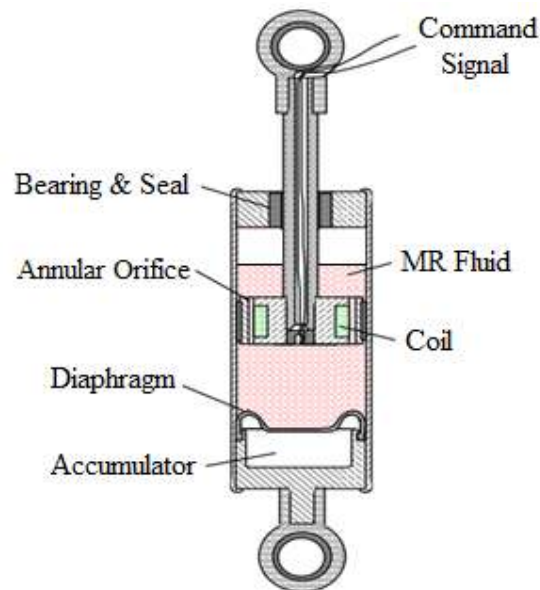


Figure 4.1 MR damper RD-1005-3

Table 4.1 Technical details of MR damper RD-1005-3

Parameter	Value	Parameter	Value
Extended Length	208 mm	Compressed Length	155 mm
Device Stroke	25 mm	Response Time	< 10 ms
Body Diameter	41.4 mm	Shaft Diameter	10 mm
Magneto-Rheological Fluid	MRF-132 DG	Max. Tensile Force	4448 N
Viscosity at 40° C	0.092 ± 0.015 N-s/m	Max. Temperature	71° C
Density	2980-3180 kg/m ³	Max. Current Supply	2 A
Solids content by weight %	80.98	Input Voltage (DC)	12 V

4.2.2 Experimental Set Up

The MR damper RD-1005-3 was tested on MTS machine to measure the dynamic test results under various excitation conditions. The MR damper test set up is shown in Figure 4.2 while the real testing work is shown in Figure 4.3. The MTS machine used for MR damper testing was same as used for testing passive dampers. The maximum magnitude of applied D.C. current to the electromagnet was kept limited up to 1 A for smooth and safe working of MR damper.

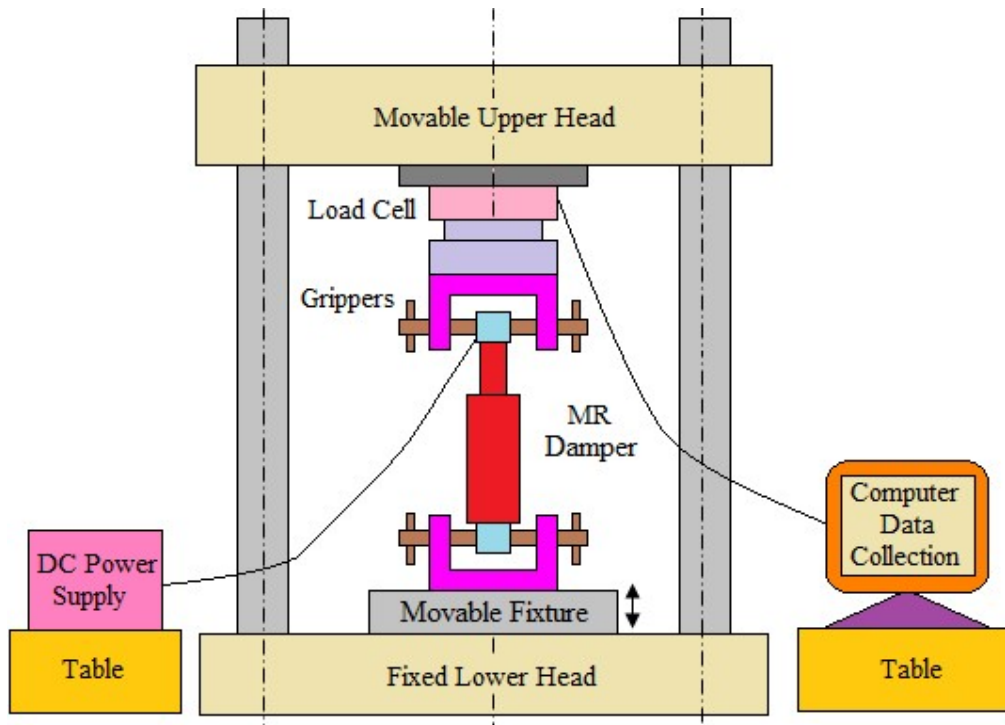


Figure 4.2 Schematic diagram of MR damper test set up on MTS machine

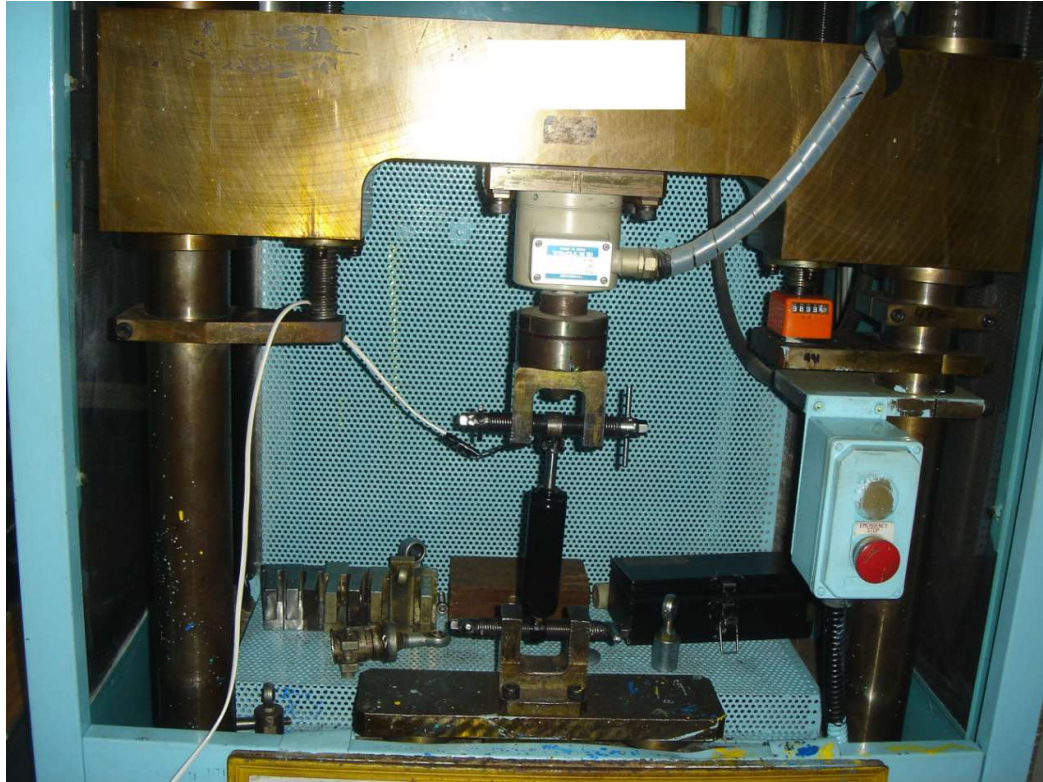


Figure 4.3 Experimental setup of MR damper with test machine

4.2.3 Test Parameters & Results

A number of experimental tests were performed under sinusoidal excitation conditions using MTS machine to measure force-velocity and force-displacement characteristics of MR damper. The influence of different parameters such as excitation frequency, stroke magnitude and supplied current on the shape of hysteretic damping force loop of MR damper was noted. Based on the experimental results, ability of MR damper to generate maximum magnitudes of damping force during compression and rebound stage were noted for various values of supplied input current ranging from 0 - 1 A. When the value of supplied current to MR damper is zero, it will behave as a passive damper. Since at the supply of zero current value, the wire windings in piston will not produce any magnetization effect near piston region. This will result into the behaviour of magnetorheological fluid as a normal flowing fluid inside the damper tube. Measured test data in shapes of force-displacement and force-velocity curves of MR damper at particular excitation frequency of 2.5 Hz and ± 6.3 mm displacement are presented in Figure 4.4.

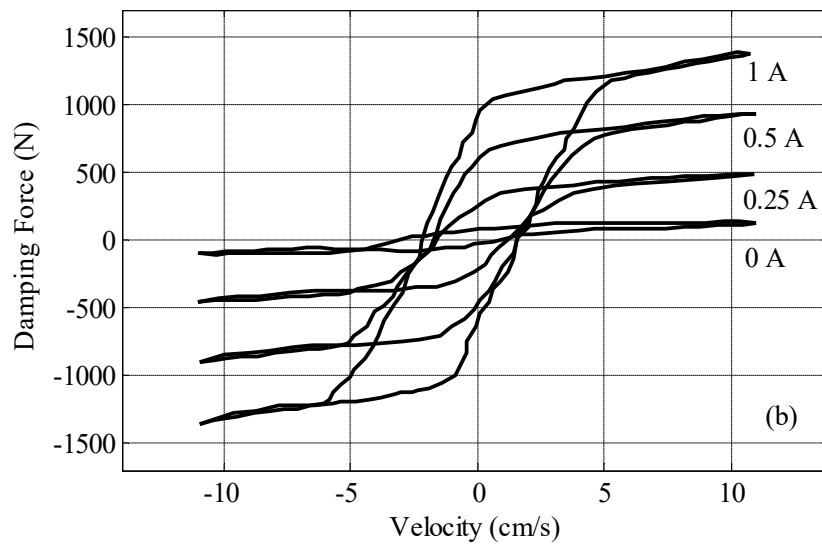
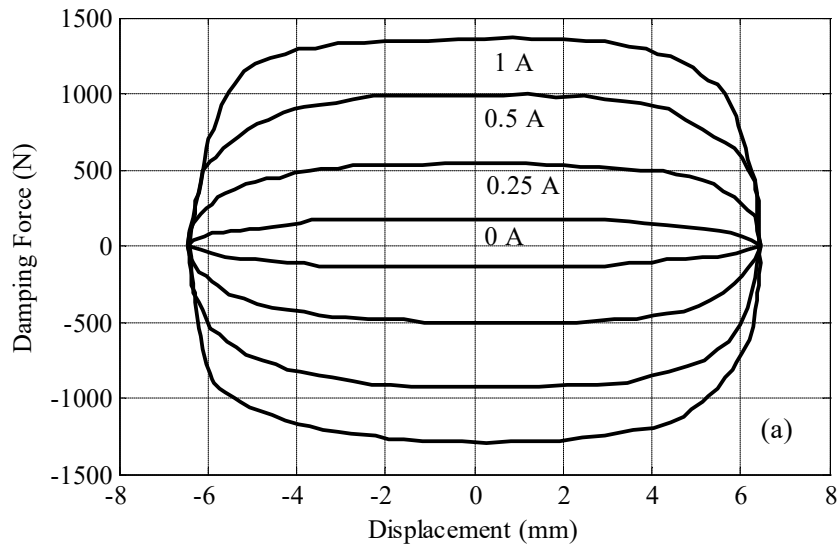


Figure 4.4 Experimental results (2.5 Hz, ± 6.3 mm):

(a) force vs. displacement; (b) force vs. velocity.

4.3 MR DAMPER MODELING

The design and development of control system is based on the MR damper experimental data. Thus, for utilization of MR damper experimental data in control system applications, a model need to be developed that can appropriately and conveniently regenerate the non-linear hysteretic behaviour of MR damper. Figure 4.5 shows the polynomial model proposed by Choi et al. for curve fitting to the MR damper test results [55]. Here, experimental data related to force-velocity hysteresis loop is divided into two parts: upper curve as negative acceleration while lower curve as positive acceleration. The presented model could describe the non-linear hysteretic properties of MR damper under specific test conditions, essential for curve fitting.

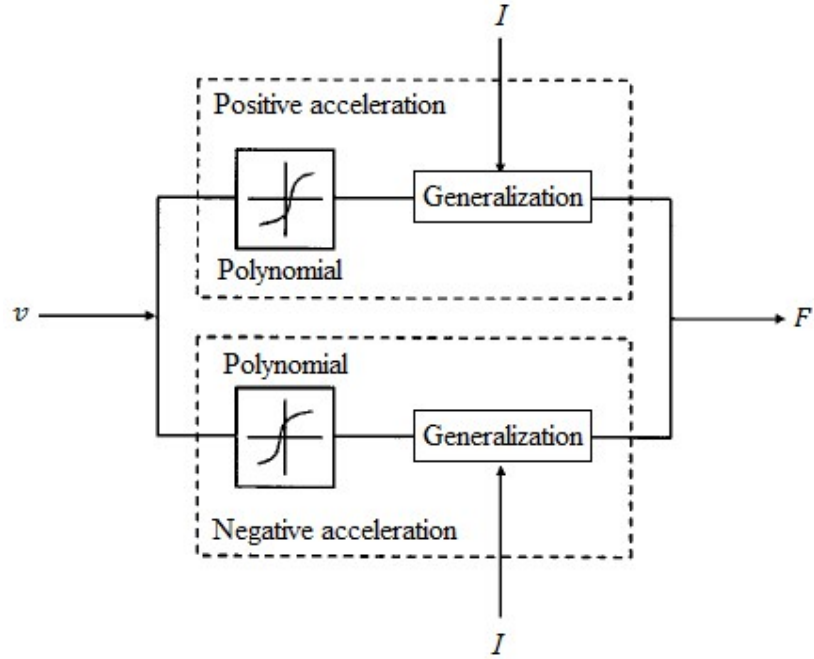


Figure 4.5 Polynomial model

These two curves are fitted by using polynomial curve fitting technique based on the power of the tested MR damper piston velocity. Therefore, the MR damper generated damping force can be represented mathematically as:

$$F_{MR} = \sum_{i=0}^n a_i v^i \quad (4.1)$$

where F_{MR} is damping force, a_i is the experimental coefficient to be find from the curve fitting, value of variable n is chosen by trial and error method based on best curve fitting of simulation results with the experimental data. In present case, $n = 10$ is selected.

Based on the curve fitting results shown in Figure 4.6, the relationship between coefficient a_i and input current I can be established as follows:

$$a_i = b_i + c_i I, i = 0,1 \dots 10 \quad (4.2)$$

Finally, the MR damping force can be represented as:

$$F_{MR} = \sum_{i=0}^{10} (b_i + c_i I) v^i \quad (4.3)$$

The calculated values of the coefficients b_i and c_i using the MR damper test results are shown in Table 4.2.

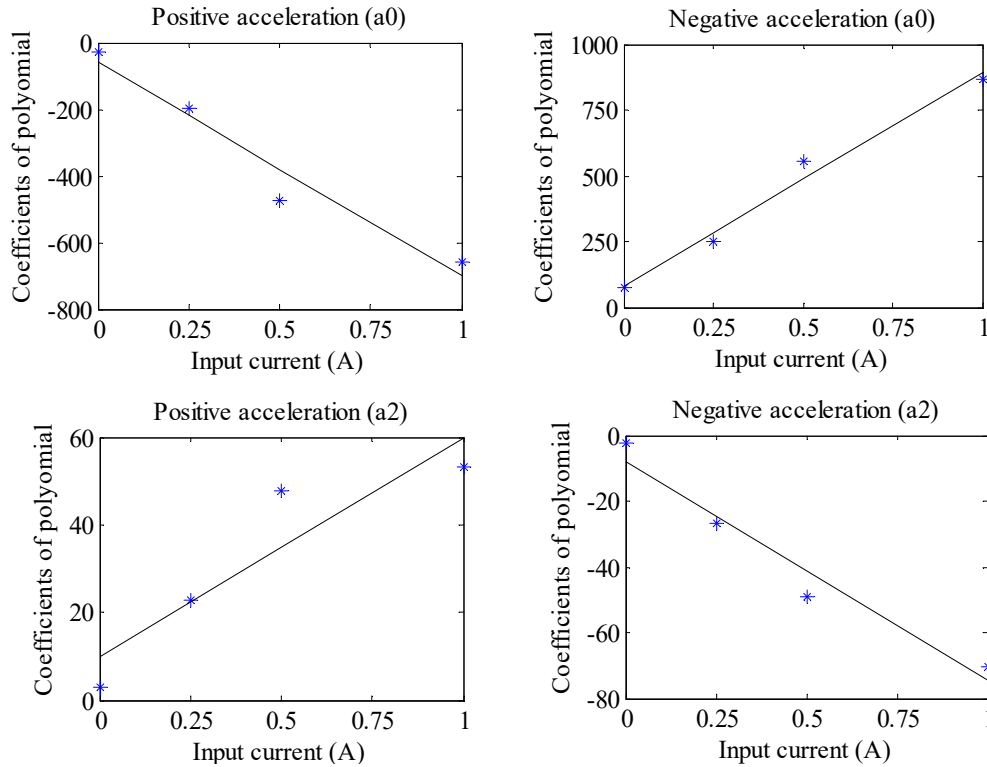


Figure 4.6 The relationship between a_i and input current

(* Coefficients, — Fitted)

Table 4.2 Calculated coefficients b_i and c_i of fitted curve with values

Positive acceleration				Negative acceleration			
Coefficients		Coefficients		Coefficients		Coefficients	
b_0	-59.46	c_0	-640.83	b_0	82.23	c_0	810.13
b_1	54.54	c_1	297.41	b_1	47.96	c_1	247.57
b_2	9.96	c_2	49.66	b_2	-7.87	c_2	-66.93
b_3	-1.96	c_3	-4.09	b_3	-0.89	c_3	-1.92
b_4	-0.44	c_4	-1.47	b_4	0.30	c_4	2.20
b_5	0.04	c_5	0.04	b_5	9.35E-03	c_5	-3.82E-05
b_6	8.24E-03	c_6	0.02	b_6	-4.93E-03	c_6	-3.51E-02
b_7	-3.26E-04	c_7	-1.35E-04	b_7	-3.83E-05	c_7	1.25E-04
b_8	-6.85E-05	c_8	-1.37E-04	b_8	3.66E-05	c_8	2.67E-04
b_9	1.02E-06	c_9	1.65E-07	b_9	2.40E-08	c_9	-5.70E-07
b_{10}	2.10E-07	c_{10}	3.44E-07	b_{10}	-1.00E-07	c_{10}	-7.74E-07

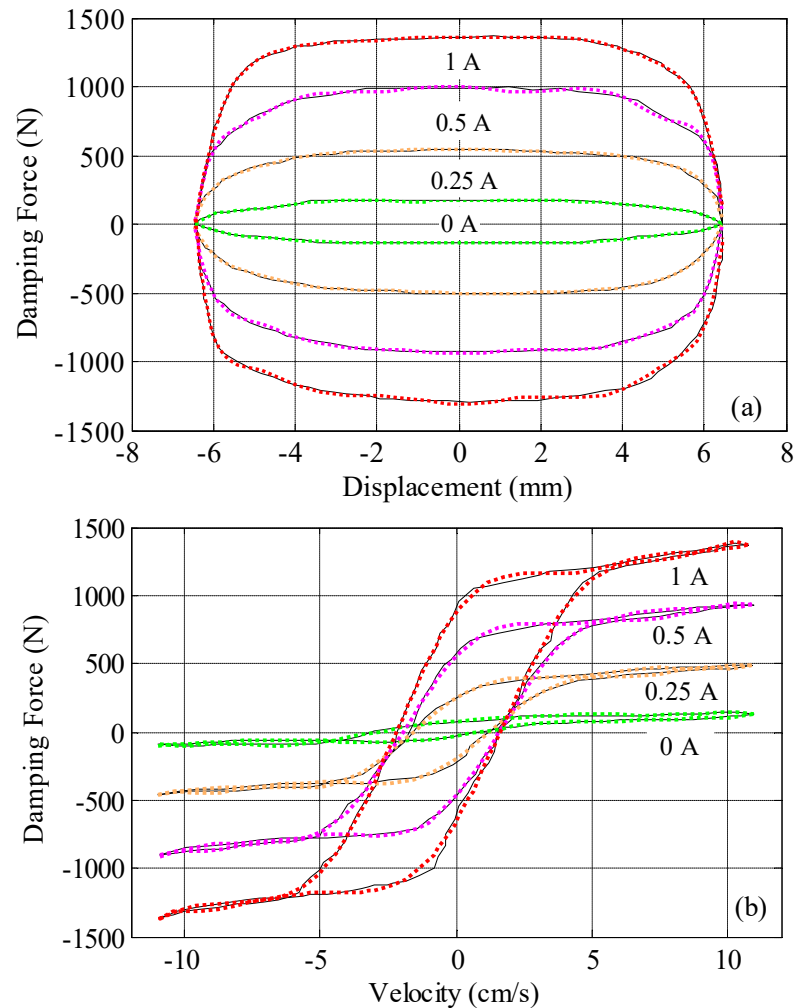


Figure 4.7 Comparison of model fitted curves and experimental results (2.5 Hz, ± 6.3 mm): (a) force vs displacement; (b) force vs velocity. (— Experimental, - - - Fitted).

The above results related to the comparison of the force-displacement and force-velocity curves between experimental data under ± 6.3 mm excitation and 2.5 Hz test conditions and fitted curve by polynomial model method under various magnitudes of supplied current are presented in Figure 4.7. The comparison of measured test results with simulated plots under different current values ranging from 0 to 1 A showed very close agreement with each other as seen in Figure 4.7.

From above figures, it can be seen and concluded that the implemented polynomial model is effective in closely following the experimental curves of MR damper. Based on the developed polynomial model, the desired damping force (F_d) to be generated by MR damper can be obtained by supplying proper current signal to MR damper as

per the piston velocity (v). The supplied current (I) to MR damper can be calculated using equation 4.4 as below:

$$I = \frac{F_d - \sum_{i=0}^{10} b_i v^i}{\sum_{i=0}^{10} c_i v^i} \quad (4.4)$$

4.4 SUMMARY

Based on the experimental data, a generalized polynomial model was presented to characterize various non-linear hysteretic force-velocity curves of MR damper at a particular sinusoidal excitation condition of fixed frequency and displacement amplitude and changing magnitudes of supplied current. The effectiveness and validation of proposed polynomial curve fitting model was presented in graphical form using least square curve fitting technique. The presented model was adequate to capture different force – velocity loops under different current values, which is the primary requirement for controller design. Based on the formulated mathematical equations, forward model for damping force and inverse model for supplied current to MR damper has been established. Thus, inverse model of MR damper can be derived for implementation in controller based technology to supply input current to the MR damper. Finally, the proposed forward and inverse models could be effectively implemented in controller design to deliver desired and timely performance of MR damper in vehicle suspension system.

CHAPTER V

MATHEMATICAL MODELING OF QUARTER CAR SYSTEM

5.1 INTRODUCTION

For simulation work and comparative analysis of passive and semi-active suspension control strategies under various road inputs, a vehicle model is required. In present study, a simple quarter car model with three degrees of freedom consisting one fourth mass of the whole vehicle body is considered. The assembled parts of the model include passenger seat, suspension components and a single wheel. The road induced vibrations are transmitted to the complete vehicle system in vertical upward direction. Quarter car model takes into account the vertical dynamics of vehicle body accurately and it is often used in literature for vehicle vibration response analysis [98-101]. Quarter car model provides certain advantages in terms of design simplicity, rapid model development, fast data generation and analysis compared to complicated full-vehicle model.

5.2 MODELLING ASSUMPTIONS

The assumptions made for the mathematical modeling of nonlinear quarter car system with three degrees of freedom are as follows:

1. Quarter car body parts are rigidly connected with each other.
2. Quarter car moves in a horizontal direction in a straight line with a constant selected velocity.
3. The passenger mass, sprung mass and unsprung mass are considered constant in magnitude during modeling and simulation work.
4. Designed and assembled controllers work instantly and supply signals in quarter car suspension system during vibration control.
5. Uneven road surface and road irregularities are responsible for vibration transfer in quarter car model in vertical direction.

5.3 QUARTER CAR WITH PASSIVE AND SEMI-ACTIVE SUSPENSION SYSTEM

In this case, two shock absorbers are assembled in the quarter vehicle system having three-degrees-of-freedom as shown in Figure 5.1. First in the primary suspension system i.e. between unsprung mass and sprung mass while the second in the secondary suspension system i.e. between the sprung mass and passenger seat. In case

of uncontrolled quarter car system, both of the assembled shock absorbers in primary and secondary suspension system are passive in nature.

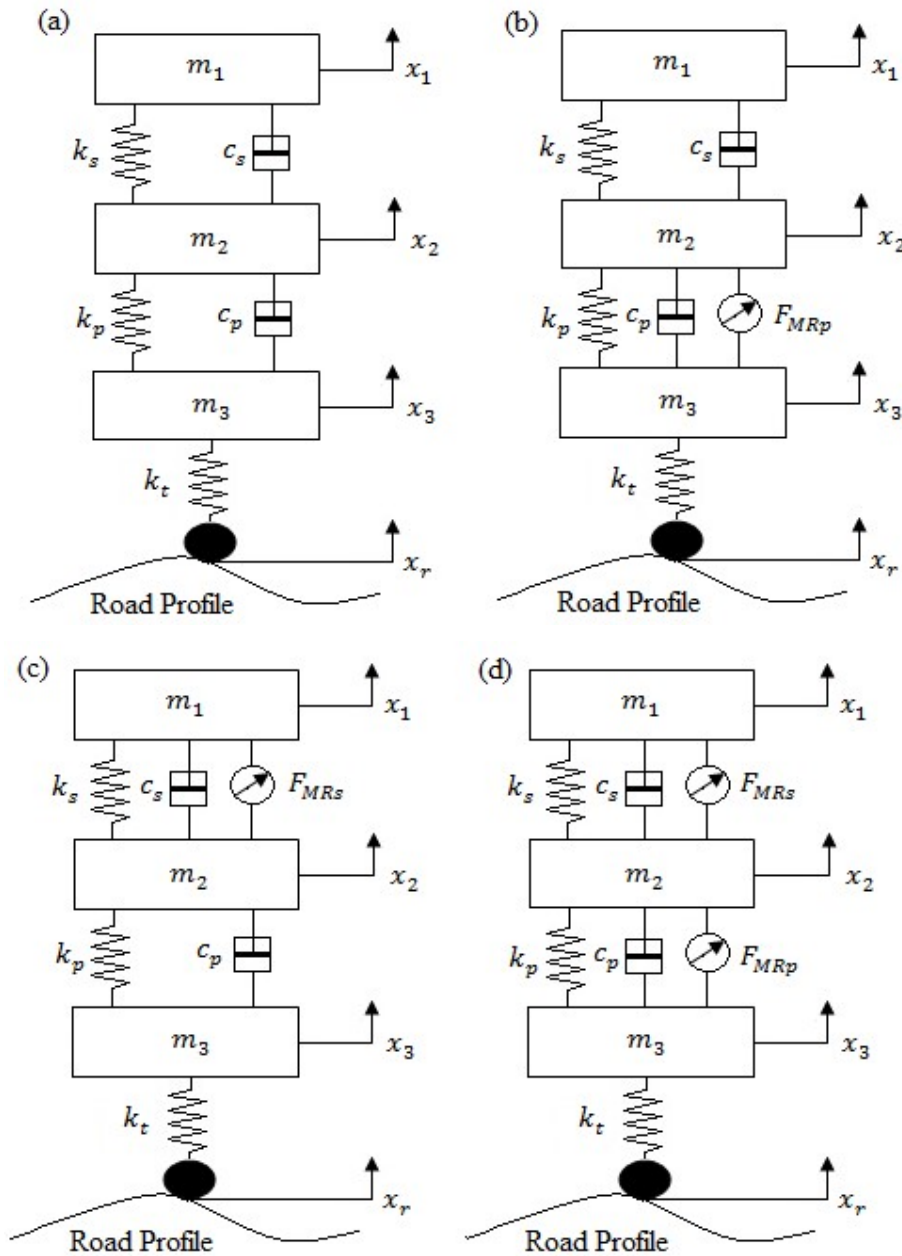


Figure 5.1 (a) Passive quarter car model (b) Primary suspension controlled semi-active quarter car model (c) Secondary suspension controlled semi-active quarter car model (d) Fully controlled semi-active quarter car model

In primary suspension controlled quarter car system, primary suspension of quarter car system is assembled with MR shock absorber whereas secondary suspension system is assembled with uncontrollable passive shock absorber. In secondary suspension controlled quarter car system, secondary suspension of quarter car system

is assembled with MR shock absorber whereas primary suspension system is assembled with uncontrollable passive shock absorber. In case of fully controlled semi-active quarter car system, primary as well as secondary suspension of quarter car system is assembled with MR shock absorbers.

The mathematical equation related to dynamic state of this model including passenger seat dynamics can be stated using Newton's second law of motion as follows:

For uncontrolled quarter car model:

$$m_1\ddot{x}_1 + c_s(\dot{x}_1 - \dot{x}_2) + k_s(x_1 - x_2) = 0 \quad (5.1)$$

$$m_2\ddot{x}_2 - c_s(\dot{x}_1 - \dot{x}_2) - k_s(x_1 - x_2) + c_p(\dot{x}_2 - \dot{x}_3) + k_p(x_2 - x_3) = 0 \quad (5.2)$$

$$m_3\ddot{x}_3 - c_p(\dot{x}_2 - \dot{x}_3) - k_p(x_2 - x_3) + k_t(x_3 - x_r) = 0 \quad (5.3)$$

For primary suspension controlled quarter car model:

$$m_1\ddot{x}_1 + c_s(\dot{x}_1 - \dot{x}_2) + k_s(x_1 - x_2) = 0 \quad (5.4)$$

$$m_2\ddot{x}_2 - c_s(\dot{x}_1 - \dot{x}_2) - k_s(x_1 - x_2) + c_p(\dot{x}_2 - \dot{x}_3) + k_p(x_2 - x_3) + F_{MRp} = 0 \quad (5.5)$$

$$m_3\ddot{x}_3 - c_p(\dot{x}_2 - \dot{x}_3) - k_p(x_2 - x_3) + k_t(x_3 - x_r) - F_{MRp} = 0 \quad (5.6)$$

For secondary suspension controlled quarter car model:

$$m_1\ddot{x}_1 + c_s(\dot{x}_1 - \dot{x}_2) + k_s(x_1 - x_2) + F_{MRS} = 0 \quad (5.7)$$

$$m_2\ddot{x}_2 - c_s(\dot{x}_1 - \dot{x}_2) - k_s(x_1 - x_2) + c_p(\dot{x}_2 - \dot{x}_3) + k_p(x_2 - x_3) - F_{MRS} = 0 \quad (5.8)$$

$$m_3\ddot{x}_3 - c_p(\dot{x}_2 - \dot{x}_3) - k_p(x_2 - x_3) + k_t(x_3 - x_r) = 0 \quad (5.9)$$

For fully controlled quarter car model:

$$m_1\ddot{x}_1 + c_s(\dot{x}_1 - \dot{x}_2) + k_s(x_1 - x_2) + F_{MRS} = 0 \quad (5.10)$$

$$m_2\ddot{x}_2 - c_s(\dot{x}_1 - \dot{x}_2) - k_s(x_1 - x_2) + c_p(\dot{x}_2 - \dot{x}_3) + k_p(x_2 - x_3) - F_{MRS} + F_{MRp} = 0 \quad (5.11)$$

$$m_3\ddot{x}_3 - c_p(\dot{x}_2 - \dot{x}_3) - k_p(x_2 - x_3) + k_t(x_3 - x_r) - F_{MRp} = 0 \quad (5.12)$$

Taking dynamic relationship into account, the following state variables can be defined

$$\begin{aligned} z_1(t) &= x_1(t) - x_2(t), & z_2(t) &= x_2(t) - x_3(t), & z_3(t) &= x_3(t) - x_r(t), \\ z_4(t) &= \dot{x}_1(t), & z_5(t) &= \dot{x}_2(t), & z_6(t) &= \dot{x}_3(t) \end{aligned} \quad (5.13)$$

where $z_1(t)$ is the secondary suspension deflection, $z_2(t)$ is the primary suspension deflection, $z_3(t)$ is the tyre deflection, $z_4(t)$ is the passenger seat vertical velocity,

$z_5(t)$ is the sprung mass velocity and $z_6(t)$ is the unsprung mass velocity while in matrix form

$$z(t) = [z_1(t) \ z_2(t) \ z_3(t) \ z_4(t) \ z_5(t) \ z_6(t)]^T, w(t) = \dot{x}_r(t) \quad (5.14)$$

where $w(t)$ is the road input disturbance.

In state-space form the equations can be represented as

$$\dot{z}(t) = Az(t) + F_d + c_w w(t) \quad (5.15)$$

where

For uncontrolled quarter car model:

$$A = \begin{bmatrix} 0 & 0 & 0 & 1 & -1 & 0 \\ 0 & 0 & 0 & 0 & 1 & -1 \\ 0 & 0 & 0 & 0 & 0 & 1 \\ -\frac{k_s}{m_1} & 0 & 0 & -\frac{c_s}{m_1} & \frac{c_s}{m_1} & 0 \\ \frac{k_s}{m_2} & -\frac{k_p}{m_2} & 0 & \frac{c_s}{m_2} & -\frac{c_s + c_p}{m_2} & \frac{c_p}{m_2} \\ 0 & \frac{k_p}{m_3} & -\frac{k_t}{m_3} & 0 & \frac{c_p}{m_3} & -\frac{c_p}{m_3} \end{bmatrix}$$

$$F_d = [0 \ 0 \ 0 \ 0 \ 0 \ 0]^T, \quad c_w = [0 \ 0 \ -1 \ 0 \ 0 \ 0]^T$$

For primary suspension controlled quarter car model:

$$A = \begin{bmatrix} 0 & 0 & 0 & 1 & -1 & 0 \\ 0 & 0 & 0 & 0 & 1 & -1 \\ 0 & 0 & 0 & 0 & 0 & 1 \\ -\frac{k_s}{m_1} & 0 & 0 & -\frac{c_s}{m_1} & \frac{c_s}{m_1} & 0 \\ \frac{k_s}{m_2} & -\frac{k_p}{m_2} & 0 & \frac{c_s}{m_2} & -\frac{c_s + c_p}{m_2} & \frac{c_p}{m_2} \\ 0 & \frac{k_p}{m_3} & -\frac{k_t}{m_3} & 0 & \frac{c_p}{m_3} & -\frac{c_p}{m_3} \end{bmatrix}$$

$$F_d = \left[0 \ 0 \ 0 \ 0 \ -\frac{F_{MRp}}{m_2} \ \frac{F_{MRp}}{m_3} \right]^T,$$

$$c_w = [0 \ 0 \ -1 \ 0 \ 0 \ 0]^T$$

For secondary suspension controlled quarter car model:

$$A = \begin{bmatrix} 0 & 0 & 0 & 1 & -1 & 0 \\ 0 & 0 & 0 & 0 & 1 & -1 \\ 0 & 0 & 0 & 0 & 0 & 1 \\ -\frac{k_s}{m_1} & 0 & 0 & -\frac{c_s}{m_1} & \frac{c_s}{m_1} & 0 \\ \frac{k_s}{m_2} & -\frac{k_p}{m_2} & 0 & \frac{c_s}{m_2} & -\frac{c_s + c_p}{m_2} & \frac{c_p}{m_2} \\ 0 & \frac{k_p}{m_3} & -\frac{k_t}{m_3} & 0 & \frac{c_p}{m_3} & -\frac{c_p}{m_3} \end{bmatrix}$$

$$F_d = \left[0 \ 0 \ 0 \ -\frac{F_{MRs}}{m_1} \ \frac{F_{MRs}}{m_2} \ 0 \right]^T,$$

$$c_w = [0 \ 0 \ -1 \ 0 \ 0 \ 0]^T$$

For fully controlled quarter car model:

$$A = \begin{bmatrix} 0 & 0 & 0 & 1 & -1 & 0 \\ 0 & 0 & 0 & 0 & 1 & -1 \\ 0 & 0 & 0 & 0 & 0 & 1 \\ -\frac{k_s}{m_1} & 0 & 0 & -\frac{c_s}{m_1} & \frac{c_s}{m_1} & 0 \\ \frac{k_s}{m_2} & -\frac{k_p}{m_2} & 0 & \frac{c_s}{m_2} & -\frac{c_s + c_p}{m_2} & \frac{c_p}{m_2} \\ 0 & \frac{k_p}{m_3} & -\frac{k_t}{m_3} & 0 & \frac{c_p}{m_3} & -\frac{c_p}{m_3} \end{bmatrix}$$

$$F_d = \left[0 \ 0 \ 0 \ -\frac{F_{MRs}}{m_1} \ \frac{F_{MRs} - F_{MRp}}{m_2} \ \frac{F_{MRp}}{m_3} \right]^T,$$

$$c_w = [0 \ 0 \ -1 \ 0 \ 0 \ 0]^T$$

represents constant matrices.

5.4 SUMMARY

In this chapter, mathematical models of a nonlinear quarter car model with three degrees of freedom were developed. The models considered passenger seat into account for comparative analysis of passenger ride comfort and safety for passive, primary suspension controlled, secondary suspension controlled and fully controlled quarter car models. Mathematical equations of developed models were also presented in state space form.

CHAPTER VI

CONTROLLERS DESIGN

6.1 INTRODUCTION

In present chapter, design of various control schemes for application in semi-active quarter car system is considered. The proposed control algorithms include PID controller, Fuzzy Logic controller, Hybrid Fuzzy PID controller (HFPID) and Hybrid Fuzzy PID controller with Coupled Rules (HFPIDCR) respectively. A vibration control system using an MR damper requires two nested controllers:

- (i) a forward controller for generating desired damping force signal, and
- (ii) an inverse controller for producing and supplying current signal to MR damper.

6.2 FORWARD CONTROLLERS

6.2.1 PID Controller

The conventional Proportional–Integral–Derivative (PID) controller is very effective, popular and mostly used in industries [102-105]. A PID controller is also known as a three-term controller and follows the input reference signal. It combines Proportional, Integral and Derivative of the difference in reference signal position and current position of signal supplied from controlled system. In the semi-active quarter car system shown in Figure 6.1, MR damper piston rod position is selected for error calculation.

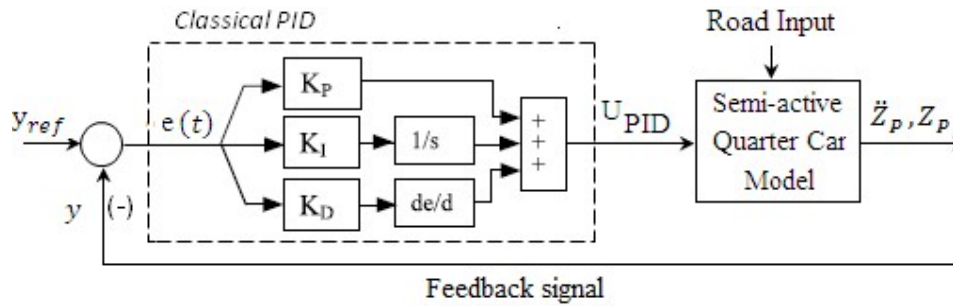


Figure 6.1 Conventional PID controller applied in secondary suspension system

The basis of PID control working is given in (6.1) and (6.2) as below:

$$e(t) = y_{ref} - y \quad (6.1)$$

$$U_{PID}(t) = K_P e(t) + K_I \sum_{i=0}^t e(t) + K_D \dot{e}(t) \quad (6.2)$$

where y_{ref} is the reference position and y is the current position of piston rod while K_P , K_I and K_D are proportional, integral and derivative gain respectively. During the MR damper working, the error signal, $e(t)$ is equal to the difference between the current position, y and selected reference value position, y_{ref} of the piston rod.

6.2.2 Fuzzy Logic Controller

The field of fuzzy logic (FL) came into existence in 1965, due to the efforts and vision of Lotfi Zadeh [106]. The first fuzzy logic controller (FLC) was developed by E. H. Mamdani in 1975 for practical application to a steam engine [107]. During the past several years, FL has emerged as one of the most powerful and promising area for research and application in control system field [108-110]. Fuzzy logic represents a branch of Artificial Intelligence which is helpful in solving mathematically complicated and imprecise real life problems by incorporating human knowledge and optimum decision making abilities into machines. It can be considered as an easy and reliable method to achieve the goal for many complex and technically complicated real-life control problems that are too problematic from understanding point of view related to its mathematical formulation and dynamics.

It requires expert knowledge and experience about the system under consideration for controlling using fuzzy logic technique. Since the formulation and application of this technique is experience based and expert system based, anyone having an expertise in particular system application can apply it. Fuzzy controller works as an artificial decision taker in a closed loop mechatronic based systems in real life. Plant output data is fed to the controller where it is compared with the reference input signal based on which decision is taken to meet the required or desired performance parameters.

Fuzzy Logic Controllers (FLCs) have been successfully developed and implemented in quarter car, half car and full car semi-active vehicle suspension systems [111-114]. The simulation and practical results have shown the benefits of FLC in improving ride comfort and safety in vehicle suspension system mainly related to two controlling parameters namely: sprung mass and unsprung mass. In present case, FLC have been integrated after design and development in quarter vehicle system having three-degrees-of-freedom specifically for improving passenger ride comfort and safety as target criterion.

In present case, the designed Forward Fuzzy Logic Controller (FFLC) has two different inputs and one output. The desired output damping force signal (F_d) supplied by fuzzy controller is determined based on the corresponding levels of piston rod position variation or delta position ($e(t) = \Delta P = \text{reference position} - \text{actual position}$) and the piston rod velocity variation, ($de(t) = \Delta V = \text{reference velocity} - \text{actual velocity}$). The supplied inputs are error signal, $[e(t) =$

$y_{ref} - y]$ and change of error signal, $[de(t) = v_{ref} - v]$ while the output generated from fuzzy controller is desired damping force signal, F_d . The complete structure of fuzzy logic controller with components is shown in Figure 6.2.

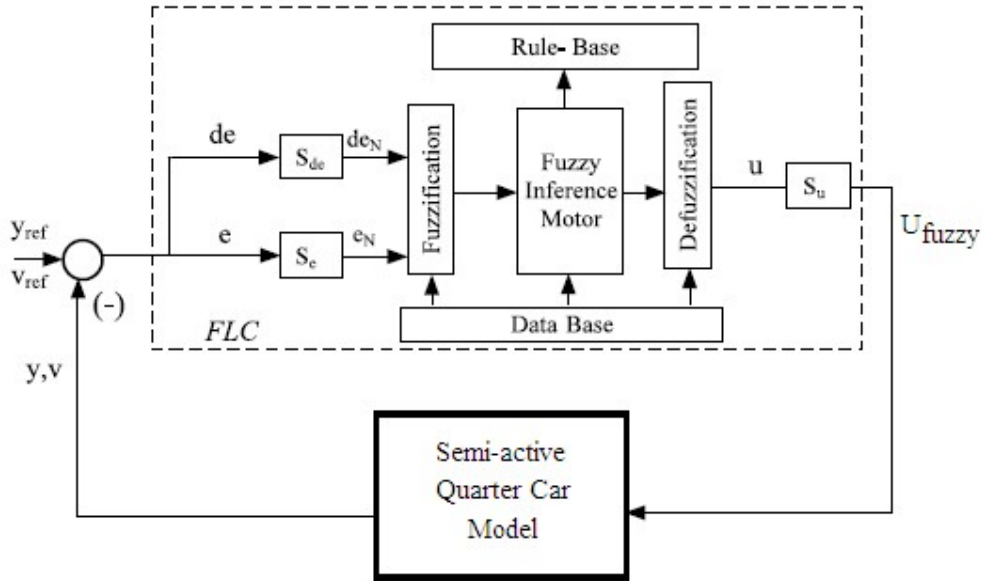
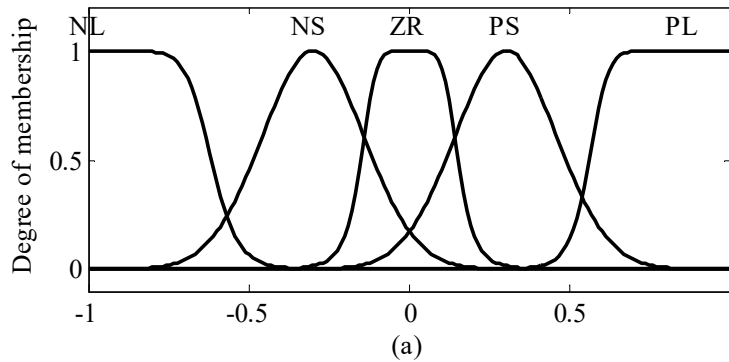


Figure 6.2 Forward FLC with plant or system

The abbreviations used for input and output side linguistic variables are as follows: NL (Negative Large), NM (Negative Medium), NS (Negative Small), ZR (Zero), PS (Positive Small), PM (Positive Medium), and PL (Positive Large) respectively. The membership functions with selected shapes and matching portions are shown in Figure 6.3. The defined intervals for input and output side are in the range of $[-1, 1]$ and $[-3, 3]$ respectively. Actual ranges for variables is decided by multiplication factors S_e , S_{de} and S_u as shown in Figure 6.2. The working of fuzzy controller is directed by if-then rules. Here, total 25 if-then rules are written in a matrix form as shown in Table 6.1 while rule base description is presented in Table 6.2.



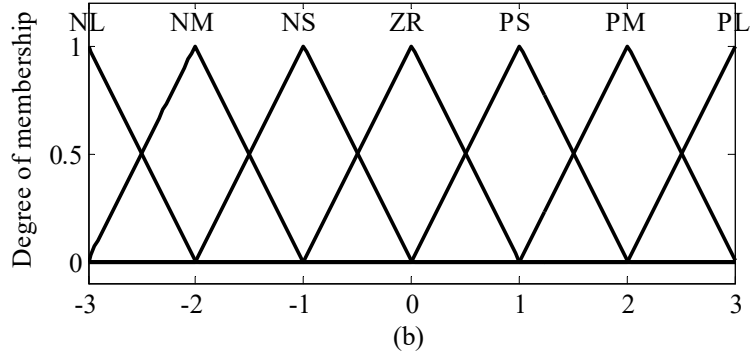


Figure 6.3 MFs for FLC (a) Input side, e and de (b) Output side, F_d

Table 6.1 Fuzzy Rule Base for computing F_d

FLC output , F_d		FLC input 1- Delta Position (ΔP) i.e. e				
		NL	NS	ZR	PS	PL
FLC input 2- Delta velocity (ΔV) i.e. de	NL	NL	NL	NL	NM	ZR
	NS	NL	NS	NS	ZR	PM
	ZR	NL	NS	ZR	PS	PL
	PS	NM	ZR	PS	PS	PL
	PL	ZR	PM	PL	PL	PL

In present work, Mamdani method is selected in fuzzy inference system whereas “max-min” inference method is selected as aggregation operator being mostly used and simplest method. For defuzzification stage, “centroid” method is employed where “center of mass” of the output generates a numerical value i.e. transformation of linguistic variables to crisp values.

Table 6.2 Rule base description of Forward FLC

Rule No.	Rule Description
1	If e is NL and de is NL Then F_d is NL
2	If e is NS and de is NL Then F_d is NL

24	If e is PS and de is PL Then F_d is PL
25	If e is PL and de is PL Then F_d is PL

Figure 6.4 represents a mesh plot for controller input- output relationship in present case. It shows the nonlinear relationship between piston rod position variation and piston rod velocity variation on the input side and the controller output in the form of desired damping force on the output side respectively.

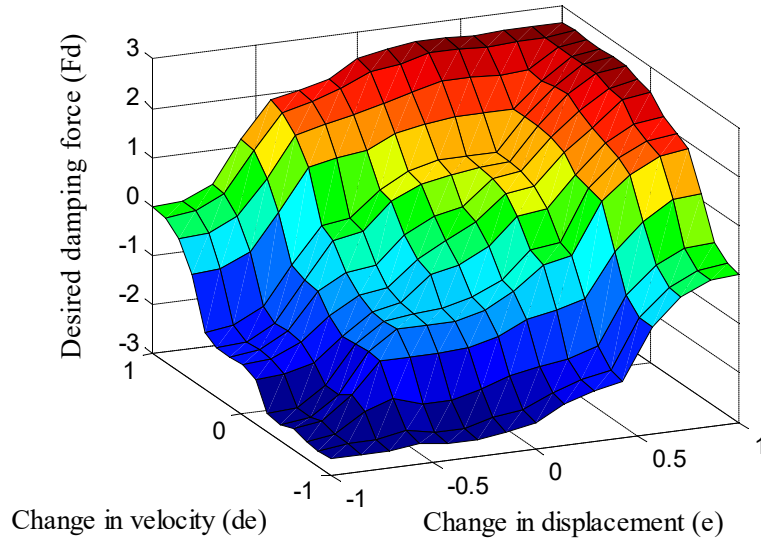


Figure 6.4 Forward FLC input / output surface

6.2.3 Hybrid Fuzzy PID Controller (HFPID)

An intelligent hybrid Fuzzy PID controller has been used by Erenoglu et al. [115]. PID controller can successfully work for linear systems under stable load conditions. However, its control performance is highly affected and drastically reduced for the systems showing highly nonlinear characteristics during working period. While, FLC controller is suitable and attractive choice in control applications of complex, highly nonlinear systems and shows superior response under the varying input conditions. Therefore, the proposed HFPID controller can provide the benefits of Fuzzy and PID controllers by further performance improvement in system response in terms of stability and fast control. The structure of HFPID controller is shown in Figure 6.5. Here, the continuous response of Fuzzy and PID controllers is based on the actuating error signal. The integrated switching mechanism shifts the working between Fuzzy and PID controller as follows:

$$Switch = \begin{cases} 1, & \text{if } |e| > w \\ 0, & \text{if } |e| \leq w \end{cases} \quad \begin{array}{l} \text{Fuzzy controller} \\ \text{PID controller} \end{array} \quad (6.3)$$

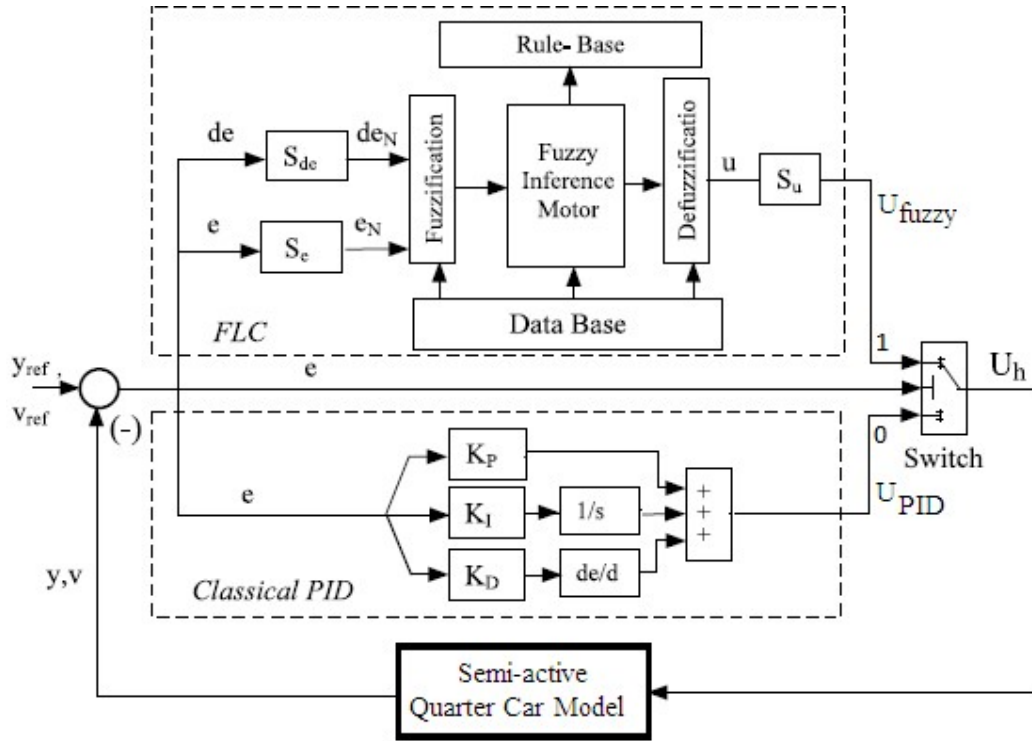


Figure 6.5 Structure of HFPID controller

In this case, if error value “ e ” is greater than the set threshold value “ w ” then the switching mechanism starts Fuzzy controller otherwise transfer of working shifts to PID controller. Thus, PID controller handles the situation better near set point while Fuzzy controller provides rapid control and stabilization when the piston rod position is far from the set point. Finally, the output signal value supplied from HFPID controller at any time can be calculated using a hybrid switching function as written below:

$$U_h = U_{Fuzzy} + U_{PID} \quad (6.4)$$

6.2.4 Hybrid Fuzzy PID Controller with Coupled Rules (HFPIDCR)

Hybrid Fuzzy-PID Controller with Coupled Rules (HFPIDCR) is the advanced stage of HFPID controller in combination with a tuning mechanism for PI and PD actions [116-117]. The overall structure of HFPIDCR with Fuzzy, PID controller, a switch and tuning mechanism is presented in Figure 6.6.

The integrated two gain parameters i.e. K_{PI} and K_{PD} can be tuned easily by supplying proper mathematical values using trial and error method to improve the controller results. The final output signal supplied from HFPIDCR controller to quarter car system can be obtained as follows:

$$U(t) = G_U [K_{PI} \sum_{t=0}^t U_h(t) + K_{PD} U_h(t)] \quad (6.5)$$

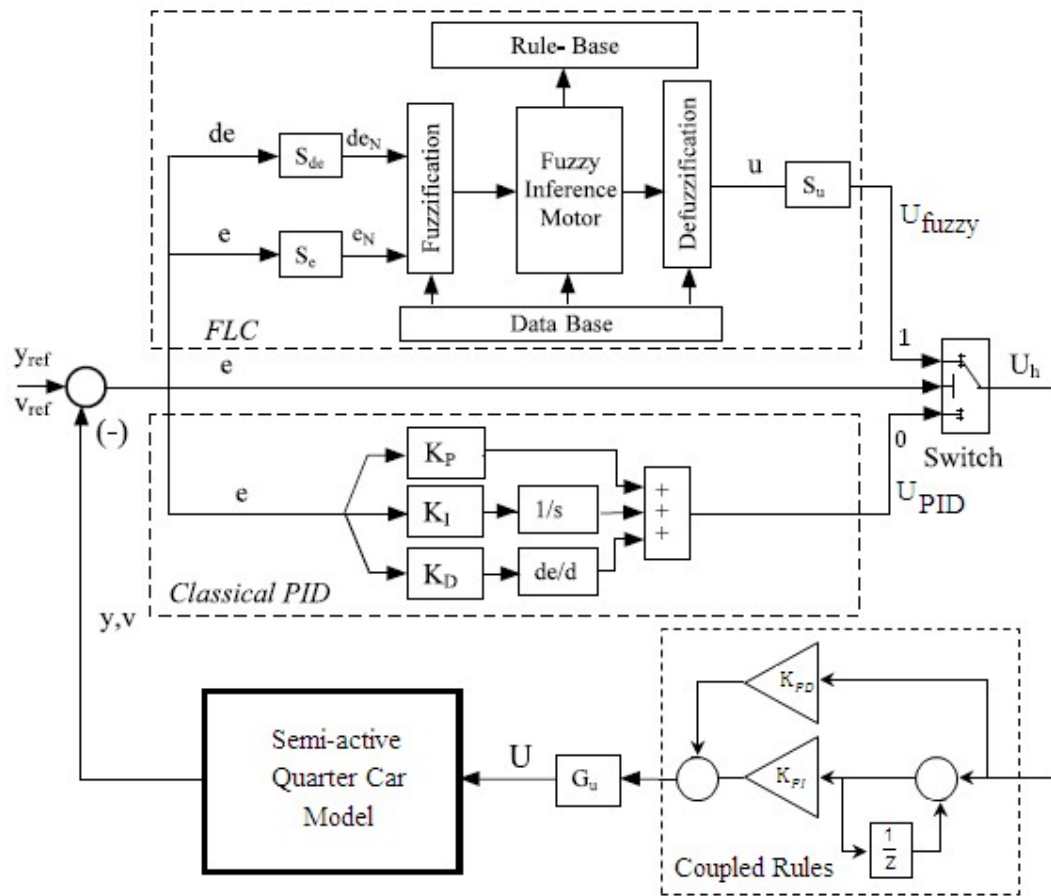


Figure 6.6 Structure of HFPIDCR controller

6.3 INVERSE CONTROLLERS

The developed forward controllers provide output in terms of desired damping force signal. It cannot be used directly for the physical MR damper in vehicle suspension system. For working of assembled MR damper, the utmost requirement is to supply the input variable in terms of current/ voltage. Thus, for the development and application of inverse FLC, the desired damping force supplied by the forward controllers should be related/ mapped in terms of supplied current/ voltage to the assembled MR damper. Later, the generated current signals are supplied to the assembled physical MR damper for necessary damping force generation. The structure of Inverse fuzzy logic controller with components is shown in Figure 6.7.

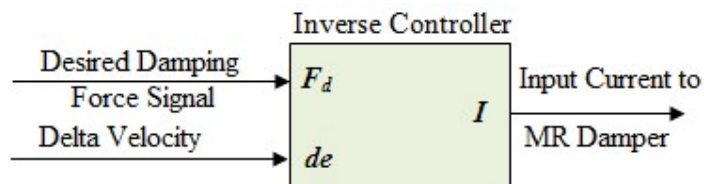


Figure 6.7 Inverse controller design using Forward controller output

In Inverse Fuzzy Logic Controller (IFLC) model, the input information in the form of two variables are: desired damping force signal, F_d which is supplied by forward controller and the piston rod velocity variation ($de(t) = \Delta V = \text{reference velocity} - \text{actual velocity}$), while the output is in the form of supplied current, I to the assembled MR damper in the vehicle suspension system. This supplied current through inverse fuzzy controller is responsible to control the generated actual damping force from the assembled MR damper. The concerned input-output for inverse FLC controller is shown in Figure 6.8.

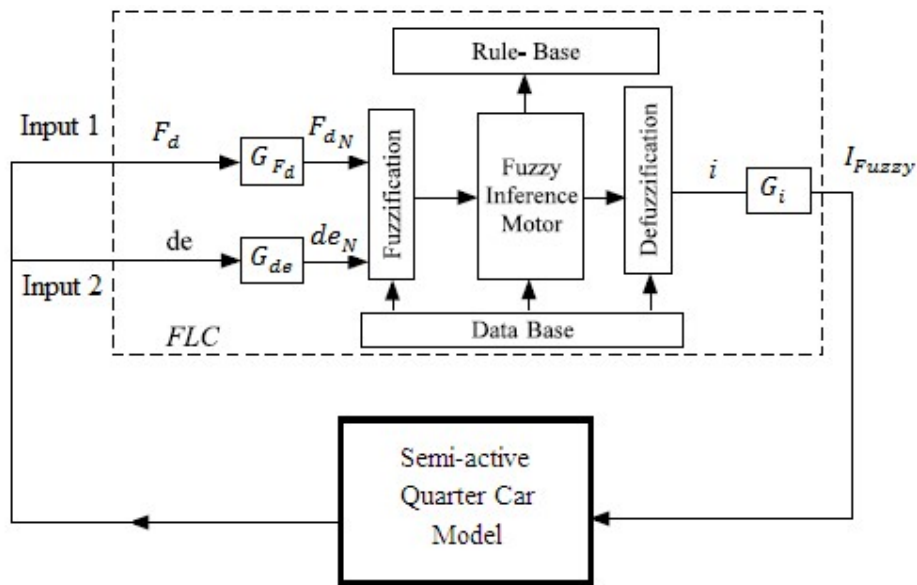


Figure 6.8 Inverse fuzzy logic controller with plant or system

In case of IFLC, membership function having triangular shape is applied, since these behave in more sensitive way for supplied inputs for generation of output current from the applied control system, which is afterwards supplied to the physical MR damper. The membership function plots for the inverse fuzzy controller with selected shapers are shown in Figure 6.9. In present case, for each input and output variable related to membership functions, seven linguistic variables are used for primary as well as secondary suspension system are as follows: PVH (Positive Very High), PH (Positive High), PM (Positive Medium), ZE (Zero), PL (Positive Low), NL (Negative Low) and NH (Negative High) respectively. The defined intervals for input side are in the range of $[-1, 1]$ while for output side are in the range of $[0, 1]$ respectively. An actual range for variables is decided by multiplication factors G_{F_d} , G_{de} and G_i as shown in Figure 6.8.

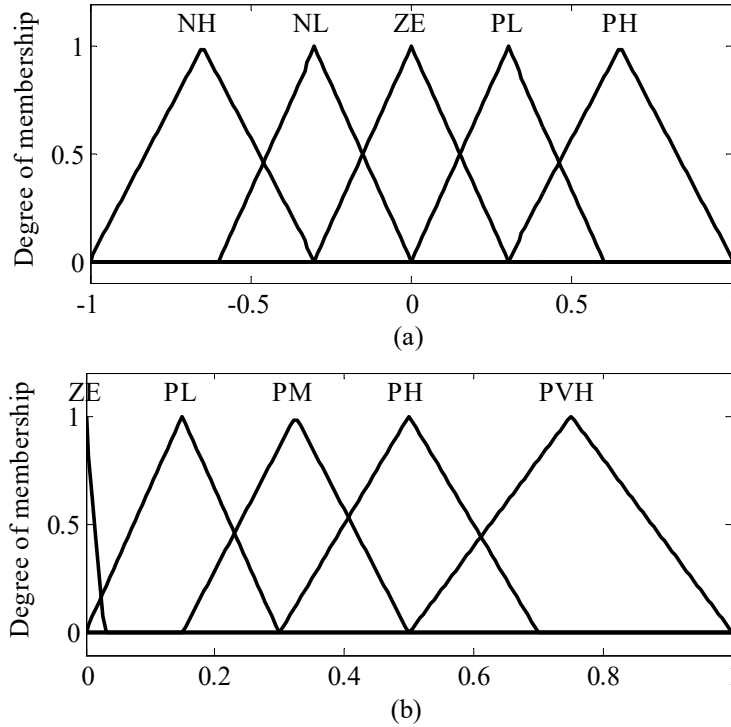


Figure 6.9 MFs for FLC (a) Input side, F_d and de (b) Output side, I

Since, the magnitude of actual damping force generated by assembled physical MR damper is directly related to the value of input current supplied. This concept puts forward the basis for fuzzy rules writing i.e. when the requirement of damping force is low the value of this supplied current must be low whereas the supplied current to MR damper must increase when the damping force requirements are high. Table 6.3 shows the used rules for the inverse controller in a 5x5 matrix (25 rules) for the designed inverse control system while Table 6.4 illustrates the used rules.

Table 6.3 Fuzzy Rule Base for computing I

FLC output, I		FLC input 1- Desired damping force signal, F_d				
		NH	NL	ZE	PL	PH
FLC input 2- Delta velocity (ΔV) i.e. de	NH	PVH	PH	PH	PM	ZE
	NL	PH	PM	PL	ZE	PM
	ZE	PH	PL	ZE	PL	PH
	PL	PM	ZE	PL	PM	PH
	PH	ZE	PM	PH	PH	PVH

In present work Mamdani method is selected in fuzzy inference system whereas “max-min” inference method is selected as aggregation operator being mostly used and simplest method. For defuzzification stage, “centroid” method is employed where “center of mass” of the output generates a numerical value i.e. transformation of linguistic variables to crisp values.

Table 6.4 Rule base description of Inverse FLC

Rule No.	Rule Description
1	If F_d is NH and de is NH Then I is PVH
2	If F_d is NL and de is NL Then I is PH

24	If F_d is PL and de is PH Then I is PH
25	If F_d is PH and de is PH Then I is PVH

Input-output mapping in present case can be represented by a surface. Figure 6.10 represents mesh plot showing the relationship between desired damping force signal and change in piston rod velocity on the input side and the controller output in the form of supplied current to the MR damper showing nonlinear relationship variation with each other.

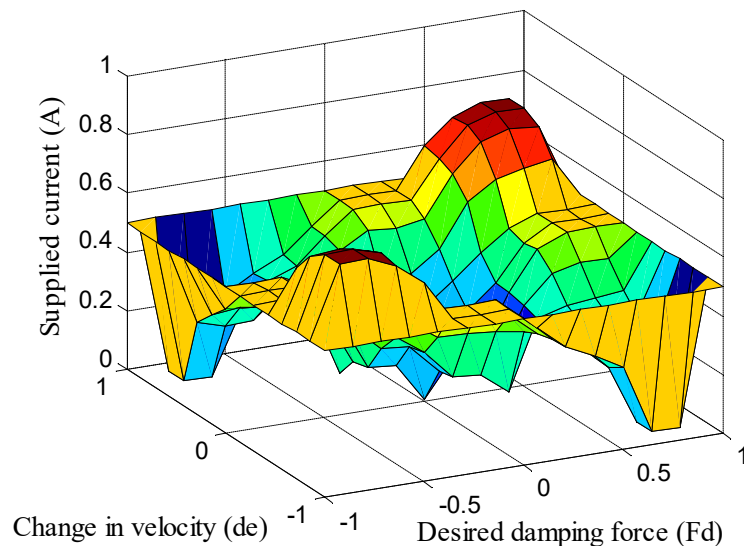


Figure 6.10 Inverse Input / Output surface

6.4 SUMMARY

The nonlinear hysteresis damping force behavior of MR damper makes the modeling and development of proper control strategy a challenging task. In present chapter, forward as well as inverse control algorithms have been developed to utilize the controlled working of MR damper in suspension system. Forward control algorithms such as PID, Fuzzy, HFPIID and HFPIIDCR were designed to keep the generated desired damping force signal within maximum limits of assembled MR damper generated actual damping force. Inverse controllers utilizing the output signals of PID, Fuzzy, HFPIID and HFPIIDCR were designed to keep the supply current to MR damper within 0 A to continuous supply current of 1 A.

CHAPTER VII

PERFORMANCE SPECIFICATIONS

7.1 OVERVIEW

In present chapter, performance specifications related to the passenger seat acceleration and displacement response are mentioned. The main goal is to achieve a best level of vibration isolation in quarter car model with passenger seat. The travelling passengers perceive these responses as transferred from the vehicle structure which is responsible for comfort and safety issues of the occupants. Numerical simulations are carried out to examine the dynamic behavior of quarter car system in terms of passenger seat acceleration and displacement responses for the uncontrolled as well as controlled cases.

7.2 PERFORMANCE EVALUATION PARAMETERS

The effectiveness of suspension shock absorbers in suppression and mitigation of vibration and shock parameters need to be presented in mathematical results. The selected parameters applied for ride comfort evaluation are peak as well root mean square (RMS) values of passenger seat acceleration and displacement. The obtained peak and RMS values provide the basis for selection of most suitable and effectively controlled semi-active suspension system.

7.2.1 Peak Amplitude Criterion

It takes into consideration the maximum values of the passenger seat parameters for evaluation for uncontrolled and controlled cases as shown graphically in Figure 7.1 and selected as:

- (i) Peak acceleration (ii) Peak displacement

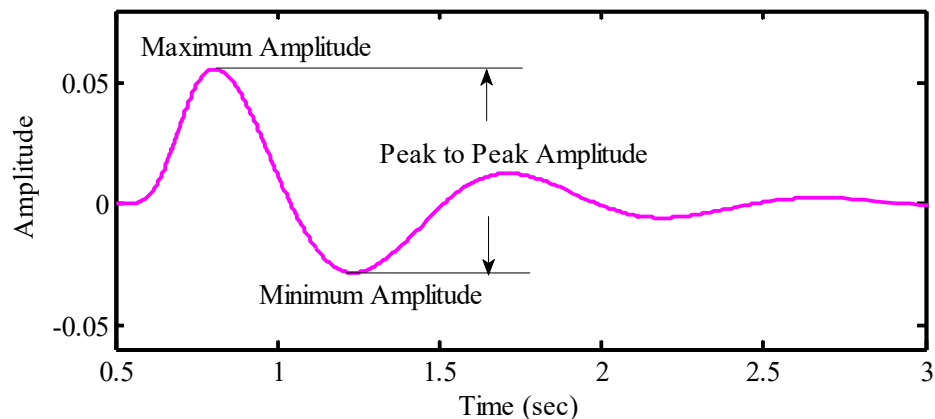


Figure 7.1 Peak / Maximum amplitude

7.2.2 RMS Criterion

It is used in present case for the evaluation and comparison of RMS values related to acceleration and displacement of passenger seat. Seat acceleration in combination with displacement values are the main cause of discomfort to the travelling passengers. These values are calculated using the mathematical term known as root mean square (RMS). RMS values of vertical acceleration (a_{RMS}) and displacement (d_{RMS}) are affected by control strategy chosen in vehicle system for vibration suppression. Taking n as number of variables in time domain from starting time to the final time, RMS values are calculated as follows:

$$a_{RMS} = \sqrt{\frac{1}{n} \sum_{i=1}^n a_i^2} = \sqrt{\frac{a_1^2 + a_2^2 + \dots + a_n^2}{n}} \quad (7.1)$$

$$d_{RMS} = \sqrt{\frac{1}{n} \sum_{i=1}^n d_i^2} = \sqrt{\frac{d_1^2 + d_2^2 + \dots + d_n^2}{n}} \quad (7.2)$$

The mathematical formula used for the calculation of percentage response improvement in vibration control for the uncontrolled and controlled system can be defined below:

$$\text{Improvement (\%)} = \left| \frac{\lambda_{uss} - \lambda_{css}}{\lambda_{uss}} \right| \times 100 \quad (7.3)$$

where:

λ_{uss} = the calculated value with uncontrolled suspension system

λ_{css} = the calculated value with controlled suspension system

7.3 SIMULATION PARAMETERS

In this section, selected parameters related to quarter car model with three degrees of freedom and various controllers are discussed. The four types of road excitations having pulse, bump, sinusoidal and random type are also mentioned. These parameters are used for simulation purpose for comparison of performance of passenger ride comfort in uncontrolled and controlled semi-active quarter car models using MATLAB/ Simulink.

7.3.1 Quarter Car Simulation Parameters

Simulation work in time domain provides valuable data and results for design and selection of optimum system. The simulation work for uncontrolled as well as semi-active quarter car models are obtained by taking simulation time as 4 seconds. The

travelling speed of vehicle was set as 40 km/h during simulation work. The selected parameters of quarter car model for simulation purpose are shown in Table 7.1.

Table 7.1 Parameters of quarter car model for simulation

S. No.	Parameter	Value (Unit)
1	m_1	70 kg
2	m_2	325 kg
3	m_3	40 kg
4	k_p	20000 N/m
5	c_p	1550 N/m/s
6	k_s	8500 N/m
7	c_s	850 N/m/s
8	k_t	180,000 N/m

7.3.2 Controller Parameters

The selected controller parameters for simulation work related to integrated forward controllers i.e. PID controller, Fuzzy controller, HFPID controller and HFPIDCR controller in primary and secondary suspension of quarter car model with three degrees of freedom are shown in Table 7.2 and Table 7.3 respectively.

Table 7.2 Forward controller parameters for primary suspension system

PID Gains		FLC input – output scaling factors
$K_p = 400$	$K_{PI} = 0.1$	$S_e = 2$
$K_I = 500$	$K_{PD} = 2.5$	$S_{de} = 1$
$K_D = 700$	$G_u = 2.5$	$S_u = 550$

Table 7.3 Forward controller parameters for secondary suspension system

PID Gains		FLC input – output scaling factors
$K_p = 50$	$K_{PI} = 0.1$	$S_e = 2$
$K_I = 10$	$K_{PD} = 2.5$	$S_{de} = 1$
$K_D = 500$	$G_u = 2.5$	$S_u = 280$

The developed Simulink models with HFPIDCR controller in present work were compared and validated for the 2-d and 3-d quarter car semi-active/ active models available in literature [118-120] with the same parameters. The simulation results in graphical form in terms of passenger seat response, sprung mass response and

unsprung mass response showed the improved results using developed HFPIDCR controller compared to results available in selected research publications.

7.4 INPUT ROAD EXCITATIONS

The vehicle travels over different types of road profiles during running period with different speeds, having various shape and size. It can generate very uncomfortable and unpleasant ride experience for travelling passengers if the transmitted vibration effects to the passenger seat are not controlled timely while the vehicle passes over it. In present case, different types of road profiles such as pulse road profile, bump road profile, sinusoidal road profile and random road profiles are considered for performance evaluation of the passenger ride comfort and safety taking uncontrolled and controlled quarter car systems into account.

7.4.1 Pulse Road Profile

The pulse road profile as input road surface with 0.05 m amplitude is shown in Figure 7.2.

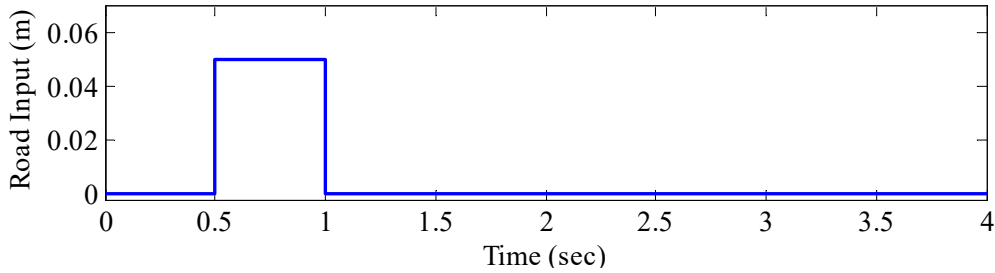


Figure 7.2 Pulse road profile

7.4.2 Bump Road Profile

Bump road input is most commonly encountered profile for travelling vehicles and can be represented by upper positive profile of single sinusoidal curve. It generally acts as a shock input having different height from place to place such as highway road or crowded road as per safety requirements for road walking people. Since it is unpredictable and suddenly comes in the way of running vehicle, giving a very short time for the driver to react, this can be very harmful to the vehicle body and travelling passengers. The bump road profile can be described by Equation 7.3. The bump height 'h' is set to 0.07 m for Simulation work in MATLAB software.

$$z(t) = \begin{cases} \frac{h[1 - \cos(8\pi t)]}{2}, & 0.5 \leq t \leq 0.75 \\ 0, & \text{otherwise} \end{cases} \quad (7.3)$$

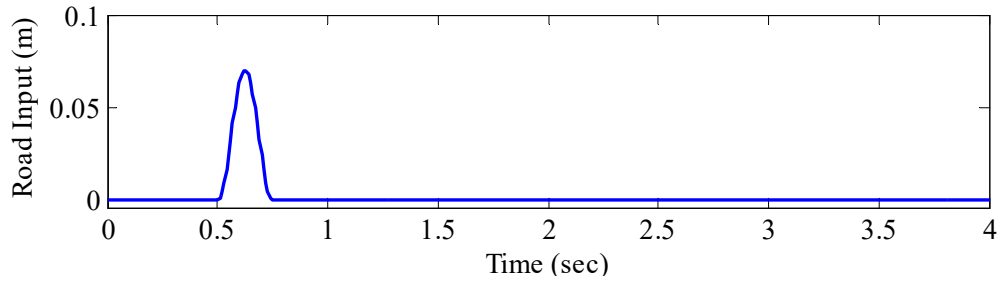


Figure 7.3 Bump road profile

7.4.3 Sinusoidal Road Profile

In present case, road is assumed to be of wavy profile having harmonic waves, approximated by a sinusoidal wave. The selected sinusoidal road profile with 0.03 m amplitude and frequency of 20 rad/sec is shown in Figure 7.4.

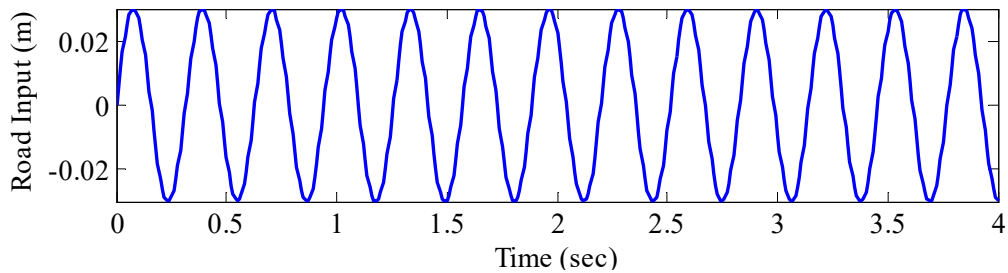


Figure 7.4 Sinusoidal road profile

7.4.4 Random Road Profile

The random road profile as input road surface is shown in Figure 7.5.

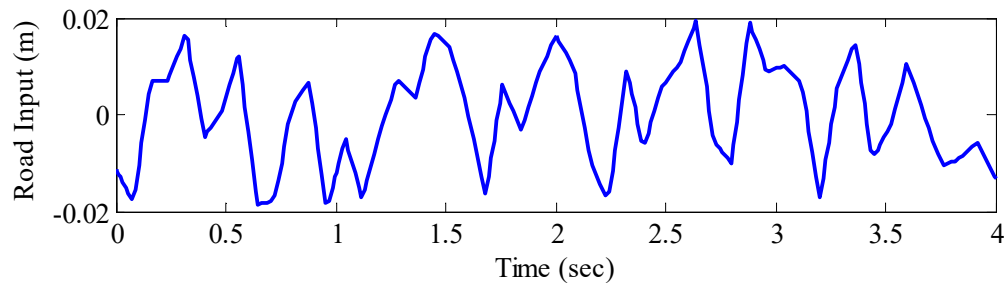


Figure 7.5 Random road profile

7.5 ROBUSTNESS ANALYSIS

In practical situations, parametric uncertainty needs to be studied for understanding the performance of quarter car suspension system. Taking such variable factors into account for evaluating vehicle system performance, it provides support for design and development of realistic and best systems. The objective of following section is to consider the robustness of the controlled semi-active quarter car system integrated

with various controllers, in terms of passenger ride compared to uncontrolled or passive one when vehicle travels with 40 km/hr.

The study about the effect of vehicle mass variation on the passenger ride comfort is crucial from practical point of view in real life. Various parameters responsible for changing the total mass of vehicle system can be mentioned as: loading and unloading of carrying mass and filling up of fuel tank as required etc. The mass of travelling passenger sitting on the seat also varies as different passengers travel from time to time. It is crucial to analyze the performance of vehicle system during such type of situations. The sprung mass, m_2 as well as the passenger mass, m_1 of quarter car model was varied ± 20 % of its selected value. Therefore, following values of sprung mass as well as passenger mass were tested for passenger ride comfort issues:

1. Variation of quarter car sprung mass, m_2 :

- (a) 80 % $m_2 = 260$ kg
- (b) 100 % $m_2 = 325$ kg
- (c) 120 % $m_2 = 390$ kg

2. Variation of passenger mass, m_1 :

- (a) 80 % $m_1 = 56$ kg
- (b) 100 % $m_1 = 70$ kg
- (c) 120 % $m_1 = 84$ kg

7.6 SUMMARY

In this chapter, performance specifications for passenger ride comfort were defined in terms of peak/ maximum and RMS values. Selected quarter car parameters for simulation work with magnitude were written. Finally, four types of road excitations for quarter car model such as pulse input, bump input, sinusoidal input and random input road profiles were also mentioned. Robustness analysis parameters in terms of variation in sprung mass and passenger mass were also considered.

CHAPTER VIII

PRIMARY SUSPENSION CONTROLLED SEMI-ACTIVE QUARTER CAR SYSTEM

8.1 INTRODUCTION

In present case, primary suspension system is assembled with MR shock absorber 1 between unsprung mass and sprung mass. The secondary suspension system is assembled with a passive shock absorber between sprung mass and passenger seat mass. The developed controllers with MR shock absorber 1 in quarter car suspension system are shown in Figure 8.1. During the vibration generation period of travelling quarter car, assembled MR shock absorber 1 and passive shock absorber starts working. Both of the shock absorbers delivers damping force in the suspension system to suppress the uneven road generated vibrations. In the primary suspension system, assembled forward controller 1 generates desired damping force signal, F_{d1} and supplies it to the assembled inverse controller 1. Based on the transfer signals, inverse controller 1 generates current signal I_1 . This generated current signal is supplied to the MR shock absorber 1 for generation of actual damping force in the primary suspension system of the quarter car model.

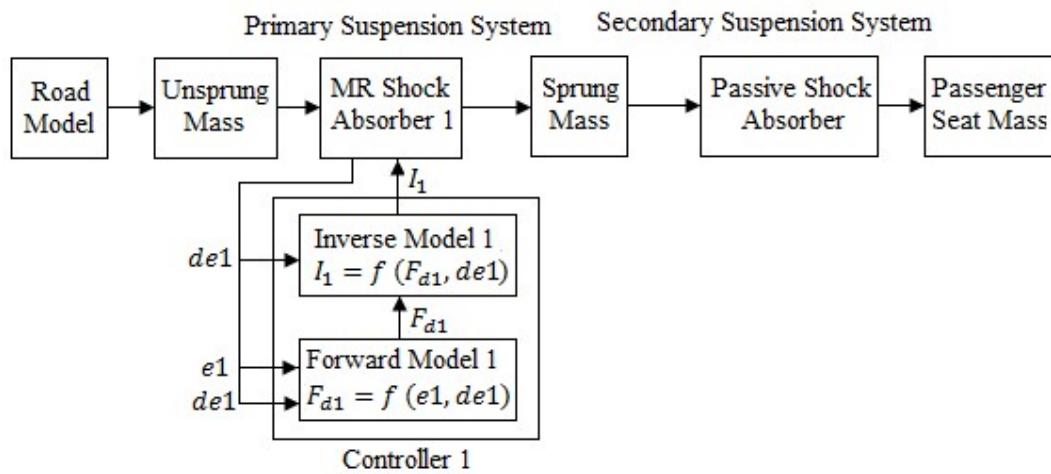


Figure 8.1 Block diagram of primary suspension controlled semi-active quarter car system

8.2 PASSENGER SEAT SIMULATION RESULTS

8.2.1 Pulse Input Disturbance

The simulation responses for uncontrolled and controlled quarter car models related to passenger seat acceleration and displacement are presented in Figure 8.2 (a)-(b)

respectively for $m_2 = 325$ kg and $m_1 = 70$ kg. The pulse road excitation is responsible for vibration generation in the quarter car model during travelling period. The calculated passenger seat acceleration and displacement response in mathematical values using peak and RMS criterion are presented in Table 8.1 and Table 8.2.

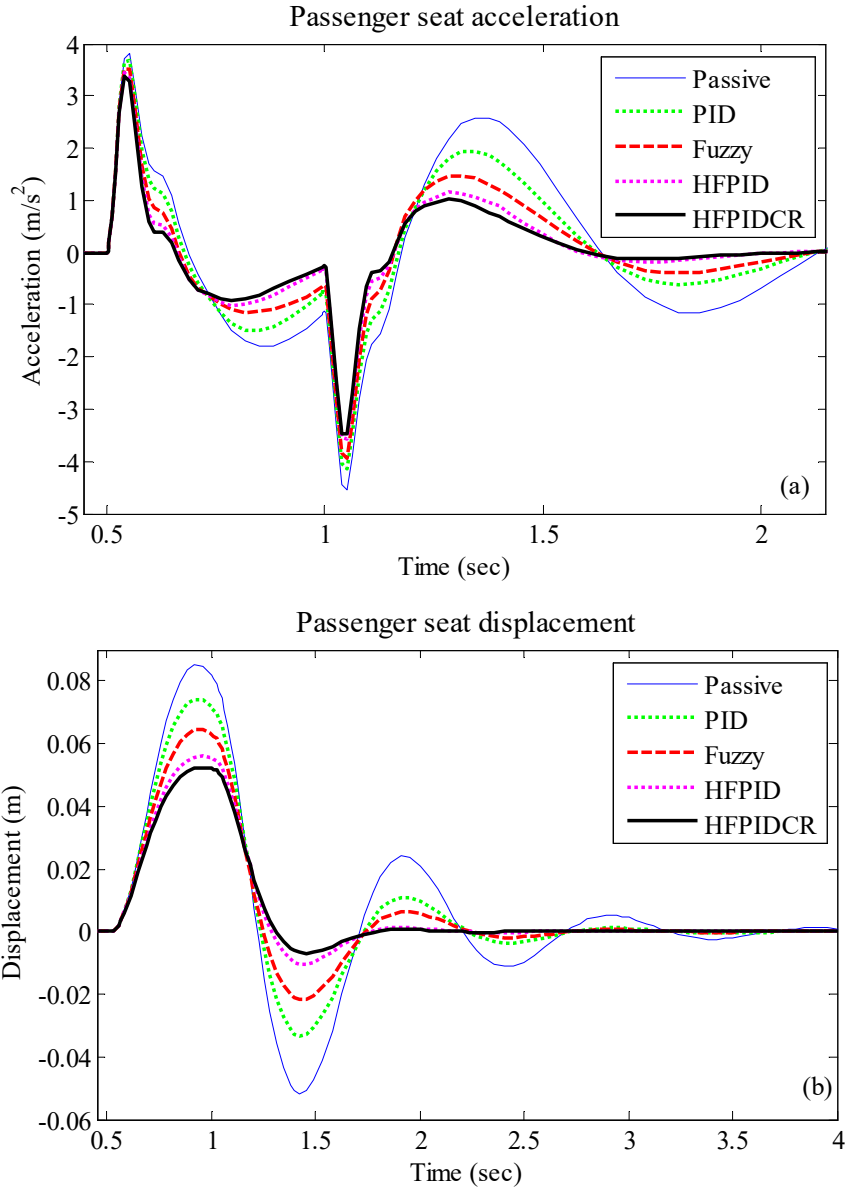


Figure 8.2 (a) Passenger seat acceleration (b) Passenger seat displacement

It can be seen in Figure 8.2 (a)-(b) that the primary suspension controlled semi-active quarter car models worked effectively in controlling the vibration amplitude of passenger seat compared to uncontrolled one.

Table 8.1 Performance comparison of Passenger seat response under Pulse road profile ($m_1 = 70$ kg)

Performance Parameters	Acceleration (m/s^2)				Displacement (m)			
	Max.		RMS		Max.		RMS	
	Magnitude	Improvement %	Magnitude	Improvement %	Magnitude	Improvement %	Magnitude	Improvement %
Controller Type	80% $m_2 = 260$ kg							
Uncontrolled	4.5541	-----	1.3679	-----	0.0842	-----	0.0324	-----
PID	4.4077	3.21	1.1709	14.40	0.0727	13.64	0.0278	14.15
Fuzzy	4.2488	6.70	1.0584	22.63	0.0634	24.66	0.0243	24.91
HFPID	4.0937	10.11	0.9355	31.61	0.0547	35.03	0.0216	33.42
HFPIDCR	4.0076	12.00	0.8936	34.68	0.0513	39.07	0.0204	37.10
Controller Type	100% $m_2 = 325$ kg							
Uncontrolled	3.8608	-----	1.2844	-----	0.0853	-----	0.0333	-----
PID	3.7535	2.78	1.0799	15.92	0.0741	13.21	0.0281	15.55
Fuzzy	3.6154	6.35	0.9571	25.48	0.0644	24.51	0.0243	27.04
HFPID	3.5008	9.32	0.8392	34.66	0.0560	34.43	0.0213	36.09
HFPIDCR	3.4311	11.13	0.7977	37.89	0.0524	38.62	0.0200	39.85
Controller Type	120% $m_2 = 390$ kg							
Uncontrolled	3.2564	-----	1.2030	-----	0.0861	-----	0.0356	-----
PID	3.1509	3.24	1.0098	16.06	0.0751	12.76	0.0301	15.47
Fuzzy	3.0450	6.49	0.8901	26.02	0.0654	23.97	0.0260	27.02
HFPID	2.9805	8.47	0.7757	35.52	0.0569	33.84	0.0227	36.43
HFPIDCR	2.9362	9.83	0.7355	38.86	0.0533	38.03	0.0213	40.31

Table 8.2 Performance comparison of Passenger seat response under Pulse road profile ($m_2 = 325$ kg)

Performance Parameters	Acceleration (m/s^2)				Displacement (m)			
	Max.		RMS		Max.		RMS	
	Magnitude	Improvement %	Magnitude	Improvement %	Magnitude	Improvement %	Magnitude	Improvement %
Controller Type	80% $m_1 = 56$ kg							
Uncontrolled	4.4652	-----	1.3329	-----	0.0839	-----	0.0327	-----
PID	4.3518	2.54	1.1324	15.04	0.0725	13.60	0.0275	15.65
Fuzzy	4.1999	5.94	1.0162	23.76	0.0628	25.21	0.0237	27.34
HFPID	4.0839	8.54	0.9082	31.86	0.0544	35.19	0.0209	35.97
HFPIDCR	4.0096	10.20	0.8703	34.70	0.0509	39.41	0.0197	39.66
Controller Type	100% $m_1 = 70$ kg							
Uncontrolled	3.8608	-----	1.2844	-----	0.0853	-----	0.0333	-----
PID	3.7535	2.78	1.0799	15.92	0.0741	13.21	0.0281	15.55
Fuzzy	3.6154	6.35	0.9571	25.48	0.0644	24.51	0.0243	27.04
HFPID	3.5008	9.32	0.8392	34.66	0.0560	34.43	0.0213	36.09
HFPIDCR	3.4311	11.13	0.7977	37.89	0.0524	38.62	0.0200	39.85
Controller Type	120% $m_1 = 84$ kg							
Uncontrolled	3.3488	-----	1.2343	-----	0.0865	-----	0.0343	-----
PID	3.2230	3.76	1.0311	16.46	0.0753	12.87	0.0291	15.21
Fuzzy	3.0756	8.16	0.9068	26.54	0.0660	23.68	0.0253	26.47
HFPID	2.9941	10.59	0.7828	36.58	0.0573	33.69	0.0220	35.84
HFPIDCR	2.9422	12.14	0.7395	40.09	0.0537	37.87	0.0207	39.66

The performance delivered by HFPIDCR controller 1 controlled suspension system is best in suppressing passenger seat acceleration and displacement responses compared to uncontrolled, PID controller 1, Fuzzy controller 1 and HFPID controller 1 controlled suspension systems. It can be seen from Table 8.1 and Table 8.2 that HFPIDCR controller 1 controlled semi-active quarter car system is best choice to achieve best ride comfort and safety to the travelling passengers.

The desired damping force signals generated by assembled forward controllers in primary suspension system of quarter car model are shown in Figure 8.3. The peak values of desired damping force signals supplied by different forward controllers are presented in Table 8.3. It can be observed that HFPIDCR controller 1 generated highest value of desired damping force signal during compression period as 915.76 N while during the rebound period it was 829.32 N respectively.

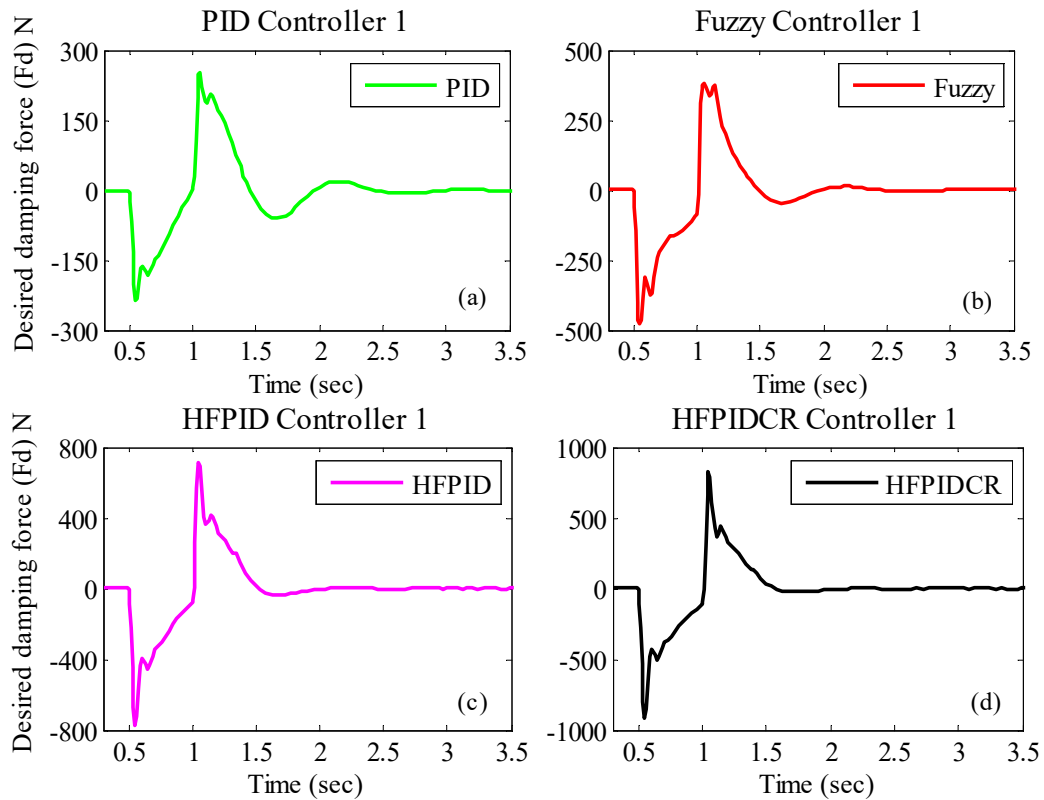


Figure 8.3 Desired damping force signals supplied by different controllers

Table 8.3 Calculated Max. desired damping force using Forward controller 1 (N)

Forward Controller 1	Max. Damping Force (N)			
	PID	Fuzzy	HFPID	HFPIDCR
Compression Stage	237.14	477.24	773.35	915.76
Rebound Stage	252.40	381.16	714.83	829.32

The input current signal generated by different assembled inverse controllers in primary suspension system of quarter car model is shown in Figure 8.4 while its peak values are presented in Table 8.4. It can be seen that the highest value of input current is 0.88 A which is generated by inverse controller with HFPIDCR controller 1.

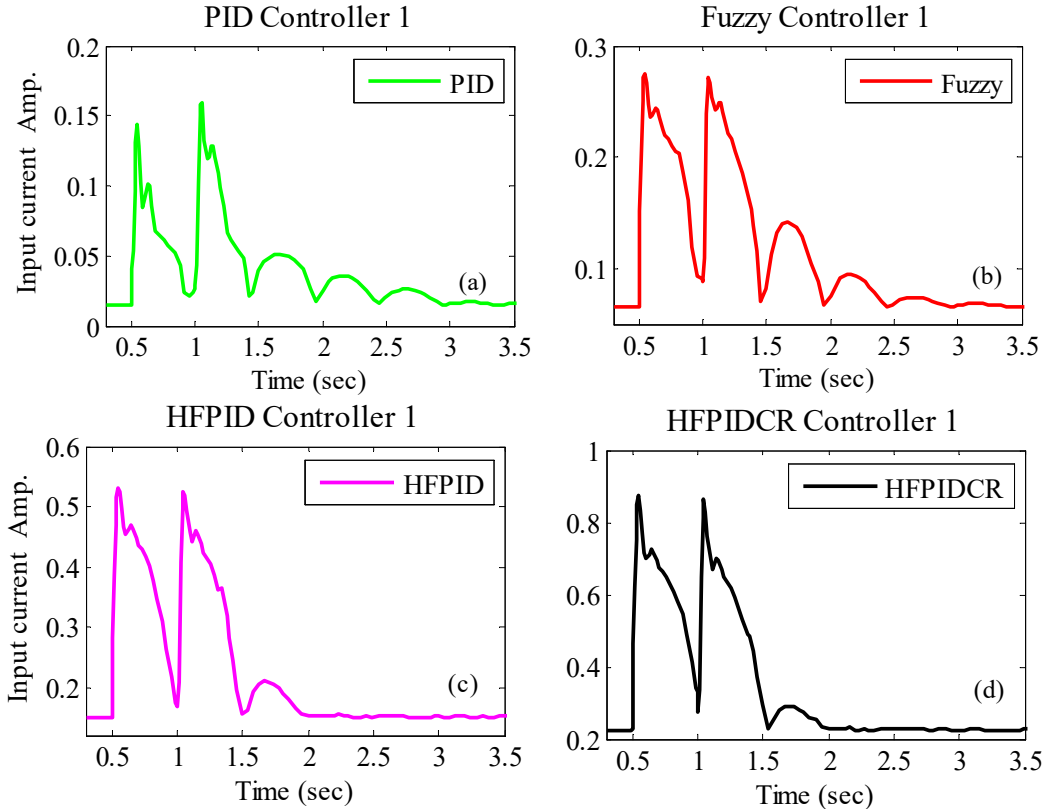


Figure 8.4 Input current signal generated by different controllers

Table 8.4 Calculated Max. input current using Inverse controller 1 (A)

Inverse Controller 1	Max. input current (A)			
	PID	Fuzzy	HFPID	HFPIDCR
Magnitude	0.16	0.28	0.53	0.88

8.2.2 Bump Input Disturbance

The simulation results of passenger seat acceleration and displacement response under bump type of road excitation for uncontrolled and controlled semi-active quarter car systems are shown in Figure 8.5 (a)-(b) for $m_2 = 325$ kg and $m_1 = 70$ kg. The mathematical results in terms of peak and RMS values related to passenger seat response are presented in Table 8.5 and Table 8.6.

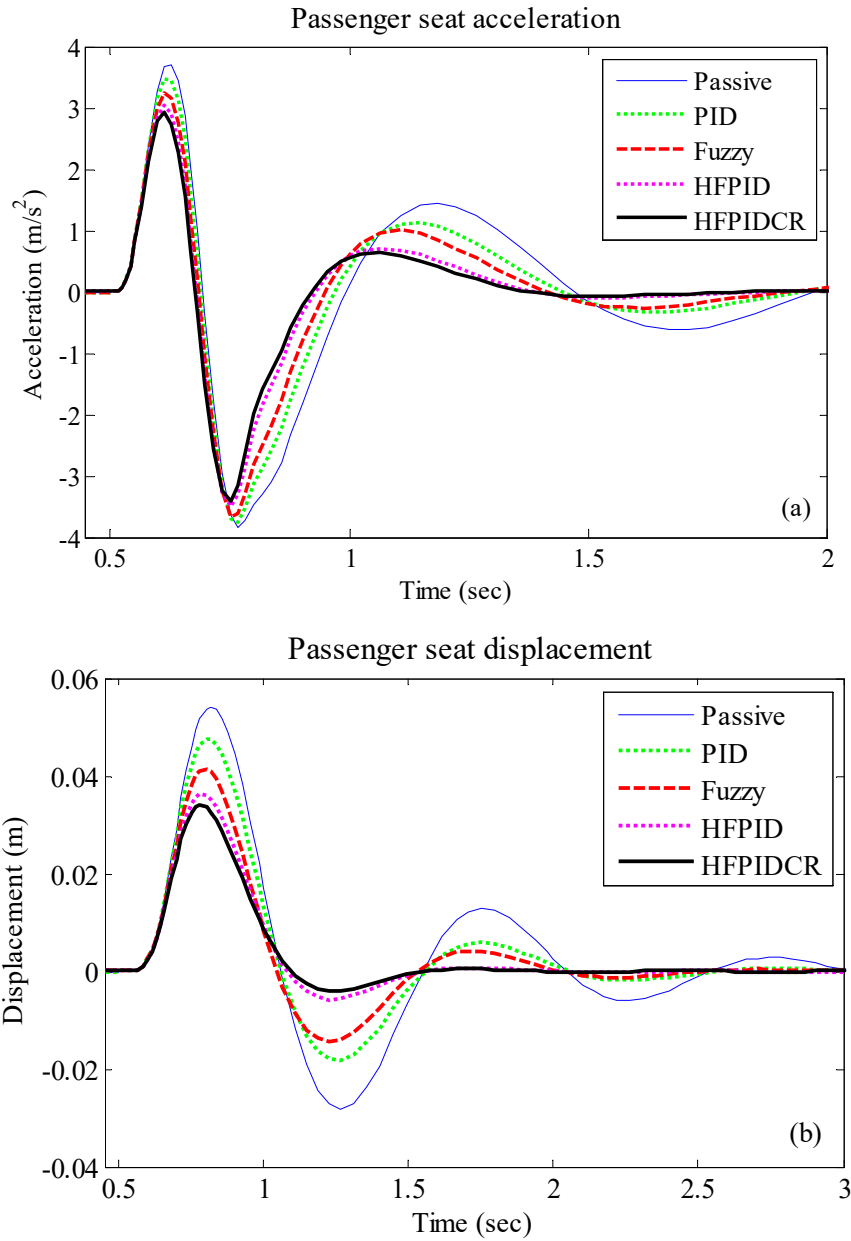


Figure 8.5 (a) Passenger seat acceleration (b) Passenger seat displacement

It can be seen from graphical and tabular results of passenger seat acceleration and displacement response that semi-active suspension system assembled with MR shock absorber in combination with HFPIDCR controller 1 provide best vibration control performance compared to uncontrolled and other semi-active suspension system controlled cases.

Table 8.5 Performance comparison of Passenger seat response under Bump road profile ($m_1 = 70$ kg)

Performance Parameters	Acceleration (m/s^2)				Displacement (m)			
	Max.		RMS		Max.		RMS	
	Magnitude	Improvement %	Magnitude	Improvement %	Magnitude	Improvement %	Magnitude	Improvement %
Controller Type	80% $m_2 = 260$ kg							
Uncontrolled	4.3291	-----	1.4607	-----	0.0574	-----	0.0178	-----
PID	4.0142	7.27	1.3102	10.31	0.0498	13.23	0.0148	16.67
Fuzzy	3.6863	14.85	1.2013	17.76	0.0437	23.82	0.0128	28.19
HFPID	3.3948	21.58	1.0563	27.69	0.0374	34.87	0.0108	39.47
HFPIDCR	3.2647	24.59	0.9994	31.58	0.0348	39.31	0.0100	43.72
Controller Type	100% $m_2 = 325$ kg							
Uncontrolled	3.7298	-----	1.2472	-----	0.0542	-----	0.0172	-----
PID	3.4853	6.55	1.1374	8.81	0.0476	12.19	0.0145	16.09
Fuzzy	3.2222	13.61	1.0545	15.45	0.0414	23.57	0.0124	28.09
HFPID	3.0324	18.70	0.9470	24.07	0.0363	33.07	0.0106	38.34
HFPIDCR	2.9237	21.61	0.9029	27.61	0.0339	37.46	0.0099	42.52
Controller Type	120% $m_2 = 390$ kg							
Uncontrolled	3.2620	-----	1.0873	-----	0.0513	-----	0.0170	-----
PID	3.0810	5.55	1.0003	8.01	0.0455	11.48	0.0143	15.89
Fuzzy	2.8906	11.38	0.9321	14.28	0.0396	22.80	0.0123	27.86
HFPID	2.7329	16.22	0.8508	21.75	0.0351	31.64	0.0105	38.32
HFPIDCR	2.6400	19.07	0.8159	24.96	0.0329	35.87	0.0098	42.44

Table 8.6 Performance comparison of Passenger seat response under Bump road profile ($m_2 = 325$ kg)

Performance Parameters	Acceleration (m/s^2)				Displacement (m)			
	Max.		RMS		Max.		RMS	
	Magnitude	Improvement %	Magnitude	Improvement %	Magnitude	Improvement %	Magnitude	Improvement %
Controller Type	80% $m_1 = 56$ kg							
Uncontrolled	4.1223	-----	1.3039	-----	0.0551	-----	0.0169	-----
PID	3.8606	6.35	1.1910	8.66	0.0485	11.91	0.0140	17.05
Fuzzy	3.5589	13.67	1.1064	15.15	0.0424	23.08	0.0120	29.19
HFPID	3.3693	18.27	0.9995	23.34	0.0372	32.49	0.0102	39.83
HFPIDCR	3.2562	21.01	0.9551	26.75	0.0347	36.93	0.0095	44.00
Controller Type	100% $m_1 = 70$ kg							
Uncontrolled	3.7298	-----	1.2472	-----	0.0542	-----	0.0172	-----
PID	3.4853	6.55	1.1374	8.81	0.0476	12.19	0.0145	16.09
Fuzzy	3.2222	13.61	1.0545	15.45	0.0414	23.57	0.0124	28.09
HFPID	3.0324	18.70	0.9470	24.07	0.0363	33.07	0.0106	38.34
HFPIDCR	2.9237	21.61	0.9029	27.61	0.0339	37.46	0.0099	42.52
Controller Type	120% $m_1 = 84$ kg							
Uncontrolled	3.4023	-----	1.1553	-----	0.0531	-----	0.0171	-----
PID	3.1892	6.26	1.0424	9.77	0.0466	12.32	0.0143	16.31
Fuzzy	2.9450	13.44	0.9585	17.04	0.0405	23.75	0.0123	28.28
HFPID	2.7258	19.88	0.8515	26.29	0.0353	33.54	0.0105	38.79
HFPIDCR	2.6324	22.63	0.8086	30.01	0.0330	37.92	0.0098	42.98

The generated desired damping force signals by forward controllers in primary suspension system of semi-active quarter car model are shown in Figure 8.6 while its highest values are presented in Table 8.7 respectively. It can be seen that the highest values of desired damping force is generated by HFPID controller 1 as 910.80 N during compression stage and 352.87 N during the rebound stage while the quarter car passes over the bump road excitation.

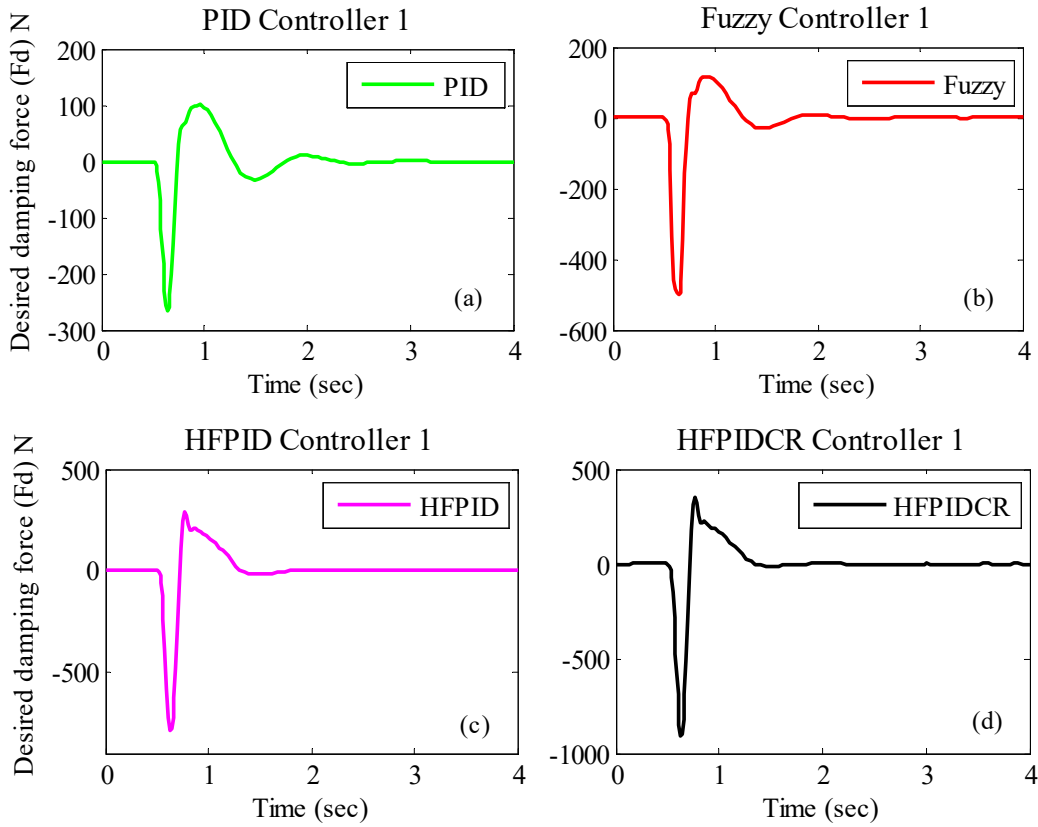


Figure 8.6 Desired damping force signals supplied by different controllers

Table 8.7 Calculated Max. desired damping force using Forward controller 1 (N)

Forward Controller 1	Max. Damping Force (N)			
	PID	Fuzzy	HFPID	HFPIDCR
Compression Stage	266.45	497.76	783.96	910.80
Rebound Stage	100.20	115.81	284.79	352.87

The generated input current signals by inverse controllers in graphical and mathematical value can be seen in Figure 8.7 and Table 8.8 respectively. The graphical and tabular results show the maximum input current is generated by inverse controller having HFPIDCR controller 1 as forward controller, having the amplitude of 0.87 A.

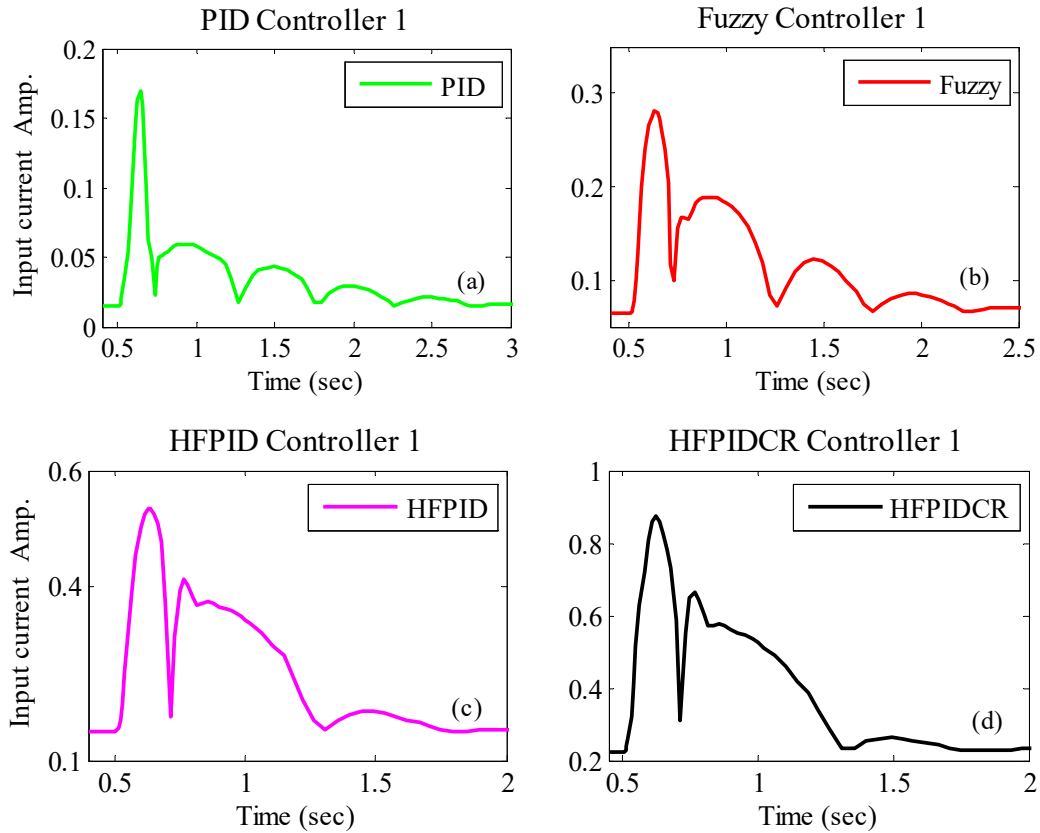


Figure 8.7 Input current signal generated by different controllers

Table 8.8 Calculated Max. input current using Inverse controller 1 (A)

Inverse Controller 1	Max. input current (A)			
	PID	Fuzzy	HFPID	HFPIDCR
Magnitude	0.17	0.28	0.54	0.87

8.2.3 Sinusoidal Input Disturbance

The simulation results for passenger seat acceleration and displacement response under sinusoidal road excitation for the uncontrolled and controlled quarter car systems are shown in Figure 8.8 (a) - (b) for $m_2 = 325$ kg and $m_1 = 70$ kg while mathematical values are given in Table 8.9 and Table 8.10.

It can be finalized from graphical and mathematical values that all the semi-active quarter car models provides better performance compared to uncontrolled one in controlling passenger seat vibrations. It can also be seen that semi-active quarter car model having MR shock absorber 1 in primary suspension system in combination with HFPIDCR controller 1 provides best results related to ride comfort and safety of travelling passengers.

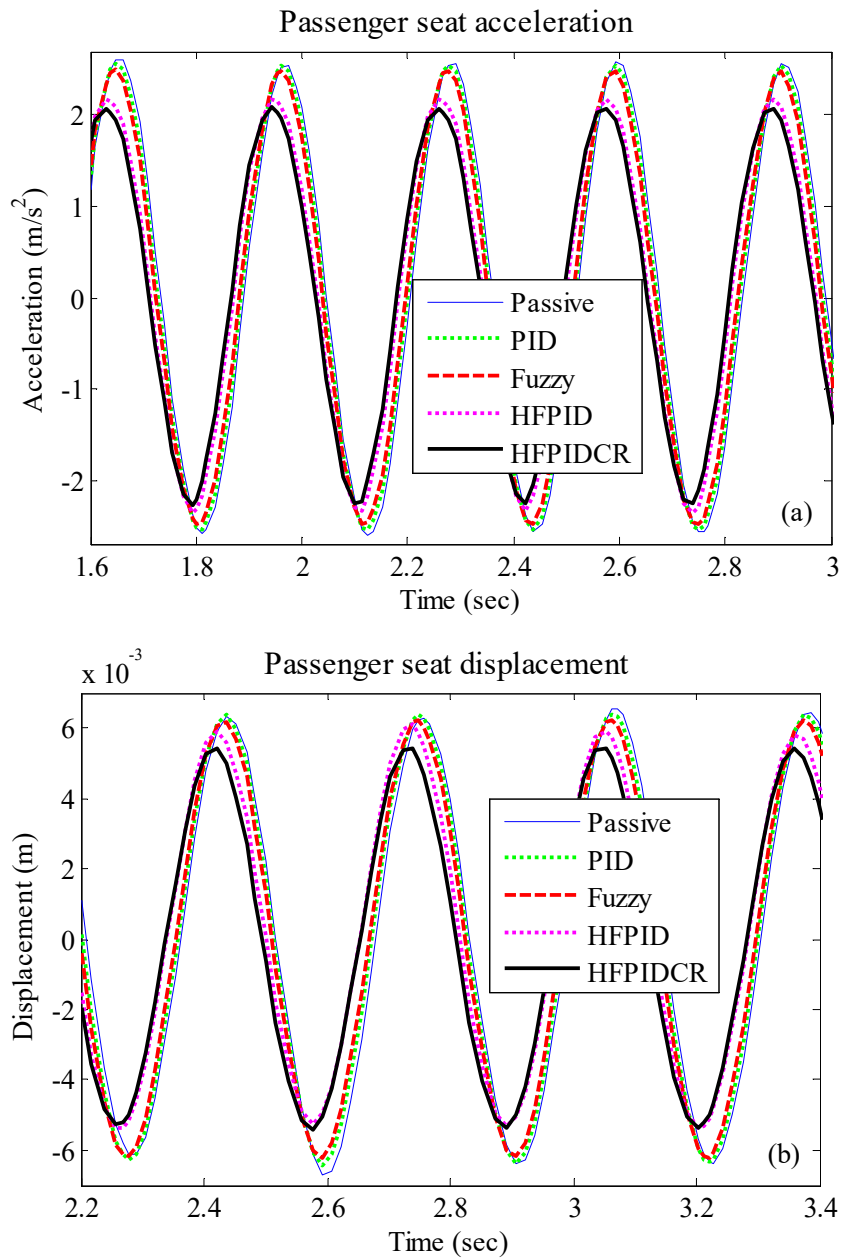


Figure 8.8 (a) Passenger seat acceleration (b) Passenger seat displacement

It can be seen from Figure 8.9 and Figure 8.10 that the desired damping force signals generated by forward controllers and input current signals generated by inverse controllers are continuous while the vehicle travels over the sinusoidal road profile. Table 8.11 shows the highest values of desired damping force generated by each controller in primary suspension system.

Table 8.9 Performance comparison of Passenger seat response under Sinusoidal road profile ($m_1 = 70$ kg)

Performance Parameters	Acceleration (m/s^2)				Displacement (m)			
	Max.		RMS		Max.		RMS	
	Magnitude	Improvement %	Magnitude	Improvement %	Magnitude	Improvement %	Magnitude	Improvement %
Controller Type	80% $m_2 = 269$ kg							
Uncontrolled	3.4765	-----	2.4832	-----	0.0187	-----	0.0070	-----
PID	3.3704	3.05	2.4101	2.94	0.0166	11.00	0.0065	6.05
Fuzzy	3.1644	8.98	2.2752	8.37	0.0150	19.92	0.0061	12.67
HFPID	2.6136	24.82	1.9361	22.03	0.0128	31.28	0.0052	25.69
HFPIDCR	2.4466	29.63	1.8098	27.12	0.0120	35.53	0.0048	30.74
Controller Type	100% $m_2 = 325$ kg							
Uncontrolled	2.7350	-----	1.9321	-----	0.0169	-----	0.0055	-----
PID	2.7204	0.54	1.9024	1.54	0.0153	9.75	0.0052	5.74
Fuzzy	2.6514	3.06	1.8504	4.23	0.0142	16.41	0.0050	10.02
HFPID	2.3445	14.28	1.6535	14.42	0.0121	28.60	0.0044	20.71
HFPIDCR	2.2348	18.29	1.5761	18.43	0.0114	32.61	0.0042	24.82
Controller Type	120% $m_2 = 390$ kg							
Uncontrolled	2.3195	-----	1.6170	-----	0.0155	-----	0.0049	-----
PID	2.2383	3.50	1.6033	0.85	0.0141	8.84	0.0046	6.24
Fuzzy	2.2328	3.74	1.5793	2.33	0.0133	14.19	0.0044	9.60
HFPID	2.0796	10.34	1.4578	9.85	0.0114	26.37	0.0039	18.81
HFPIDCR	2.0030	13.64	1.4058	13.06	0.0108	30.19	0.0038	22.17

Table 8.10 Performance comparison of Passenger seat response under Sinusoidal road profile ($m_2 = 325$ kg)

Performance Parameters	Acceleration (m/s^2)				Displacement (m)			
	Max.		RMS		Max.		RMS	
	Magnitude	Improvement %	Magnitude	Improvement %	Magnitude	Improvement %	Magnitude	Improvement %
Controller Type	80% $m_1 = 56$ kg							
Uncontrolled	3.1733	-----	2.2499	-----	0.0178	-----	0.0064	-----
PID	3.1616	0.37	2.2088	1.82	0.0161	10.00	0.0060	5.38
Fuzzy	3.0839	2.82	2.1453	4.65	0.0148	16.87	0.0058	9.73
HFPID	2.7890	12.11	1.9063	15.27	0.0128	28.29	0.0050	21.05
HFPIDCR	2.6618	16.12	1.8169	19.24	0.0121	32.40	0.0048	25.26
Controller Type	100% $m_1 = 70$ kg							
Uncontrolled	2.7350	-----	1.9321	-----	0.0169	-----	0.0055	-----
PID	2.7204	0.54	1.9024	1.54	0.0153	9.75	0.0052	5.74
Fuzzy	2.6514	3.06	1.8504	4.23	0.0142	16.41	0.0050	10.02
HFPID	2.3445	14.28	1.6535	14.42	0.0121	28.60	0.0044	20.71
HFPIDCR	2.2348	18.29	1.5761	18.43	0.0114	32.61	0.0042	24.82
Controller Type	120% $m_1 = 84$ kg							
Uncontrolled	2.4032	-----	1.7175	-----	0.0161	-----	0.0053	-----
PID	2.3351	2.83	1.6956	1.28	0.0145	9.77	0.0049	6.81
Fuzzy	2.2816	5.06	1.6511	3.86	0.0135	16.28	0.0047	11.62
HFPID	2.0185	16.01	1.4781	13.94	0.0114	28.94	0.0041	22.73
HFPIDCR	1.9155	20.29	1.4087	17.98	0.0108	32.89	0.0039	26.77

The highest value of desired damping force was generated by HFPIDCR controller 1 among all the assembled controllers, which is 669.8 N during the compression stage and 878.66 N during the rebound stage.

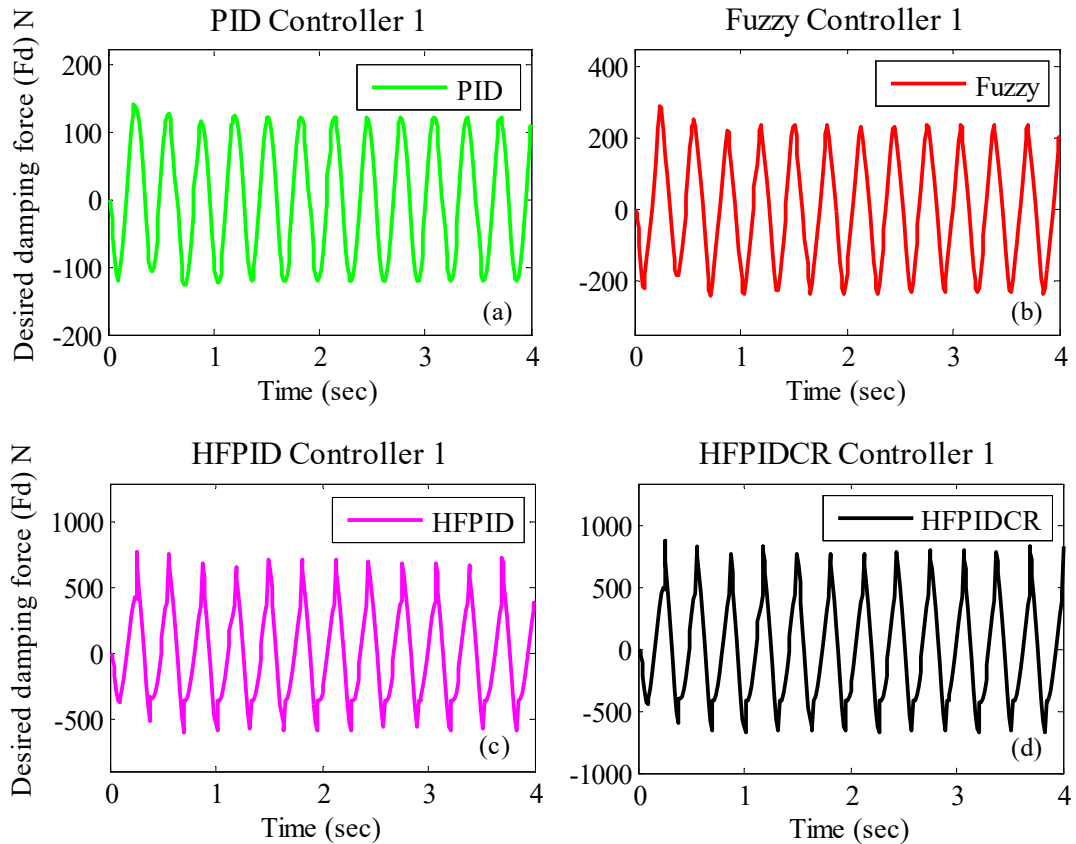


Figure 8.9 Desired damping force signals supplied by different controllers

Table 8.11 Calculated Max. desired damping force using Forward controller 1 (N)

Forward Controller 1	Max. Damping Force (N)			
	PID	Fuzzy	HFPID	HFPIDCR
Compression Stage	125.80	242.25	600.57	669.80
Rebound Stage	139.77	288.79	780.52	878.66

Figure 8.10 and Table 8.12 shows the current signals generated by inverse controllers and highest values of current signals generated by inverse controllers in primary suspension system of quarter car model. It can be seen from Table 8.12 that inverse controller with HFPIDCR controller 1 produced maximum current signal of 0.81 A.

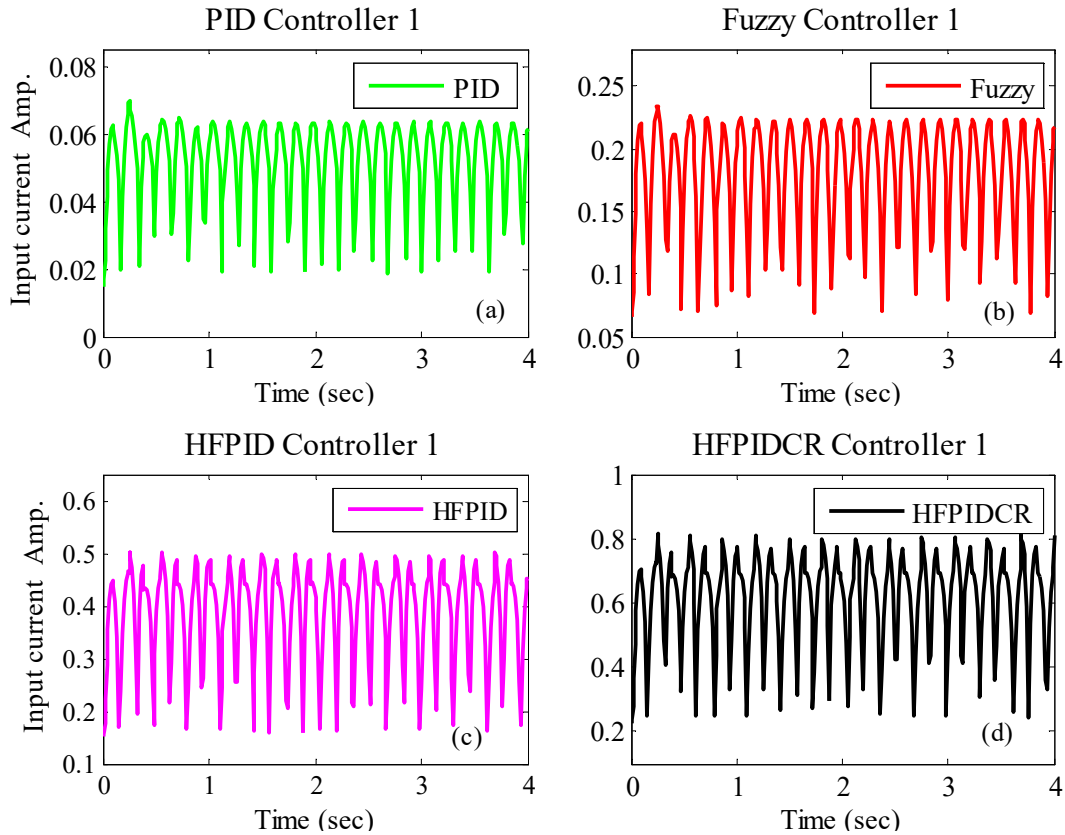


Figure 8.10 Input current signal generated by different controllers

Table 8.12 Calculated Max. input current using Inverse controller 1 (A)

Inverse Controller 1	Max. input current (A)			
	PID	Fuzzy	HFPID	HFPIDCR
Magnitude	0.07	0.23	0.50	0.81

8.2.4 Random Input Disturbance

The simulation response under random road excitation related to passenger seat vibration control responses are shown in Figure 8.11 for $m_2 = 325$ kg and $m_1 = 70$ kg. The calculated mathematical values are presented in Table 8.13 and Table 8.14. Based on the graphical and mathematical results, it can be observed that controlled semi-active quarter car models provide improved response compared to uncontrolled one. Finally, the MR shock absorber 1 in combination with HFPIDCR controller 1 provide best results in terms of passenger seat acceleration and displacement vibration suppression.

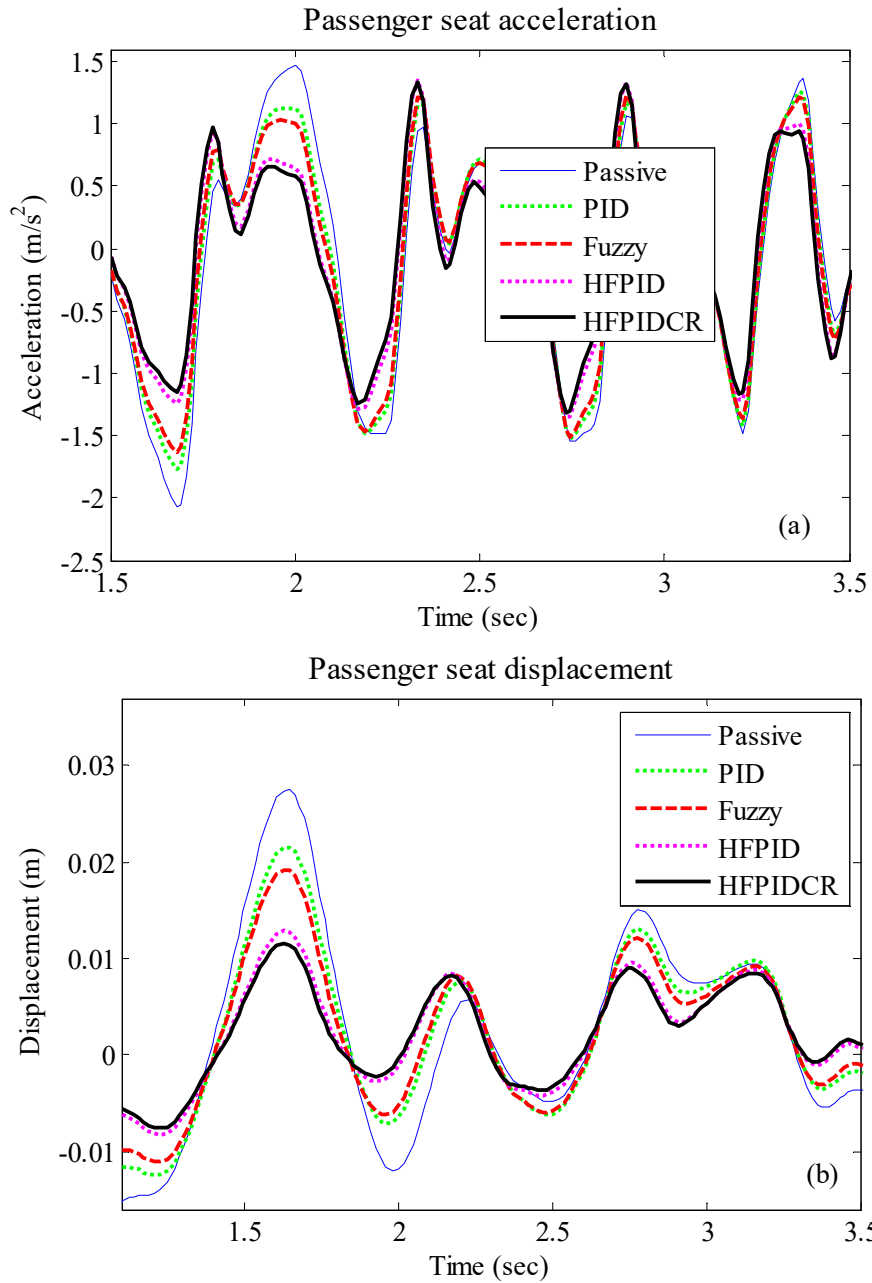


Figure 8.11 (a) Passenger seat acceleration (b) Passenger seat displacement

It can be seen from Figure 8.12 and Figure 8.13 that the desired damping force signals generated by forward controllers and input current signals generated by inverse controllers are continuous while the vehicle travels over the sinusoidal road profile. Table 8.15 shows the highest values of desired damping force generated by each controller in primary suspension system.

Table 8.13 Performance comparison of Passenger seat response under Random road profile ($m_1 = 70$ kg)

Performance Parameters	Acceleration (m/s ²)				Displacement (m)			
	Max.		RMS		Max.		RMS	
	Magnitude	Improvement %	Magnitude	Improvement %	Magnitude	Improvement %	Magnitude	Improvement %
Controller Type	80% $m_2 = 260$ kg							
Uncontrolled	1.8803	-----	1.0206	-----	0.0262	-----	0.0101	-----
PID	1.7212	8.46	0.9322	8.66	0.0212	19.22	0.0083	17.72
Fuzzy	1.6462	12.45	0.8914	12.66	0.0189	28.05	0.0075	25.90
HFPID	1.6007	14.87	0.7473	26.78	0.0128	51.23	0.0053	47.22
HFPIDCR	1.5735	16.31	0.7102	30.42	0.0115	56.09	0.0049	51.42
Controller Type	100% $m_2 = 325$ kg							
Uncontrolled	1.5311	-----	0.8625	-----	0.0274	-----	0.0100	-----
PID	1.3849	9.55	0.7949	7.83	0.0216	21.34	0.0081	18.44
Fuzzy	1.3580	11.31	0.7667	11.11	0.0192	30.15	0.0073	26.45
HFPID	1.3020	14.96	0.6574	23.78	0.0128	53.41	0.0052	47.57
HFPIDCR	1.2993	15.13	0.6296	27.01	0.0115	58.11	0.0048	51.68
Controller Type	120% $m_2 = 390$ kg							
Uncontrolled	1.2896	-----	0.7364	-----	0.0279	-----	0.0101	-----
PID	1.1646	9.69	0.6859	6.86	0.0217	22.30	0.0081	19.43
Fuzzy	1.1324	12.19	0.6665	9.49	0.0193	30.91	0.0073	27.42
HFPID	1.0882	15.61	0.5827	20.87	0.0127	54.42	0.0052	48.44
HFPIDCR	1.1022	14.53	0.5610	23.81	0.0114	59.07	0.0048	52.52

Table 8.14 Performance comparison of Passenger seat response under Random road profile ($m_2 = 325$ kg)

Performance Parameters	Acceleration (m/s^2)				Displacement (m)			
	Max.		RMS		Max.		RMS	
	Magnitude	Improvement %	Magnitude	Improvement %	Magnitude	Improvement %	Magnitude	Improvement %
Controller Type	80% $m_1 = 56$ kg							
Uncontrolled	1.6697		0.9562		0.0268	-----	0.0098	
PID	1.6055	3.85	0.8932	6.59	0.0212	20.80	0.0081	17.71
Fuzzy	1.5774	5.53	0.8657	9.46	0.0188	29.63	0.0073	25.46
HFPID	1.5500	7.17	0.7567	20.86	0.0127	52.70	0.0053	46.34
HFPIDCR	1.4300	14.36	0.7267	24.00	0.0114	57.38	0.0048	50.58
Controller Type	100% $m_1 = 70$ kg							
Uncontrolled	1.5311	-----	0.8625	-----	0.0274	-----	0.0100	-----
PID	1.3849	9.55	0.7949	7.83	0.0216	21.34	0.0081	18.44
Fuzzy	1.3580	11.31	0.7667	11.11	0.0192	30.15	0.0073	26.45
HFPID	1.3020	14.96	0.6574	23.78	0.0128	53.41	0.0052	47.57
HFPIDCR	1.2993	15.13	0.6296	27.01	0.0115	58.11	0.0048	51.68
Controller Type	120% $m_1 = 84$ kg							
Uncontrolled	1.4184	-----	0.7896		0.0280	-----	0.0102	
PID	1.2594	11.21	0.7221	8.55	0.0220	21.53	0.0083	18.76
Fuzzy	1.1961	15.67	0.6946	12.03	0.0195	30.14	0.0074	26.91
HFPID	1.0856	23.46	0.5866	25.70	0.0130	53.64	0.0053	48.13
HFPIDCR	1.0763	24.12	0.5591	29.19	0.0117	58.36	0.0049	52.29

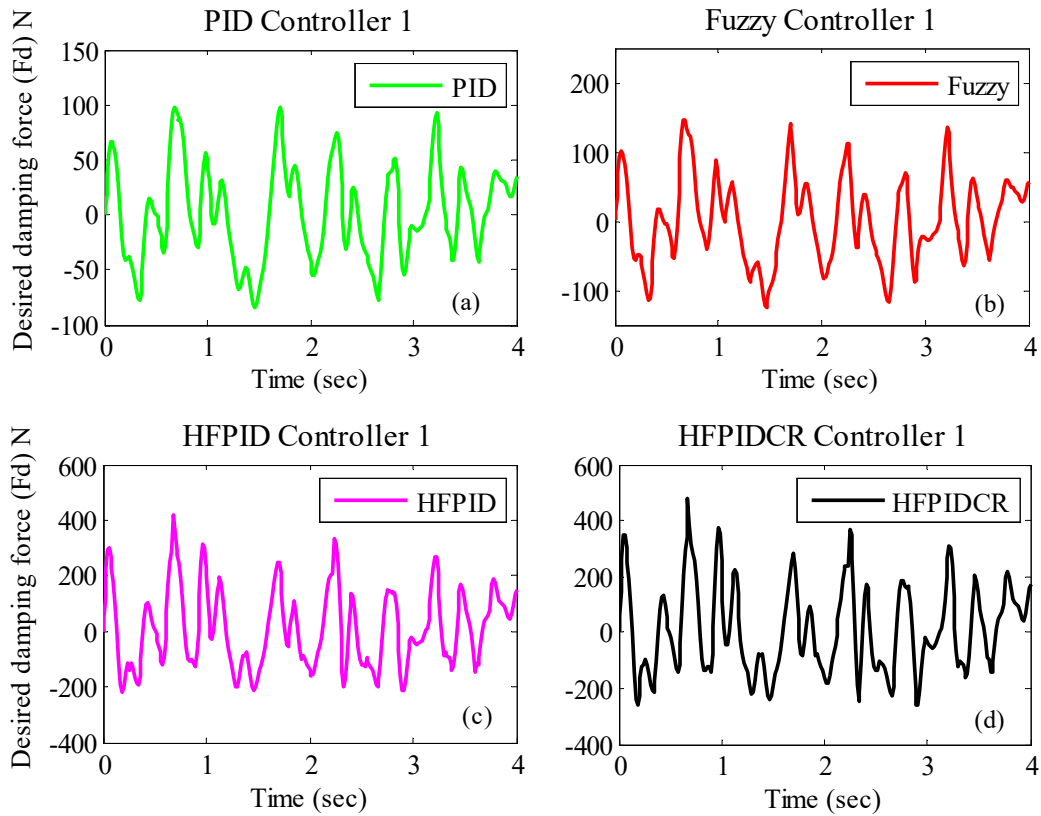


Figure 8.12 Desired damping force signals supplied by different controllers

The highest value of desired damping force is generated by HFPIDCR controller 1 among all the assembled controllers, which is 262.70 N during the compression stage and 477.53 N during the rebound stage.

Table 8.15 Calculated Max. desired damping force using Forward controller 1 (N)

Forward Controller 1	Max. Damping Force (N)			
	PID	Fuzzy	HFPID	HFPIDCR
Compression Stage	84.91	124.37	220.35	262.70
Rebound Stage	97.88	147.17	418.57	477.53

Figure 8.13 and Table 8.16 shows the current signals generated by inverse controllers and highest values of current signals generated by inverse controllers in primary suspension system of quarter car model. It can be seen from Table 8.16 that inverse controller with HFPIDCR controller 1 produces maximum current signal of 0.72 A.

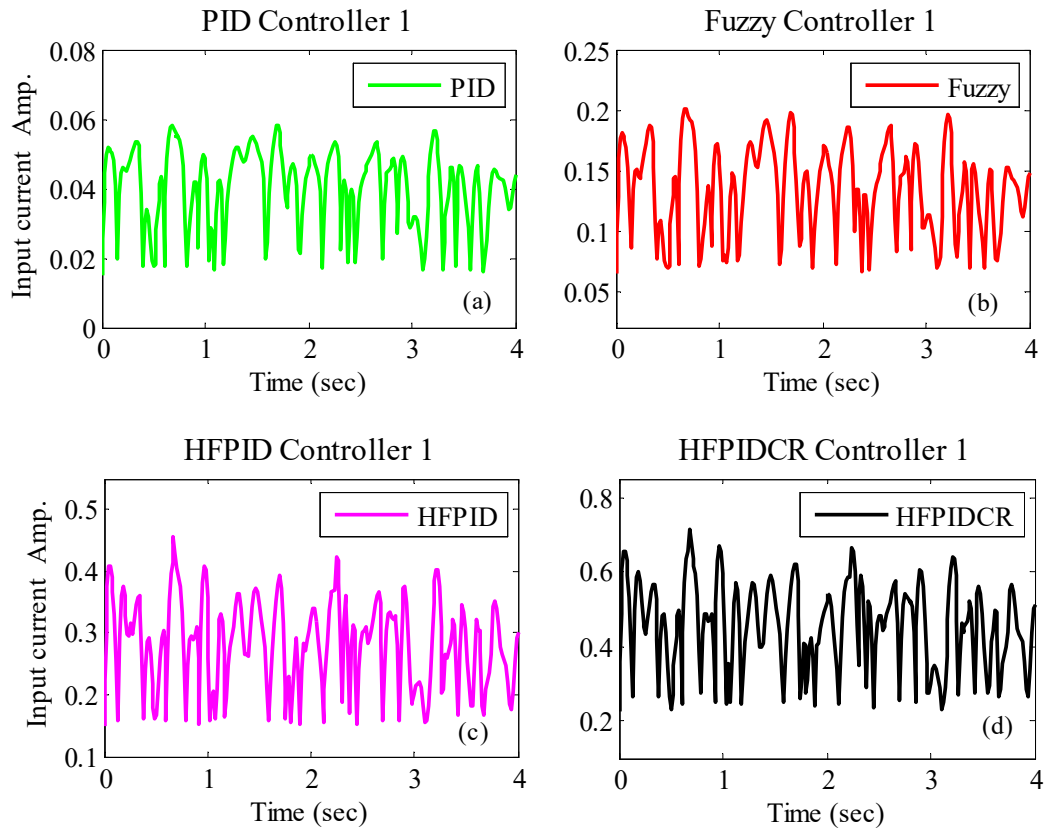


Figure 8.13 Input current signal generated by different controllers

Table 8.16 Calculated Max. input current using Inverse controller 1 (A)

Inverse Controller 1	Max. input current (A)			
	PID	Fuzzy	HFPID	HFPIDCR
Magnitude	0.06	0.20	0.46	0.72

8.3 SPRUNG MASS SIMULATION RESULTS

The simulation results of sprung mass acceleration and displacement response for pulse, bump, sinusoidal and random road input profile are shown in Figure 8.14 to Figure 8.17 respectively. The mathematical results in terms of peak and RMS values for passenger seat response for selected road profiles are shown in Table 8.17.

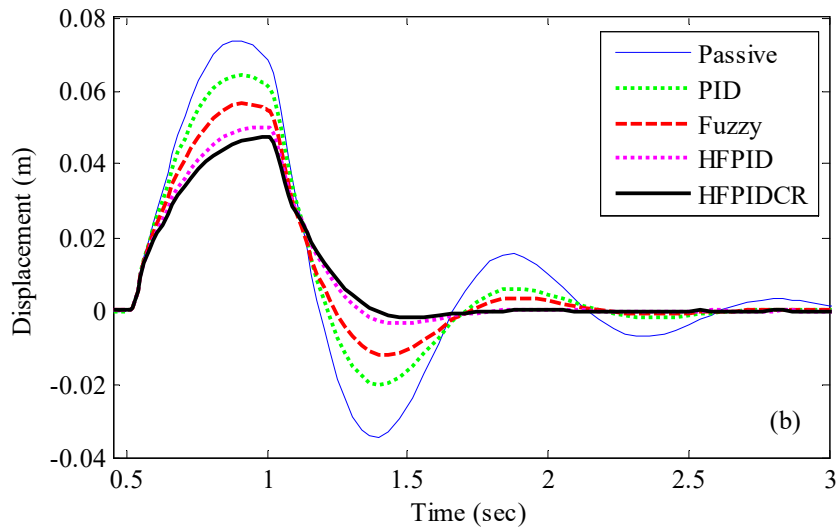
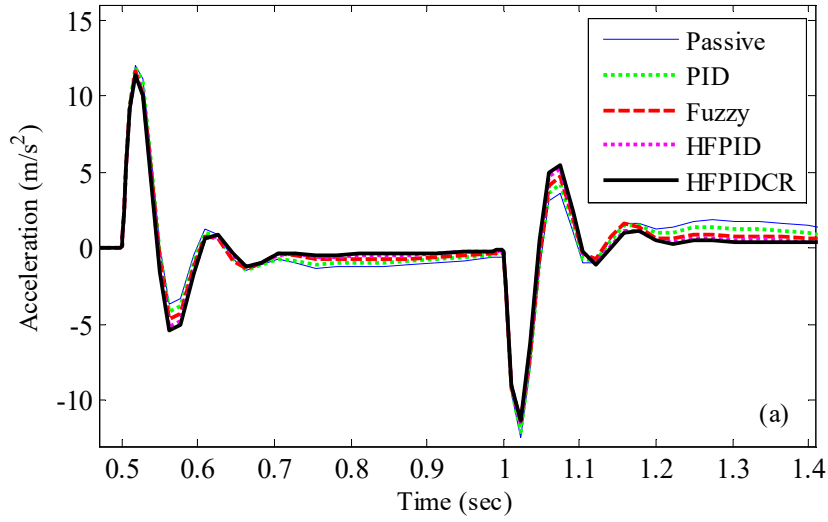
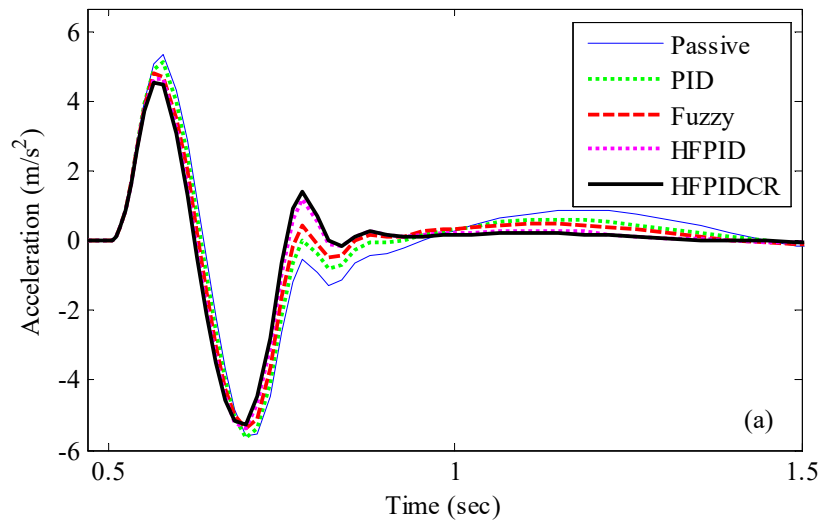


Figure 8.14 Sprung mass response under pulse road input (a) Acceleration (b) Displacement



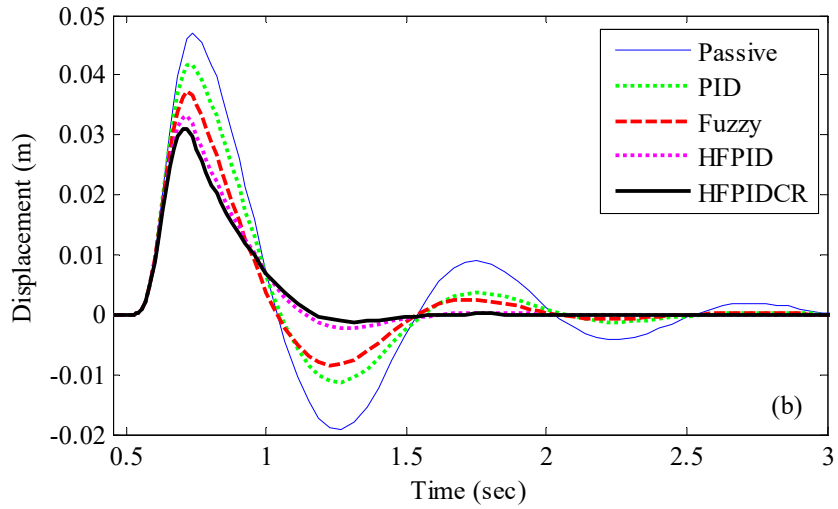


Figure 8.15 Sprung mass response under bump road input (a) Acceleration (b) Displacement

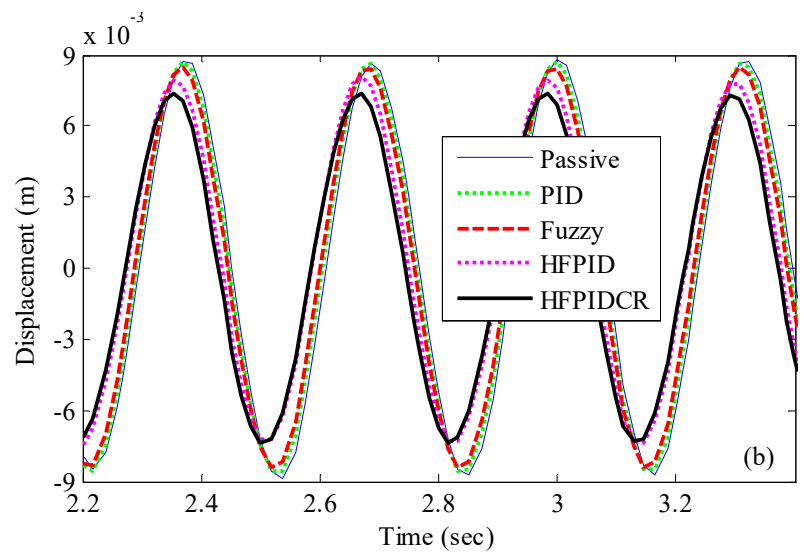
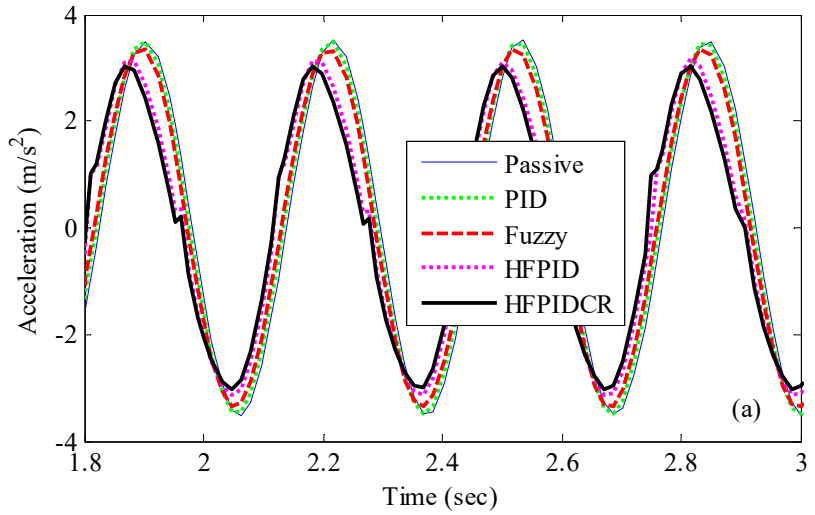


Figure 8.16 Sprung mass response under sinusoidal road input (a) Acceleration (b) Displacement

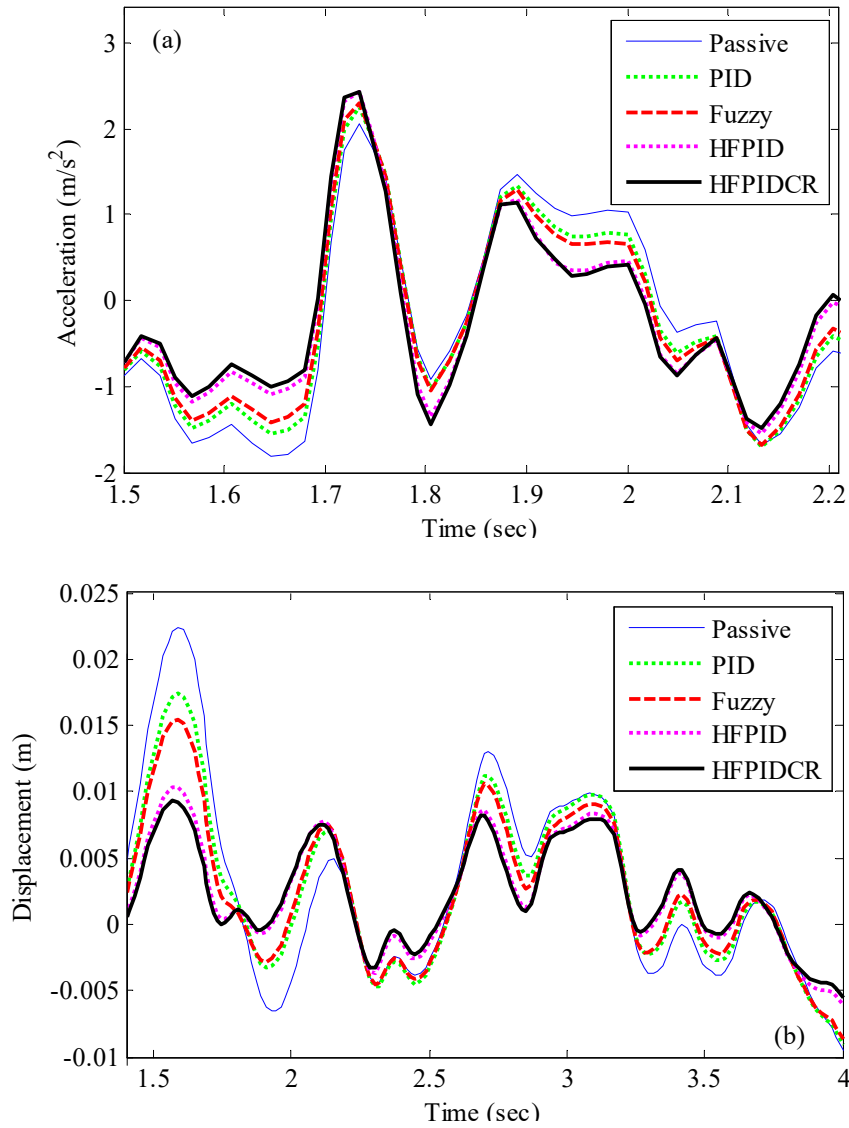


Figure 8.17 Sprung mass response under random road input (a) Acceleration (b) Displacement

Table 8.17 Performance comparison of Sprung mass response ($m_1 = 70$ kg, $m_2 = 325$ kg, $m_3 = 40$ kg)

Controller Type	Acceleration (m/s ²)				Displacement (m)			
	Max.		RMS		Max.		RMS	
	Magnitude	Improvement %	Magnitude	Improvement %	Magnitude	Improvement %	Magnitude	Improvement %
Pulse road profile								
Uncontrolled	12.1845	-----	2.5766	-----	0.0740	-----	0.0299	-----
PID	11.8096	3.08	2.3445	9.01	0.0643	13.00	0.0249	16.73
Fuzzy	11.6044	4.76	2.2763	11.65	0.0565	23.58	0.0219	26.86
HFPIID	11.4312	6.18	2.2768	11.63	0.0501	32.26	0.0198	33.84
HFPIIDCR	11.3237	7.07	2.2663	12.04	0.0476	35.64	0.0188	37.22
Bump road profile								
Uncontrolled	5.4038	-----	1.4669	-----	0.0469	-----	0.0154	-----
PID	5.1597	4.52	1.3882	5.36	0.0418	10.83	0.0130	15.54
Fuzzy	4.8095	11.00	1.3225	9.84	0.0373	20.58	0.0112	27.58
HFPIID	4.6610	13.75	1.2999	11.39	0.0331	29.47	0.0098	36.37
HFPIIDCR	4.5751	15.34	1.2777	12.90	0.0310	33.83	0.0092	40.42
Sinusoidal road profile								
Uncontrolled	3.6476	-----	2.4159	-----	0.0166	-----	0.0064	-----
PID	3.5732	2.04	2.3179	4.06	0.0152	8.66	0.0060	5.84
Fuzzy	3.4090	6.54	2.2426	7.17	0.0141	15.01	0.0058	9.35
HFPIID	3.2815	10.04	2.1011	13.03	0.0124	25.44	0.0053	17.82

Table 8.17 Performance comparison of Sprung mass response ($m_1 = 70$ kg, $m_2 = 325$ kg, $m_3 = 40$ kg)								
Random road profile								
Uncontrolled	2.5499	-----	1.1746	-----	0.0224	-----	0.0083	-----
PID	2.6253	-2.96	1.1651	0.81	0.0174	22.24	0.0069	16.76
Fuzzy	2.6270	-3.02	1.1460	2.43	0.0155	30.92	0.0063	24.51
HFPIID	2.6788	-5.06	1.1305	3.75	0.0103	53.89	0.0046	44.15
HFPIIDCR	2.6373	-3.42	1.1223	4.45	0.0093	58.50	0.0043	48.02

8.4 SUMMARY

In present case, vertical response of passenger seat vibrations are studied at the 40 km/h running speed of quarter car model with three degrees of freedom under pulse, bump, sinusoidal and random road profiles. Simulation results in terms of passenger seat acceleration and displacement response showed the effectiveness of semi-active controlled quarter car system compared to uncontrolled one. The MR shock absorber 1 assembled with HFPIIDCR controller 1 was most effective in vibration control of passenger seat compared to uncontrolled, PID controller 1, Fuzzy controller 1, HFPIID controller 1 and HFPIIDCR controller 1 controlled suspension systems. The desired damping force signals generated by forward controllers and input current to be supplied to MR shock absorber 1 as generated by inverse controllers were maximum for suspension system assembled with HFPIID controller 1. The generated peak values of input current by inverse controllers in each case of travelling quarter car model under pulse, bump, sinusoidal and random road profile remained below 1 A in primary suspension system. Thus, resulting into lower power consumption by inverse controllers for working of MR shock absorber 1.

CHAPTER IX

SECONDARY SUSPENSION CONTROLLED SEMI-ACTIVE QUARTER CAR SYSTEM

9.1 INTRODUCTION

Here, quarter car model is having two shock absorbers for vibration control of passenger seat as well as suspension system. Passive shock absorber is assembled in primary suspension system i.e. between unsprung mass and sprung mass. The developed controller with MR shock absorber 2 is assembled in secondary suspension system i.e. between sprung mass and passenger seat mass as shown in Figure 9.1.

During the quarter car travelling period, assembled passive as well as MR shock absorber 2 reacts and starts delivering damping force to control the road induced vibrations. In the secondary suspension system, assembled forward controller 2 generates desired damping force signal, F_{d2} and supplies it to the inverse controller 2. Inverse controller 2 is responsible for the generation and supply of current to the MR shock absorber 2. The supplied current, I_2 to MR shock absorber 2 generates the actual damping force in the secondary suspension system of the quarter car model.

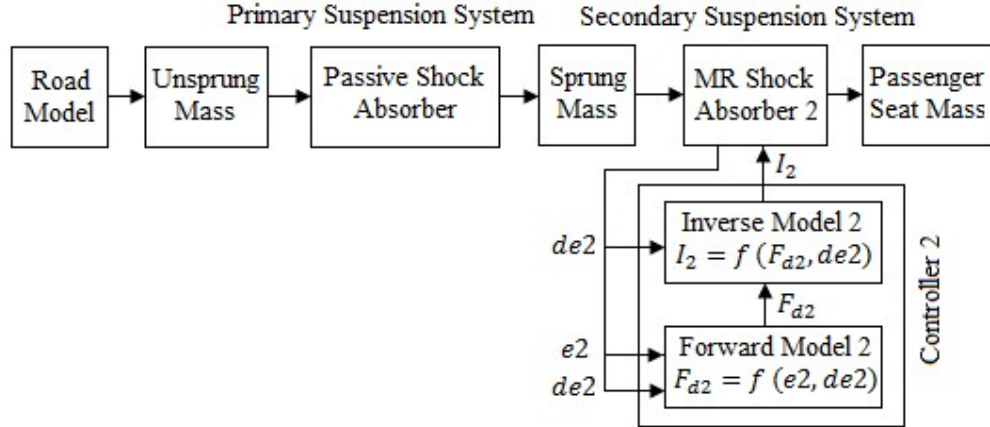


Figure 9.1 Block diagram of secondary suspension controlled semi-active quarter car system

9.2 PASSENGER SEAT SIMULATION RESULTS

9.2.1 Pulse Input Disturbance

The simulation results for passenger seat acceleration and displacement response are shown in Figure 9.2 (a)-(b) for $m_2 = 325$ kg and $m_1 = 70$ kg under pulse input road excitation for uncontrolled and controlled quarter car models. The passenger seat response in mathematical values are calculated in terms of peak and RMS values for

passenger seat acceleration and displacement response are shown in Table 9.1 and Table 9.2.

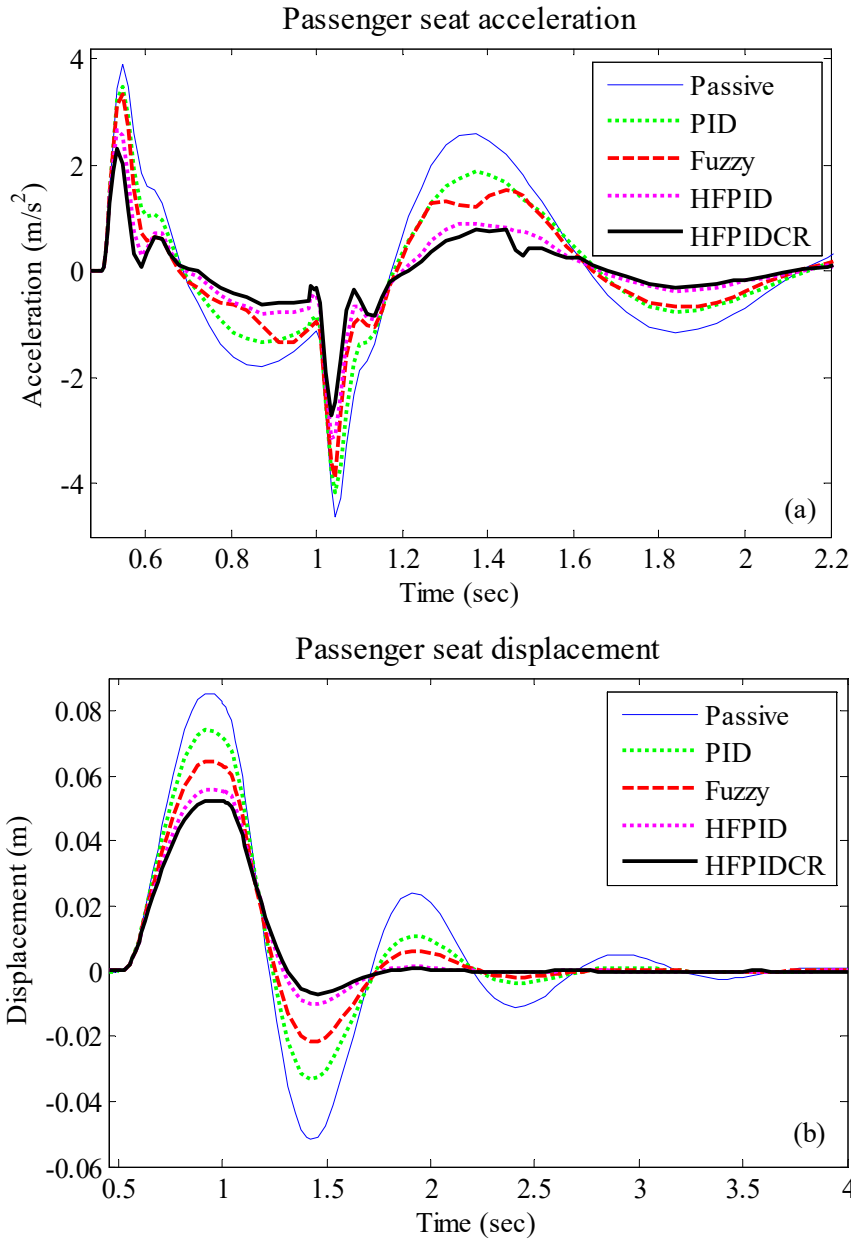


Figure 9.2 (a) Passenger seat acceleration (b) Passenger seat displacement

Figure 9.2 (a)-(b) reveals that the passenger seat acceleration and displacement vibration amplitudes are significantly reduced for all controlled semi-active suspension systems compared to uncontrolled one. It can be seen that HFPIDCR controller 2 is most effective in controlling the passenger seat vibrations under pulse road input compared to uncontrolled, PID controller 2, Fuzzy controller 2 and HFPID controller 2 controlled suspension systems.

Table 9.1 Performance comparison of Passenger seat response under Pulse road profile ($m_1 = 70$ kg)

Performance Parameters	Acceleration (m/s^2)				Displacement (m)			
	Max.		RMS		Max.		RMS	
	Magnitude	Improvement %	Magnitude	Improvement %	Magnitude	Improvement %	Magnitude	Improvement %
Controller Type	80% $m_2 = 260$ kg							
Uncontrolled	4.5541	-----	1.3679	-----	0.0842	-----	0.0324	-----
PID	4.1896	8.00	1.1166	18.38	0.0710	15.70	0.0276	14.94
Fuzzy	4.0198	11.73	0.9631	29.60	0.0633	24.79	0.0242	25.18
HFPID	3.3350	26.77	0.7589	44.52	0.0502	40.40	0.0199	38.64
HFPIDCR	2.8046	38.42	0.6250	54.31	0.0409	51.43	0.0164	49.40
Controller Type	100% $m_2 = 325$ kg							
Uncontrolled	3.8608	-----	1.2844	-----	0.0853	-----	0.0333	-----
PID	3.5113	9.05	1.0396	19.06	0.0732	14.26	0.0282	15.39
Fuzzy	3.3554	13.09	0.9084	29.28	0.0657	22.96	0.0250	25.04
HFPID	2.6869	30.41	0.6898	46.29	0.0528	38.17	0.0201	39.67
HFPIDCR	2.2353	42.10	0.5595	56.44	0.0430	49.65	0.0165	50.44
Controller Type	120% $m_2 = 390$ kg							
Uncontrolled	3.2564	-----	1.2030	-----	0.0861	-----	0.0356	-----
PID	2.9518	9.36	0.9786	18.65	0.0748	13.07	0.0304	14.58
Fuzzy	2.8373	12.87	0.8833	26.58	0.0677	21.39	0.0272	23.66
HFPID	2.3405	28.13	0.6425	46.59	0.0545	36.73	0.0217	39.04
HFPIDCR	1.9630	39.72	0.5184	56.91	0.0442	48.59	0.0178	50.12

Table 9.2 Performance comparison of Passenger seat response under Pulse road profile ($m_2 = 325$ kg)

Performance Parameters	Acceleration (m/s^2)				Displacement (m)			
	Max.		RMS		Max.		RMS	
	Magnitude	Improvement %	Magnitude	Improvement %	Magnitude	Improvement %	Magnitude	Improvement %
Controller Type	80% $m_1 = 56$ kg							
Uncontrolled	4.4652	-----	1.3329	-----	0.0839	-----	0.0327	-----
PID	4.0269	9.81	1.0889	18.30	0.0724	13.80	0.0280	14.23
Fuzzy	3.8257	14.32	0.9380	29.62	0.0651	22.46	0.0248	24.00
HFPID	3.0250	32.25	0.7260	45.53	0.0526	37.39	0.0202	38.23
HFPIDCR	2.4517	45.09	0.5893	55.79	0.0429	48.87	0.0166	49.16
Controller Type	100% $m_1 = 70$ kg							
Uncontrolled	3.8608	-----	1.2844	-----	0.0853	-----	0.0333	-----
PID	3.5113	9.05	1.0396	19.06	0.0732	14.26	0.0282	15.39
Fuzzy	3.3554	13.09	0.9084	29.28	0.0657	22.96	0.0250	25.04
HFPID	2.6869	30.41	0.6898	46.29	0.0528	38.17	0.0201	39.67
HFPIDCR	2.2353	42.10	0.5595	56.44	0.0430	49.65	0.0165	50.44
Controller Type	120% $m_1 = 84$ kg							
Uncontrolled	3.3488	-----	1.2343	-----	0.0865	-----	0.0343	-----
PID	3.0399	9.22	0.9911	19.70	0.0738	14.70	0.0288	16.10
Fuzzy	2.9406	12.19	0.8819	28.55	0.0662	23.44	0.0255	25.63
HFPID	2.4902	25.64	0.6530	47.10	0.0530	38.73	0.0204	40.67
HFPIDCR	2.1341	36.27	0.5284	57.19	0.0430	50.27	0.0167	51.39

It can be seen from mathematical results that the semi-active suspension with HFPIDCR controller 2 is the best choice for achieving maximum ride comfort and safety to the travelling passengers.

The desired damping force signal generated by assembled forward controllers for the pulse road excitation is shown in Figure 9.3. The highest values of desired damping force signals supplied by different controllers in semi-active quarter car model are shown in Table 9.3. It can be observed from Table 9.3 that the desired damping force generated by forward controllers lies within the limits of the damping force generated by the tested MR shock absorber. It can be seen that HFPIDCR controller 2 generated maximum value of desired damping force during compression stage as 409.27 N and during rebound stage as 438.35 N respectively.

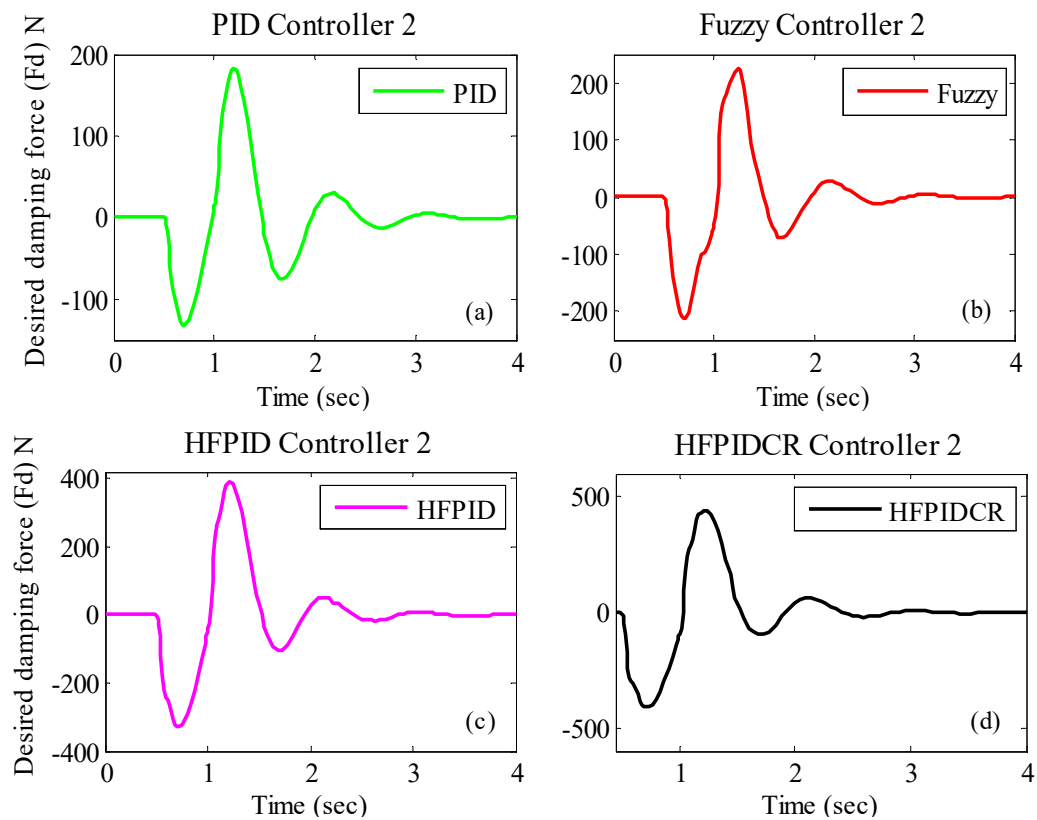


Figure 9.3 Desired damping force signals supplied by different controllers

Table 9.3 Calculated Max. desired damping force using Forward controller 2 (N)

Forward Controller 2	Max. Damping Force (N)			
	PID	Fuzzy	HFPID	HFPIDCR
Compression Stage	132.25	211.47	327.56	409.27
Rebound Stage	183.27	223.71	388.28	438.35

Input current signals generated by different inverse controllers are shown in Figure 9.4. and presented in mathematical value in Table 9.4. It can be seen that the highest value of input current is 0.68 A which is generated by inverse controller with HFPIDCR controller 2.

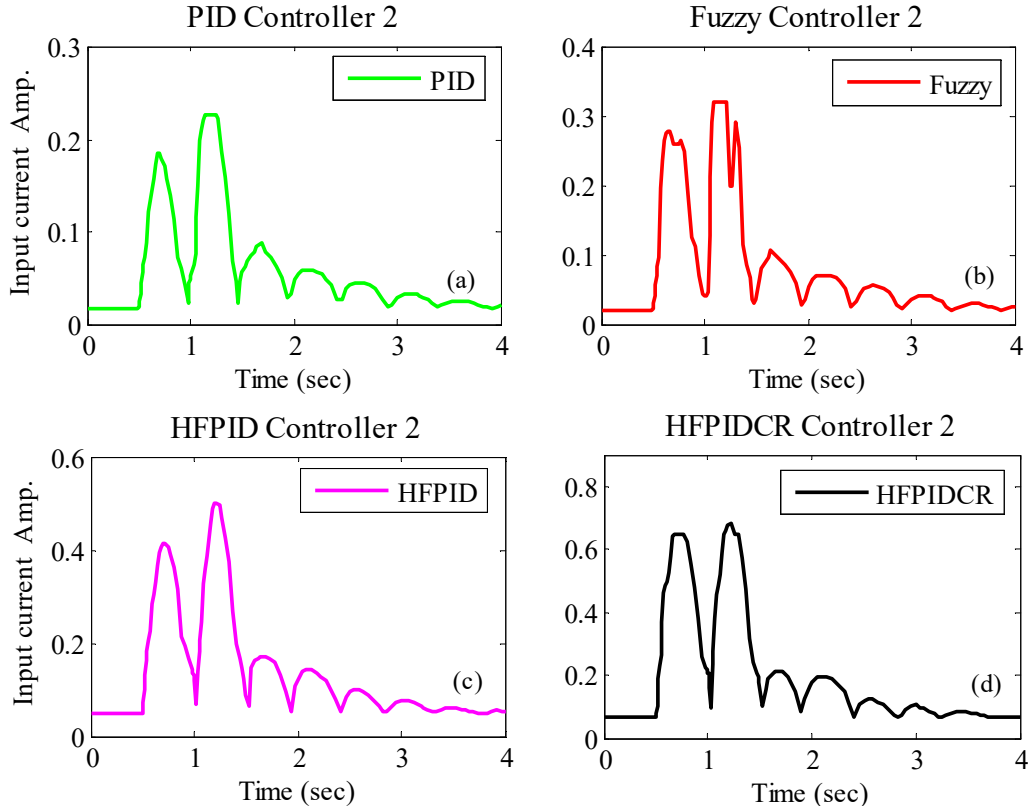


Figure 9.4 Input current signal generated by different controllers

Table 9.4 Calculated Max. input current using Inverse controller 2 (A)

Inverse Controller 2	Max. input current (A)			
	PID	Fuzzy	HFPID	HFPIDCR
Magnitude	0.23	0.32	0.50	0.68

9.2.2 Bump Input Disturbance

The simulation response under bump road excitation are shown in Figure 9.5 (a)-(b) for $m_2 = 325$ kg and $m_1 = 70$ kg. It can be observed that semi-active suspension systems with controllers provide better performance compared to uncontrolled one. Figure 9.5 (a)-(b) shows that passenger seat response in terms of acceleration and displacement response is significantly improved for all semi-active suspension systems. The calculated results for passenger seat acceleration and displacement

response in peak and RMS values are shown in Table 9.5 and Table 9.6. It can be finalized from graphical response and tabular values that the best performance is delivered by HFPIDCR controller 2 in combination with MR shock absorber 2 for passenger seat vibration control compared to other cases.

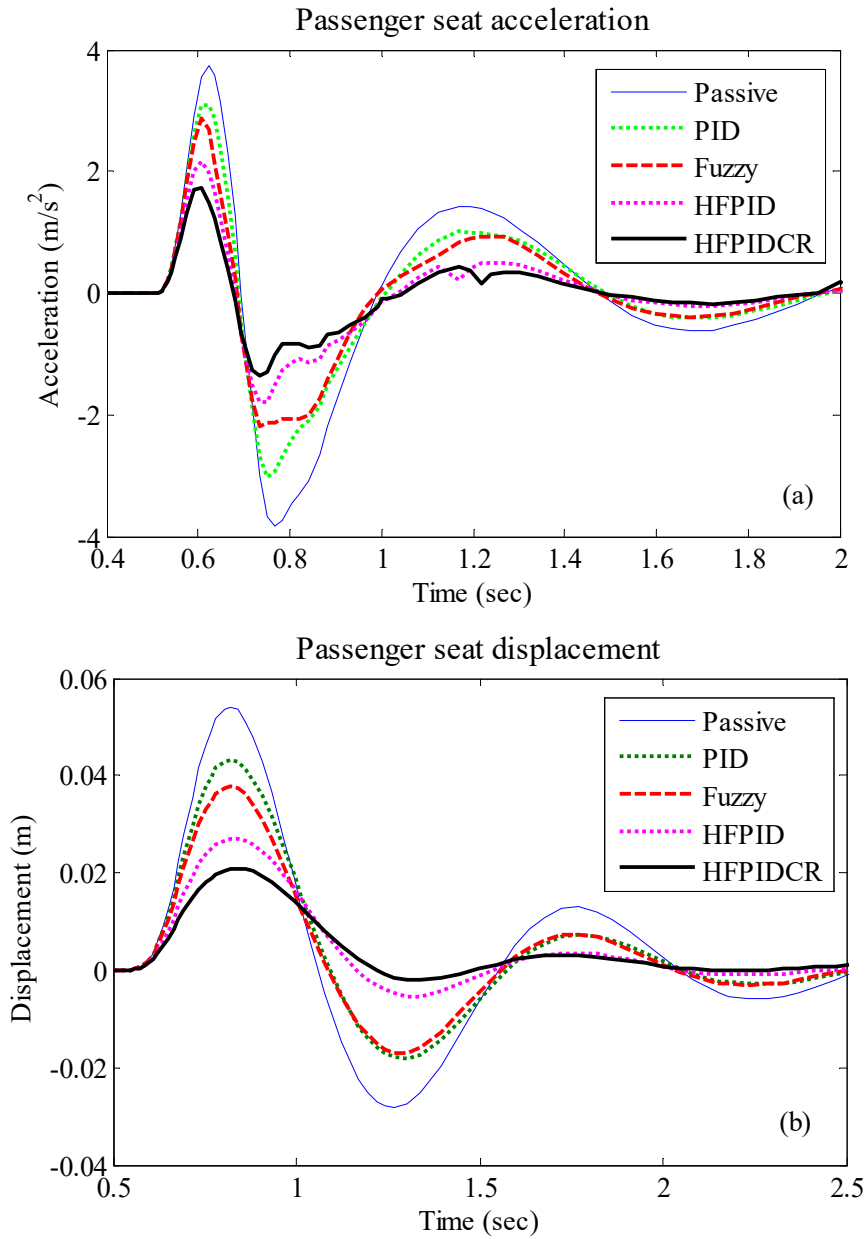


Figure 9.5 (a) Passenger seat acceleration (b) Passenger seat displacement

Table 9.5 Performance comparison of Passenger seat response under Bump road profile ($m_1 = 70$ kg)

Performance Parameters	Acceleration (m/s^2)				Displacement (m)			
	Max.		RMS		Max.		RMS	
	Magnitude	Improvement %	Magnitude	Improvement %	Magnitude	Improvement %	Magnitude	Improvement %
Controller Type	80% $m_2 = 260$ kg							
Uncontrolled	4.3291	-----	1.4607	-----	0.0574	-----	0.0178	-----
PID	3.6209	16.36	1.1506	21.23	0.0457	20.45	0.0140	21.57
Fuzzy	3.3083	23.58	0.9790	32.98	0.0400	30.33	0.0123	31.12
HFPID	2.5468	41.17	0.7140	51.12	0.0284	50.56	0.0089	50.33
HFPIDCR	2.0369	52.95	0.5548	62.02	0.0217	62.25	0.0069	61.00
Controller Type	100% $m_2 = 325$ kg							
Uncontrolled	3.7298	-----	1.2472	-----	0.0542	-----	0.0172	-----
PID	3.1078	16.68	0.9738	21.92	0.0432	20.32	0.0137	20.77
Fuzzy	2.8814	22.75	0.8214	34.14	0.0379	30.04	0.0121	30.10
HFPID	2.1192	43.18	0.5960	52.22	0.0272	49.86	0.0088	49.15
HFPIDCR	1.7473	53.15	0.4609	63.04	0.0210	61.28	0.0069	59.86
Controller Type	120% $m_2 = 390$ kg							
Uncontrolled	3.2620	-----	1.0873	-----	0.0513	-----	0.0170	-----
PID	2.7475	15.77	0.8448	22.30	0.0410	20.14	0.0135	20.43
Fuzzy	2.5440	22.01	0.7187	33.90	0.0364	29.14	0.0121	28.93
HFPID	1.8599	42.98	0.5140	52.73	0.0262	48.88	0.0087	49.00
HFPIDCR	1.5142	53.58	0.3971	63.48	0.0204	60.25	0.0068	59.81

Table 9.6 Performance comparison of Passenger seat response under Bump road profile ($m_2 = 325$ kg)

Performance Parameters	Acceleration (m/s^2)				Displacement (m)			
	Max.		RMS		Max.		RMS	
	Magnitude	Improvement %	Magnitude	Improvement %	Magnitude	Improvement %	Magnitude	Improvement %
Controller Type	80% $m_1 = 56$ kg							
Uncontrolled	4.1223	-----	1.3039	-----	0.0551	-----	0.0169	-----
PID	3.3884	17.80	0.9966	23.57	0.0435	20.98	0.0133	21.19
Fuzzy	3.0771	25.36	0.8261	36.65	0.0381	30.85	0.0117	30.70
HFPID	2.2964	44.29	0.6728	48.40	0.0273	50.48	0.0088	48.07
HFPIDCR	1.8149	55.97	0.4646	64.36	0.0210	61.87	0.0067	60.26
Controller Type	100% $m_1 = 70$ kg							
Uncontrolled	3.7298	-----	1.2472	-----	0.0542	-----	0.0172	-----
PID	3.1078	16.68	0.9738	21.92	0.0432	20.32	0.0137	20.77
Fuzzy	2.8814	22.75	0.8214	34.14	0.0379	30.04	0.0121	30.10
HFPID	2.1192	43.18	0.5960	52.22	0.0272	49.86	0.0088	49.15
HFPIDCR	1.7473	53.15	0.4609	63.04	0.0210	61.28	0.0069	59.86
Controller Type	120% $m_1 = 84$ kg							
Uncontrolled	3.4023	-----	1.1553	-----	0.0531	-----	0.0171	-----
PID	2.8822	15.29	0.9161	20.71	0.0427	19.63	0.0135	21.24
Fuzzy	2.6834	21.13	0.7893	31.68	0.0377	29.06	0.0120	30.02
HFPID	2.0140	40.80	0.6145	46.81	0.0270	49.16	0.0089	48.33
HFPIDCR	1.6061	52.79	0.4443	61.55	0.0209	60.67	0.0068	60.59

Figure 9.6 shows the simulation response for changes in desired damping force values generated by forward controller when the vehicle passes through bump road excitation. Table 9.7 shows the maximum values of desired damping force supplied by integrated controllers in quarter car model. It can be seen that the highest value of desired damping force is generated by HFPIDCR controller 2 as 436.36 N during compression and 241.10 N during rebound stage.

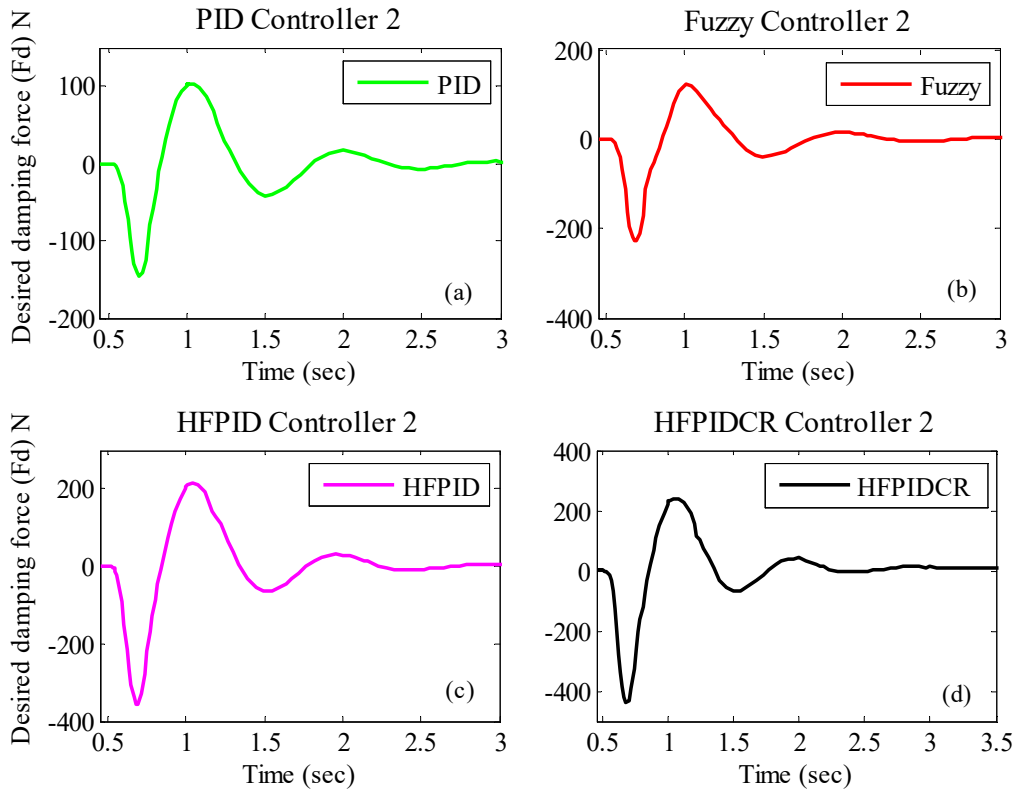


Figure 9.6 Desired damping force signals supplied by different controllers

Table 9.7 Calculated Max. desired damping force using Forward controller 2 (N)

Forward Controller 2	Max. Damping Force (N)			
	PID	Fuzzy	HFPID	HFPIDCR
Compression Stage	146.71	226.87	356.52	436.36
Rebound Stage	103.87	120.54	213.63	241.10

Figure 9.7 shows the generated current signals by inverse controllers. The highest value of generated input current by inverse controller with HFPIDCR controller 2 is 0.65 A as shown in Table 9.8.

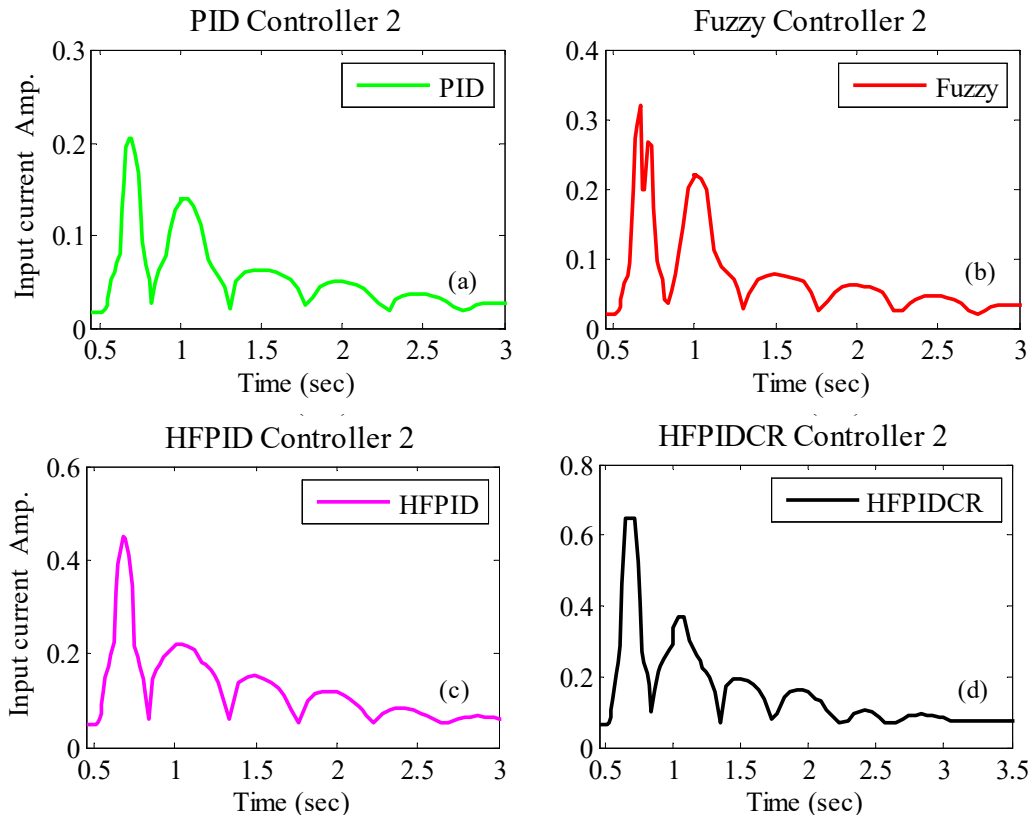


Figure 9.7 Input current signal generated by different controllers

Table 9.8 Calculated Max. input current using Inverse controller 2 (A)

Inverse Controller 2	Max. input current (A)			
	PID	Fuzzy	HFPID	HFPIDCR
Magnitude	0.21	0.32	0.45	0.65

9.2.3 Sinusoidal Input Disturbance

The simulation response of various controlled and uncontrolled quarter car systems under sinusoidal excitation is shown in Figure 9.8 (a)-(b) for $m_2 = 325$ kg and $m_1 = 70$ kg. It can be observed that response delivered by all controlled cases is different in each case related to passenger seat acceleration and displacement control but better as compared to uncontrolled system. The graphical response shows that best performance is delivered by HFPIDCR controller 2 controlled semi-active quarter car system compared to uncontrolled, PID controller 2, Fuzzy controller 2 and HFPID controller 2 controlled suspension systems.

The calculated results in mathematical values for passenger seat acceleration and displacement response are shown in Table 9.9 and Table 9. Based on the graphical and mathematical results, it can be decided that the semi-active suspension with

HFPIDCR controller 2 is the best choice for achieving maximum ride comfort and safety to the travelling passengers.

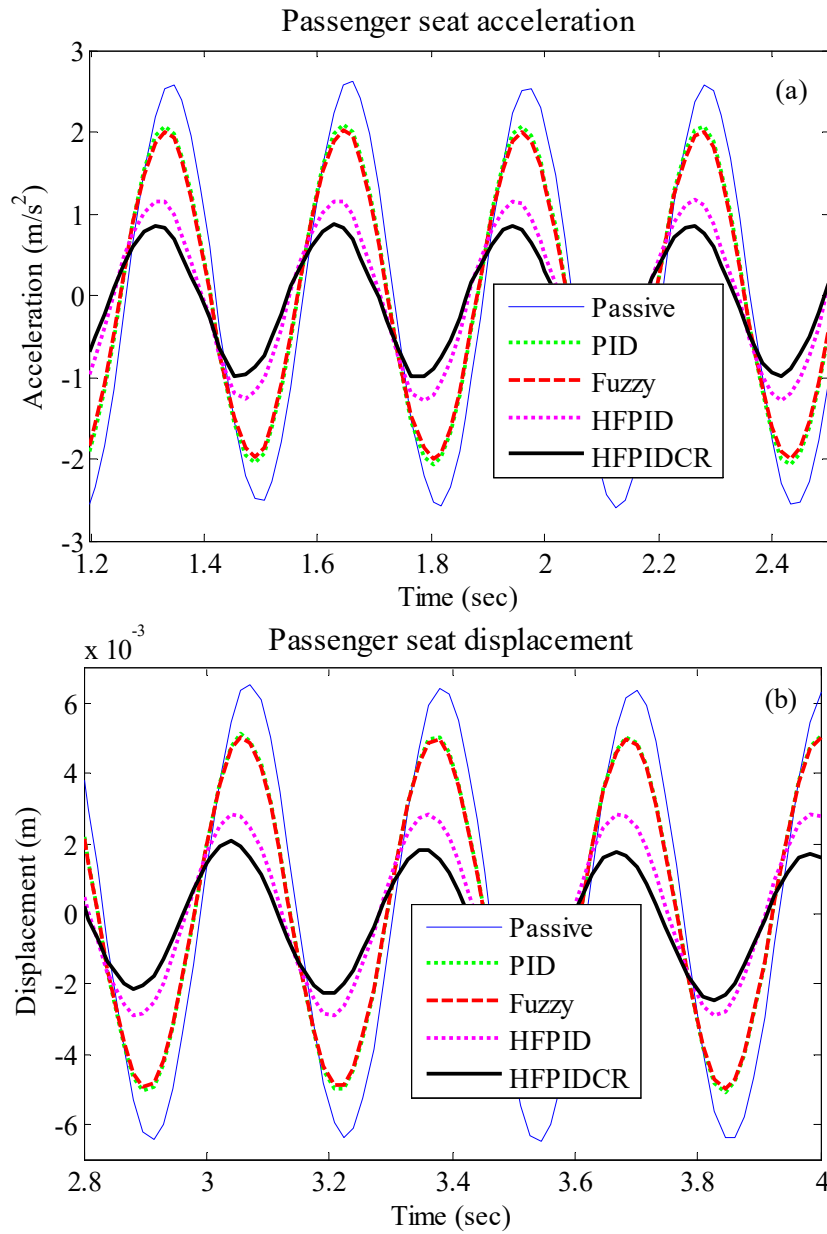


Figure 9.8 (a) Passenger seat acceleration (b) Passenger seat displacement

Table 9.9 Performance comparison of Passenger seat response under Sinusoidal road profile ($m_1 = 70$ kg)

Performance Parameters	Acceleration (m/s^2)				Displacement (m)			
	Max.		RMS		Max.		RMS	
	Magnitude	Improvement %	Magnitude	Improvement %	Magnitude	Improvement %	Magnitude	Improvement %
Controller Type	80% $m_2 = 260$ kg							
Uncontrolled	3.4765	-----	2.4832	-----	0.0187	-----	0.0070	-----
PID	2.6721	23.14	1.9715	20.61	0.0149	20.21	0.0054	21.92
Fuzzy	2.5821	25.73	1.9198	22.69	0.0143	23.41	0.0053	23.96
HFPID	1.5153	56.41	1.1262	54.64	0.0091	51.43	0.0031	55.40
HFPIDCR	1.1577	66.70	0.8332	66.45	0.0069	63.30	0.0023	67.09
Controller Type	100% $m_2 = 325$ kg							
Uncontrolled	2.7350	-----	1.9321	-----	0.0169	-----	0.0055	-----
PID	2.1939	19.79	1.5266	20.99	0.0135	20.49	0.0043	22.67
Fuzzy	2.1109	22.82	1.4860	23.09	0.0130	23.48	0.0042	24.41
HFPID	1.2613	53.88	0.8688	55.03	0.0082	51.84	0.0024	55.99
HFPIDCR	0.9708	64.51	0.6454	66.60	0.0061	63.72	0.0018	67.43
Controller Type	120% $m_2 = 390$ kg							
Uncontrolled	2.3195	-----	1.6170	-----	0.0155	-----	0.0049	-----
PID	1.8737	19.22	1.2715	21.36	0.0123	20.76	0.0038	22.69
Fuzzy	1.8122	21.87	1.2404	23.29	0.0118	23.69	0.0037	24.46
HFPID	1.0348	55.38	0.7193	55.51	0.0074	52.15	0.0021	55.85
HFPIDCR	0.8306	64.19	0.5328	67.05	0.0056	64.01	0.0016	67.10

Table 9.10 Performance comparison of Passenger seat response under Sinusoidal road profile ($m_2 = 325$ kg)

Performance Parameters	Acceleration (m/s^2)				Displacement (m)			
	Max.		RMS		Max.		RMS	
	Magnitude	Improvement %	Magnitude	Improvement %	Magnitude	Improvement %	Magnitude	Improvement %
Controller Type	80% $m_1 = 56$ kg							
Uncontrolled	3.1733	-----	2.2499	-----	0.0178	-----	0.0064	-----
PID	2.4030	24.27	1.6700	25.77	0.0139	22.04	0.0047	26.40
Fuzzy	2.3185	26.94	1.6149	28.22	0.0133	25.21	0.0046	28.35
HFPID	1.2867	59.45	0.8977	60.10	0.0083	53.68	0.0025	60.11
HFPIDCR	1.0584	66.65	0.6648	70.45	0.0062	65.28	0.0019	70.79
Controller Type	100% $m_1 = 70$ kg							
Uncontrolled	2.7350	-----	1.9321	-----	0.0169	-----	0.0055	-----
PID	2.1939	19.79	1.5266	20.99	0.0135	20.49	0.0043	22.67
Fuzzy	2.1109	22.82	1.4860	23.09	0.0130	23.48	0.0042	24.41
HFPID	1.2613	53.88	0.8688	55.03	0.0082	51.84	0.0024	55.99
HFPIDCR	0.9708	64.51	0.6454	66.60	0.0061	63.72	0.0018	67.43
Controller Type	120% $m_1 = 84$ kg							
Uncontrolled	2.4032	-----	1.7175	-----	0.0161	-----	0.0053	-----
PID	1.9905	17.17	1.4291	16.79	0.0130	19.22	0.0042	19.53
Fuzzy	1.9616	18.37	1.4030	18.31	0.0125	22.03	0.0040	24.26
HFPID	1.2021	49.98	0.8632	49.74	0.0080	50.02	0.0025	51.95
HFPIDCR	0.9089	62.18	0.6440	62.50	0.0061	62.13	0.0019	64.16

While the vehicle passes over the sinusoidal profile road, it can be seen from simulation response in Figure 9.9 and Figure 9.10 that the desired damping force values generated by forward controller as well current supplied by inverse controller are continuous during that period.

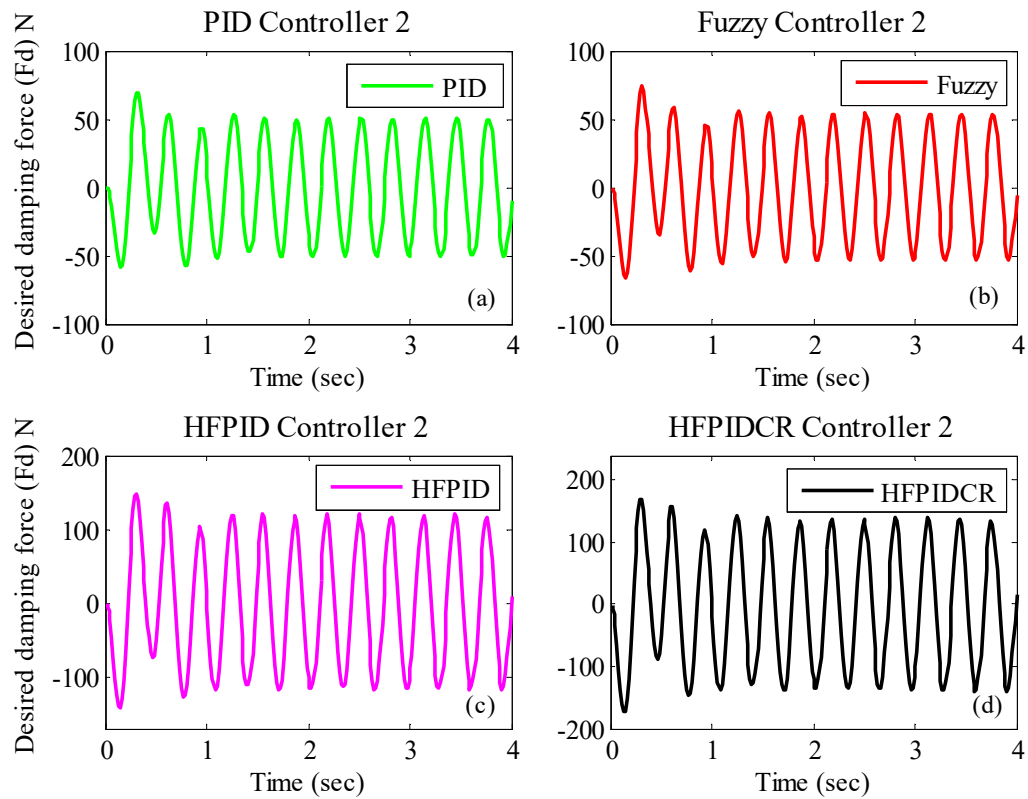
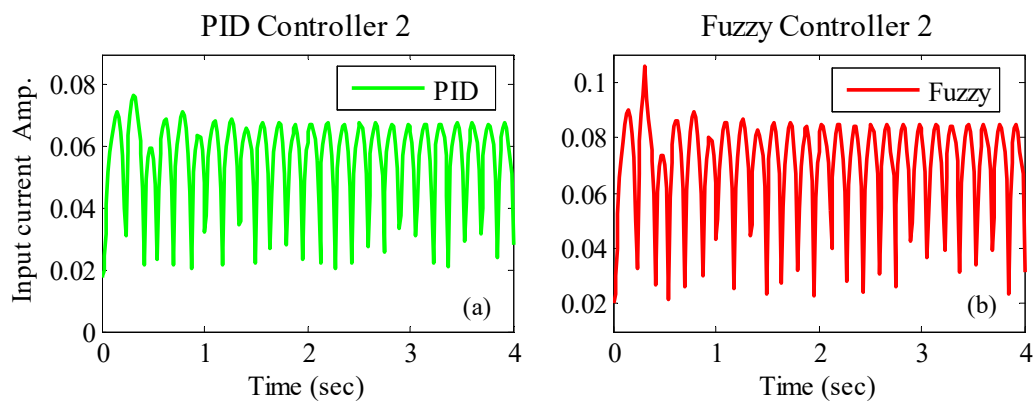


Figure 9.9 Desired damping force signals supplied by different controllers



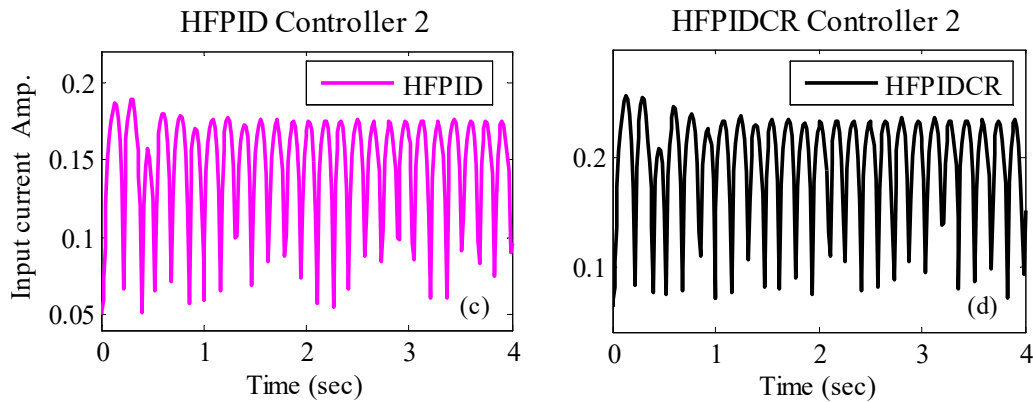


Figure 9.10 Input current signal generated by different controllers

Table 9.11 shows the maximum values of desired damping force generated by forward controllers during compression and rebound stage. It can be observed that the semi-active quarter car model with HFPIDCR controller 2 generated highest values of desired damping force values for best response related to passenger seat vibration control. The highest value of input current is generated by inverse controller with HFPIDCR controller 2 as 0.26 A as shown in Table 9.12.

Table 9.11 Calculated Max. desired damping force using Forward controller 2 (N)

Forward Controller 2	Max. Damping Force (N)			
	PID	Fuzzy	HFPID	HFPIDCR
Compression Stage	57.98	66.76	142.72	173.11
Rebound Stage	69.16	74.94	148.24	168.37

Table 9.12 Calculated Max. input current using Inverse controller 2 (A)

Inverse Controller 2	Max. input current (A)			
	PID	Fuzzy	HFPID	HFPIDCR
Magnitude	0.08	0.11	0.19	0.26

9.2.4 Random Input Disturbance

The simulation results under random road excitation for passenger seat acceleration and displacement results are shown in Figure 9.11 for $m_2 = 325$ kg and $m_1 = 70$ kg while Table 9.13 and Table 9.14 shows calculated mathematical values for the same. It can be observed from graphical and tabular values that controlled semi-active quarter car model with MR shock absorber 2 in combination with HFPIDCR controller 2 provided best response for passenger seat ride comfort issues.

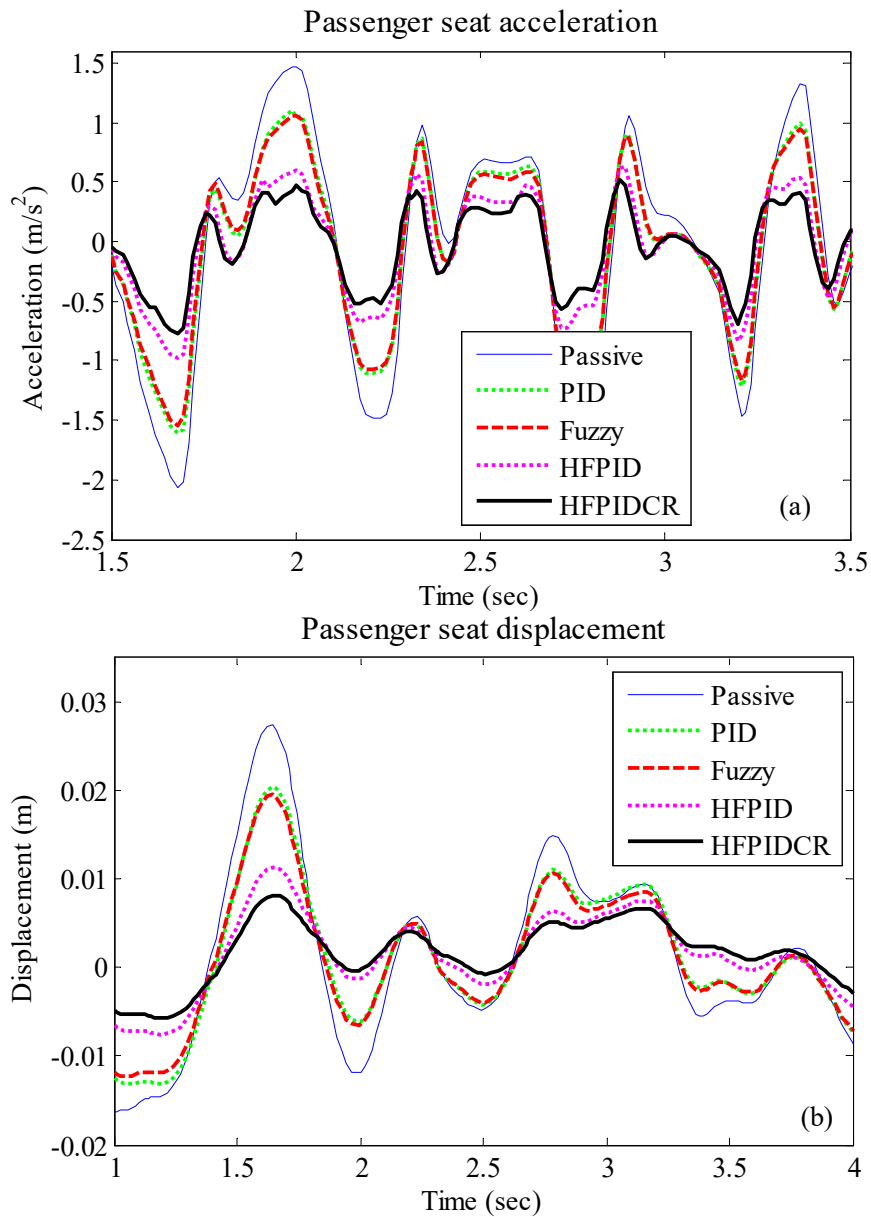


Figure 9.11 (a) Passenger seat acceleration (b) Passenger seat displacement

It can be seen from Figure 9.12 and Figure 9.13 that the desired damping force signals generated by forward controllers and input current signals generated by inverse controllers are continuous while the vehicle travels over the random road profile. Table 9.15 shows the highest values of desired damping force generated by each controller in secondary suspension system.

Table 9.13 Performance comparison of Passenger seat response under Random road profile ($m_1 = 70$ kg)

Performance Parameters	Acceleration (m/s ²)				Displacement (m)			
	Max.		RMS		Max.		RMS	
	Magnitude	Improvement %	Magnitude	Improvement %	Magnitude	Improvement %	Magnitude	Improvement %
Controller Type	80% $m_2 = 260$ kg							
Uncontrolled	1.8803	-----	1.0206	-----	0.0262	-----	0.0101	-----
PID	1.4381	23.52	0.8073	20.90	0.0197	25.03	0.0077	23.29
Fuzzy	1.3604	27.65	0.7749	24.07	0.0188	28.32	0.0073	27.13
HFPID	0.8373	55.47	0.4934	51.66	0.0109	58.31	0.0046	54.57
HFPIDCR	0.6888	63.37	0.3811	62.66	0.0079	69.78	0.0036	64.17
Controller Type	100% $m_2 = 325$ kg							
Uncontrolled	1.5311	-----	0.8625	-----	0.0274	-----	0.0100	-----
PID	1.0922	28.67	0.6749	21.75	0.0204	25.73	0.0077	22.90
Fuzzy	1.0542	31.15	0.6493	24.72	0.0196	28.65	0.0073	26.84
HFPID	0.6357	58.48	0.4054	53.00	0.0114	58.52	0.0046	54.14
HFPIDCR	0.5069	66.89	0.3126	63.76	0.0083	69.88	0.0036	63.52
Controller Type	120% $m_2 = 390$ kg							
Uncontrolled	1.2896	-----	0.7364	-----	0.0279	-----	0.0101	-----
PID	0.9505	26.30	0.5720	22.32	0.0207	25.72	0.0079	22.16
Fuzzy	0.9205	28.62	0.5502	25.29	0.0200	28.45	0.0074	26.24
HFPID	0.5673	56.01	0.3406	53.75	0.0117	58.12	0.0047	53.34
HFPIDCR	0.4948	61.63	0.2628	64.31	0.0085	69.53	0.0038	62.64

Table 9.14 Performance comparison of Passenger seat response under Random road profile ($m_2 = 325$ kg)

Performance Parameters	Acceleration (m/s^2)				Displacement (m)			
	Max.		RMS		Max.		RMS	
	Magnitude	Improvement %	Magnitude	Improvement %	Magnitude	Improvement %	Magnitude	Improvement %
Controller Type	80% $m_1 = 56$ kg							
Uncontrolled	1.6697	-----	0.9562	-----	0.0268	-----	0.0098	-----
PID	1.2228	26.77	0.7338	23.26	0.0202	24.53	0.0076	22.32
Fuzzy	1.1572	30.70	0.7005	26.74	0.0194	27.69	0.0072	26.38
HFPID	0.7140	57.24	0.4286	55.18	0.0114	57.32	0.0046	53.43
HFPIDCR	0.5472	67.23	0.3300	65.49	0.0083	68.94	0.0036	62.83
Controller Type	100% $m_1 = 70$ kg							
Uncontrolled	1.5311	-----	0.8625	-----	0.0274	-----	0.0100	-----
PID	1.0922	28.67	0.6749	21.75	0.0204	25.73	0.0077	22.90
Fuzzy	1.0542	31.15	0.6493	24.72	0.0196	28.65	0.0073	26.84
HFPID	0.6357	58.48	0.4054	53.00	0.0114	58.52	0.0046	54.14
HFPIDCR	0.5069	66.89	0.3126	63.76	0.0083	69.88	0.0036	63.52
Controller Type	120% $m_1 = 84$ kg							
Uncontrolled	1.4184	-----	0.7896	-----	0.0280	-----	0.0102	-----
PID	1.0412	26.59	0.6250	20.84	0.0206	26.40	0.0078	23.46
Fuzzy	1.0212	28.00	0.6050	23.38	0.0198	29.30	0.0074	27.27
HFPID	0.6209	56.22	0.3857	51.15	0.0114	59.12	0.0046	54.70
HFPIDCR	0.4813	66.07	0.3002	61.98	0.0083	70.36	0.0037	63.97

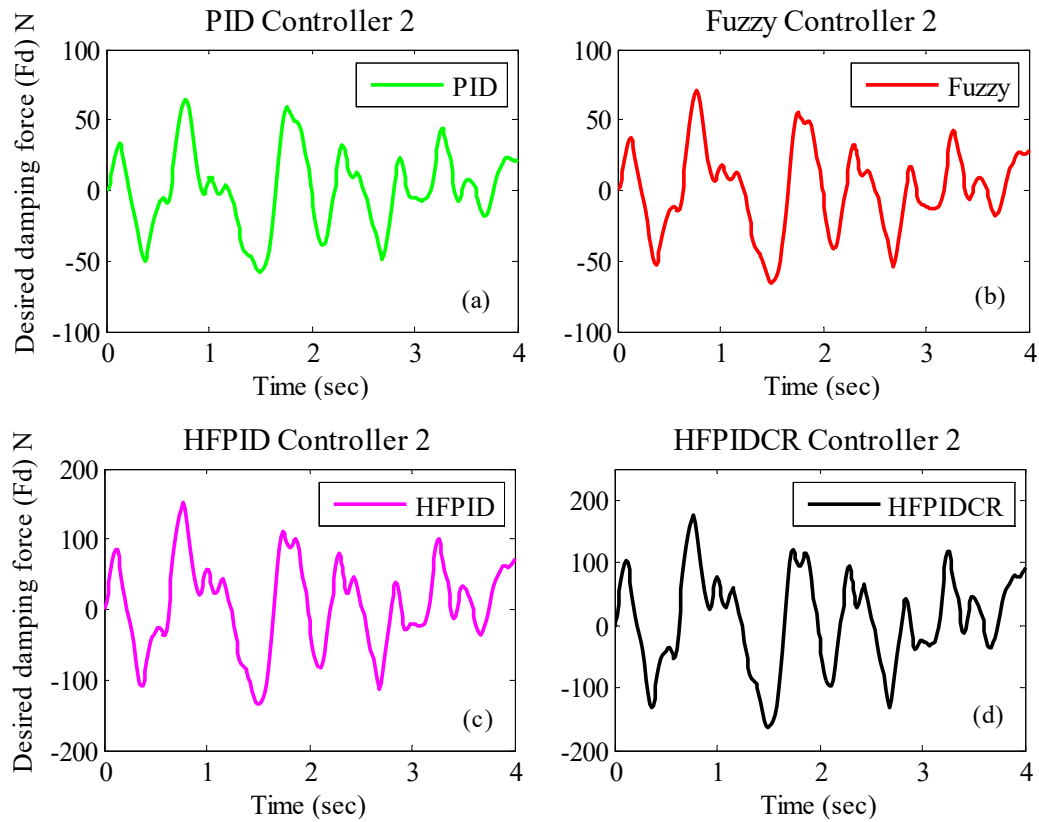


Figure 9.12 Desired damping force signals supplied by different controllers

The highest value of desired damping force generated by HFPIDCR controller 2 are 162.82 N during the compression stage and 174.77 N during the rebound stage.

Table 9.15 Calculated Max. desired damping force using Forward controller 2 (N)

Forward Controller 2	Max. Damping Force (N)			
	PID	Fuzzy	HFPID	HFPIDCR
Compression Stage	58.08	65.48	135.47	162.82
Rebound Stage	64.62	70.96	153.08	174.77

Figure 9.13 shows the current signals generated by inverse controllers. Table 9.16 represents the highest values of current signals generated by inverse controllers in secondary suspension system of quarter car model where HFPIDCR controller 2 produced maximum current signal of 0.26 A.

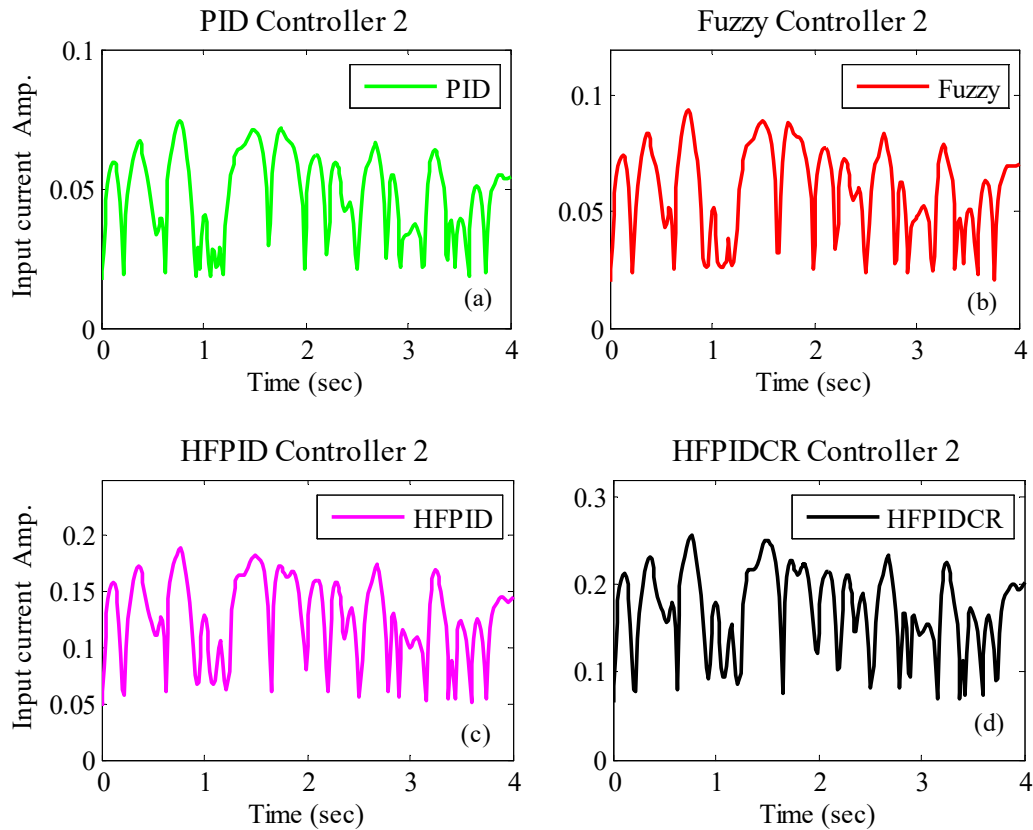


Figure 9.13 Input current signal generated by different controllers

Table 9.16 Calculated Max. input current using Inverse controller 2 (A)

Inverse Controller 2	Max. input current (A)			
	PID	Fuzzy	HFPID	HFPIDCR
Magnitude	0.08	0.10	0.20	0.26

9.3 SPRUNG MASS SIMULATION RESULTS

The simulation results of sprung mass acceleration and displacement response for pulse, bump, sinusoidal and random road input profile are shown in Figure 9.14 to Figure 9.17 respectively. The mathematical results in terms of peak and RMS values for passenger seat response for selected road profiles are shown in Table 9.17.

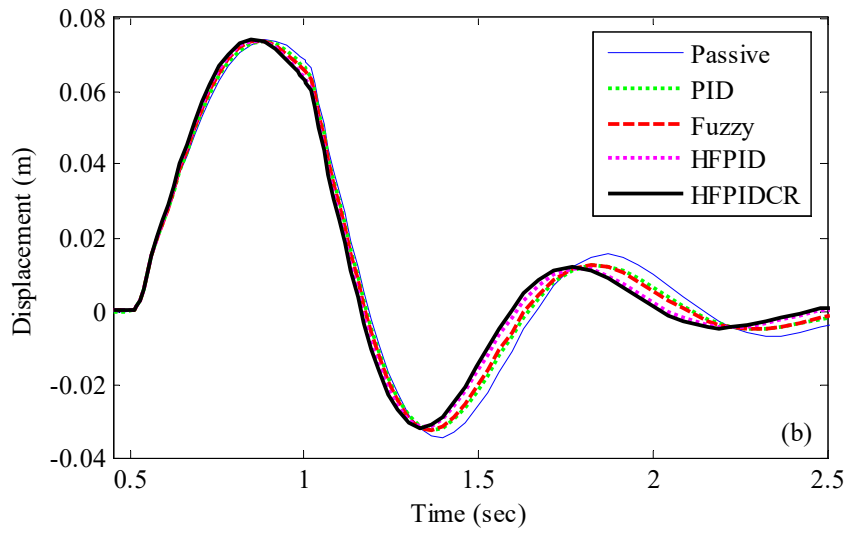
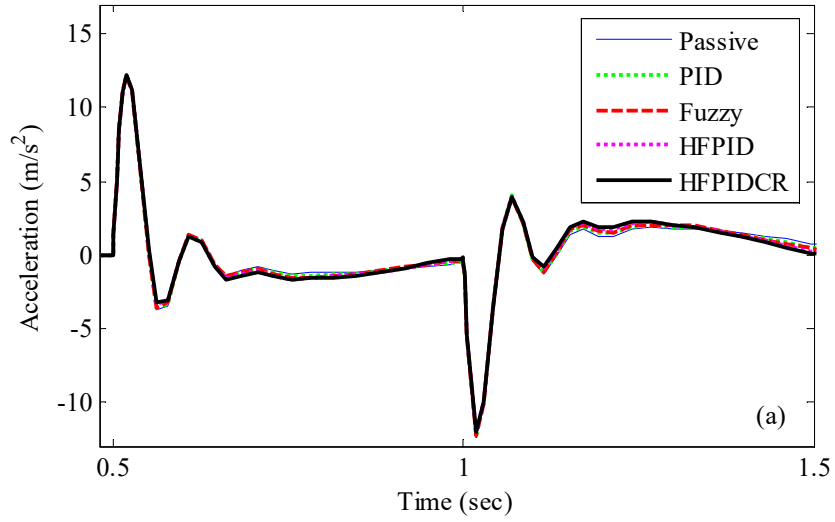
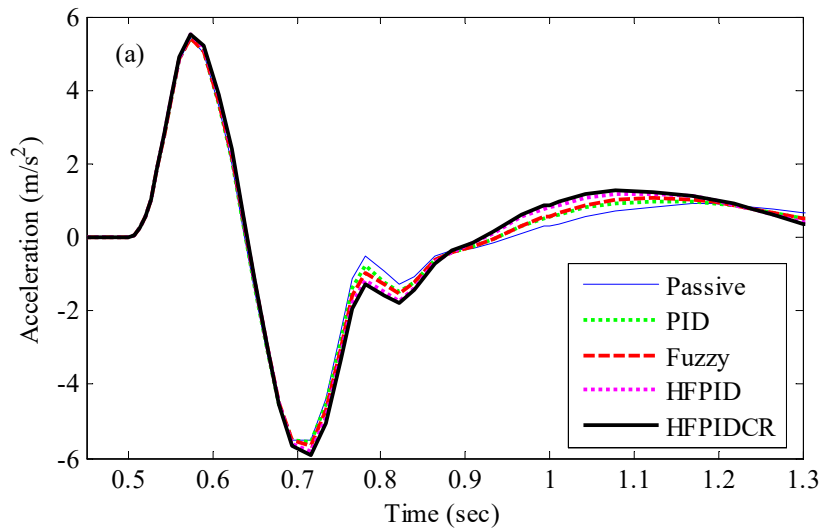


Figure 9.14 Sprung mass response under pulse road input (a) Acceleration (b) Displacement



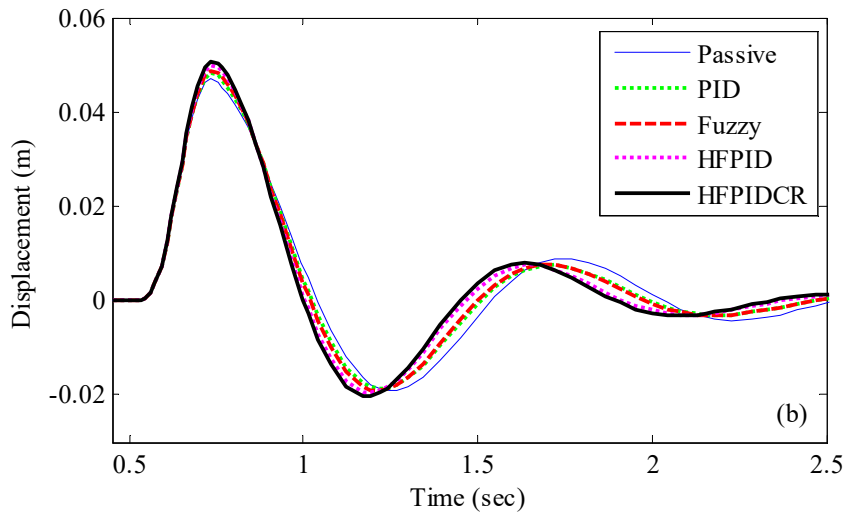


Figure 9.15 Sprung mass response under bump road input (a) Acceleration (b) Displacement

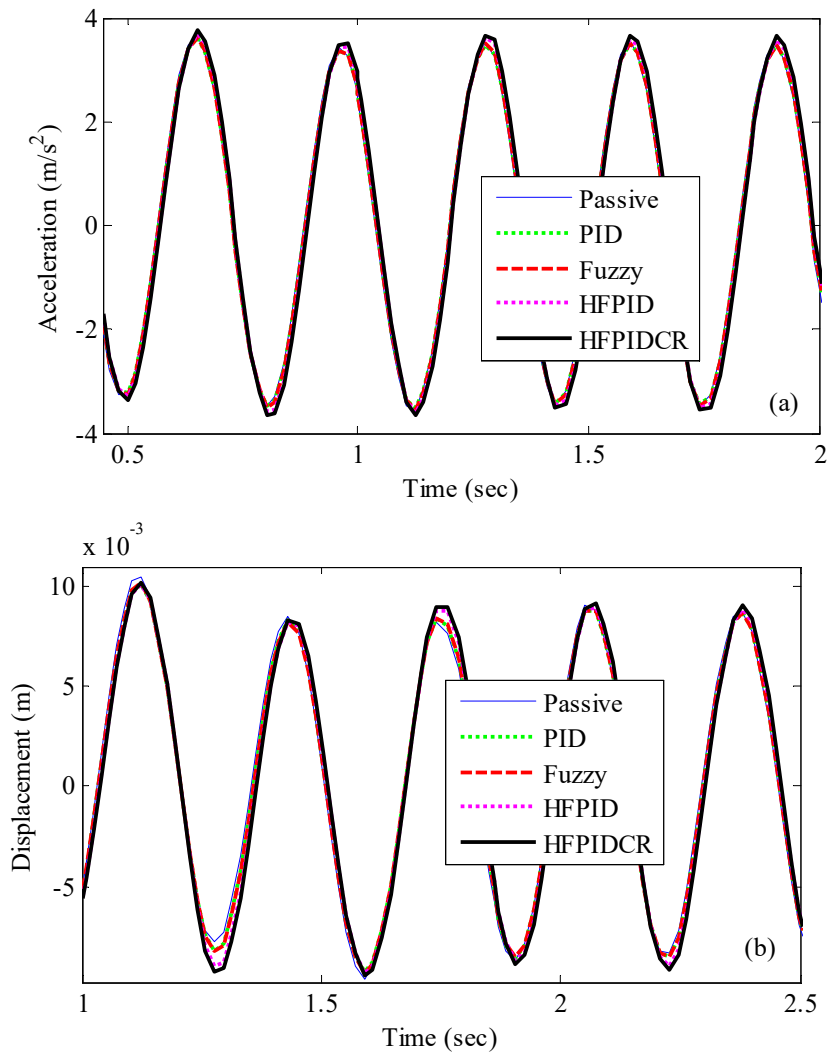


Figure 9.16 Sprung mass response under sinusoidal road input (a) Acceleration (b) Displacement

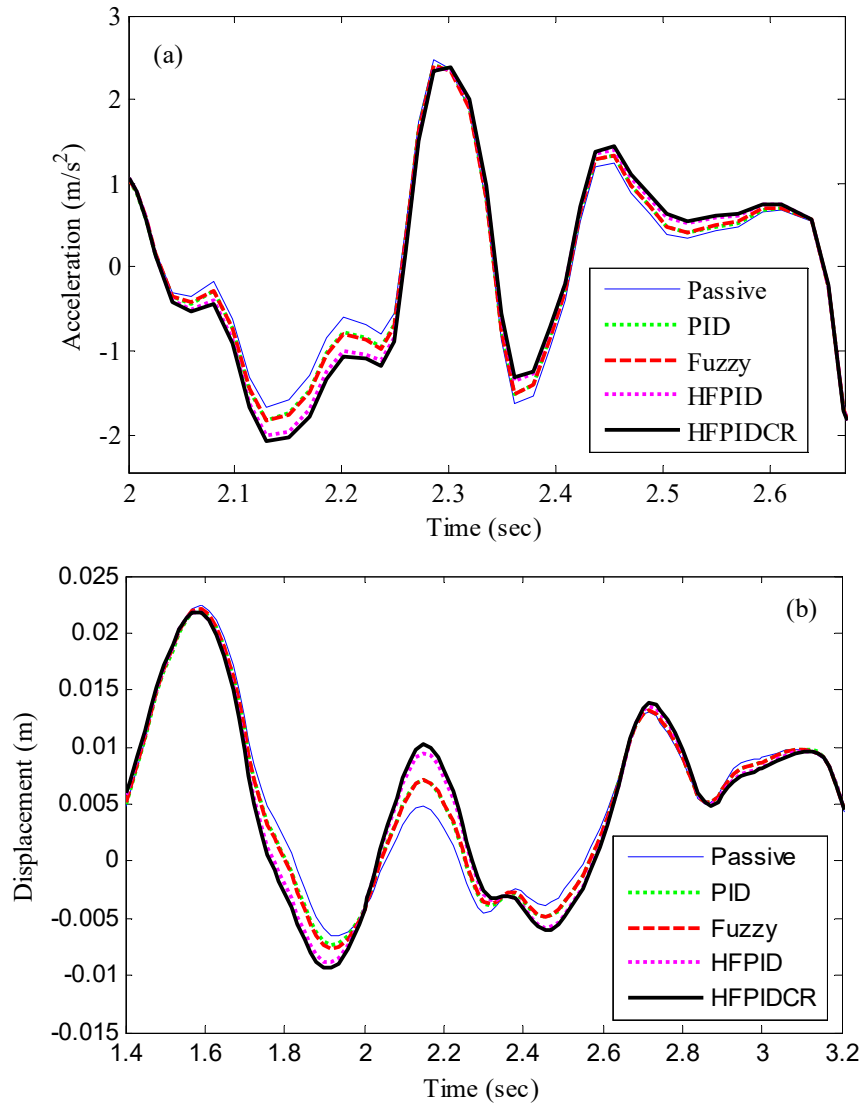


Figure 9.17 Sprung mass response under random road input (a) Acceleration (b) Displacement

Table 9.17 Performance comparison of Sprung mass response ($m_1 = 70$ kg, $m_2 = 325$ kg, $m_3 = 40$ kg)

Controller Type	Acceleration (m/s^2)				Displacement (m)			
	Max.		RMS		Max.		RMS	
	Magnitude	Improvement %	Magnitude	Improvement %	Magnitude	Improvement %	Magnitude	Improvement %
Pulse road profile								
Uncontrolled	12.1845	-----	2.5766	-----	0.0740	-----	0.0299	-----
PID	12.1984	-0.11	2.5673	0.36	0.0736	0.42	0.0292	2.41
Fuzzy	12.2049	-0.17	2.5676	0.35	0.0735	0.62	0.0291	2.94
HFPIID	12.2363	-0.42	2.5685	0.31	0.0737	0.40	0.0285	4.64
HFPIIDCR	12.2638	-0.65	2.5741	0.09	0.0739	0.03	0.0284	5.14
Bump road profile								
Uncontrolled	5.4038	-----	1.4669	-----	0.0469	-----	0.0154	-----
PID	5.4205	-0.31	1.4904	-1.60	0.0481	-2.55	0.0155	-0.65
Fuzzy	5.4342	-0.56	1.5070	-2.73	0.0488	-3.98	0.0157	-1.63
HFPIID	5.4914	-1.62	1.5462	-5.40	0.0500	-6.60	0.0159	-2.95
HFPIIDCR	5.5327	-2.38	1.5723	-7.18	0.0508	-8.21	0.0160	-4.09
Sinusoidal road profile								
Uncontrolled	3.6476	-----	2.4159	-----	0.0166	-----	0.0064	-----
PID	3.6067	1.12	2.4032	0.53	0.0170	-1.97	0.0064	0.23
Fuzzy	3.6195	0.77	2.4082	0.32	0.0170	-2.29	0.0064	0.05
HFPIID	3.7018	-1.49	2.4708	-2.27	0.0176	-5.87	0.0066	-2.91
HFPIIDCR	3.7537	-2.91	2.5094	-3.87	0.0179	-7.57	0.0067	-4.67

Table 9.17 Performance comparison of Sprung mass response ($m_1 = 70$ kg, $m_2 = 325$ kg, $m_3 = 40$ kg)								
Random road profile								
Uncontrolled	2.5499	-----	1.1746	-----	0.0224	-----	0.0083	-----
PID	2.4888	2.40	1.1759	-0.12	0.0220	2.02	0.0082	0.15
Fuzzy	2.4871	2.46	1.1788	-0.36	0.0221	1.39	0.00831	-0.36
HFPIID	2.4871	2.46	1.2051	-2.60	0.0218	2.64	0.00845	-2.12
HFPIIDCR	2.4987	2.01	1.2199	-3.86	0.0219	2.50	0.0085	-3.21

9.4 SUMMARY

In this case, vertical response of passenger seat has been studied at 40 km/h running speed of semi-active quarter car model on four different road surfaces. The secondary suspension system of semi-active quarter car model was controlled by using a PID controller 2, Fuzzy controller 2, HFPIID controller 2 and HFPIIDCR controller 2 separately. Simulation results demonstrate that the vibration control performance of passenger seat is different in case of each controlled suspension system and highly affected by designed controllers. It can be observed that HFPIIDCR controller 2 produced highest desired damping force than other controllers for passenger seat vibration suppression. In conclusion, application of HFPIIDCR controller 2 in secondary suspension of semi-active quarter car system highly improved the acceleration and displacement responses of travelling passenger seat to enhance ride comfort experience compared to uncontrolled and other controlled cases. The power requirement for running the inverse controllers in each case is less since generated highest values by assembled inverse controllers in each case remained below 1 A.

CHAPTER X

FULLY CONTROLLED SEMI-ACTIVE QUARTER CAR SYSTEM

10.1 INTRODUCTION

Fully controlled suspension system represents fully mechatronics based system where primary as well as secondary suspension systems are both semi-active in nature as shown in Figure 10.1. It can be considered as a combination of primary suspension system and secondary suspension system, both assembled with controllers and MR shock absorbers. During the vibration transfer period from road surface to the quarter car model, both MR shock absorber 1 and MR shock absorber 2 starts delivering damping force in the primary and secondary suspension system respectively.

In the primary suspension system, assembled forward and inverse controllers generates desired damping force signal F_{d1} and input current signal I_1 respectively. While in the secondary suspension system, assembled forward and inverse controllers generates desired damping force signal F_{d2} and input current signal I_2 respectively.

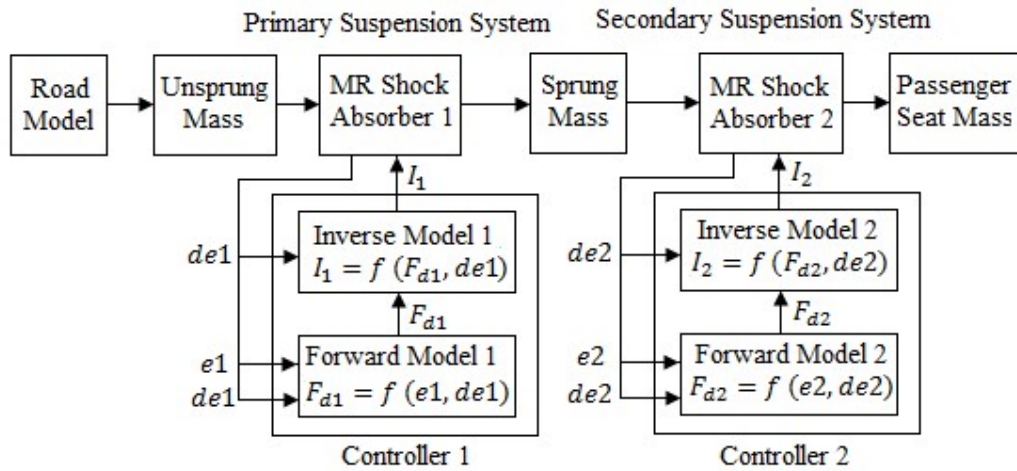


Figure 10.1 Block diagram of fully suspension controlled semi-active quarter car system

10.2 PASSENGER SEAT SIMULATION RESULTS

10.2.1 Pulse Input Disturbance

Figure 10.2 (a)-(b) shows the simulation results of passenger seat acceleration and displacement response in graphical form for $m_2 = 325$ kg and $m_1 = 70$ kg and in mathematical form in Table 10.1 and Table 10.2 while the vehicle passes over the pulse road excitation. It can be seen from graphical and mathematical results that all

controlled semi-active quarter car models achieves better passenger ride comfort and safety issues compared to uncontrolled one. It can be observed that semi-active quarter car model with HFPIDCR controller 1 and HFPIDCR controller 2 is most effective in controlling passenger seat vibrations compared to uncontrolled and other controlled cases.

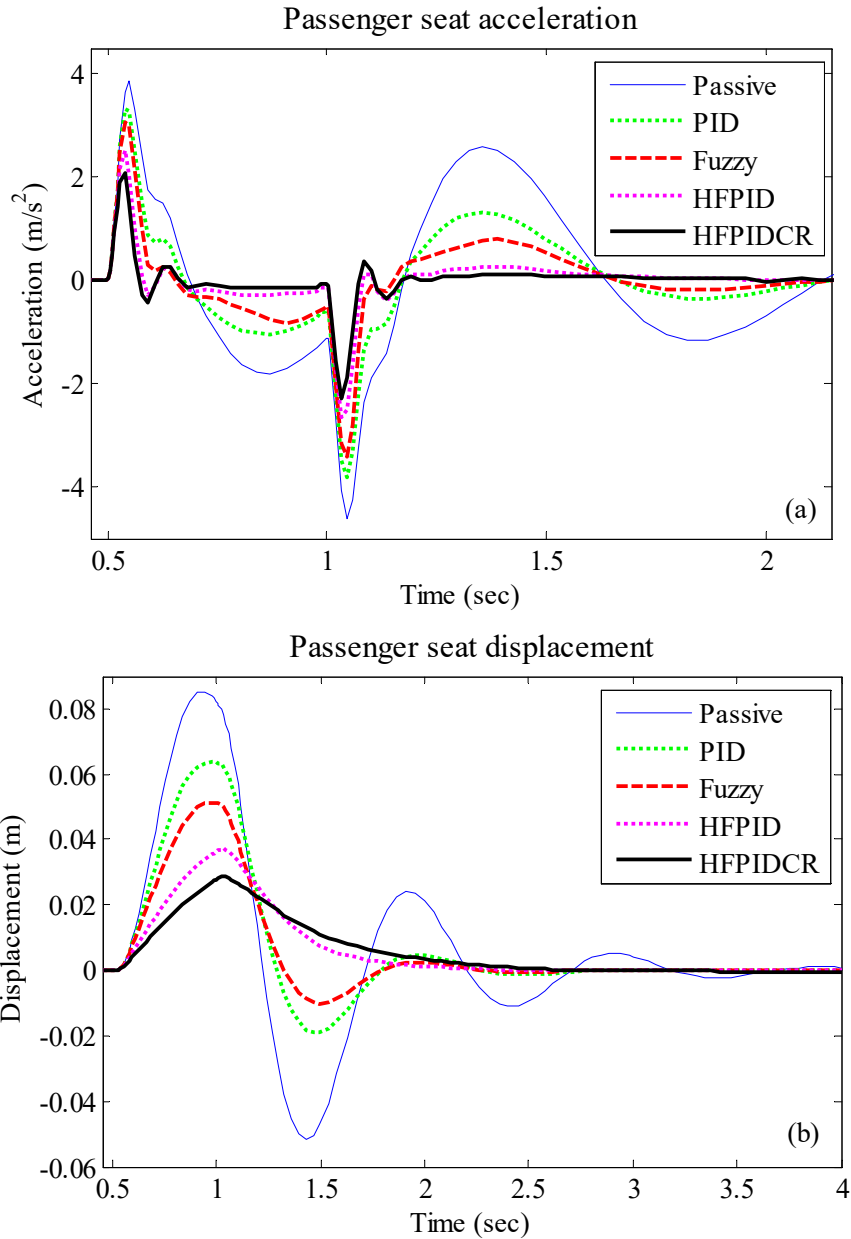


Figure 10.2 (a) Passenger seat acceleration (b) Passenger seat displacement

Table 10.1 Performance comparison of Passenger seat response under Pulse road profile ($m_1 = 70$ kg)

Performance Parameters	Acceleration (m/s^2)				Displacement (m)			
	Max.		RMS		Max.		RMS	
	Magnitude	Improvement %	Magnitude	Improvement %	Magnitude	Improvement %	Magnitude	Improvement %
Controller Type	80% $m_2 = 260$ kg							
Uncontrolled	4.5541	-----	1.3679	-----	0.0842	-----	0.0324	-----
PID	4.0615	10.82	0.9756	28.68	0.0618	26.60	0.0242	25.14
Fuzzy	3.7521	17.61	0.8100	40.79	0.0496	41.12	0.0194	40.22
HFPID	2.9615	34.97	0.6024	55.96	0.0366	56.52	0.0150	53.70
HFPIDCR	2.4030	47.23	0.4962	63.73	0.0285	66.20	0.0121	62.58
Controller Type	100% $m_2 = 325$ kg							
Uncontrolled	3.8608	-----	1.2844	-----	0.0853	-----	0.0333	-----
PID	3.4096	11.69	0.8876	30.89	0.0638	25.26	0.0244	26.78
Fuzzy	3.1323	18.87	0.7297	43.19	0.0514	39.81	0.0194	41.71
HFPID	2.3936	38.00	0.5154	59.88	0.0372	56.43	0.0148	55.72
HFPIDCR	2.0466	46.99	0.4181	67.45	0.0288	66.30	0.0119	64.16
Controller Type	120% $m_2 = 390$ kg							
Uncontrolled	3.2564	-----	1.2030	-----	0.0861	-----	0.0356	-----
PID	2.8887	11.29	0.8300	31.01	0.0656	23.84	0.0262	26.36
Fuzzy	2.6902	17.39	0.6841	43.14	0.0530	38.38	0.0210	41.17
HFPID	2.1539	33.86	0.4632	61.49	0.0377	56.15	0.0155	56.51
HFPIDCR	1.7616	45.91	0.3707	69.19	0.0290	66.31	0.0124	65.17

Table 10.2 Performance comparison of Passenger seat response under Pulse road profile ($m_2 = 325$ kg)

Performance Parameters	Acceleration (m/s^2)				Displacement (m)			
	Max.		RMS		Max.		RMS	
	Magnitude	Improvement %	Magnitude	Improvement %	Magnitude	Improvement %	Magnitude	Improvement %
Controller Type	80% $m_1 = 56$ kg							
Uncontrolled	4.4652	-----	1.3329	-----	0.0839	-----	0.0327	-----
PID	3.9202	12.21	0.9380	29.62	0.0629	25.01	0.0242	25.89
Fuzzy	3.5878	19.65	0.7709	42.16	0.0505	39.83	0.0192	41.13
HFPID	2.7214	39.05	0.5540	58.44	0.0371	55.83	0.0148	54.73
HFPIDCR	2.2253	50.16	0.4468	66.48	0.0287	65.76	0.0120	63.28
Controller Type	100% $m_1 = 70$ kg							
Uncontrolled	3.8608	-----	1.2844	-----	0.0853	-----	0.0333	-----
PID	3.4096	11.69	0.8876	30.89	0.0638	25.26	0.0244	26.78
Fuzzy	3.1323	18.87	0.7297	43.19	0.0514	39.81	0.0194	41.71
HFPID	2.3936	38.00	0.5154	59.88	0.0372	56.43	0.0148	55.72
HFPIDCR	2.0466	46.99	0.4181	67.45	0.0288	66.30	0.0119	64.16
Controller Type	120% $m_1 = 84$ kg							
Uncontrolled	3.3488	-----	1.2343	-----	0.0865	-----	0.0343	-----
PID	2.9642	11.49	0.8400	31.95	0.0647	25.19	0.0250	27.23
Fuzzy	2.7680	17.34	0.6913	43.99	0.0523	39.56	0.0200	41.90
HFPID	2.2633	32.42	0.4771	61.34	0.0373	56.85	0.0149	56.52
HFPIDCR	1.8864	43.67	0.3879	68.57	0.0288	66.71	0.0120	64.95

Figure 10.3 and Figure 10.5 shows the desired damping force signals generated by assembled forward controller 1 in primary suspension system and forward controller 2 in secondary suspension system respectively.

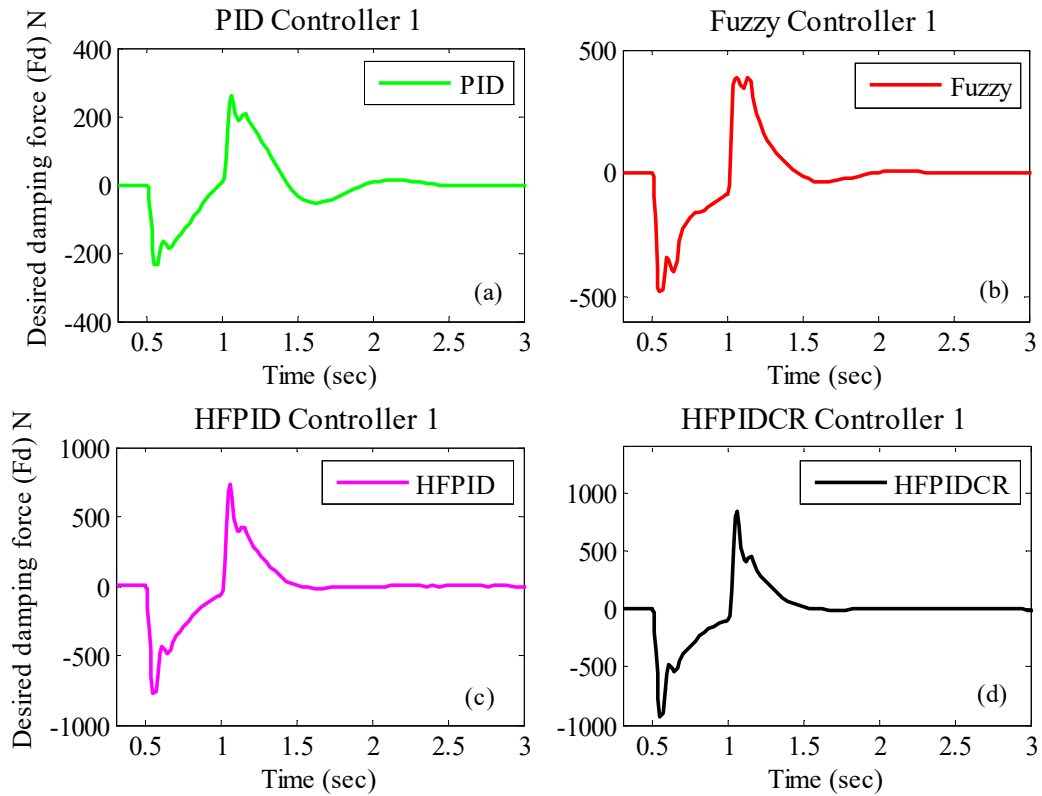


Figure 10.3 Desired damping force signals supplied by different controller

Table 10.3 shows that the highest value of the desired damping force signal is generated by HFPIDCR controller 1 assembled in primary suspension system as 925.34 N during compression stage and 848.08 N during the rebound stage. The highest value of desired damping force signal generated by assembled HFPIDCR controller 2 in the secondary suspension system is presented in Table 10.5 as 241.40 N during the compression stage and 143.57 N during the rebound stage respectively.

Table 10.3 Calculated Max. desired damping force using Forward controller 1 (N)

Forward Controller 1	Max. Damping Force (N)			
	PID	Fuzzy	HFPID	HFPIDCR
Compression Stage	235.70	477.48	776.57	925.34
Rebound Stage	259.29	385.10	729.42	848.08

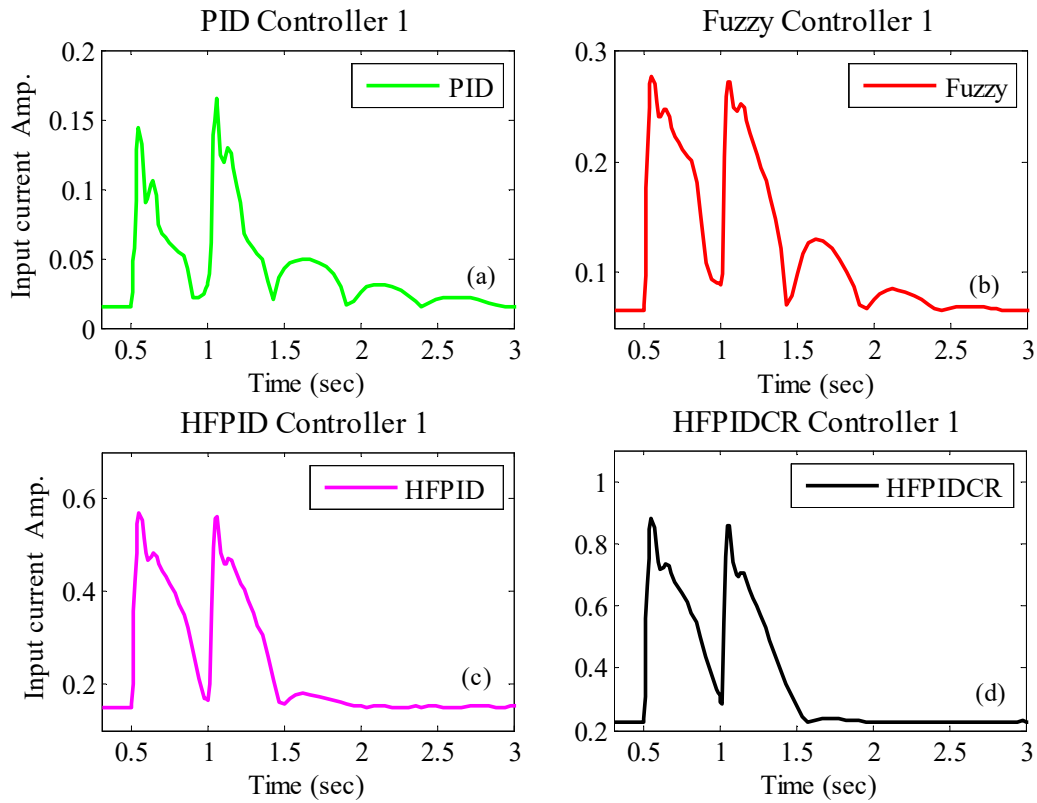


Figure 10.4 Input current signal generated by different controllers

Figure 10.4 and Figure 10.6 shows the input current generated by assembled inverse controller 1 in primary suspension system and inverse controller 2 in secondary suspension system respectively. Table 10.4 and Table 10.6 shows the highest values of generated input current signals by assembled inverse controller 1 and inverse controller 2 respectively. It can be observed from Table 10.4 and Table 10.6 that the HFPIDCR based inverse controller 1 generated peak value of input current of 0.88 A while inverse controller 2 generated peak value of input current of 0.37 A.

Table 10.4 Calculated Max. input current using Inverse controller 1 (A)

Inverse Controller 1	Max. input current (A)			
	PID	Fuzzy	HFPID	HFPIDCR
Magnitude	0.17	0.28	0.57	0.88

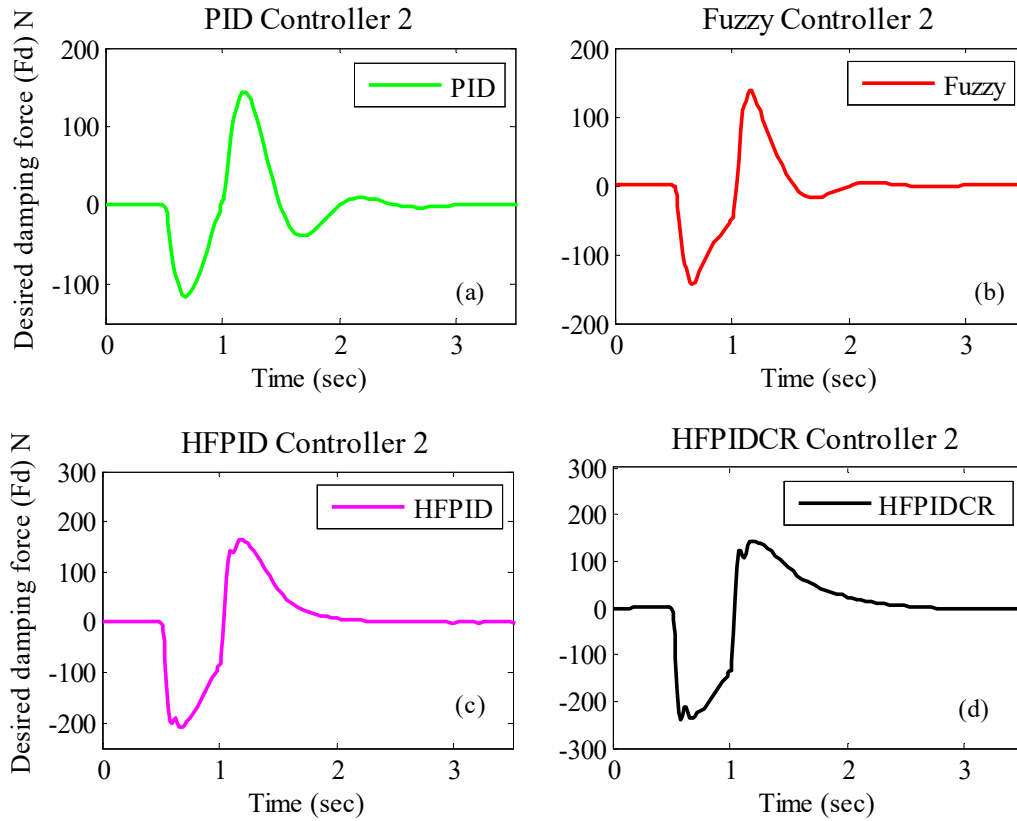
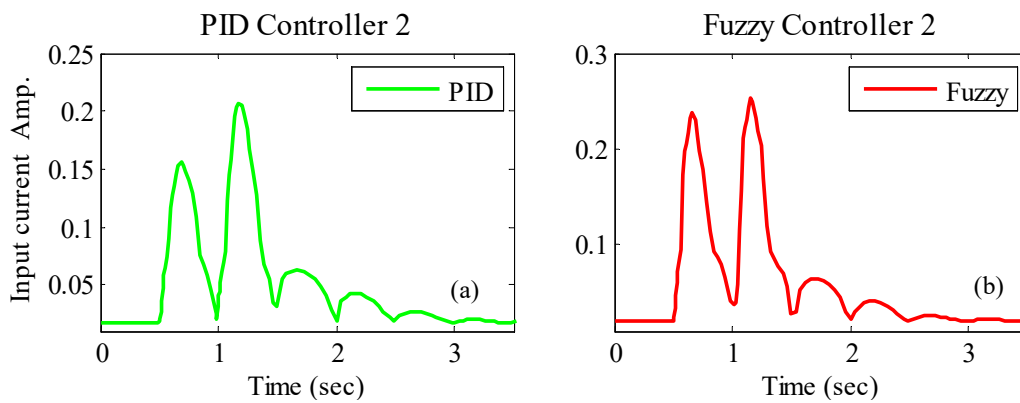


Figure 10.5 Desired damping force signals supplied by different controllers

Table 10.5 Calculated Max. desired damping force using Forward controller 2 (N)

Forward Controller 2	Max. Damping Force (N)			
	PID	Fuzzy	HFPID	HFPIDCR
Compression Stage	115.92	144.28	208.83	241.40
Rebound Stage	144.06	138.57	165.26	143.57



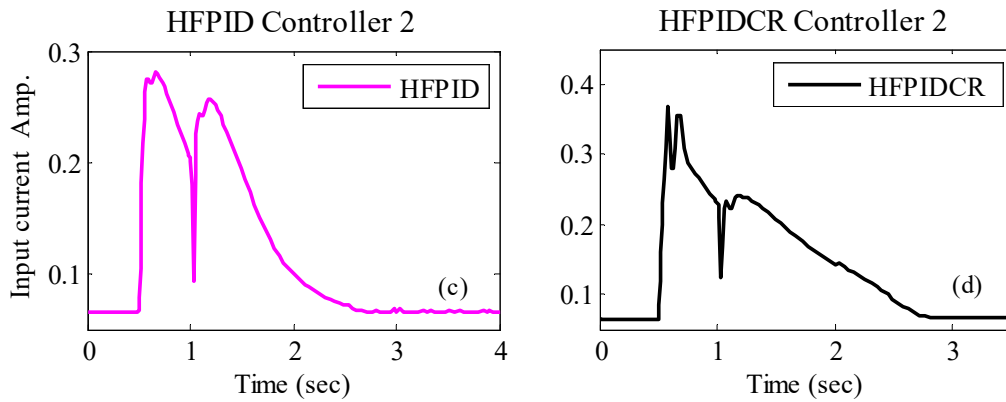


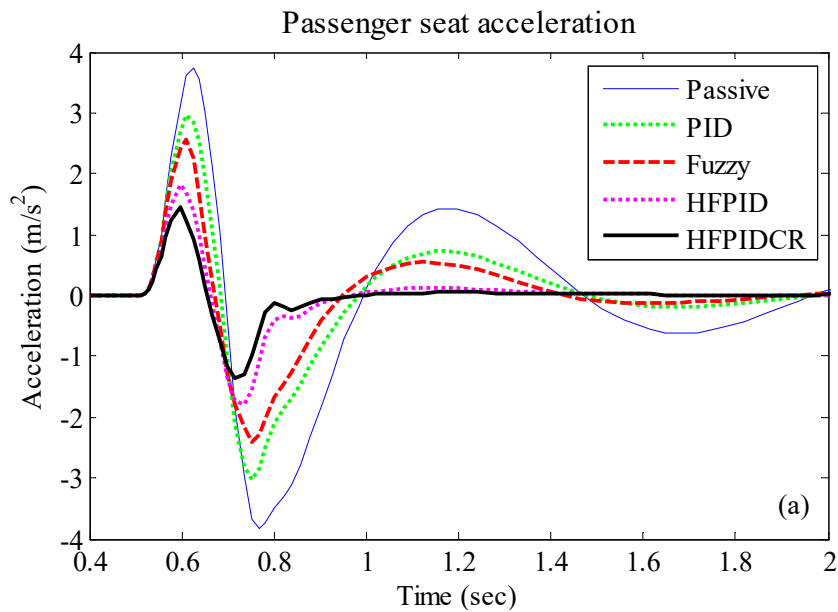
Figure 10.6 Input current signal generated by different controllers

Table 10.6 Calculated Max. input current using Inverse controller 2 (A)

Inverse Controller 2	Max. input current (A)			
	PID	Fuzzy	HFPID	HFPIDCR
Magnitude	0.21	0.25	0.28	0.37

10.2.2 Bump Input Disturbance

The simulation results in terms of passenger seat acceleration as well as displacement response are presented in Figure 10.7 (a)-(b) for $m_2 = 325$ kg and $m_1 = 70$ kg as well as in Table 10.7 and Table 10.8 for graphical and mathematical values respectively while the quarter car passes over the bump road excitation.



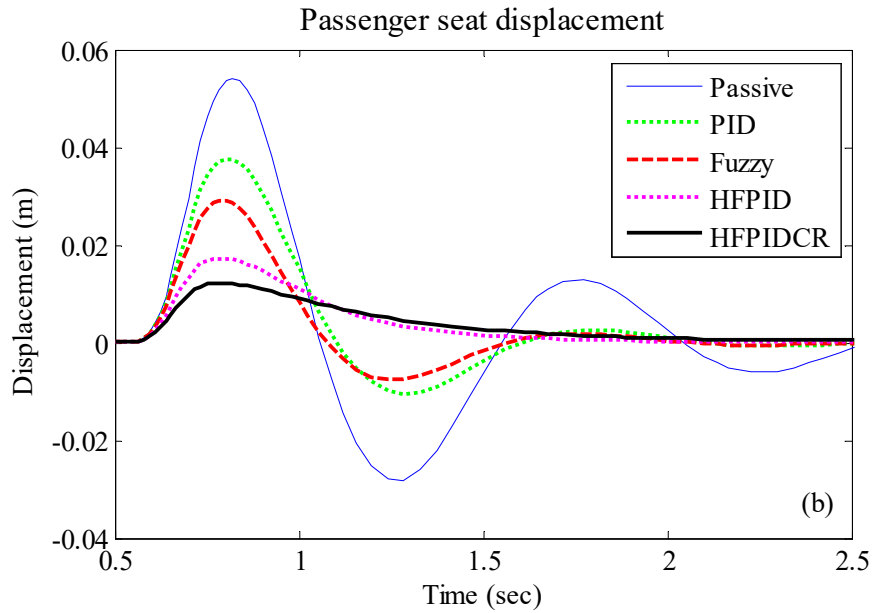


Figure 10.7 (a) Passenger seat acceleration (b) Passenger seat displacement

The graphical and mathematical results show that semi-active controlled suspension systems provide improved ride comfort and safety response to travelling passengers compared to uncontrolled one under bump road excitation. The best results are provided by HFPIIDCR controller in controlling the passenger seat vibrations in terms of acceleration and displacement responses.

Figure 10.8 shows the desired damping force signal generated by assembled forward controller 1 in primary suspension system. Table 10.9 shows that the highest values of the desired damping force signals was generated in primary suspension system by HFPIIDCR controller 1 as 956.55 N during compression stage while 409.91 N during rebound stage.

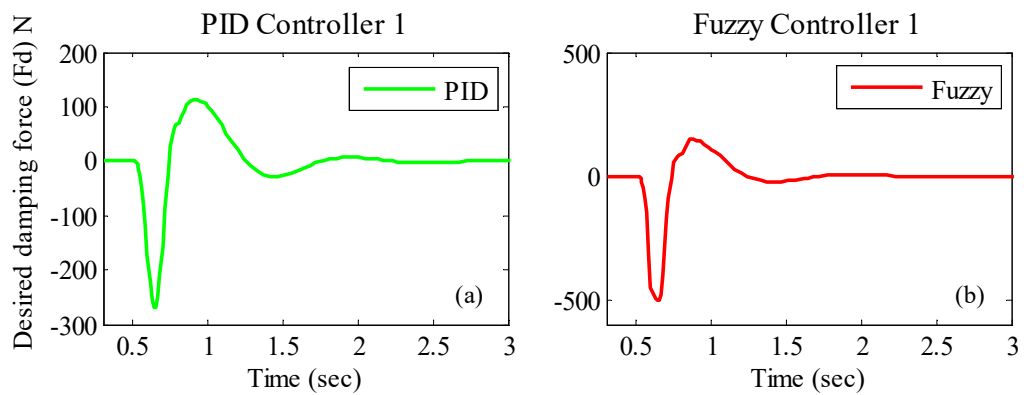


Table 10.7 Performance comparison of Passenger seat response under Bump road profile ($m_1 = 70$ kg)

Performance Parameters	Acceleration (m/s^2)				Displacement (m)			
	Max.		RMS		Max.		RMS	
	Magnitude	Improvement %	Magnitude	Improvement %	Magnitude	Improvement %	Magnitude	Improvement %
Controller Type	80% $m_2 = 260$ kg							
Uncontrolled	4.3291	-----	1.4607	-----	0.0574	-----	0.0178	-----
PID	3.3869	21.77	1.0370	29.00	0.0395	31.12	0.0118	33.71
Fuzzy	2.9288	32.35	0.8162	44.12	0.0304	47.06	0.0090	49.57
HFPID	2.0190	53.36	0.5406	62.99	0.0178	68.98	0.0060	66.49
HFPIDCR	1.6155	62.68	0.4037	72.36	0.0124	78.40	0.0046	74.27
Controller Type	100% $m_2 = 325$ kg							
Uncontrolled	3.7298	-----	1.2472	-----	0.0542	-----	0.0172	-----
PID	2.9412	21.14	0.8900	28.65	0.0377	30.40	0.0116	32.66
Fuzzy	2.5589	31.39	0.7136	42.78	0.0291	46.37	0.0088	48.78
HFPID	1.8185	51.24	0.4663	62.61	0.0173	68.05	0.0060	65.26
HFPIDCR	1.4349	61.53	0.3472	72.16	0.0121	77.64	0.0046	73.18
Controller Type	120% $m_2 = 390$ kg							
Uncontrolled	3.2620	-----	1.0873	-----	0.0513	-----	0.0170	-----
PID	2.6083	20.04	0.7778	28.46	0.0361	29.60	0.0115	32.29
Fuzzy	2.2643	30.58	0.6345	41.65	0.0282	45.02	0.0086	49.49
HFPID	1.6127	50.56	0.4110	62.20	0.0170	66.96	0.0059	65.34
HFPIDCR	1.2587	61.41	0.3066	71.80	0.0120	76.55	0.0045	73.57

Table 10.8 Performance comparison of Passenger seat response under Bump road profile ($m_2 = 325$ kg)

Performance Parameters	Acceleration (m/s^2)				Displacement (m)			
	Max.		RMS		Max.		RMS	
	Magnitude	Improvement %	Magnitude	Improvement %	Magnitude	Improvement %	Magnitude	Improvement %
Controller Type	80% $m_1 = 56$ kg							
Uncontrolled	4.1223	-----	1.3039	-----	0.0551	-----	0.0169	-----
PID	3.2182	21.93	0.9100	30.21	0.0381	30.92	0.0112	33.71
Fuzzy	2.7543	33.19	0.7151	45.16	0.0292	46.92	0.0085	50.08
HFPID	1.9117	53.63	0.4680	64.11	0.0173	68.54	0.0058	65.82
HFPIDCR	1.5178	63.18	0.3491	73.22	0.0121	78.02	0.0045	73.39
Controller Type	100% $m_1 = 70$ kg							
Uncontrolled	3.7298	-----	1.2472	-----	0.0542	-----	0.0172	-----
PID	2.9412	21.14	0.8900	28.65	0.0377	30.40	0.0116	32.66
Fuzzy	2.5589	31.39	0.7136	42.78	0.0291	46.37	0.0088	48.78
HFPID	1.8185	51.24	0.4663	62.61	0.0173	68.05	0.0060	65.26
HFPIDCR	1.4349	61.53	0.3472	72.16	0.0121	77.64	0.0046	73.18
Controller Type	120% $m_1 = 84$ kg							
Uncontrolled	3.4023	-----	1.1553	-----	0.0531	-----	0.0171	-----
PID	2.6904	20.92	0.8301	28.15	0.0372	29.94	0.0115	33.18
Fuzzy	2.3837	29.94	0.6763	41.46	0.0289	45.56	0.0088	48.61
HFPID	1.6662	51.03	0.4414	61.79	0.0172	67.58	0.0058	65.89
HFPIDCR	1.3304	60.90	0.3312	71.33	0.0120	77.41	0.0045	73.70

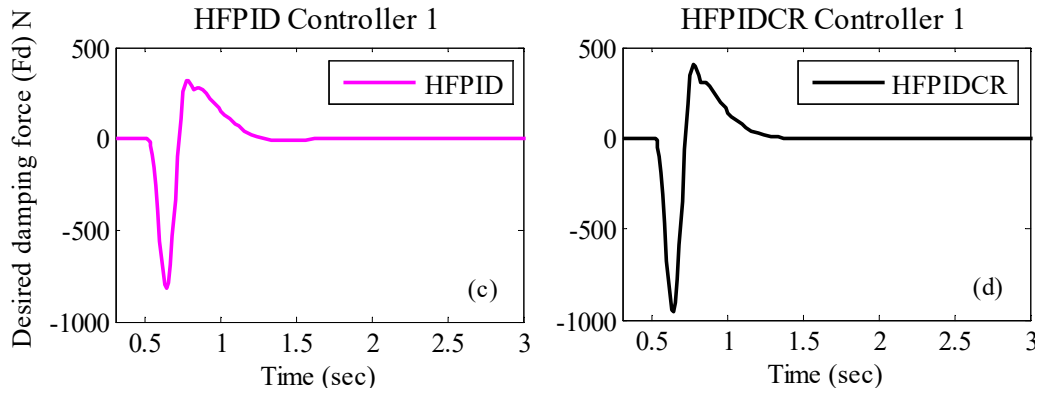


Figure 10.8 Desired damping force signals supplied by different controllers

Table 10.9 Calculated Max. desired damping force using Forward controller 1 (N)

Forward Controller 1	Max. Damping Force (N)			
	PID	Fuzzy	HFPID	HFPIDCR
Compression Stage	269.44	499.79	820.29	956.55
Rebound Stage	112.18	150.73	317.59	409.91

Figure 10.9 represents the input current signal generated by assembled inverse controller 1 in primary suspension system.

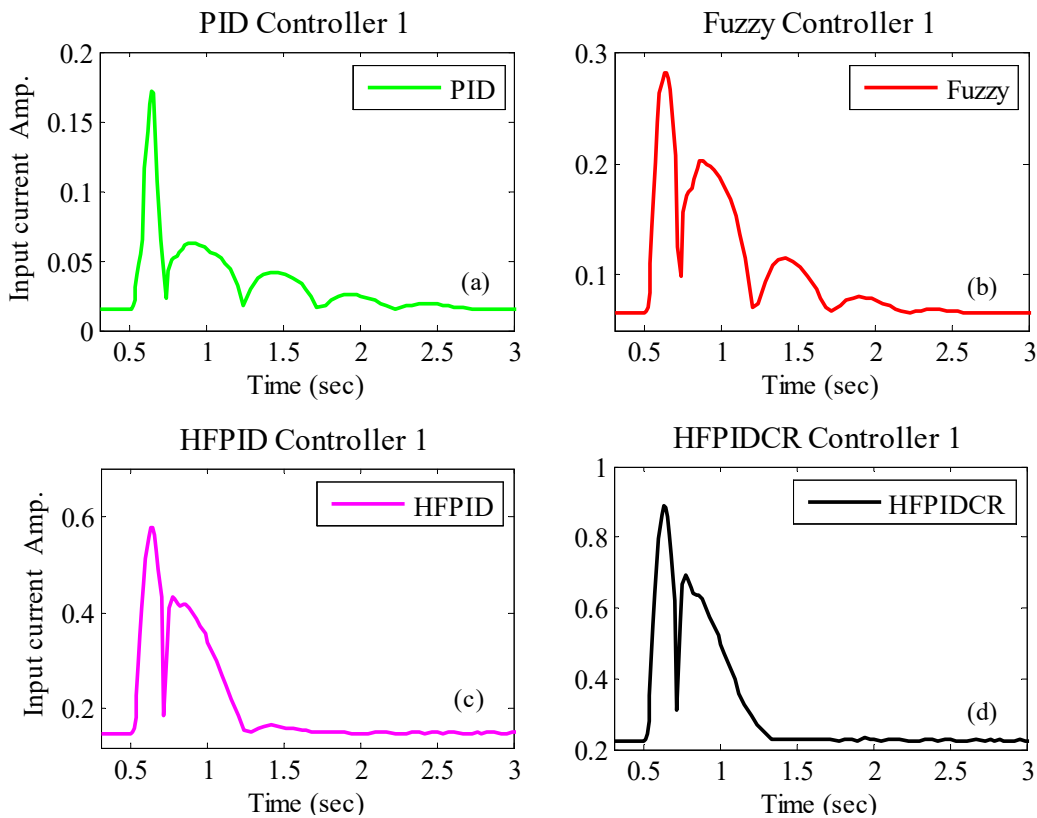


Figure 10.9 Input current signal generated by different controllers

Table 10.10 shows the highest values of input current generated by inverse controller 1 in primary suspension system.

Table 10.10 Calculated Max. input current using Inverse controller 1 (A)

Inverse Controller 1	Max. input current (A)			
	PID	Fuzzy	HFPID	HFPIDCR
Magnitude	0.17	0.28	0.58	0.89

Figure 10.10 shows the generated desired damping force signal by assembled forward controller 2 in the secondary suspension system. Table 10.11 shows that the highest values of the desired damping force signals was generated in the secondary suspension system by HFPIDCR controller 2 as 308.43 N during compression stage and 60.65 N during the rebound stage respectively.

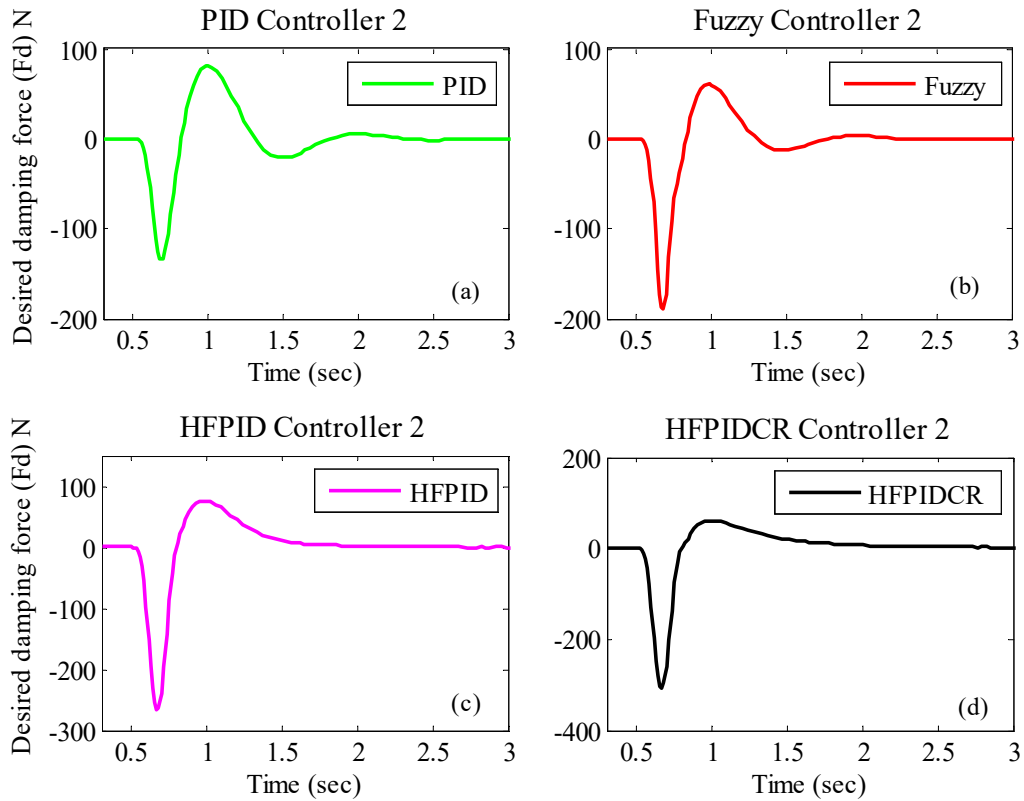


Figure 10.10 Desired damping force signals supplied by different controllers

Table 10.11 Calculated Max. desired damping force using Forward controller 2 (N)

Forward Controller 2	Max. Damping Force (N)			
	PID	Fuzzy	HFPID	HFPIDCR
Compression Stage	133.16	188.10	267.31	308.43
Rebound Stage	81.21	61.17	76.31	60.65

Figure 10.11 represents the input current signal generated by assembled inverse controller 2 as well as Table 10.12 shows the highest values of input current generated by inverse controller 2 in secondary suspension system. It can be seen from Table 10.12 that highest values of input current generated by inverse controller in secondary suspension system is 0.50 A having HFPIDCR controller 2 as forward controller.

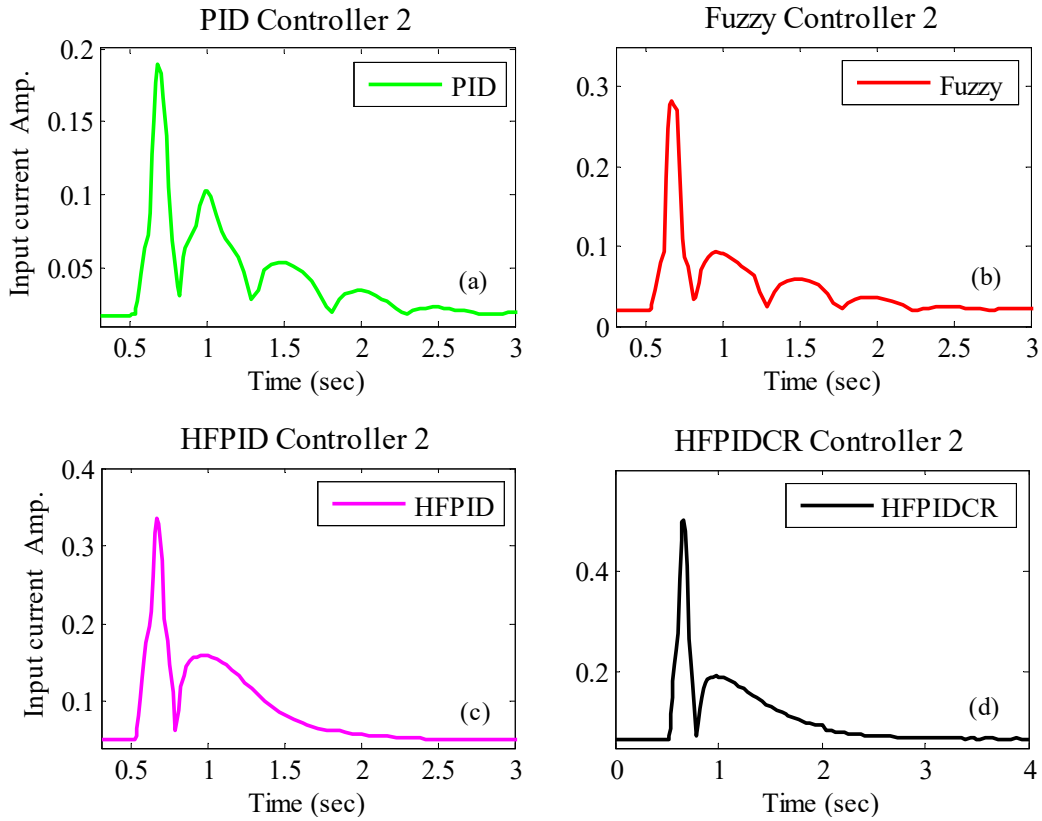


Figure 10.11 Input current signal generated by different controllers

It can also be seen from Table 10.12 that highest values of input current generated by inverse controller 2 in secondary suspension system is 0.50 A having HFPIDCR assembled controller.

Table 10.12 Calculated Max. input current using Inverse controller 2 (A)

Inverse Controller 2	Max. input current (A)			
	PID	Fuzzy	HFPID	HFPIDCR
Magnitude	0.19	0.28	0.44	0.50

10.2.3 Sinusoidal Input Disturbance

The simulation results of passenger seat acceleration and displacement response under sinusoidal input excitation are shown in Figure 10.12 (a)-(b) for $m_2 = 325$ kg and $m_1 = 70$ kg while the mathematical values are shown in Table 10.13 and Table 10.14.

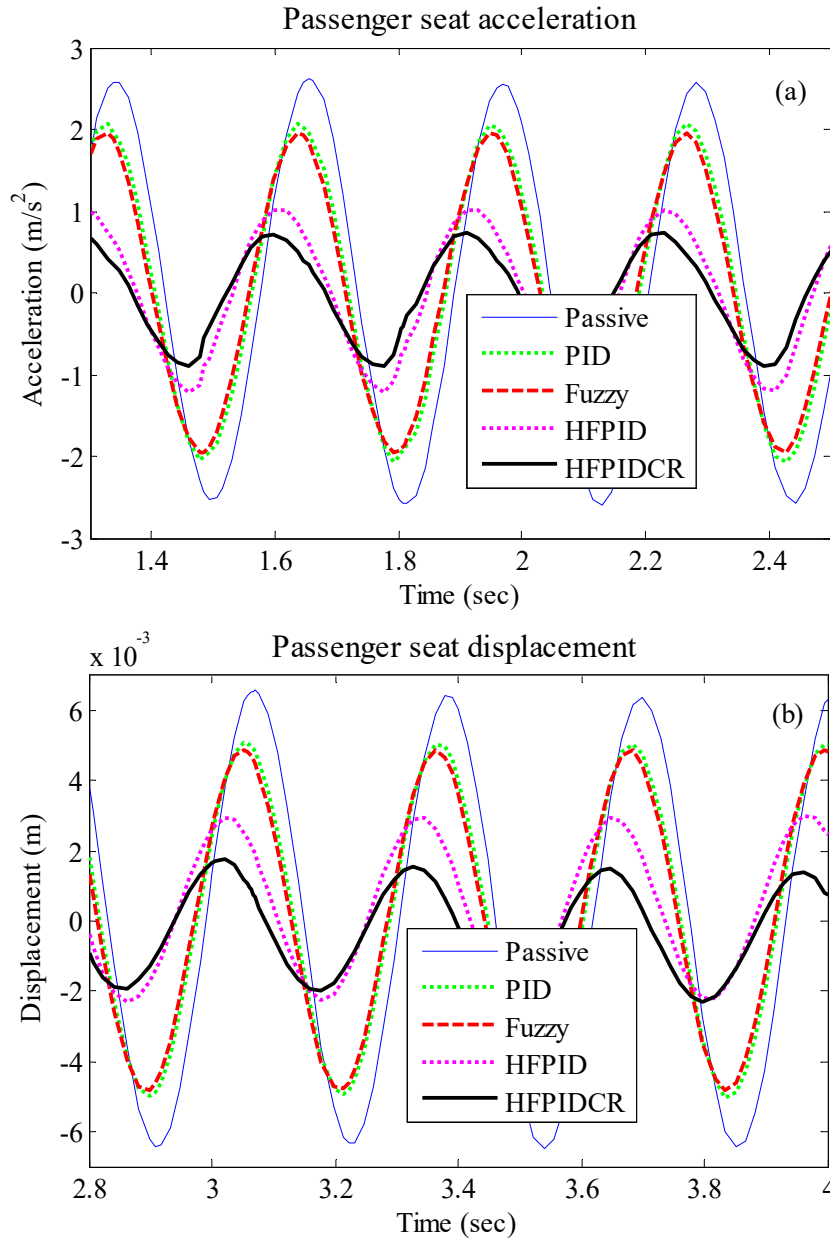


Figure 10.12 (a) Passenger seat acceleration (b) Passenger seat displacement

It can be observed from graphical and mathematical results that the vibration control of passenger seat is better for all controlled cases compared to uncontrolled one. It can be seen that the fully controlled semi-active quarter car system with HFPIDCR controllers in primary and secondary suspension system provided best response related to passenger ride comfort issues.

Table 10.13 Performance comparison of Passenger seat response under Sinusoidal road profile ($m_1 = 70$ kg)

Performance Parameters	Acceleration (m/s ²)				Displacement (m)			
	Max.		RMS		Max.		RMS	
	Magnitude	Improvement %	Magnitude	Improvement %	Magnitude	Improvement %	Magnitude	Improvement %
Controller Type	80% $m_2 = 260$ kg							
Uncontrolled	3.4765	-----	2.4832	-----	0.0187	-----	0.0070	-----
PID	2.6410	24.03	1.9126	22.98	0.0132	29.56	0.0051	26.38
Fuzzy	2.3994	30.98	1.7643	28.95	0.0115	38.72	0.0047	32.86
HFPID	1.2085	65.24	0.8590	65.41	0.0062	66.99	0.0024	66.11
HFPIDCR	0.9714	72.06	0.5958	76.01	0.0043	76.89	0.0016	76.40
Controller Type	100% $m_2 = 325$ kg							
Uncontrolled	2.7350	-----	1.9321	-----	0.0169	-----	0.0055	-----
PID	2.1351	21.94	1.5041	22.15	0.0121	28.74	0.0041	26.78
Fuzzy	1.9972	26.98	1.4268	26.15	0.0108	36.42	0.0038	31.19
HFPID	1.0368	62.09	0.7502	61.17	0.0058	66.05	0.0020	63.82
HFPIDCR	0.8354	69.46	0.5378	72.16	0.0041	76.02	0.0014	73.98
Controller Type	120% $m_2 = 390$ kg							
Uncontrolled	2.3195	-----	1.6170	-----	0.0155	-----	0.0049	-----
PID	1.8141	21.79	1.2603	22.06	0.0111	28.21	0.0035	27.33
Fuzzy	1.7139	26.11	1.2114	25.08	0.0101	34.88	0.0033	31.16
HFPID	1.0143	56.27	0.6525	59.65	0.0054	65.23	0.0018	63.44
HFPIDCR	0.7641	67.06	0.4719	70.82	0.0038	75.32	0.0013	73.48

Table 10.14 Performance comparison of Passenger seat response under Sinusoidal road profile ($m_2 = 325$ kg)

Performance Parameters	Acceleration (m/s^2)				Displacement (m)			
	Max.		RMS		Max.		RMS	
	Magnitude	Improvement %	Magnitude	Improvement %	Magnitude	Improvement %	Magnitude	Improvement %
Controller Type	80% $m_1 = 56$ kg							
Uncontrolled	3.1733	-----	2.2499	-----	0.0178	-----	0.0064	-----
PID	2.3393	26.28	1.6412	27.05	0.0124	30.28	0.0044	30.51
Fuzzy	2.1800	31.30	1.5417	31.47	0.0111	37.57	0.0041	35.27
HFPID	1.1301	64.39	0.7700	65.77	0.0058	67.28	0.0020	68.18
HFPIDCR	0.8952	71.79	0.5501	75.55	0.0041	77.07	0.0014	77.65
Controller Type	100% $m_1 = 70$ kg							
Uncontrolled	2.7350	-----	1.9321	-----	0.0169	-----	0.0055	-----
PID	2.1351	21.94	1.5041	22.15	0.0121	28.74	0.0041	26.78
Fuzzy	1.9972	26.98	1.4268	26.15	0.0108	36.42	0.0038	31.19
HFPID	1.0368	62.09	0.7502	61.17	0.0058	66.05	0.0020	63.82
HFPIDCR	0.8354	69.46	0.5378	72.16	0.0041	76.02	0.0014	73.98
Controller Type	120% $m_1 = 84$ kg							
Uncontrolled	2.4032	-----	1.7175	-----	0.0161	-----	0.0053	-----
PID	1.9087	20.58	1.4089	17.97	0.0117	27.47	0.0040	24.44
Fuzzy	1.8141	24.51	1.3488	21.46	0.0104	35.43	0.0037	29.24
HFPID	0.9935	58.66	0.7300	57.50	0.0057	64.84	0.0020	61.81
HFPIDCR	0.7821	67.45	0.5194	69.76	0.0040	74.96	0.0014	72.75

The generated desired damping force signals by assembled forward controllers in primary and secondary suspension system are shown in Figure 10.13 and Figure 10.15. Table 10.15 and Table 10.17 shows the calculated highest values of desired damping force. The highest desired damping force values are generated by HFPIDCR controllers as 759.08 N during compression stage and 1009.8 N during rebound stage in primary suspension system while in secondary suspension system; it is 130.93 N during compression stage and 131.19 N during rebound stages respectively.

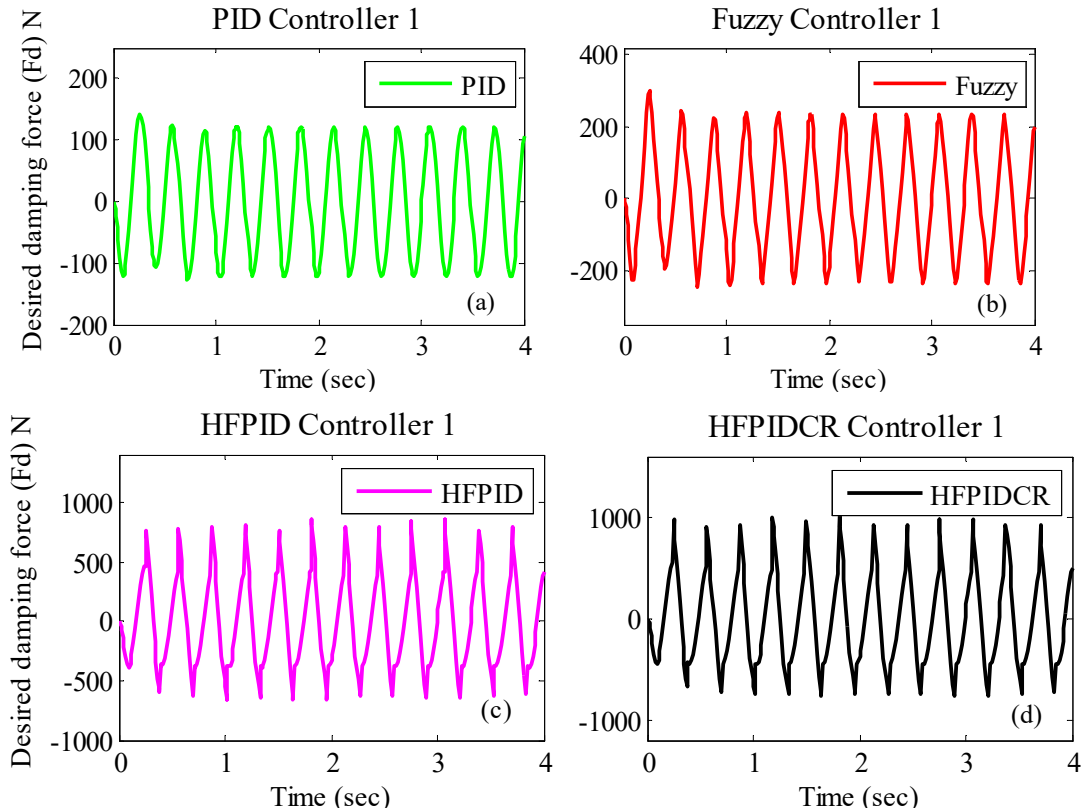


Figure 10.13 Desired damping force signals supplied by different controllers

Table 10.15 Calculated Max. desired damping force using Forward controller 1 (N)

Forward Controller 1	Max. Damping Force (N)			
	PID	Fuzzy	HFPID	HFPIDCR
Compression Stage	126.01	244.99	658.93	759.08
Rebound Stage	143.03	299.79	853.71	1009.8

The input current signals generated by assembled inverse controllers in primary and secondary suspension systems are shown in Figure 10.14 Figure 10.16 respectively while the peak values of the same is shown in Table 10.16 and Table 10.18. It can be

seen that the highest value of input current is generated by HFPIDCR based inverse controller 1 as 0.83 A and inverse controller 2 as 0.24 A respectively.

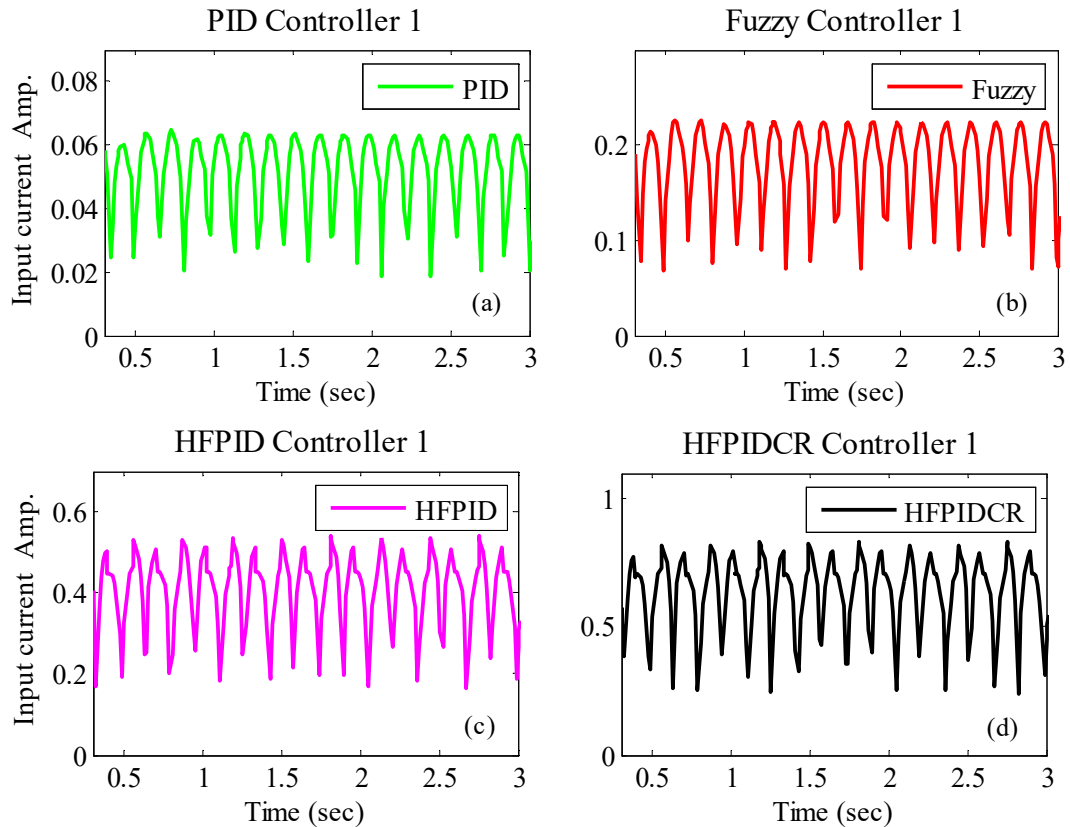
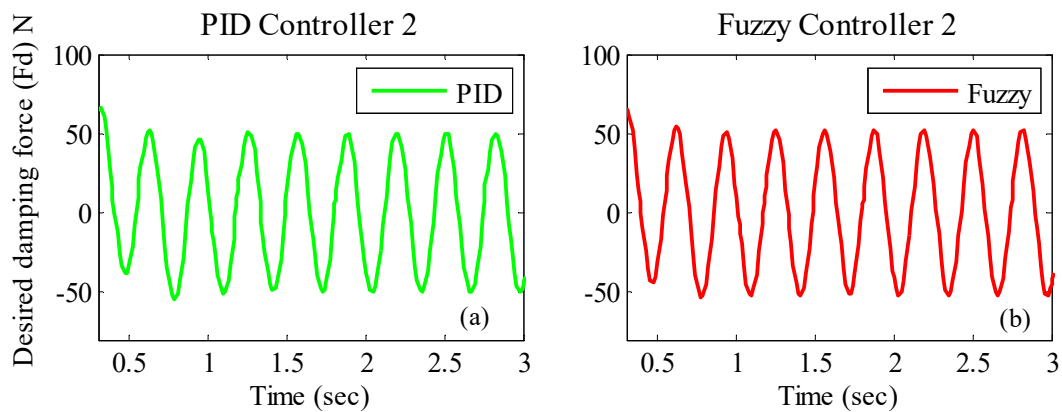


Figure 10.14 Input current signal generated by different controllers

Table 10.16 Calculated Max. input current using Inverse controller 1 (A)

Inverse Controller 1	Max. input current (A)			
	PID	Fuzzy	HFPID	HFPIDCR
Magnitude	0.07	0.24	0.54	0.83



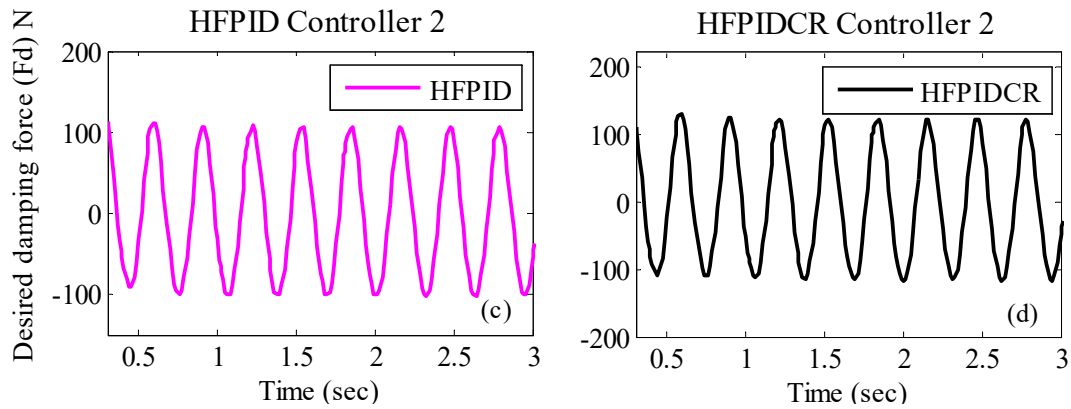


Figure 10.15 Desired damping force signals supplied by different controllers

Table 10.17 Calculated Max. desired damping force using Forward controller 2 (N)

Forward Controller 2	Max. Damping Force (N)			
	PID	Fuzzy	HFPID	HFPIDCR
Compression Stage	54.23	57.28	113.07	130.93
Rebound Stage	65.77	64.81	120.13	131.19

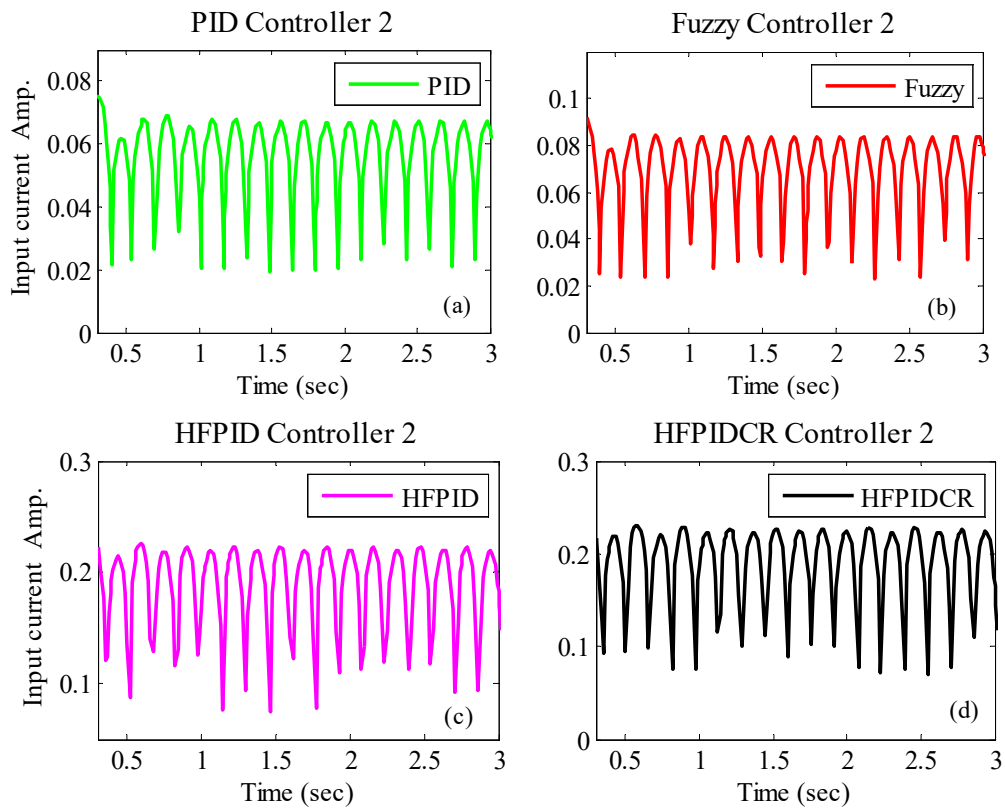


Figure 10.16 Input current signal generated by different controllers

Table 10.18 Calculated Max. input current using Inverse controller 2 (A)

Inverse Controller 2	Max. input current (A)			
	PID	Fuzzy	HFPID	HFPIDCR
Magnitude	0.07	0.09	0.23	0.24

10.2.4 Random Input Disturbance

The simulated passenger seat acceleration and displacement response under random road profile are shown in Figure 10.17 (a)-(b) for $m_2 = 325$ kg and $m_1 = 70$ kg while the mathematical values are shown in Table 10.19 and Table 10.20 respectively.

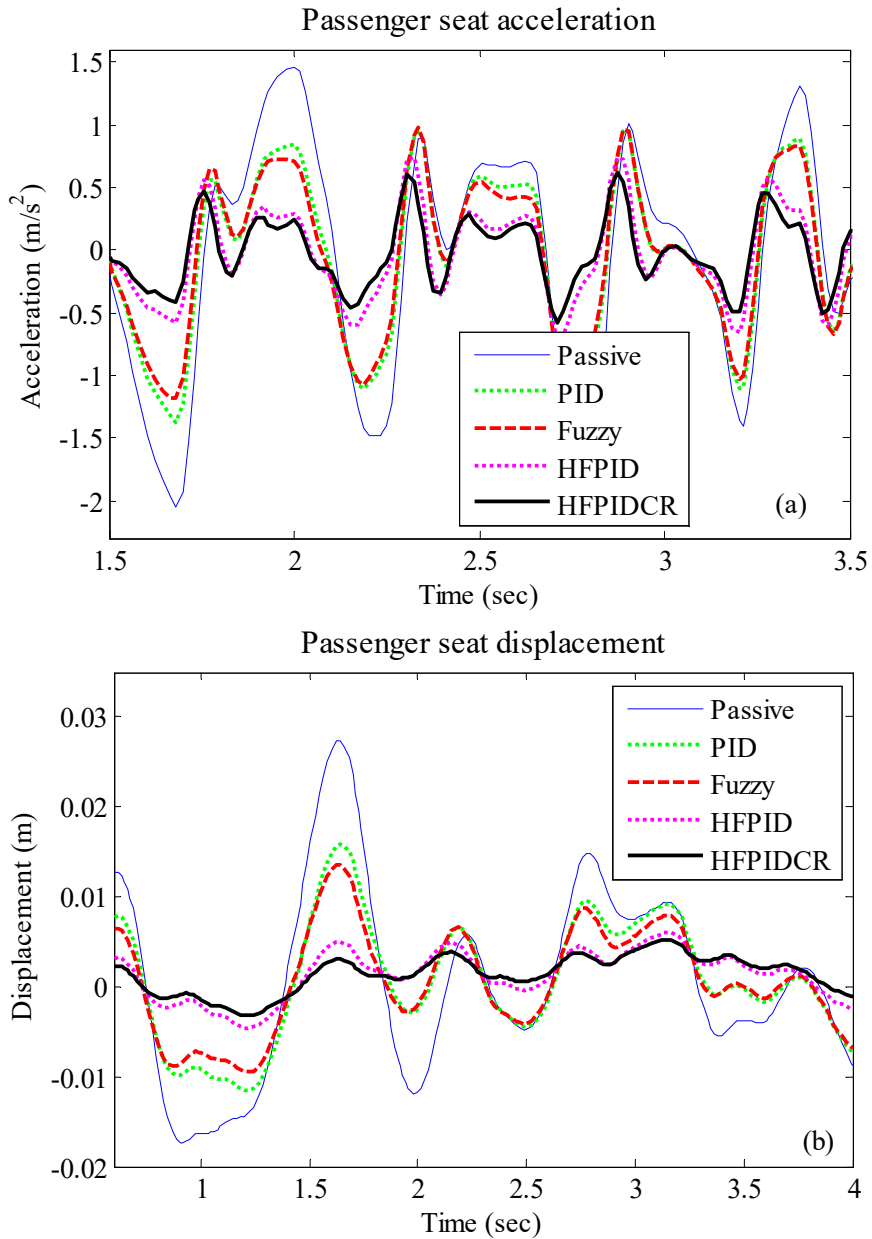


Figure 10.17 (a) Passenger seat acceleration (b) Passenger seat displacement

Table 10.19 Performance comparison of Passenger seat response under Random road profile ($m_1 = 70$ kg)

Performance Parameters	Acceleration (m/s ²)				Displacement (m)			
	Max.		RMS		Max.		RMS	
	Magnitude	Improvement %	Magnitude	Improvement %	Magnitude	Improvement %	Magnitude	Improvement %
Controller Type	80% $m_2 = 260$ kg							
Uncontrolled	1.8803	-----	1.0206	-----	0.0262	-----	0.0101	-----
PID	1.3485	28.28	0.7434	27.16	0.0157	39.99	0.0064	36.18
Fuzzy	1.3564	27.86	0.6883	32.56	0.0135	48.56	0.0055	45.19
HFPID	0.9774	48.02	0.3971	61.10	0.0060	77.15	0.0028	72.61
HFPIDCR	0.7709	59.00	0.3034	70.28	0.0051	80.38	0.0023	77.33
Controller Type	100% $m_2 = 325$ kg							
Uncontrolled	1.5311	-----	0.8625	-----	0.0274	-----	0.0100	-----
PID	1.0505	31.39	0.6266	27.36	0.0159	41.99	0.0064	36.28
Fuzzy	1.0067	34.25	0.5850	32.17	0.0137	50.21	0.0055	45.39
HFPID	0.7876	48.56	0.3369	60.94	0.0061	77.86	0.0028	72.16
HFPIDCR	0.6472	57.73	0.2563	70.29	0.0052	80.99	0.0023	77.00
Controller Type	120% $m_2 = 390$ kg							
Uncontrolled	1.2896	-----	0.7364	-----	0.0279	-----	0.0101	-----
PID	0.8544	33.75	0.5355	27.27	0.0159	42.85	0.0064	36.48
Fuzzy	0.8311	35.55	0.5035	31.63	0.0137	50.82	0.0055	45.76
HFPID	0.6352	50.74	0.2892	60.73	0.0061	78.26	0.0028	72.36
HFPIDCR	0.5341	58.58	0.2198	70.15	0.0052	81.41	0.0023	77.29

Table 10.20 Performance comparison of Passenger seat response under Random road profile ($m_2 = 325$ kg)

Performance Parameters	Acceleration (m/s^2)				Displacement (m)			
	Max.		RMS		Max.		RMS	
	Magnitude	Improvement %	Magnitude	Improvement %	Magnitude	Improvement %	Magnitude	Improvement %
Controller Type	80% $m_1 = 56$ kg							
Uncontrolled	1.6697	-----	0.9562	-----	0.0268	-----	0.0098	-----
PID	1.2347	26.06	0.6881	28.03	0.0158	40.83	0.0063	35.49
Fuzzy	1.2171	27.11	0.6402	33.04	0.0136	49.32	0.0054	44.62
HFPID	0.8676	48.04	0.3631	62.02	0.0061	77.26	0.0028	71.59
HFPIDCR	0.7048	57.79	0.2754	71.19	0.0052	80.41	0.0023	76.42
Controller Type	100% $m_1 = 70$ kg							
Uncontrolled	1.5311	-----	0.8625	-----	0.0274	-----	0.0100	-----
PID	1.0505	31.39	0.6266	27.36	0.0159	41.99	0.0064	36.28
Fuzzy	1.0067	34.25	0.5850	32.17	0.0137	50.21	0.0055	45.39
HFPID	0.7876	48.56	0.3369	60.94	0.0061	77.86	0.0028	72.16
HFPIDCR	0.6472	57.73	0.2563	70.29	0.0052	80.99	0.0023	77.00
Controller Type	120% $m_1 = 84$ kg							
Uncontrolled	1.4184	-----	0.7896	-----	0.0280	-----	0.0102	-----
PID	0.9387	33.82	0.5777	26.84	0.0160	42.70	0.0064	36.77
Fuzzy	0.9151	35.48	0.5421	31.35	0.0138	50.64	0.0055	45.79
HFPID	0.7313	48.44	0.3187	59.63	0.0061	78.24	0.0028	72.47
HFPIDCR	0.5945	58.09	0.2462	68.82	0.0052	81.34	0.0023	77.27

It can be seen from graphical and mathematical results that vibration control of passenger seat is better for all controlled cases compared to uncontrolled one. It can be seen that the fully controlled semi-active quarter car system with HFPIDCR controllers in primary and secondary suspension system provided best response related to passenger ride comfort issues. The generated desired damping force signals by assembled forward controllers in primary and secondary suspension system are shown in Figure 10.18 and Figure 10.20 respectively.

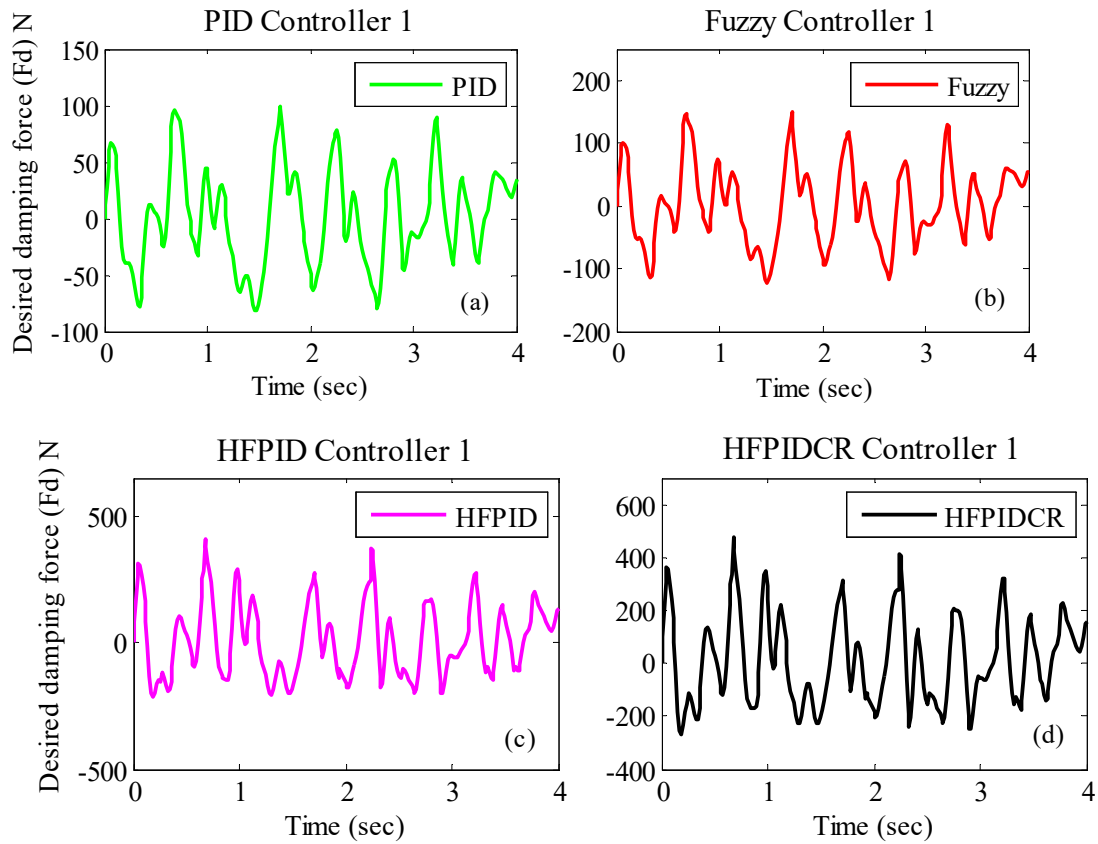


Figure 10.18 Desired damping force signals supplied by different controllers

Table 10.21 and Table 10.23 shows the calculated highest values of desired damping force for the same. The highest desired damping force values are generated by HFPIDCR controllers 1 as 265.18 N during compression stage and 475.17 N during rebound stage in primary suspension system while generated by HFPIDCR controllers 2 in secondary suspension system; it is 82.98 N during compression stage and 84.39 N during rebound stages respectively.

The input current signals generated by assembled inverse controllers in primary and secondary suspension systems are shown in Figure 10.19 Figure 10.21 respectively while the peak values of the same is shown in Table 10.22 and Table 10.24. It can be seen that the

highest value of input current is generated by HFPIDCR based inverse controller 1 as 0.72 A and inverse controller 2 as 0.22 A respectively.

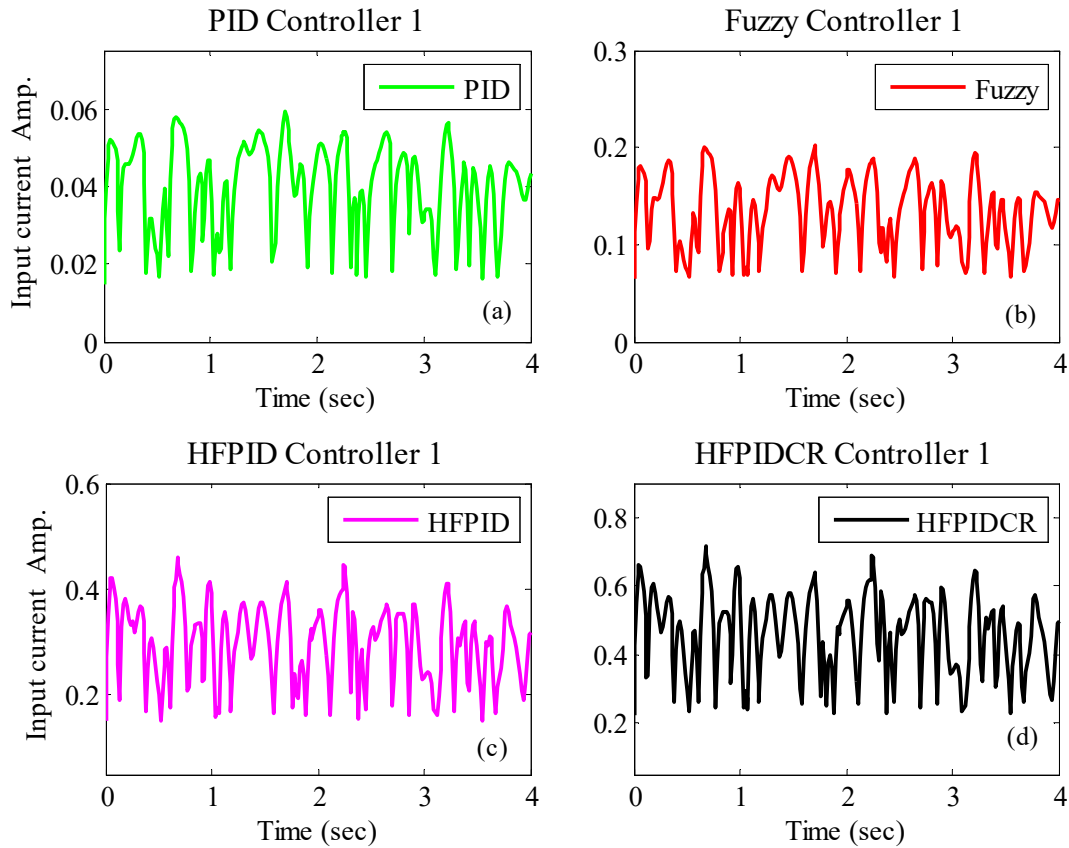


Figure 10.19 Input current signal supplied to MR shock absorber by different controllers

Table 10.21 Calculated Max. desired damping force using Forward controller 1 (N)

Forward Controller 1	Max. Damping Force (N)			
	PID	Fuzzy	HFPID	HFPIDCR
Compression Stage	81.63	121.75	218.03	265.18
Rebound Stage	98.81	149.58	410.78	475.17

Table 10.22 Calculated Max. input current using Inverse controller 1 (A)

Inverse Controller 1	Max. input current (A)			
	PID	Fuzzy	HFPID	HFPIDCR
Magnitude	0.06	0.20	0.46	0.72

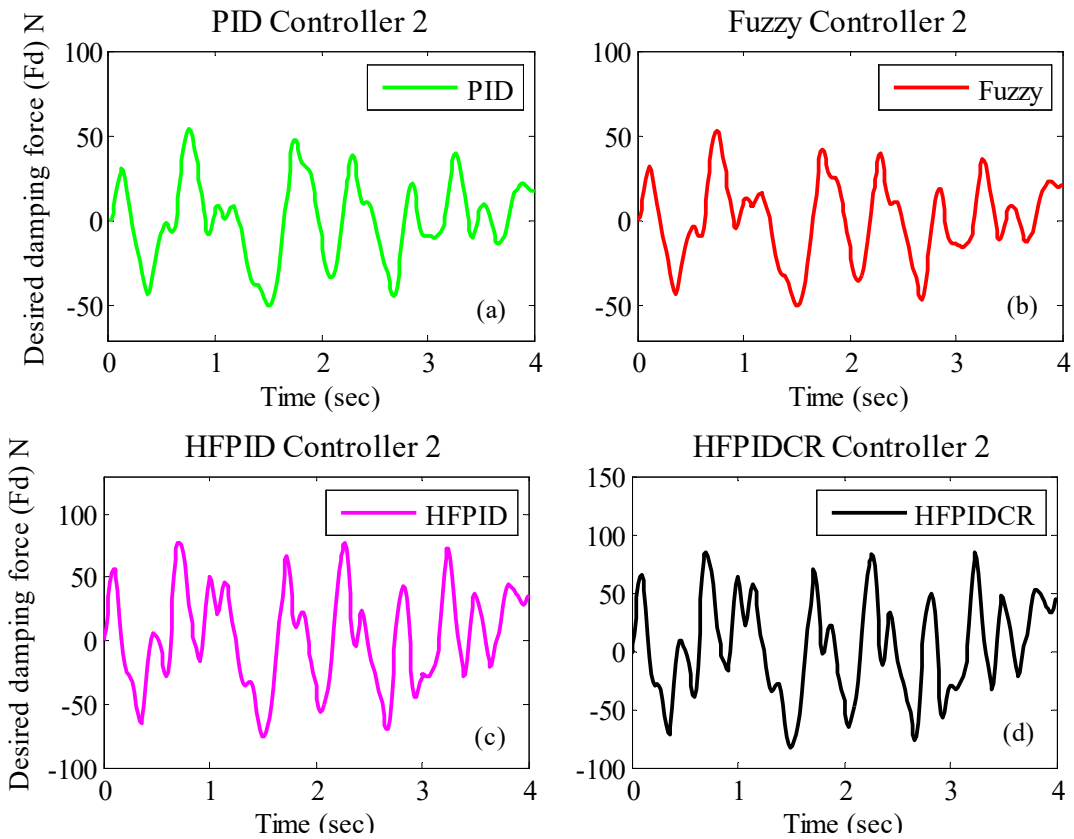


Figure 10.20 Desired damping force signals supplied by different controllers

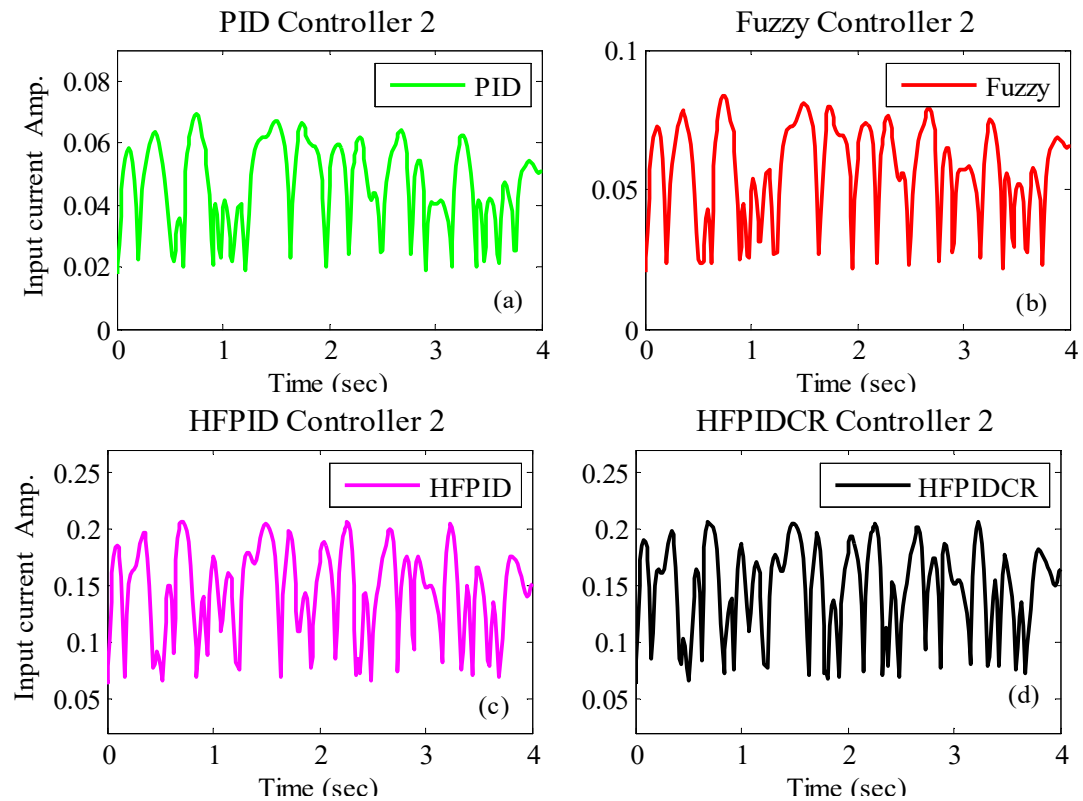


Figure 10.21 Input current signal supplied to MR shock absorber by different controllers

Table 10.23 Calculated Max. desired damping force using Forward controller 2 (N)

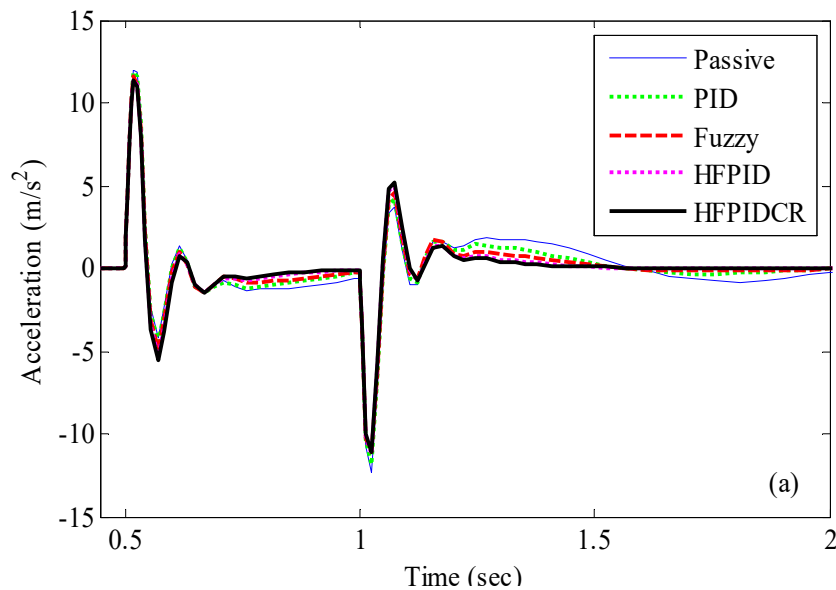
Forward Controller 2	Max. Damping Force (N)			
	PID	Fuzzy	HFPID	HFPIDCR
Compression Stage	49.63	49.48	75.11	82.98
Rebound Stage	54.00	53.49	77.83	84.39

Table 10.24 Calculated Max. input current using Inverse controller 2 (A)

Inverse Controller 2	Max. input current (A)			
	PID	Fuzzy	HFPID	HFPIDCR
Magnitude	0.07	0.08	0.21	0.22

10.3 SPRUNG MASS SIMULATION RESULTS

The simulation results of sprung mass acceleration and displacement response for pulse, bump, sinusoidal and random road input profile are shown in Figure 10.22 to Figure 10.25 respectively.



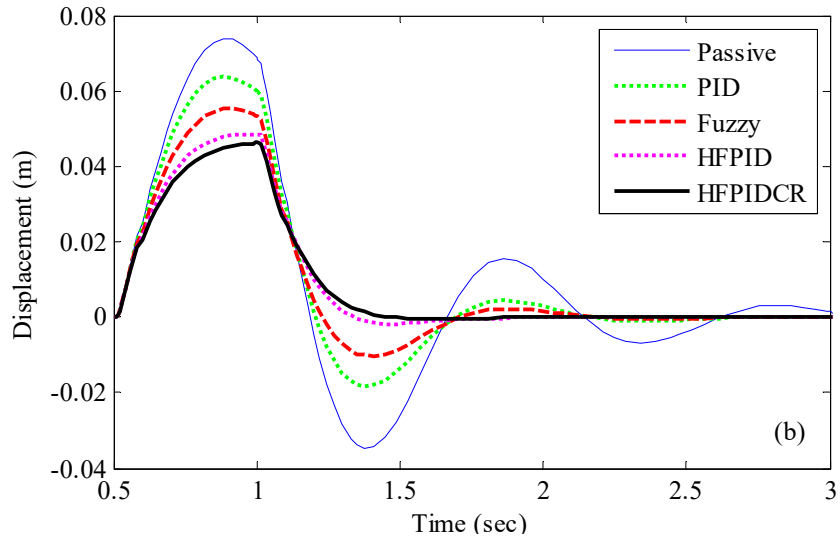


Figure 10.22 Sprung mass response under pulse road input (a) Acceleration (b) Displacement

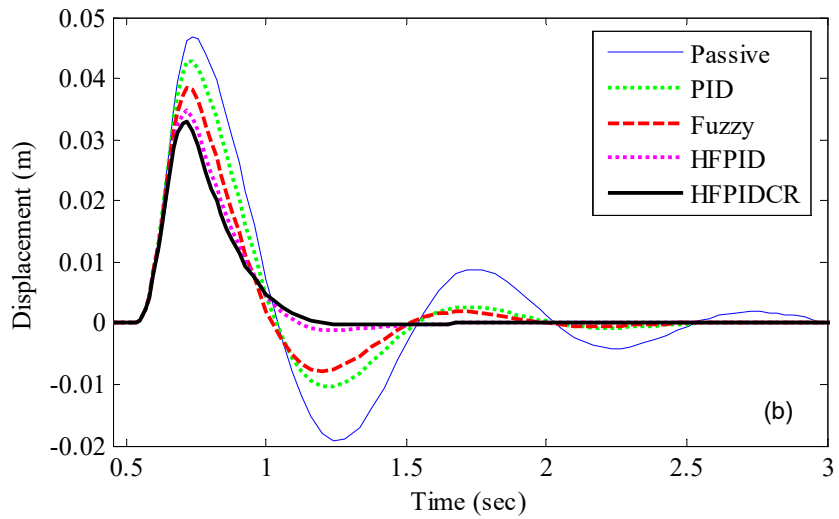
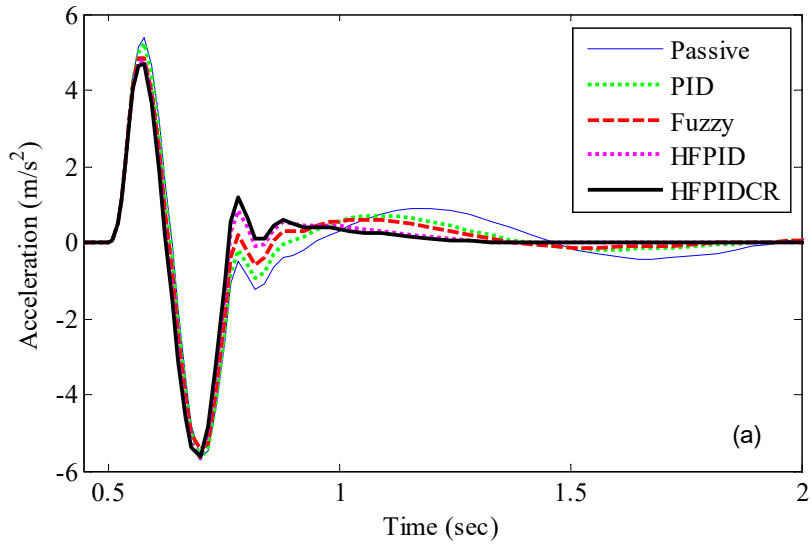


Figure 10.23 Sprung mass response under bump road input (a) Acceleration (b) Displacement

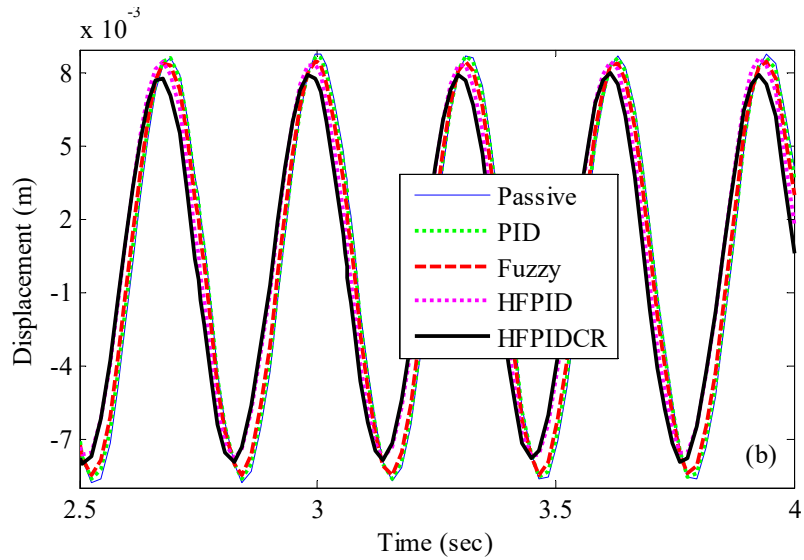
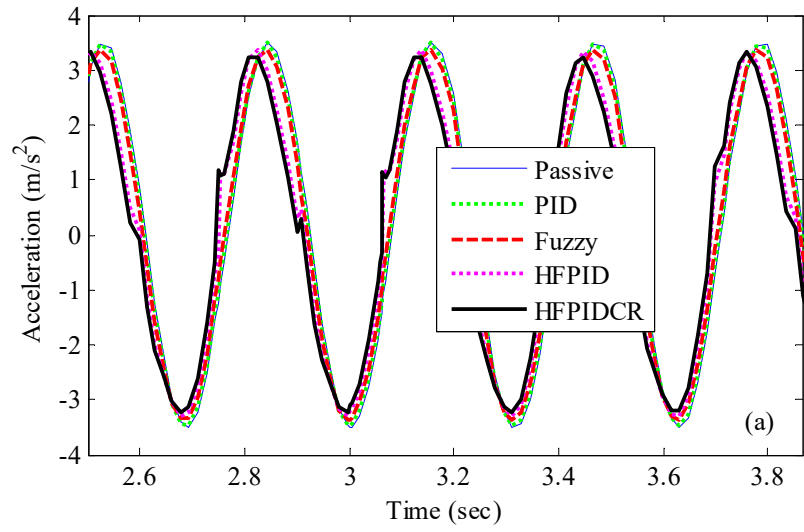
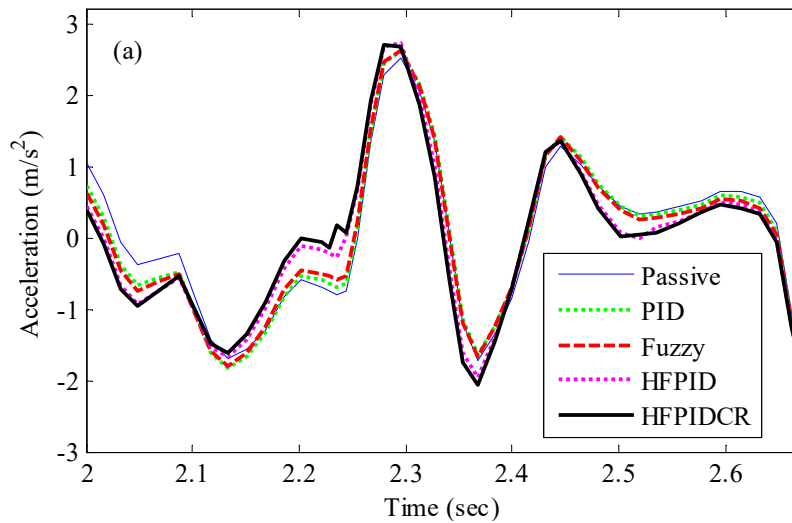


Figure 10.24 Sprung mass response under sinusoidal road input (a) Acceleration (b) Displacement



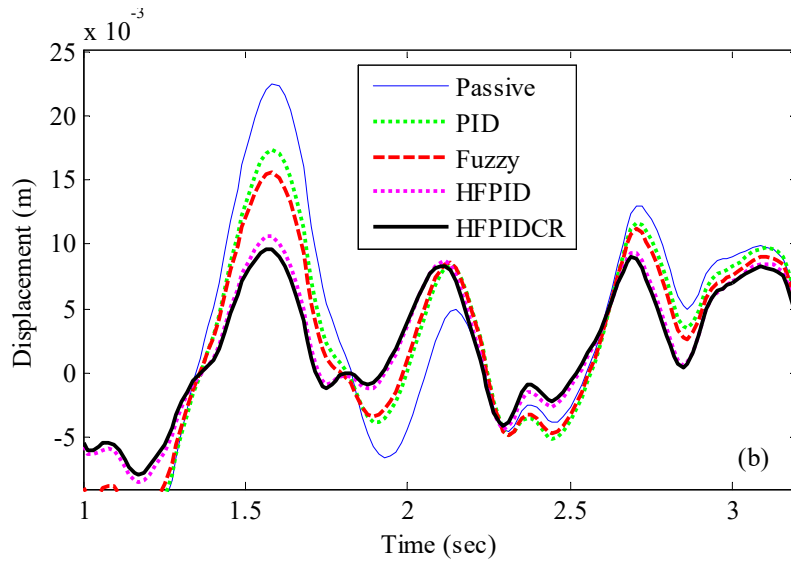


Figure 10.25 Sprung mass response under random road input (a) Acceleration (b) Displacement

The mathematical results in terms of peak and RMS values for passenger seat response for selected road profiles are shown in Table 10.25.

Table 10.25 Performance comparison of Sprung mass response ($m_1 = 70$ kg, $m_2 = 325$ kg, $m_3 = 40$ kg)

Controller Type	Acceleration (m/s^2)				Displacement (m)			
	Max.		RMS		Max.		RMS	
	Magnitude	Improvement %	Magnitude	Improvement %	Magnitude	Improvement %	Magnitude	Improvement %
Pulse road profile								
Uncontrolled	12.1845	-----	2.5766	-----	0.0740	-----	0.0299	-----
PID	11.8045	3.12	2.5365	1.55	0.0637	13.85	0.0240	19.96
Fuzzy	11.6214	4.62	2.4687	4.19	0.0552	25.31	0.0210	29.97
HFPIID	11.4098	6.36	2.4603	4.51	0.0485	34.36	0.0190	36.64
HFPIIDCR	11.3098	7.18	2.4507	4.88	0.0462	37.54	0.0180	39.84
Bump road profile								
Uncontrolled	5.4038	-----	1.4669	-----	0.0469	-----	0.0154	-----
PID	5.2281	3.25	1.4092	3.93	0.0428	8.71	0.0128	16.73
Fuzzy	4.8637	9.99	1.3512	7.89	0.0385	17.91	0.0111	28.07
HFPIID	4.8107	10.98	1.3410	8.58	0.0347	26.02	0.0097	36.79
HFPIIDCR	4.7158	12.73	1.3315	9.23	0.0328	30.05	0.0091	40.68
Sinusoidal road profile								
Uncontrolled	3.6476	-----	2.4159	-----	0.0166	-----	0.0064	-----
PID	3.5489	2.71	2.3336	3.41	0.0155	6.99	0.0060	5.63
Fuzzy	3.4657	4.99	2.2692	6.07	0.0145	13.07	0.0059	8.68
HFPIID	3.5249	3.36	2.2244	7.93	0.0130	22.04	0.0056	12.86
HFPIIDCR	3.4969	4.13	2.2009	8.90	0.0124	25.52	0.0055	14.87

Table 10.25 Performance comparison of Sprung mass response ($m_1 = 70$ kg, $m_2 = 325$ kg, $m_3 = 40$ kg)								
Random road profile								
Uncontrolled	2.5499	-----	1.1746	-----	0.0224	-----	0.0083	-----
PID	2.6398	-3.52	1.1669	0.65	0.0173	22.58	0.0069	16.97
Fuzzy	2.6346	-3.32	1.1493	2.15	0.0156	30.57	0.0063	24.18
HFPIID	2.7741	-8.79	1.1431	2.68	0.0106	52.82	0.0047	42.96
HFPIIDCR	2.7806	-9.05	1.1426	2.72	0.0096	57.14	0.0044	46.62

10.4 SUMMARY

In this case, passenger seat acceleration and displacement responses of fully controlled semi-active quarter car model has been studied under pulse, bump, sinusoidal and random road excitations running at 40 km/h. Simulation results show that fully controlled semi-active quarter car model with HFPIIDCR controllers is most effective in controlling passenger seat vibrations compared to uncontrolled and other controlled cases. It can also be seen that HFPIIDCR controller integrated suspension systems generated highest desired damping force and input current values. The generated peak values of input current by inverse controllers in primary and secondary suspension system remained below 1 A, thus the power requirements for running inverse controller 1 and inverse controller 2 are lower for working of MR shock absorber 1 and MR shock absorber 2 respectively.

CHAPTER XI

FREQUENCY RESPONSE ANALYSIS OF QUARTER CAR MODEL

11.1 INTRODUCTION

The concept of natural frequencies of any dynamic system plays a crucial role in deciding the location of the resonance while the harmonic excitation is given to the system. The considered system is quarter car model with three degrees of freedom. Thus, there will be three natural frequencies for this system. In present case, the natural frequencies of the quarter car model are found using the undamped and free vibrations of the equations of motions.

Equation 5.1 to 5.3 may be written in matrix form as follows:

$$\begin{bmatrix} m_1 & 0 & 0 \\ 0 & m_2 & 0 \\ 0 & 0 & m_3 \end{bmatrix} \begin{bmatrix} \ddot{x}_1 \\ \ddot{x}_2 \\ \ddot{x}_3 \end{bmatrix} + \begin{bmatrix} c_s & -c_s & 0 \\ -c_s & c_s + c_p & -c_p \\ 0 & -c_p & c_p \end{bmatrix} \begin{bmatrix} \dot{x}_1 \\ \dot{x}_2 \\ \dot{x}_3 \end{bmatrix} + \begin{bmatrix} k_s & -k_s & 0 \\ -k_s & k_s + k_p & -k_p \\ 0 & -k_p & k_p + k_t \end{bmatrix} \begin{bmatrix} x_1 \\ x_2 \\ x_3 \end{bmatrix} = \begin{bmatrix} 0 \\ 0 \\ k_t x_r \end{bmatrix} \quad (11.1)$$

Equation 11.1 can be represented in the matrix form as follows:

$$M \cdot \ddot{x} + C \cdot \dot{x} + K \cdot x = f_a \quad (11.2)$$

where M, C and K represents the mass, damping and stiffness matrices respectively as shown below while x is the displacement and f_a is the road excitation.

$$[M] = \begin{bmatrix} m_1 & 0 & 0 \\ 0 & m_2 & 0 \\ 0 & 0 & m_3 \end{bmatrix}$$

$$[K] = \begin{bmatrix} k_s & -k_s & 0 \\ -k_s & k_s + k_p & -k_p \\ 0 & -k_p & k_p + k_t \end{bmatrix}$$

$$[C] = \begin{bmatrix} c_s & -c_s & 0 \\ -c_s & c_s + c_p & -c_p \\ 0 & -c_p & c_p \end{bmatrix}$$

11.2 NATURAL FREQUENCIES OF QUARTER CAR MODEL

The natural frequencies of quarter car model are extracted using the MATLAB command 'eig' as mentioned below and represented in Table 11.1:

```
>> syms m1 m2 m3 ks kp kt
m1=70;
m2=325;
m3=45;
ks=8000;
kp=25000;
kt=180000;

M=[m1 0 0;0 m2 0;0 0 m3];
K=[ks -ks 0;-ks ks+kp -kp;0 -kp kp+kt];
ff=sqrt(eig(K,M))

ff =

    6.9985
   12.5407
   67.5658

>> nf=ff/(2*pi)

nf =

    1.1138
    1.9959
   10.7534
```

Table 11.1 Quarter car model natural frequencies

Sr. No.	Frequency	rad/sec	Hz
1	First natural frequency	6.9985	1.1138
2	Second natural frequency	12.5407	1.9959
3	Third natural frequency	67.5658	10.7534

11.3 ROAD PROFILE AND QUARTER CAR TRAVEL

The road profile is considered as infinite cam having wavy profile with harmonic waves whereas the moving wheel of the quarter car model is considered as follower. The road will give harmonic excitation to the quarter car model. The road profile is approximated with a sine wave as seen in Figure 11.1 which can be represented by following equation:

$$y(t) = Y \sin(\omega t) \quad (11.3)$$

where,

$y(t)$ = Road profile excitation at time t ,
 Y = Amplitude of sinusoidal road profile = 0.03 m,
 λ = Wavelength of the sinusoidal road profile = 8 m.

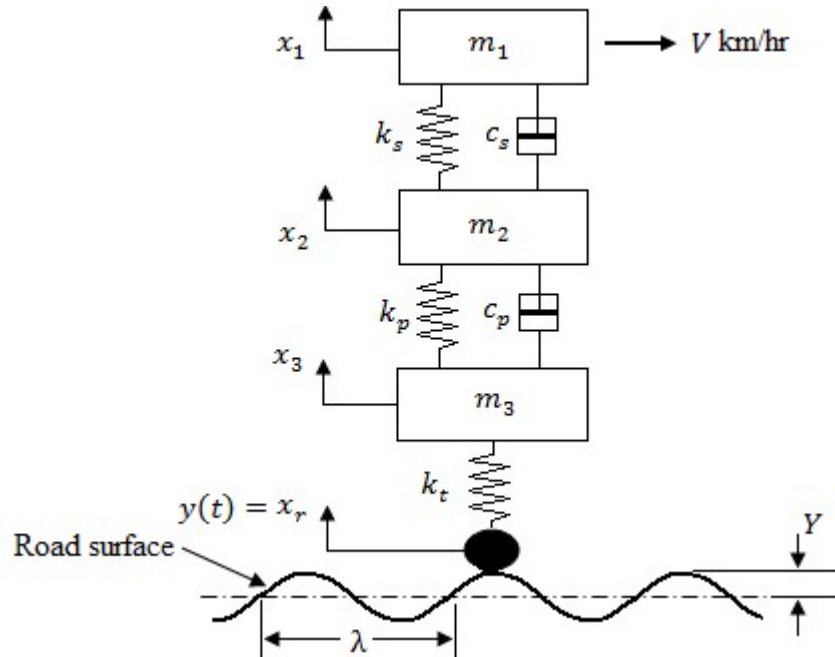


Figure 11.1 Quarter car travel over sinusoidal road profile

The excitation frequency from the base (ω_b) depends on the quarter car velocity V as well as on the road surface wavelength λ as follows:

$$\omega_b = \frac{2\pi V}{\lambda} \quad (11.4)$$

In present case, the quarter car model is considered to be travelling over the sinusoidal road profile with the velocity ranging from 20 km/hr to 120 km/hr. For different velocities of quarter car model, the excitation frequencies are calculated as mentioned below and tabulated in Table 11.1 for various velocities.

For 20 km/hr, the base excitation frequency is:

$$\omega_b = \frac{2\pi V}{\lambda} = \frac{2\pi \times 20 \times 1000}{8 \times 3600} = 4.36 \text{ rad/sec} = 0.69 \text{ Hz}$$

For 120 km/hr, the base excitation frequency is:

$$\omega_b = \frac{2\pi V}{\lambda} = \frac{2\pi \times 120 \times 1000}{8 \times 3600} = 26.18 \text{ rad/sec} = 4.16 \text{ Hz}$$

Table 11.2 Base excitation frequency at various quarter car velocities

Sr. No.	Quarter car velocity (km/hr)	Base excitation frequency (Hz)
1	20	0.69
2	40	1.39
3	60	2.08
4	80	2.77
5	100	3.47
6	120	4.16

It can be observed from Table 11.2 that the magnitude of base excitation frequency at 120 km/hr speed of quarter car model is 4.16 Hz, which is much lower than the natural frequency of 10.7534 Hz. Thus design of present quarter car model having three degrees of freedom is safe with selected parameters as resonance phenomenon will not take place in quarter car model.

11.4 SUMMARY

In present chapter, three natural frequencies of quarter car model with three degrees of freedom have been calculated. Finally, sinusoidal road profile was considered to calculate base excitation frequency in Hz for the running speed of model from 20 km/hr to 120 km/hr to evaluate the safe design of the quarter car model.

CHAPTER XII

CONCLUSIONS AND SCOPE FOR FURTHER WORK

12.1 CONCLUSIONS

12.1.1 SUMMARY

Based on the research gaps identified in the available literature, the objectives of the thesis work were to the development and testing of dual tube passive dampers for passenger seat with various piston design and valve design parameters as well to study the application of MR shock absorber in semi-active quarter car system with three degrees of freedom for passenger ride comfort and safety issues. Experimental works were performed on MTS machine using developed passive and available MR damper to obtain force-displacement and force-velocity curves. Various forward controllers such as PID, Fuzzy, HFPID and HFPIDCR as well as fuzzy logic based inverse controllers were developed for working of MR shock absorber in semi-active suspension system. Finally, simulation work was performed under pulse, bump, sinusoidal and random road excitations using quarter car model, developed in MATLAB/ Simulink environment. Based on the simulation results, comparative analysis of passive and semi-active suspension system with various developed controllers were performed for passenger ride comfort and safety. The mathematical results of quarter car model under various road excitations for passenger seat acceleration and displacement response are shown in Table 12.1 to Table 12.4 for $m_2 = 325$ kg and $m_1 = 70$ kg.

Present research work has made a significant contribution in the field of hydraulic dampers related to its damping capabilities during test work as well as its effectiveness in the quarter car model to achieve desired ride comfort and safety of travelling passengers. In particular, simulation work was used to compare the obtained data in graphical and mathematical form of passive and semi-active quarter car models with three degrees of freedom.

Table 12.1 Performance comparison of Passenger seat response under Pulse road profile

Controller Type	Acceleration (m/s ²)				Displacement (m)			
	Max.		RMS		Max.		RMS	
	Mag.	Improvement %	Mag.	Improvement %	Mag.	Improvement %	Mag.	Improvement %
Primary Suspension Controlled								
Uncontrolled	3.8608	-----	1.2844	-----	0.0853	-----	0.0333	-----
PID	3.7535	2.78	1.0799	15.92	0.0741	13.21	0.0281	15.55
Fuzzy	3.6154	6.35	0.9571	25.48	0.0644	24.51	0.0243	27.04
HFPIID	3.5008	9.32	0.8392	34.66	0.0560	34.43	0.0213	36.09
HFPIIDCR	3.4311	11.13	0.7977	37.89	0.0524	38.62	0.0200	39.85
Secondary Suspension Controlled								
Uncontrolled	3.8608	-----	1.2844	-----	0.0853	-----	0.0333	-----
PID	3.5113	9.05	1.0396	19.06	0.0732	14.26	0.0282	15.39
Fuzzy	3.3554	13.09	0.9084	29.28	0.0657	22.96	0.0250	25.04
HFPIID	2.6869	30.41	0.6898	46.29	0.0528	38.17	0.0201	39.67
HFPIIDCR	2.2353	42.10	0.5595	56.44	0.0430	49.65	0.0165	50.44
Fully Suspension Controlled								
Uncontrolled	3.8608	-----	1.2844	-----	0.0853	-----	0.0333	-----
PID	3.4096	11.69	0.8876	30.89	0.0638	25.26	0.0244	26.78
Fuzzy	3.1323	18.87	0.7297	43.19	0.0514	39.81	0.0194	41.71
HFPIID	2.3936	38.00	0.5154	59.88	0.0372	56.43	0.0148	55.72
HFPIIDCR	2.0466	46.99	0.4181	67.45	0.0288	66.30	0.0119	64.16

Table 12.2 Performance comparison of Passenger seat response under Bump road profile

Controller Type	Acceleration (m/s^2)				Displacement (m)			
	Max.		RMS		Max.		RMS	
	Mag.	Improvement %	Mag.	Improvement %	Mag.	Improvement %	Mag.	Improvement %
Primary Suspension Controlled								
Uncontrolled	3.7298	-----	1.2472	-----	0.0542	-----	0.0172	-----
PID	3.4853	6.55	1.1374	8.81	0.0476	12.19	0.0145	16.09
Fuzzy	3.2222	13.61	1.0545	15.45	0.0414	23.57	0.0124	28.09
HFPIID	3.0324	18.70	0.9470	24.07	0.0363	33.07	0.0106	38.34
HFPIIDCR	2.9237	21.61	0.9029	27.61	0.0339	37.46	0.0099	42.52
Secondary Suspension Controlled								
Uncontrolled	3.7298	-----	1.2472	-----	0.0542	-----	0.0172	-----
PID	3.1078	16.68	0.9738	21.92	0.0432	20.32	0.0137	20.77
Fuzzy	2.8814	22.75	0.8214	34.14	0.0379	30.04	0.0121	30.10
HFPIID	2.1192	43.18	0.5960	52.22	0.0272	49.86	0.0088	49.15
HFPIIDCR	1.7473	53.15	0.4609	63.04	0.0210	61.28	0.0069	59.86
Fully Suspension Controlled								
Uncontrolled	3.7298	-----	1.2472	-----	0.0542	-----	0.0172	-----
PID	2.9412	21.14	0.8900	28.65	0.0377	30.40	0.0116	32.66
Fuzzy	2.5589	31.39	0.7136	42.78	0.0291	46.37	0.0088	48.78
HFPIID	1.8185	51.24	0.4663	62.61	0.0173	68.05	0.0060	65.26
HFPIIDCR	1.4349	61.53	0.3472	72.16	0.0121	77.64	0.0046	73.18

Table 12.3 Performance comparison of Passenger seat response under Sinusoidal road profile

Controller Type	Acceleration (m/s ²)				Displacement (m)			
	Max.		RMS		Max.		RMS	
	Mag.	Improvement %	Mag.	Improvement %	Mag.	Improvement %	Mag.	Improvement %
Primary Suspension Controlled								
Uncontrolled	2.7350	-----	1.9321	-----	0.0169	-----	0.0055	-----
PID	2.7204	0.54	1.9024	1.54	0.0153	9.75	0.0052	5.74
Fuzzy	2.6514	3.06	1.8504	4.23	0.0142	16.41	0.0050	10.02
HFPID	2.3445	14.28	1.6535	14.42	0.0121	28.60	0.0044	20.71
HFPIDCR	2.2348	18.29	1.5761	18.43	0.0114	32.61	0.0042	24.82
Secondary Suspension Controlled								
Uncontrolled	2.7350	-----	1.9321	-----	0.0169	-----	0.0055	-----
PID	2.1939	19.79	1.5266	20.99	0.0135	20.49	0.0043	22.67
Fuzzy	2.1109	22.82	1.4860	23.09	0.0130	23.48	0.0042	24.41
HFPID	1.2613	53.88	0.8688	55.03	0.0082	51.84	0.0024	55.99
HFPIDCR	0.9708	64.51	0.6454	66.60	0.0061	63.72	0.0018	67.43
Fully Suspension Controlled								
Uncontrolled	2.7350	-----	1.9321	-----	0.0169	-----	0.0055	-----
PID	2.1351	21.94	1.5041	22.15	0.0121	28.74	0.0041	26.78
Fuzzy	1.9972	26.98	1.4268	26.15	0.0108	36.42	0.0038	31.19
HFPID	1.0368	62.09	0.7502	61.17	0.0058	66.05	0.0020	63.82
HFPIDCR	0.8354	69.46	0.5378	72.16	0.0041	76.02	0.0014	73.98

Table 12.4 Performance comparison of Passenger seat response under Random road profile

Controller Type	Acceleration (m/s ²)				Displacement (m)			
	Max.		RMS		Max.		RMS	
	Mag.	Improvement %	Mag.	Improvement %	Mag.	Improvement %	Mag.	Improvement %
Primary Suspension Controlled								
Uncontrolled	1.5311	-----	0.8625	-----	0.0274	-----	0.0100	-----
PID	1.3849	9.55	0.7949	7.83	0.0216	21.34	0.0081	18.44
Fuzzy	1.3580	11.31	0.7667	11.11	0.0192	30.15	0.0073	26.45
HFPIID	1.3020	14.96	0.6574	23.78	0.0128	53.41	0.0052	47.57
HFPIIDCR	1.2993	15.13	0.6296	27.01	0.0115	58.11	0.0048	51.68
Secondary Suspension Controlled								
Uncontrolled	1.5311	-----	0.8625	-----	0.0274	-----	0.0100	-----
PID	1.0922	28.67	0.6749	21.75	0.0204	25.73	0.0077	22.90
Fuzzy	1.0542	31.15	0.6493	24.72	0.0196	28.65	0.0073	26.84
HFPIID	0.6357	58.48	0.4054	53.00	0.0114	58.52	0.0046	54.14
HFPIIDCR	0.5069	66.89	0.3126	63.76	0.0083	69.88	0.0036	63.52
Fully Suspension Controlled								
Uncontrolled	1.5311	-----	0.8625	-----	0.0274	-----	0.0100	-----
PID	1.0505	31.39	0.6266	27.36	0.0159	41.99	0.0064	36.28
Fuzzy	1.0067	34.25	0.5850	32.17	0.0137	50.21	0.0055	45.39
HFPIID	0.7876	48.56	0.3369	60.94	0.0061	77.86	0.0028	72.16
HFPIIDCR	0.6472	57.73	0.2563	70.29	0.0052	80.99	0.0023	77.00

Based on the experimental work of dual tube passive damper and MR damper as well as simulation results, the major conclusion drawn and contributions of this research work can be concluded as follows:

❖ **An extensive literature review on passive shock absorbers and semi-active quarter car system with various controllers is presented.**

The studied published research work in the field of passive as well as MR shock absorber design, development and testing resulted into highlight of research gaps in this area. Applications of various controllers in semi-active quarter car model with MR shock absorber were also studied.

❖ **Piston design parameters influence the damping capabilities of passenger seat passive dampers.**

Dual tube passive hydraulic dampers with various piston design parameters were tested under piston rod velocity of 0.05 m/s, 0.1 m/s and 0.3 m/s respectively, on MTS machine to observe the influence of these parameters on the force-displacement and force-velocity curves. Table 12.5 shows the conclusions based on the test results.

Table 12.5 Influence of various piston design parameters

Sr. No.	Parameters	Peak Damping Force	
		Rebound Force	Compressive Force
1.	Increase in number of orifice from 1 to 3	Decreases	Decreases
2.	Increase in diameter of orifice from 0.8 mm to 1 mm.	Decreases	Decreases
3.	The difference in variation in generated peak rebound force is small at small piston rod velocity while it is larger at higher piston rod velocity		

❖ **The damping capabilities of passenger seat passive damper vary with valve design parameters.**

Dual tube passive hydraulic dampers with various valve design parameters were tested under piston rod velocity of 0.05 m/s, 0.1 m/s and 0.3 m/s respectively, on MTS machine to know the influence of valve design parameters on the force-displacement and force-velocity curves. Table 12.6 presents the conclusions based on the test results.

Table 12.6 Influence of various valve design parameters

Sr. No.	Parameters	Peak Damping Force	
		Rebound Force	Compressive
1.	Variation in valve thickness on rebound side from 0.15 mm to 0.45 mm.	Increases	Remains approx. same
2.	Variation in cuts in valve on rebound side from 1 to 3	Decreases	Remains approx. same
3.	The difference in variation in generated peak rebound force is small at small piston rod velocity while it is larger at higher piston rod velocity		

❖ **Piston with different materials and different weight has negligible effect on the damping characteristics of passive hydraulic dampers.**

Experimental work was done on the passive dampers with two pistons having different materials as: Ductile iron and 7075 Aluminium Alloy as well as with two pistons of different thickness of 11.7 mm and 12.7 mm. Experimental results showed that different materials and different weight has negligible effect on the damping characteristics of passive hydraulic dampers.

❖ **Taguchi method has been used for optimization of no. of piston holes and shim thickness parameters to maximize the generated damping force values in dual tube passive damper.**

Taguchi L9 experimental design method has been selected for selection of optimum combinations of no. of holes, dia. of holes and shim thickness to maximize the generated damping force values in dual tube damper. Optimum no. of piston holes and shim thickness parameters which response to maximum damping force values were no. of holes = 4, dia. of holes = 0.8 mm and shim thickness = 0.45 mm respectively for piston velocity of 0.3 m/s and at the piston rod displacement of 25 mm.

❖ **Polynomial model has been successfully used to trace the forward dynamics of MR damper.**

The experimental data of MR damper was fitted using polynomial model. The polynomial model fitted curves matched very closely with the MR damper experimental results. Based on the developed polynomial model, the actual damping

force to be generated by MR damper can be obtained by supplying proper current signal to MR damper as per the piston rod velocity (v).

❖ **Semi-active quarter car model with three degrees of freedom is introduced.**

An extensive literature is available on semi-active quarter car system with MR shock absorber having two degrees of freedom. But a semi-active quarter car model with MR shock absorber to describe the passenger ride comfort and safety is not available in the literature. Therefore, semi-active quarter car model with three degrees of freedom having MR shock absorbers is introduced.

❖ **Various Forward control strategies were designed for getting desired damping force signal.**

A combination of non-hybrid and hybrid control strategies were developed for generation of desired damping force signal in primary and secondary suspension system of semi-active quarter car model. The selected forward controllers include PID Controller, Fuzzy Controller, HFPID Controller and HFPIDCR Controller. It was shown through numerical simulation results that generated desired damping force signals lies within the maximum damping force capability of MR damper.

❖ **Various Inverse control strategies were designed for generation and supply of input current to physical MR damper.**

Inverse control strategies were designed for supply of input current to MR damper in semi-active quarter car suspension systems. The designed fuzzy based inverse controller has desired damping force signal (F_d) and change in error signal (de) as two inputs while output is the current signal. Simulation results revealed that the current signal generated by PID, Fuzzy, HFPID and HFPIDCR based inverse controllers produced input current of less than 1 A magnitude. This magnitude of supply current ensures the low power consumption and extended working life of MR damper. Thus the designed inverse controllers can be used in real life control problems related to vibration control of semi-active suspension systems.

❖ **Comparative analysis of passenger ride comfort performance of passive and various semi-active quarter car systems is presented.**

In order to compare the various controlled and uncontrolled quarter car systems, the same road excitations, quarter car parameters and vehicle running speed were considered. The objective was to achieve best passenger ride comfort for travelling passengers. The criterion considered were peak and RMS values of passenger seat acceleration and displacement response.

❖ The passenger ride comfort of a semi-active suspension system is affected by the selected control strategy.

The used control strategies as PID, Fuzzy, HFPID and HFPIDCR showed different simulation results under four types of road excitations. The mathematical results achieved using various control strategies were different in terms of passenger seat acceleration and passenger seat displacement in quarter car model. Simulation results showed the effectiveness of semi-active quarter car system with MR shock absorber in combination with HFPIDCR controller. The results achieved by HFPIDCR controller were best in primary suspension controlled, secondary suspension controlled and fully suspension controlled cases for passenger ride comfort issues compared to uncontrolled and other controlled cases.

❖ Fully semi-active quarter car system was very promising in achieving best ride comfort and safety of travelling passengers.

The fully controlled semi-active quarter car system with HFPIDCR controller in combination with MR shock absorber provided best performance related to passenger ride comfort issues out of passive, primary suspension controlled and secondary suspension controlled quarter car systems for various passenger and sprung mass values.

❖ Damping force ranges of hydraulic shock absorbers were found out for which the operator can say the shock absorbers are good, fair and unacceptable for particular requirement.

Simulation results using MR shock absorber in semi-active quarter car model demonstrated that the vibration control performance of passenger seat was different in case of each controlled suspension system and highly affected by designed controllers. Based on the simulation results related to passenger ride comfort and safety under various road conditions, it can be concluded to have following damping force ranges in primary and secondary suspension system, for which the operator can say about the performance of shock absorbers in automotive vehicles in the quarter car model:

a) In semi-active suspension system, MR shock absorber with controllers was used which provided the controlled damping force to achieve maximum ride comfort and safety of passengers. The MR shock absorbers in combination with HFPIDCR or

HFPID controllers provided the sufficient controlled damping force and have been called “Good”. In this case, the range of desired damping force generated by integrated controllers in primary and secondary suspension systems are shown in Table 12.7 and Table 12.8 as follows :

Table 12.7 Primary suspension system good desired damping force range

Criterion	Damping Force Range (N)	
Suspension System	Primary Suspension System	
Forward Controller 1	HFPID 1	HFPIDCR 1
Compression Stage	218.03 - 820.29	262.7 - 956.55
Rebound Stage	284.79 - 853.71	352.87 - 1009.8

Table 12.8 Secondary suspension system good desired damping force range

Criterion	Damping Force Range (N)	
Suspension System	Secondary Suspension System	
Forward Controller 2	HFPID 2	HFPIDCR 2
Compression Stage	75.11 - 356.52	82.98 - 436.36
Rebound Stage	76.31 - 388.28	60.65 - 438.35

b) The MR shock absorber generated damping force in combination with PID or Fuzzy controllers have been called “Fair”. In this case, the range of desired damping force generated by assembled controllers in primary and secondary suspension system are shown in Table 12.9 and Table 12.10 as follows :

Table 12.9 Primary suspension system fair desired damping force range

Criterion	Damping Force Range (N)	
Suspension System	Primary Suspension System	
Forward Controller 1	PID 1	Fuzzy 1
Compression Stage	81.63 - 269.44	121.75 - 499.79
Rebound Stage	97.88 - 259.29	115.81 - 385.1

Table 12.10 Secondary suspension system fair desired damping force range

Criterion	Damping Force Range (N)	
Suspension System	Secondary Suspension System	
Forward Controller 2	PID 2	Fuzzy 2
Compression Stage	49.63 - 146.71	49.48 - 226.87
Rebound Stage	54 - 183.27	53.49 - 223.71

c) The uncontrollable passive shock absorber provided lesser damping force as

compared to controlled MR shock absorber and therefore it has been put under the category of “unacceptable” for achieving desired passenger ride comfort and safety in quarter car model.

d) The operator can measure the MR damper damping force under different values of input current and excitation conditions using MTS machine. Based on the desired damping force generation capability of developed controllers in semi-active quarter car suspension model, the operator can decide that the shock absorbers are good, fair and unacceptable for passenger ride comfort and safety.

❖ **Frequency response analysis was performed to analyze the safe design of quarter car model at various road excitation velocities under sinusoidal road profile.**

The calculated three natural frequencies of the quarter car model were 1.1138 Hz, 1.9959 Hz and 10.7534 Hz respectively. The natural frequency of unsprung mass is 10.7534 Hz which is much lower than the magnitude of base excitation frequency at the quarter car selected velocity of 120 km/ hr. Thus design of quarter car model with selected parameters is safe.

12.2 RESEARCH LIMITATIONS

Research limitations based on present work in the field of passive and MR damper technology can be described as follows:

1. The damping force generation behavior of designed and developed dual tube passive hydraulic dampers is based on the test results on MTS machine. Real testing of these dampers is required in real vehicle under passenger seat in terms of effectiveness and damping force generation capability.
2. For comparative analysis of passenger ride comfort and safety, simulation based work has been used in this research work. An experimental test rig related to semi-active quarter car model with three degrees of freedom is required using proposed controllers for validation of simulation results.
3. The considered MR damper in present work can only be used in small vehicles due to small size and limited damping force generation capability with supply current range of 0 to 2 Amp.

12.3 SCOPE FOR FURTHER WORK

The knowledge gained from present research work can provide a support and direction for further research work as follows:

1. Simulation results of quarter car model related to passenger ride comfort can be compared and validated through laboratory and field testing with real setup.
2. Current research work considered Fuzzy and PID controllers as well their combinations to achieve the desired task. Future research studies may be considered to compare the performance of various available and latest controllers to achieve enhanced performance.
3. A half car model as well as full car model may be studied with passive and controllable magnetorheological and electrorheological shock absorbers with various available controllers, taking passenger ride comfort factor into account.
4. In present case, MR shock absorber, RD-1005-3, manufactured by Lord Corporation, was selected for study. Future studies may investigate and compare application of various types of designed and developed magnetorheological shock absorbers in vehicle suspension system as well as work related to optimization of its design parameters.
5. In automotive sector, application of magnetorheological and electrorheological fluid based shock absorbers in suspension systems can be studied for development of latest technology based vehicles.

REFERENCES

- [1] D. Fischer and R. Isermann, "Mechatronic semi-active and active vehicle suspensions," in *Control Engineering Practice*, Vol. 12, No. 11, 2004, pp. 1353-1367.
- [2] A. Alleyne and J. K. Hedrick, "Non-linear adaptive control of active suspensions," in *IEEE Transactions on Control Systems Technology*, Vol. 3, No. 1, 1995, pp. 94–101.
- [3] I. Ursu, F. Ursu, and M. Vladimirescu, "The synthesis of two suboptimal electrohydraulic suspensions, active and semiactive, employing the receding horizon method," in *Nonlinear Analysis Theory, Methods & Applications*, Vol. 30, No. 4, 1997, pp. 1977–1984.
- [4] W. K. Kim, and S. B. Choi, "Vibration control of a semi-active suspension featuring electro-rheological fluid dampers," in *Journal of Sound and Vibration*, Vol. 234, No. 3, 2000, pp. 537–546.
- [5] R. Rajamani, *Vehicle Dynamics and Control*, New York, NY, USA: Springer Science & Business Media, 2006.
- [6] S. Sassi, K. Cherif, L. Mezghani, M. Thomas, and A. Kotrane, "An innovative magnetorheological damper for automotive suspension: from design to experimental characterization," in *Smart Materials and Structures*, Vol. 14, No. 4, 2005, pp. 811–822.
- [7] D. Karnopp, M. J. Crosby, and R. A. Farwood, "Vibration control using semi-active force generators," in *Journal of Manufacturing Science and Engineering*, Vol. 96, No. 2, 1974, pp. 619-626.
- [8] D. Ledezma-Ramirez, N. Ferguson, and M. Brennan, "Shock performance of different semiactive damping strategies," in *Journal of Applied Research and Technology*, Vol. 8, No. 2, 2010, pp. 249–259.
- [9] R. S. Sharp and S. A. Hassan, "The relative performance capabilities of passive, active and semi-active car suspension systems," in *Proceedings of the Institution of Mechanical Engineers, Part D: Journal of Automobile Engineering*, Vol. 200, No. 3, 1986, pp. 219–228.
- [10] T. Gillespie, *Development of semi-active damper for heavy off-road military vehicles*, M.Sc. Thesis, University of Waterloo, 2006.

- [11] A. Preumont, “Vibration control of active structures: an introduction,” 2nd ed., Kluwer Academic Publishers Dordrecht, 2002.
- [12] Z. D. Xu, Y.P. Shen, and Y.Q. Guo, “Semi-active control of structures incorporated with magnetorheological dampers using neural networks”, in *Smart Materials and Structures*, Vol. 12, No. 1, 2003, pp. 80–87.
- [13] C. M. D. Wilson and M. M. Abdullah, “Structural vibration reduction using self-tuning fuzzy control of magnetorheological dampers”, in *Bulletin of Earthquake Engineering*, Vol. 8, No. 4, 2010, pp. 1037–1054.
- [14] X. Song, M. Ahmadian, S. Southward, and L. R. Miller, “An adaptive semiactive control algorithm for magnetorheological suspension systems,” in *Journal of Vibration and Acoustics*, Vol. 127, No. 5, 2005, pp. 493–502.
- [15] M. Ahmadian and J. C. Poynor, “An evaluation of magneto rheological dampers for controlling gun recoil dynamics,” in *Shock and Vibration*, Vol. 8, No. 3–4, 2001, pp. 147–155.
- [16] W. H. Liao, and D. H. Wang, “Semi-active vibration control of train suspension systems via magnetorheological dampers,” in *Intelligent Material Systems and Structures*, Vol. 14, 2003, pp. 161-172.
- [17] J. Rabinow, “The Magnetic Fluid Clutch,” Transactions of the AIEE, Vol. 67, 1948, pp. 1308-1315.
- [18] J. Rabinow, “Magnetic fluid torque and force transmitting device,” U.S. Patent 2,575,360, 1951.
- [19] K. D. Weiss and D. A. Nixon, “Viscoelastic properties of magneto - and electrorheological fluids,” in *Journal of Intelligent Material Systems and Structures*, Vol. 5, 1994, pp. 772-775.
- [20] F. D. Goncalves, J. H. Koo and M. Ahmadian, “A review of the state of the art in magnetorheological fluid technologies – Part I: MR fluid and MR fluid models,” in *Shock and Vibration Digest*, Vol. 38, No. 3, 2006, pp. 203–219.
- [21] M. R. Jolly, J. W. Bender, and J. D. Carlson, “Properties and Application of Commercial Magnetorheological Fluids,” in *Journal of Intelligent Material Systems and Structures*, Vol. 10, 1999, pp. 5-13.
- [22] Y. Shen, “Vehicle Suspension Vibration Control with Magnetorheological Dampers,” Ph.D. Dissertation, University of Waterloo, Canada, 2005.

- [23] K. Lee, "Numerical modelling for the hydraulic performance prediction of automotive monotube dampers," in *Vehicle System Dynamics*, Vol. 28, No. 1, 1997, pp. 25-39.
- [24] M. S. Talbott and J. Starkey "An experimentally validated physical model of a high-performance mono-tube damper," No. 2002-01-3337, SAE Technical Paper, 2002.
- [25] X. C. Akutain, J. Viñolas, J. Savall, and J. Biera, "A parametric damper model validated on a track," in *International Journal of Heavy Vehicle Systems*, Vol. 13, No. 3, 2006, pp. 145–162
- [26] C. T. Lee and B. Y. Moon, "Simulation and experimental validation of vehicle dynamic characteristics for displacement-sensitive shock absorber using fluid-flow modeling," in *Mechanical Systems and signal processing*, Vol. 20, No. 2, 2006, pp. 373-388.
- [27] F. G. Guzzomi, P. L. O'Neill, and A. C. R. Tavner, "Investigation of damper valve dynamics using parametric numerical methods," in *16th Australasian Fluid Mechanics Conference (AFMC), School of Engineering, The University of Queensland*, 2007, pp. 1123-1130.
- [28] M. Shams, R. Ebrahimi, A. Raoufi, and B. J. Jafari, "CFD-FEA analysis of hydraulic shock absorber valve behavior," in *International Journal of Automotive Technology*, Vol. 8, No. 5, 2007, pp. 615-622.
- [29] A. Farjoud and M. Ahmadian, "Shim stack deflection analysis in hydraulic dampers using energy methods," in *SPIE Smart Structures and Materials+ Nondestructive Evaluation and Health Monitoring, International Society for Optics and Photonics*, 2010, pp. 764325-764325.
- [30] C. C. Zhou and Y. Z. Xu, "Analytic Computation Method of the Equivalent Thickness of Superposition Multi-Throttle-Slices of Twin-Tubes Shock Absorber," in *Engineering*, Vol. 2, No. 2, 2010, pp. 103-106.
- [31] J. Gołdasz, "Modelling of amplitude-selective-damping valves," in *Mechanics and Control*, Vol. 30, 2011, pp. 60-64.
- [32] P. Czop, D. Gąsiorek, J. Gniłka, D. Sławik, and G. Wszolek, "Fluid-structure simulation of a valve system used in hydraulic dampers," in *Modelowanie Inzynierskie*, Vol. 45, No. 14, 2012, pp. 197-205.
- [33] A. Farjoud, M. Ahmadian, M. Craft, and W. Burke, "Nonlinear modeling and experimental characterization of hydraulic dampers: effects of shim stack and

- orifice parameters on damper performance," in *Nonlinear Dynamics*, Vol. 67, No. 2, 2012, pp. 1437-1456.
- [34] L. Liang, X. Zhang, M. Peng, and G. Qin, "Non-linear Characteristic Simulation of Hydraulic Shock Absorbers Considering the Contact of Valves," in *Proceedings of the 2nd International Conference on Computer Application and System Modeling*, 2012, pp. 1132-1134.
- [35] N. V. Satpute, S. Singh, and S. M. Sawant, "Fluid flow modelling of a fluid damper with shim loaded relief valve," in *International Journal of Mechanical Engineering*, Vol. 2, No. 1, 2013, pp. 65-74.
- [36] G. Yang, B. F. Spencer Jr., J. D. Carlson, and M. K. Sain, "Large-scale MR fluid dampers: modeling and dynamic performance considerations," in *Engineering Structures*, 2002, Vol. 24, pp. 309–323.
- [37] S. R. Hong, S. B. Choi, Y. T. Choi, and N. M. Wereley, "Non-dimensional analysis and design of a magnetorheological damper," in *Journal of Sound and Vibration*, Vol. 288, 2005, pp. 847–863.
- [38] W. W. Chooi and S. O. Oyadiji, "Design, modelling and testing of magnetorheological (MR) dampers using analytical flow solutions," in *Computers and Structures*, Vol. 86, 2008, pp. 473–482.
- [39] Q. H. Nguyen and S. B. Choi, "Optimal design of MR shock absorber and application to vehicle suspension," in *Smart materials and Structures*, Vol. 18, No. 3, 2009, 035012.
- [40] S. Kciuk, A. Mezyk, and W. Klein, "The numerical and experimental studies of the prototype MR damper," in *Active Noise and Vibration Control Methods, Krakow-Wojanow, Poland*, 2011, pp. 231-245.
- [41] Z. Parlak, T. Engin, and I. Çalli, "Optimal design of MR damper via finite element analyses of fluid dynamic and magnetic field," in *Mechatronics*, Vol. 22, No. 6, 2012, pp. 890–903.
- [42] R. S. Prabakar, C. Sujatha, and S. Narayanan, "Response of a quarter car model with optimal magnetorheological damper parameters," in *Journal of Sound and Vibration*, Vol. 332, No. 9, 2013, pp. 2191–2206.
- [43] J. H. Lee, C. Han, D. Ahn, J. K. Lee, S. H. Park, and S. Park, "Design and performance evaluation of a rotary magnetorheological damper for unmanned vehicle suspension systems," in *The Scientific World Journal Volume 2013*, Article ID 894016, 10 pages.

- [44] S. K. Mangal and A. Kumar, “Experimental and numerical studies of magnetorheological (MR) damper,” in *Chinese Journal of Engineering*, Volume 2014, Article ID 915694, 7 pages.
- [45] I. I. M. Yazid, S. A. Mazlan, T. Kikuchi, H. Zamzuri, and F. Imaduddin, “Design of magnetorheological damper with a combination of shear and squeeze modes,” in *Materials and Design*, Vol. 54, 2014, pp. 87–95.
- [46] N. M. Kwok, Q. P. Ha, M. T. Nguyen, J. Li, and B. Samali, “Bouc–Wen model parameter identification for a MR fluid damper using computationally efficient GA,” in *ISA transactions*, Vol. 46, 2007, No. 2, pp. 167–179.
- [47] R. Stanway, J. L. Sproston, and N. G. Stevens, “Non-linear modelling of an electro-rheological vibration damper,” in *Journal of Electrostatics*, Vol. 20, No. 2, 1987, pp. 167–84.
- [48] Y. Wen, “Method for random vibration of hysteretic systems,” in *Journal of the Engineering Mechanics Division*, 1976, pp. 249-263.
- [49] B. F. Spencer, S. J. Dyke, M. K. Sain, and J. D. Carlson, “Phenomenological model of a magnetorheological damper,” in *Journal of Engineering Mechanics*, Vol. 123, No. 3, 1997, pp. 230–238.
- [50] B. J. Bass and R. E. Christenson, “System identification of a 200 kN magnetorheological fluid damper for structural control in large-scale smart structures,” in *American Control Conference, ACC'07*, 2007, pp. 2690–2695.
- [51] P. R. Dahl, “Solid friction damping of mechanical vibrations” in *AIAA Journal*, Vol. 14, No. 12, 1976, pp. 1675–1682.
- [52] Q. Zhou and W. L. Qu, “Two mechanic models for magnetorheological damper and corresponding test verification,” in *Earthq. Eng. Eng. Vib. (in Chinese)*, Vol. 22, 2002, pp. 144–150.
- [53] R. C. Ehrgott and S. F. Masri, “Modeling the oscillatory dynamic behaviour of electrorheological materials in shear,” in *Smart Materials Structures*, Vol. 1, No. 4, 1992, pp. 275 – 285.
- [54] K. C. Schurter and P. N. Roschke, “Fuzzy modeling of a magnetorheological damper using ANFIS,” in *Proceedings of the IEEE International Conference on Fuzzy Systems*, 2000, pp. 122–127.
- [55] S. B. Choi, S. K. Lee, and Y. P. Park, “A hysteresis model for the field-dependent damping force of a magnetorheological damper,” in *Journal of Sound and Vibration*, Vol. 245, No. 2, 2001, pp. 375–383.

- [56] D. H. Wang and W. H. Liao, "Modeling and control of magnetorheological fluid dampers using neural networks," in *Smart Materials and Structures*, Vol. 14, No. 1, 2004, pp. 111–26.
- [57] H. Du, J. Lam, and N. Zhang, "Modeling of a magneto-rheological damper by evolving radial basis function networks," in *Engineering Applications of Artificial Intelligence*, Vol. 19, No. 8, 2006, pp. 869–81.
- [58] D. Q. Truong and K. K. Ahn, "Identification and application of black-box model for a self-sensing damping system using a magneto-rheological fluid damper," in *Sensors and Actuators A*, Vol. 161, No. 1-2, 2010, pp. 305–321.
- [59] M. J. L. Boada, J. A. Calvo, B. L. Boada, and V. Diaz, "Modeling of a Magnetorheological damper by recursive lazy learning," in *International Journal of Non-Linear Mechanics*, Vol. 46, No. 3, 2011, pp. 479–485.
- [60] K. Kim and D. Jeon, "Vibration suppression in an MR fluid damper suspension system," in *Journal of Intelligent Material Systems and Structures*, Vol. 10, No. 10, 1999, pp. 779-786.
- [61] M. Ahmadian and C. A. Pare, "A Quarter-Car Experimental Analysis of Alternative Semiactive Control Methods," in *Journal of Intelligent Material Systems and Structures*, Vol. 11, No. 8, 2000, pp. 604-612.
- [62] G. Z. Yao, F. F. Yap, G. Chen, W. H. Li, and S. H. Yeo, "MR damper and its application for semi-active control of vehicle suspension system," in *Mechatronics*, Vol. 12, No. 7, 2002, pp. 963–973.
- [63] A. H. F. Lam and W. H. Liao, "Semi-active control of automotive suspension systems with magneto-rheological dampers," in *International Journal of Vehicle Design, Inderscience Publishers*, Vol. 33, No. 1, 2003, pp. 50-75.
- [64] F. D. Goncalves and M. Ahmadian, "A hybrid control policy for semi-active vehicle suspensions," in *Shock and Vibration*, Vol. 10, No. 1, 2003, pp. 59–69.
- [65] D. L. Guo, H. Y. Hu, and J. Q. Yi, "Neural network control for a semi-active vehicle suspension with a magnetorheological damper," in *Journal of Vibration and Control*, Vol. 10, No. 3, 2004, pp. 461–471.
- [66] K. Hudha, H. Jamaluddin, P. M. Samin, and R. A. Rahman, "Effects of control techniques and damper constraint on the performance of a semi-active magnetorheological damper," in *International Journal of Vehicle Autonomous Systems*, Vol. 3, No. 2, 2005, pp. 230-252.

- [67] H. Du, K. Y. Sze, and J. Lam, "Semi-active H_∞ control of vehicle suspension with magneto-rheological dampers," in *Journal of Sound and Vibration*, Vol. 283, 2005, pp. 981–996.
- [68] Y. Miao, D. X. Min, L. C. Rong, and C. W. Min, "Adaptive Fuzzy-Neural Network Control for Magneto-Rheological Suspension," in *IJCSNS International Journal of Computer Science and Network Security*, Vol. 6, No.10, 2006, pp. 66-71.
- [69] M. M. Rashid, M. A. Hussain, N. A. Rahim, and J. S. Momoh, "Development of a semi-active car suspension control system using magneto-rheological damper model," in *International Journal of Mechanical and Materials Engineering*, Vol. 2, No. 2, 2007, pp. 93-108.
- [70] D. C. Batterbee and N. D. Sims, "Hardware-in-the-loop simulation of magnetorheological dampers for vehicle suspension systems," in *Proceedings of the Institution of Mechanical Engineers, Part I: Journal of Systems and Control Engineering*, Vol. 221, No. 2, 2007, pp. 265–278.
- [71] M. M. Rashid, N. A. Rahim, M. A. Hussain, F. Mohamed, and M. A. Rahman, "Development and Testing of Hybrid Fuzzy Logic Controller for Car Suspension System Using Magneto-Rheological Damper," in *Industry Applications Society Annual Meeting, 2008. IAS'08. IEEE*, 2008, pp. 1-8.
- [72] A. Turnip, K. S. Hong, and S. Park, "Control of a Semi-Active MR-Damper Suspension System: A New Polynomial Model," in *Proceedings of the 17th World Congress, The International Federation of Automatic Control Seoul, Korea*, July 6-11, 2008.
- [73] J. Uradniecek and M. Musil, "Study of adaptive control algorithm using hysteretic magneto-rheological damper model in 1/4 car suspension, in *Strojnický Casopis*, Vol. 59, No. 4, 2008, pp. 175-187.
- [74] K. Ubaidillah, F. Hudha, H. Jamaluddin, and M. R. Said, "Simulation and Experimental Investigation on Direct Multiorder PI Control for Magnetorheological Damper to Improve Vehicle Ride Performance," in *Jurnal Teknik Mesin*, Vol. 9, No. 2, 2009, pp. 115-129.
- [75] X. M. Dong, M. Yu, C. R. Liao, and W. M. Chen, "Comparative research on semi-active control strategies for magneto-rheological suspension," in *Nonlinear Dynamics*, Vol. 59, 2010, pp. 433–453.

- [76] L. H. Nguyen, K. S. Hong, and S. Park, "Road-Frequency Adaptive Control for Semi-Active Suspension Systems," in *International Journal of Control, Automation, and Systems*, Vol. 8, No. 5, 2010, pp. 1029-1038.
- [77] M. M. Rashid, N. A. Rahim, M. A. Hussain, and M. A. Rahman, "Analysis and experimental study of magnetorheological-based damper for semiactive suspension system using fuzzy hybrids," in *IEEE Transactions on Industry Applications*, Vol. 47, No. 2, 2011, pp. 1051–1059.
- [78] K. Hudha, and H. Jamaluddin, "Simulation and experimental evaluation on a skyhook policy-based fuzzy logic control for semi-active suspension system," in *International Journal of Structural Engineering* Vol. 2, No. 3, 2011, pp. 243-272.
- [79] X. Z. Jiang, W. Jiong, and H. S. Hu, "Semi-active control of a vehicle suspension using magneto-rheological damper," in *Journal of Central South University*, Vol. 19, 2012, pp. 1839-1845.
- [80] M. El-Kafafy, S.M. El-Demerdash, and A. A. M. Rabeih, "Automotive ride comfort control using MR fluid damper," in *Engineering*, Vol. 4, No. 4, 2012, pp. 179–187.
- [81] L. H. Zong, X. L. Gong, C. Y. Guo, and S. H. Xuan, "Inverse neuro-fuzzy MR damper model and its application in vibration control of vehicle suspension system," in *International Journal of Vehicle Mechanics and Mobility, Vehicle System Dynamics*, Vol. 50, No. 7, 2012, pp. 1025–1041.
- [82] M. Rahman, M. M. Rashid, A. G. A. Muthalif, and B. Kasemi, "Evaluation of Different Control Policies of Semi-Active MR Fluid Damper of a Quarter-Car Model," in *Applied Mechanics and Materials*, Vol. 165, 2012, pp. 310-315.
- [83] A. Shojaei, H. Metered, S. Shojaei, and S. O. Oyadiji, "Theoretical and Experimental Investigation of Magneto-Rheological Damper based Semi-Active Suspension Systems," in *International Journal of Vehicle Structures and Systems*, Vol. 5, No. 3-4, 2013.
- [84] A. S. Yildiz, S. Sivrioglu, E. Zergeroglu, and S. Cetin, "Adaptive Control of Semiactive Quarter Car Model with MR Damper," in *Control Conference (ASCC), 2013 9th Asian*, pp. 1-6, June 2013.
- [85] A. J. Qazi, C. W. de Silva, A. Khan, and M. T. Khan, "Performance Analysis of a Semiactive Suspension System with Particle Swarm Optimization and

- Fuzzy Logic Control,” in *The Scientific World Journal*, Volume 2014, Article ID 174102, 12 pages.
- [86] P. W. Nugroho, W. Li, H. Du, G. Alici, and J. Yang, “An adaptive Neuro Fuzzy hybrid control strategy for a semiactive suspension with magneto rheological damper,” in *Advances in Mechanical Engineering*, Volume 2014, Article ID 487312, 11 pages.
- [87] G. A. Malmedahl, “Analysis of Automotive Damper Data and Design of a Portable Measurement System,” Bachelor of Science with Distinction Research Report, The Ohio State University, 2005.
- [88] A. M. Salem, T. Salahudien, "Evaluation of Characteristics of Tracked Vehicles Torsion Bars", 13th international conference on Applied Mechanics and Mechanical engineering, Military Technical College, Cairo, Egypt, 27-29 May 2008.
- [89] V B Bhandari, Design of Machine Elements, McGraw Hill Education (India) Private Limited, Third Edition, pp. 605.
- [90] G. K. Grover, Mechanical Vibrations, Nem Chand and Brothers, Fourth Edition, pp. 95.
- [91] A. M. Salem , W. Galal, “Identification of characteristics of hydraulic shock absorbers used in light weight tracked vehicles,” in *13th International Conference on Aerospace Science & Aviation Technology, ASAT- 13*, May 26 – 28, 2009, pp. 1-13.
- [92] Y. Lu, S. Li, and N. Chen, “Research on Damping Characteristics of Shock Absorber for Heavy Vehicle,” in *Research Journal of Applied Sciences, Engineering and Technology*, Vol. 5, No. 3, 2013, pp. 842-847.
- [93] W. H. Wang and Y. S. Tarn, “Design optimization of cutting parameters for turning operations based on the Taguchi method,” in *Journal of Material Processing Technology*, Vol. 84, No. 1-3, 1998, pp. 122-129.
- [94] B. H. Lee, J. Abdullah, and Z.A. Khan, “Optimization of rapid prototyping parameters for production of flexible ABS object,” in *Journal of Material Processing Technology*, Vol. 169, No. 1, 2005, pp. 54-61.
- [95] J. Laeng, Z. A. Khan, and S. Y. Khu, “Optimizing flexible behaviour of bow prototype using Taguchi approach,” in *Journal of Applied Sciences*, Vol. 6, 2006, pp. 622-630.

- [96] S. Kamaruddin, Z. A. Khan, and K. S. Wan, "The use of the Taguchi method in determining the optimum plastic injection moulding parameters for the production of a consumer product," in *Jurnal Mekanikal*, Vol. 18, 2004, pp. 98-110.
- [97] E. R. Wang, X. Q. Ma, S. Rakheja, and C.Y. Su, "Analysis of a Semi-active MR-damper with Hysteretic and Asymmetric Properties," in *Proceedings of the American Control Conference*, Denver, Colorado, June 4-6, 2003, pp. 4920-4925.
- [98] Y. Chen, "Fuzzy skyhook surface control using micro-genetic algorithm for vehicle suspension ride comfort," in *Intelligent Computational Optimization in Engineering*, Springer Berlin Heidelberg, 2011, pp. 357-394.
- [99] H. K. Shik and S. Park, "Road-frequency adaptive control for semi-active suspension systems," in *International Journal of Control, Automation and Systems*, Vol. 8, No. 5, 2010, pp. 1029-1038.
- [100] G. Verros, S. Natsiavas, and C. Papadimitriou, "Design optimization of quarter-car models with passive and semi-active suspensions under random road excitation," in *Journal of Vibration and Control*, Vol. 11, No. 5, 2005, pp. 581-606.
- [101] A. Colina, G. Lerma, I. Cabanes, and I. Iglesias, "Modelling and Control of a Semi-active Suspension System," in *Mechanisms and Machine Science*, Vol. 17, 2014, pp. 25-32.
- [102] H. Shabani, B. Vahidi, and M. Ebrahimpour, "A robust PID controller based on imperialist competitive algorithm for load–frequency control of power systems," in *ISA Transactions*, Vol. 52, 2013, pp. 88–95.
- [103] M. A. S. Aboelela, M. F. Ahmed, and H. T. Dorrah, "Design of aerospace control systems using fractional PID controller," in *Journal of Advanced Research*, Vol. 3, No. 3, 2012, pp. 225–232.
- [104] B. Vanavil, K. K. Chaitanya, and A. S. Rao, "Improved PID controller design for unstable time delay processes based on direct synthesis method and maximum sensitivity," in *International Journal of Systems Science* in Vol. 46, No. 8, 2015, pp. 1349–1366.
- [105] R. A. Krohling, H. Jaschek, and J. P. Rey, "Designing PI/PID Controller for a Motion Control System Based on Genetic Algorithm," in *12th IEEE International Symposium on Intelligent Control*, July 1997, pp. 125-130.

- [106] L. A. Zadeh, "Fuzzy sets," in *Information and Control*, Vol. 8, No. 3, 1965, pp. 338–353.
- [107] E. Mamdani and S. Assilian, "An experiment in linguistic synthesis with a fuzzy logic controller," in *International Journal of Man-Machine Studies*, Vol. 7, No. 1, 1975, pp. 1-13.
- [108] A. V. Topalov, O. Yesim, E. Kayacan, and O. Kaynak, "Neuro-fuzzy control of antilock braking system using sliding mode incremental learning algorithm," in *Neurocomputing*, Vol. 74, No. 11, 2011, pp.1883-1893.
- [109] B. L. Boada, M. J. L. Boada, and V. Diaz. "Fuzzy-logic applied to yaw moment control for vehicle stability," in *Vehicle System Dynamics*, Vol. 43, No. 10, 2005, pp. 753-770.
- [110] Y. J. Lin, Y. Q. Lu, and J. Padovan, "Fuzzy logic control of vehicle suspension systems," in *International Journal of Vehicle Design*, Vol. 14, No. 5, 1993, pp. 457-470.
- [111] Y. Chen, Z. L. Wang, J. Qiu, and H. Z. Huang, "Hybrid fuzzy skyhook surface control using multi-objective microgenetic algorithm for semi-active vehicle suspension system ride comfort stability analysis," in *Journal of Dynamic Systems, Measurement, and Control*, Vol. 134, No. 4, 2012, 041003.
- [112] M. A. Eltantawie, "Decentralized neuro-fuzzy control for half car with semi-active suspension system," in *International Journal of Automotive Technology*, Vol. 13, No. 3, 2012, pp. 423-431.
- [113] C. F. Nicolas, J. Landaluze, E. Castrillo, M. Gaston, and R. Reyeroy, "Application of fuzzy logic control to the design of semi-active suspension systems," in *Proceedings of the Sixth IEEE International Conference on Fuzzy Systems, IEEE*, Vol. 2, 1997, pp. 987-993.
- [114] S. H. Zareh, A. Sarrafan, A. A. A. Khayyat, and A. Zabihollah. "Intelligent semi-active vibration control of eleven degrees of freedom suspension system using magnetorheological dampers," in *Journal of Mechanical Science and Technology*, Vol. 26, No. 2, 2012, pp. 323-334.
- [115] I. Erenoglu, I. Eksin, E. Yesil, and M. Guzelkaya, "An intelligent hybrid fuzzy PID controller," in *European Conference on Modelling and Simulation*, 2006, pp. 62-67.

- [116] S. Çetin and A. V. Akkaya, "Simulation and hybrid fuzzy-PID control for positioning of a hydraulic system," in *Nonlinear Dynamics*, Vol. 61, No. 3, 2010, pp. 465–476.
- [117] O. Demir, I. Keskin, and S. Cetin, "Modeling and control of a nonlinear half-vehicle suspension system: a hybrid fuzzy logic approach," in *Nonlinear Dynamics*, Vol. 67, No. 3, 2012, pp. 2139–2151.
- [118] K. H. Ubaidillah, F. Imaduddin and Md. R. Said, "Simulation and Experimental Investigation on Direct Multiorder PI Control for Magnetorheological Damper to Improve Vehicle Ride Performance," in *Jurnal Teknik Mesin (JTM)*, Vol. 9, No. 2, 2009, pp.115-129.
- [119] A.S. Yildiz, S. Sivrioglu, E. Zergeroglu, and S. Cetin, "Adaptive control of semiactive quarter car model with MR damper," in 2013 9th Asian *Control Conference (ASCC)*, pp. 1-6, June 2013, doi: 10.1109/ASCC.2013.6606324.
- [120] M. S. Kumar and S. Vijayarangan, "Design of LQR controller for active suspension system," in *Indian Journal of Engineering & Materials Sciences*, Vol. 13, 2006, pp. 173-179.

APPENDIX A

MATALB / SIMULINK MODELS OF QUARTER CAR MODEL

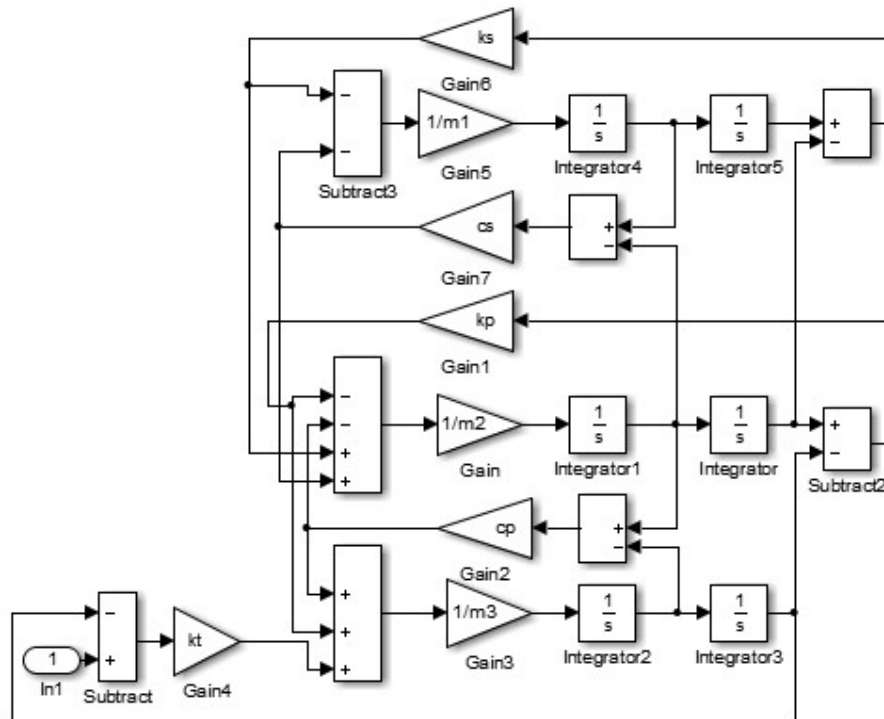


Figure A.1.1: Overview of passive/ uncontrolled quarter car model

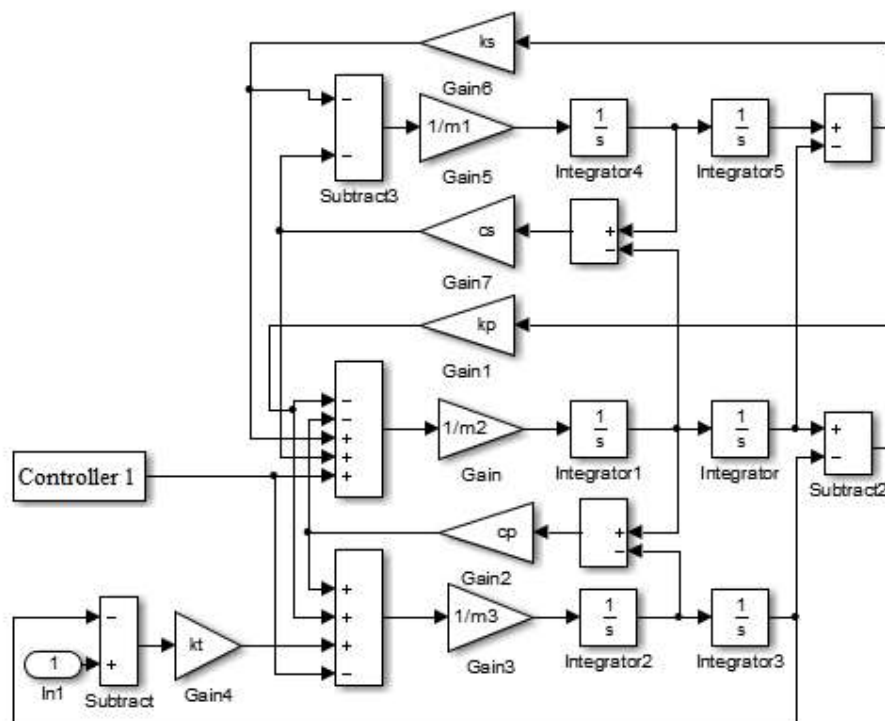


Figure A.1.2: Overview of primary suspension controlled quarter car model

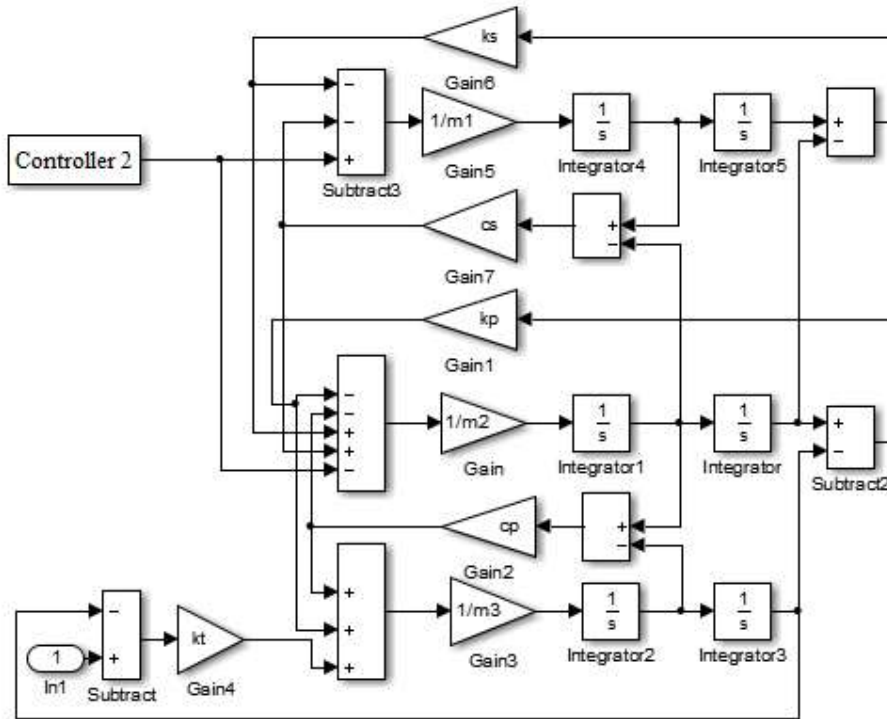


Figure A.1.3: Overview of secondary suspension controlled quarter car model

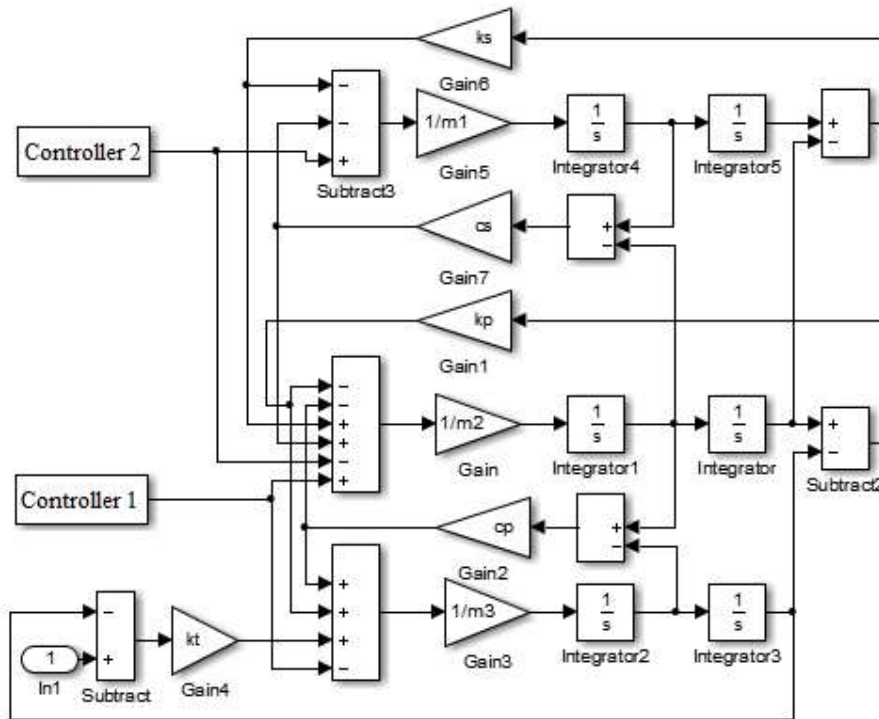


Figure A.1.4: Overview of fully suspension controlled quarter car

Figure A.1: Uncontrolled and controlled quarter car simulink models

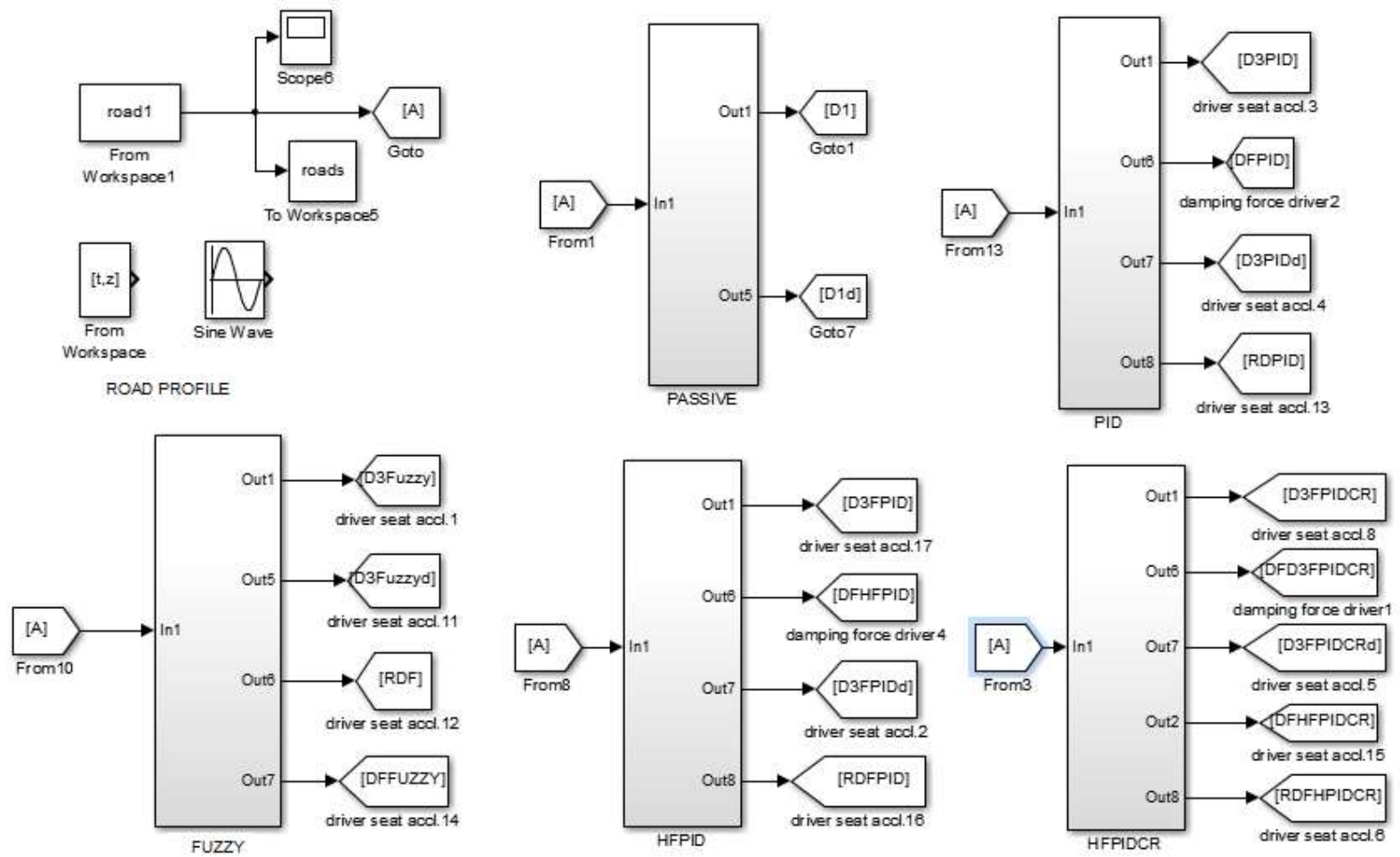


Figure A.2: Overview of quarter car model input-output signals

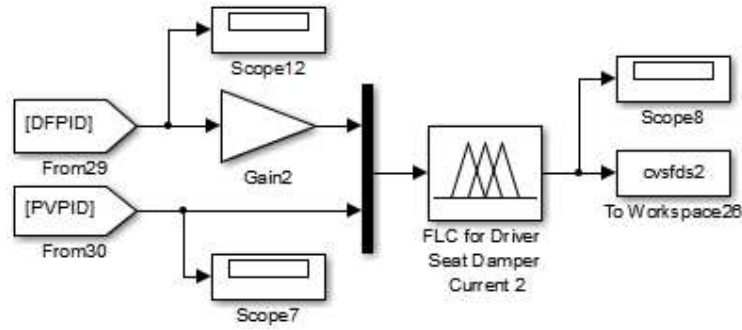


Figure A.3.1: Matlab/Simulink implementation of current signal for PID controller

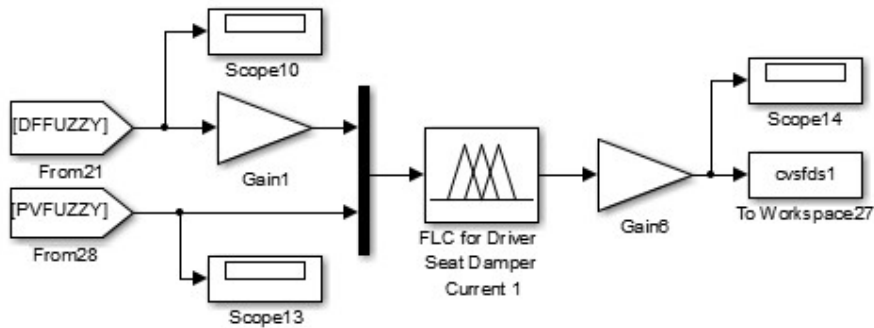


Figure A.3.2: Matlab/Simulink implementation of current signal for Fuzzy controller

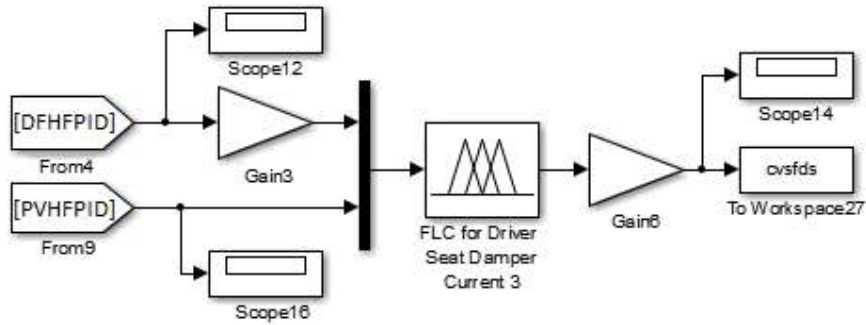


Figure A.3.3: Matlab/Simulink implementation of current signal for HFPID controller

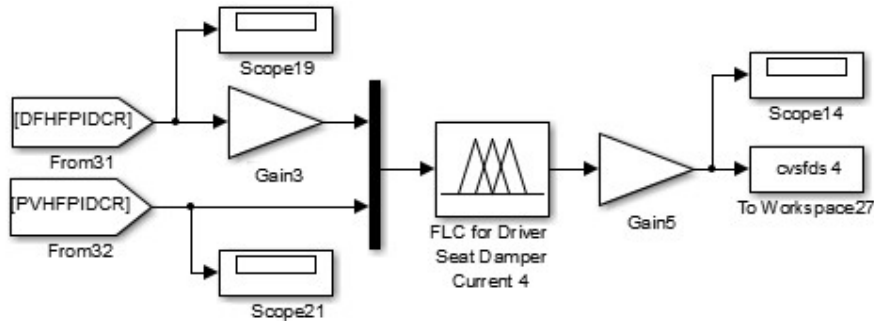


Figure A.3.4: Matlab/Simulink implementation of current signal for HFPIDCR controller

Figure A.3: Overview of Inverse Fuzzy Logic Controller in quarter car model

PROGRAMME FOR POLYNOMIAL CURVE FITTING PLOT

```
%% POLYNOMIAL CURVE FITTING PLOT %%  
  
%% Force Velocity Curve --- P VALUES %%  
  
p1dv=polyfit(x0uv,y0uv,10)    %% Upper Curve p Values  
f1dv=polyval(p1dv,x0uv);  
  
p2dv=polyfit(x25uv,y25uv,10);  
f2dv=polyval(p2dv,x25uv);  
  
p3dv=polyfit(x50uv,y50uv,10);  
f3dv=polyval(p3dv,x50uv);  
  
p5dv=polyfit(x100uv,y100uv,10);  
f5dv=polyval(p5dv,x100uv);  
  
p11dv=polyfit(x0dv,y0dv,10)    %% Lower Curve p Values  
f11dv=polyval(p11dv,x0dv);  
  
p22dv=polyfit(x25dv,y25dv,10);  
f22dv=polyval(p22dv,x25dv);  
  
p33dv=polyfit(x50dv,y50dv,10);  
f33dv=polyval(p33dv,x50dv);  
  
p55dv=polyfit(x100dv,y100dv,10);  
f55dv=polyval(p55dv,x100dv);
```

BRIEF PROFILE OF THE RESEARCH SCHOLAR

Devdutt completed his B.E. (Production Engineering) in First Division with Distinction from Swami Ramanand Teerth Marathwada University, Nanded in 2001 and M.Tech. (Manufacturing Technology & Automation) in First Division with Distinction from YMCAIE, Faridabad-Maharishi Dayanand University, Rohtak in 2007. He is Ph D student under the guidance of Dr. M. L. Aggarwal, in the Department of Mechanical Engineering, YMCA University of Science and Technology, Faridabad. Presently he is working as Assistant Professor in the Department of Mechanical Engineering, Faculty of Engineering and Technology, Manav Rachna International University, Faridabad from 2010. He is having 7 years of teaching and 4 years of industrial experience. His research areas of interest are noise, vibration and ride quality related to semi-active and active vehicle suspension system.



LIST OF PUBLICATIONS OUT OF THESIS

List of Published Papers

S. No.	Title of the Paper along with Volume, Issue No., Year of Publication	Publisher	Impact Factor	Referred or Non-Referred	Whether you paid any money or not for publication	Remarks
1	Fuzzy control of semi-active quarter car suspension system with MR damper, Proceedings of the National Conference on Trends and Advances in Mechanical Engineering, YMCA University of Science & Technology, Faridabad, Haryana, Oct 19-20, 2012, pp. 296-304.	YMCA University of Science & Technology, Faridabad, Haryana	---	---	Conference Fees	National Conference
2	Fuzzy control of seat vibrations for semi-active quarter vehicle system utilizing magneto-rheological damper, Volume 1, Issue 12, December 2012, pp. 51-56.	IJEI	1.212	Referred	Yes	International Journal of Engineering Inventions
3	Fuzzy Logic Control of a Semi-Active Quarter Car System, Volume 8, No. 1, 2014, pp. 163-167.	World Academy of Science, Engineering and Technology	---	Referred	No	International Journal of Mechanical, Industrial Science and Engineering

List of Published Papers (Contd..)

S. No.	Title of the Paper along with Volume, Issue No., Year of Publication	Publisher	Impact Factor	Referred or Non-Referred	Whether you paid any money or not for publication	Remarks
4	Passenger seat vibration control of semi-active quarter car system with fuzzy controller, Volume 2, Issue 1, 2014, pp. 6-14.	YMCA University of Science & Technology, Faridabad, Haryana	---	Referred	No	YMCAUST International Journal of Research
5	Passenger Seat Vibration Control of Quarter Car System with MR Shock Absorber, Volume 8, No. 5, 2014, pp. 707-714.	World Academy of Science, Engineering and Technology	---	Referred	No	International Journal of Computer, Information, Mechatronics, Systems Science and Engineering
6	Comparative Analysis of Passenger Ride Comfort Using Various Semi-Active Suspension Alternatives, Volume 3, No. 3, 2014, pp. 79-89.	Wireilla Scientific Publications, New South Wales, Australia	---	Referred	No	International Journal of Recent advances in Mechanical Engineering (IJMECH),

List of Published Papers (Contd..)

S. No.	Title of the Paper along with Volume, Issue No., Year of Publication	Publisher	Impact Factor	Referred or Non-Referred	Whether you paid any money or not for publication	Remarks
7	Fuzzy control of passenger ride performance using MR shock absorber suspension in quarter car model, DOI 10.1007/s40435-014-0128-z, 2014.	Springer-Verlag Berlin Heidelberg	---	Referred	No	International Journal of Dynamics and Control
8	Hybrid Fuzzy-PID Control of a Semi-Active Quarter Car System, Paradigm in Mechanical Engineering, MRIU, Faridabad, 2014, pp. 217-221.	Manav Rachna International University, Faridabad, Haryana	---	---	Conference Fees	National Conference
9	Passenger seat vibration control of a semi-active quarter car system with hybrid Fuzzy - PID approach, DOI 10.1007/s40435-015-0175-0	Springer-Verlag Berlin Heidelberg	---	Referred	No	International Journal of Dynamics and Control